UNIVERSITÉ DE STRASBOURG

ÉCOLE DOCTORALE des Sciences de la Vie et de la Santé

UMR_S INSERM 1109
(IRM – Group Tumor Microenvironment)

THÈSE présentée par :

Devadarssen MURDAMOOTHOO

soutenue le : **14 septembre 2018**

pour obtenir le grade de : **Docteur de l'université de Strasbourg**

Discipline : Sciences de la Vie et de la Santé

Spécialité : Immunologie et Cancer

Immuno-modulatory functions of Tenascin-C in a tumor progression model

THÈSE dirigée par :

Dr OREND Gertraud   Université de Strasbourg, France

Rapporteurs :

Pr HEROLD-MENDE Christel   Université de Heidelberg, Allemagne

Pr RÜEGG Curzio   Université de Fribourg, Suisse

Examinateur interne:

Pr Kilhoffer Marie-Claude   Université de Strasbourg, France

உ

Acknowledgements

I would like to express my gratitude to my supervisor Dr Gertraud Orend for giving me the opportunity to do my PhD studies in her research group. Thank you for your trust right from the start, your support and your encouragement.

I would like to thank Pr Marie-Claude Kilhoffer, Pr Christel Herold-Mende and Pr Curzio Rüegg for their interest in my work and for accepting to be part of my thesis committee. I also like to thank Dr Dominique Guenot, Dr Olivier Lefebvre and Pr Philippe Georgel, the members of my half term committee.

I wish to thank the Worldwide Cancer Research and "La foundation ARC" to have funded my PhD project and allowed me to produce this scientific work.

I will now switch to French

Mes chers collègues de l'équipe GO, je tiens à tous vous remercier pour ces bons moments passés en votre compagnie. La thèse est un long parcours, pas toujours très simple mais avec vous à mes côtés ça l'était déjà un peu plus. Merci pour les échanges scientifiques et les échanges « un peu moins scientifiques ». William, Fanny, Alev, Chérine, Thomas, Mika et Rolando, je vous dis un énorme MERCI. Ça a été un immense plaisir de travailler avec vous.

Je ne pourrais oublier ceux qui étaient présents dès le début :

Mes très chères Annick et Isabelle, Que de souvenirs mémorables avec vous ! Je vous remercie de tout cœur pour votre bienveillance à mon égard.

Sun, Constance, Christiane, Patricia et Olivier. Un grand merci pour avoir partagé vos connaissances respectives avec moi. Cela a été pour moi un privilège.

Aux membres de l'unité U1113 et en particulier Cyril, Radhia, Damien, Ahlam, Asma, Elisabeth, Léo, Marine et Emilie… (Honnêtement je serais bien parti pour tous vous citer mais j'ai peur d'en omettre quelques uns), Je vous remercie tous pour les bons moments passés ensemble.

2

Je souhaite également reconnaître la contribution des personnes « plus éloignées de la science » à ce travail. Leurs soutiens a été pour moi un moteur essentiel à la réalisation de ce projet.

Mes très chers parents Souba et Barlen, je ne sais pas par où commencer pour vous exprimer mon infinie gratitude. Tous vos sacrifices à l'échelle d'une vie ont fait de moi ce que je suis aujourd'hui. Vous n'imaginez même pas à quel point je suis fier d'être votre fils. Merci d'avoir toujours été là pour moi et de m'avoir aidé à réaliser ce travail.

Nadia, Jayssen, Veena, Mam Vassen et Tatie Kam, je vous remercie d'avoir été présents pour moi. Vos encouragements respectifs m'ont toujours aidé à aller de l'avant.

Raphaële et Christian, tout comme pour mes parents, je ne saurais vous remercier pour vos encouragements quotidiens. Vous avez été toujours formidables envers moi et je souhaite vous en exprimer toute ma gratitude du plus profond de mon cœur. Malika, Guillaume et Noah je vous remercie pour votre soutien et de m'avoir toujours apporté le sourire.

Cid et Filoche…bien sûr que je ne vous ai pas oubliés ! Merci pour tout !!!

Rom, Tu as été un soutien incessant pour moi. Tu as toujours trouvé les bons mots pour me remotiver et pour m'aider à aller de l'avant. Le fruit de ce long travail est en très grande partie grâce à toi. Je ne pourrais jamais suffisamment te remercier pour tout cela.

En relisant ces remerciements, je me rends compte que bien des mots reviennent encore et encore. Ces répétitions montrent surtout que j'ai eu la chance de côtoyer des personnes formidables au cours de ces dernières années…

Table of content

Table of figures

I.   French abstract

Introduction

Le cancer du sein demeure à ce jour l'une des causes de mortalité majeures chez la femme et ce malgré un diagnostic et une prise en charge thérapeutique précoces (Fitzmaurice et al. 2015). La principale cause de cette forte mortalité est le développement de métastases se disséminant à des organes secondaires tels que l'os, le cerveau et les poumons (Minn et al. 2005). Il est désormais bien établi que le caractère invasif des tumeurs est déterminé non seulement par les caractéristiques intrinsèques des cellules tumorales mais également par leurs interactions dynamiques avec le microenvironnement tumoral (MET) (Bissell and Hines 2011).

La composante cellulaire de ce MET comprend les cellules tumorales, les fibroblastes associés au cancer (CAF), les cellules endothéliales, les adipocytes et les cellules immunitaires. Toutes ces cellules sont étroitement intriquées dans la matrice extracellulaire (MEC), une composante déterminante du MET (Midwood et al. 2016). La MEC est constituée d'un réseau complexe de protéines telles que les collagènes, les laminines et les glycoprotéines. Longtemps restreinte à un rôle de soutien tissulaire, la MEC s'est révélée être un acteur dynamique dans l'homéostasie tissulaire dans les conditions physiologiques (Frantz, Stewart, and Weaver 2010). En effet, les protéines matricielles peuvent par exemple interagir activement avec les cellules via des récepteurs de surface, aboutissant à l'activation de voies de signalisations pouvant moduler le cycle cellulaire (Hynes 2009a). Lors de phénomènes pathologiques tels que les cancers, l'homéostasie tissulaire est rompue et la composition de la MEC est considérablement altérée (Bonnans, Chou, and Werb 2014). La ténascine-C (TNC) est l'une des protéines dont l'expression est considérablement modifiée lors de la tumorigenèse.

La TNC est une glycoprotéine matricellulaire physiologiquement exprimée lors du développement embryonnaire mais absente ou faiblement exprimée dans les tissus adultes. Toutefois, elle est de nouveau exprimée lors de processus cicatriciels et lors de processus pathologiques tels que l'inflammation chronique et le cancer (Midwood et al. 2016). La TNC est surexprimée dans le cancer du sein et cette expression est corrélée avec l'apparition précoce de métastases pulmonaires ainsi qu'un faible taux

de survie des patients (Oskarsson et al. 2011). De plus il a été observé qu'au sein de la tumeur, la TNC est sécrétée non seulement par les cellules tumorales mais également par les cellules du stroma, rendant les tumeurs encore plus agressives (Ishihara et al. 1995). En effet dans des modèles cellulaires de tumeurs mammaires, il a été montré que TNC augmente la malignité des cellules tumorales en favorisant la survie cellulaire, la prolifération et la migration (W. Huang et al. 2001; Nagaharu et al. 2011). L'impact de la TNC sur les cellules cancéreuses est donc relativement bien décrit mais qu'en est-il de son impact sur les autres cellules du MET, notamment les cellules immunitaires ?

Les cellules immunitaires jouent un rôle prépondérant dans l'homéostasie tissulaire et à plus forte raison dans le MET où ils assurent l'immunité antitumorale. Toutefois, cette réponse immunitaire antitumorale évolue au cours du temps et se divise en trois phases dites des « 3E » pour Elimination, Equilibre et Echappement tumoral (Schreiber, Old, and Smyth 2011). Durant la phase d'élimination, les cellules immunitaires reconnaissent les cellules tumorales et les éliminent. Cependant, certaines cellules tumorales peuvent persister et on voit apparaître un équilibre entre la prolifération de ces dernières et la réponse antitumorale. La croissance tumorale reste à ce stade sous le contrôle du système immunitaire. Cette phase d'équilibre peut durer plusieurs années et engendre des mutations dans les cellules cancéreuses qui leur permettent d'échapper aux cellules immunitaires.

Lors de processus inflammatoires, la TNC est fortement exprimée, notamment dans l'arthrite rhumatoïde où elle promeut l'inflammation chronique par la voie de signalisation du « Toll-like receptor 4 » (TLR4) (K. Midwood et al. 2009a). L'hypothèse a alors été émise que la TNC pourrait être reconnue par le système immunitaire comme une molécule associée au danger (DAMP). D'autre part, en mesurant les cytokines sécrétées par les lymphocytes T comme l'IFNγ, des études ont montré *in vitro* que la TNC peut inhiber l'activation de ces cellules immunitaires (Parekh et al. 2005; Rüegg, Chiquet-Ehrismann, and Alkan 1989). Plus récemment, une étude réalisée dans un modèle de cancer de la prostate a décrit que la TNC peut inhiber l'activation des lymphocytes en inhibant la polymérisation des filaments d'actine, corrompant ainsi leur cytosquelette (Jachetti et al. 2015). Les études précédentes montrent que la TNC peut favoriser la tumorigenèse en inhibant la réponse antitumorale médiée par les lymphocytes T. D'autre part, selon l'étude

d'Oskarsson et al., la TNC produite par les cellules cancéreuses favorise le développement de métastases dans un modèle de cancer du sein (Oskarsson et al. 2011). Cependant cette étude a été réalisée dans un modèle immunodéprimé, écartant ainsi la contribution d'une composante principale de la MET, les cellules immunitaires.

Notre hypothèse est que dans le cancer du sein, la TNC peut avoir différents rôles dans la réponse immunitaire antitumorale, en impactant distinctement les différentes cellules immunitaires comme les lymphocytes, les macrophages ou encore les cellules dendritiques. Le compartiment immunitaire étant très complexe et dynamique, nous supposons que la TNC pourrait d'une part moduler le MET vers un microenvironnement pro-tumoral en inhibant la réponse antitumorale. D'autre part, la TNC pourrait être reconnue comme un DAMP et de ce fait générer un microenvironnement antitumoral. **Le but de ce travail de thèse a donc été de déterminer comment la TNC peut impacter la réponse immunitaire antitumorale en utilisant des modèles immunocompétents murins de cancer du sein**.

Résultats

Pour ce travail de thèse, nous avons utilisé 2 modèles murins préalablement établis dans le laboratoire. Le premier est un modèle génétique ErbB2-dépendant, le MMTV-NeuNT (Muller et al. 1988), dont l'expression de la TNC a été invalidé au laboratoire. Ce modèle génétique de carcinome mammaire génère des tumeurs multifocales et des métastases pulmonaires au bout de 9 mois de développement. A partir d'une tumeur primaire de ce dernier modèle, une lignée de cellules cancéreuses a été établie, la lignée NT193. Afin de déterminer distinctement l'impact de la TNC stromale ou tumorale dans la tumorigenèse et le développement de métastase, un modèle de greffe syngénique orthotopique NT193 a été généré en modulant l'expression de la TNC dans la lignée NT193 (shC ou shTNC) avant de les injecter dans un hôte exprimant la TNC (WT) ou non (KO). Ce modèle de greffe génère une tumeur primaire et des métastases pulmonaires au bout de 3 mois après la greffe. L'analyse histologique comparative des tumeurs primaires issues des 2 modèles a montré une organisation tissulaire très similaire, validant l'utilisation du modèle de greffe comme un modèle pertinent.

Nous avons donc poursuivi avec la caractérisation de ce modèle de greffe NT193. De façon intéressante, nous avons observé un rejet partiel, voire totale de la tumeur lorsqu'on injecte des cellules cancéreuses exprimant la TNC (shC) dans des hôtes exprimant également la TNC (WT). Ce rejet n'est observé que dans cette condition précise et se produit au bout de 3 semaines après la greffe. 3 semaines plus tard, les tumeurs ayant subi seulement un rejet partiel entament une nouvelle pousse tumorale, s'accompagnant d'une croissance plus importante ainsi que d'un taux de formation de métastases pulmonaires plus important que les autres conditions de greffes étudiées. D'autre part, l'injection des cellules NT193 shC dans des hôtes immunodéprimés ne présente pas de rejet, suggérant que la TNC produite par les cellules cancéreuses pourrait être reconnue par le système immunitaire comme un DAMP. Le séquençage de l'ARN provenant de tumeurs à 3 semaines de développement dans des hôtes KO pour la TNC a révélé qu'en présence de TNC produite par les cellules tumorales, il y avait surexpression de gènes impliqués dans le traitement et la présentation d'antigènes. Cette signature de gènes est retrouvée dans les hôtes exprimant la TNC. De façon intéressante, cette signature a été corrélée à une meilleure survie des patientes atteintes de cancer du sein.

D'autre part nous avons étudié l'infiltration immunitaire dans le modèle de greffe NT193. Comme nous venons de le voir, ce modèle présente un rôle duplice de la TNC avec un rejet tumoral à un stade précoce (3 semaines) puis un fort taux de métastases à un stade tardif (11 semaines). Nous avons réalisé une analyse comparative de l'infiltrat immunitaire dans les tumeurs primaires par immunomarquage (CD4, CD8, CD11c, F4/80, CD45) en fonction de l'expression de la TNC et aux deux différents stades susnommés. Les différences majeures de cette analyse concernent l'infiltration des lymphocytes T CD8+ dans les tumeurs. En effet, au stade précoce, l'infiltration des lymphocytes T CD8+ est plus importante en présence de TNC. L'infiltration au stade précoce est aussi plus importante qu'au stade tardif. Cependant au stade tardif, en dépit du nombre réduit de cellules CD8+ infiltrées, ces dernières étaient préférentiellement localisées dans des réseaux organisés de matrice en présence de TNC alors qu'en absence de TNC les lymphocytes T CD8+ pouvaient envahir le lit tumoral. La distribution spatiale de l'infiltrat immunitaire étant essentielle à une bonne réponse anti-tumorale (Fridman et al. 2012), nous nous sommes intéressés aux raisons de cette localisation

préférentielle des cellules CD8+. Notre hypothèse était que les réseaux organisés de TNC pouvaient attirer les lymphocytes CD8+ infiltrés dans la tumeur et les séquestrer, les empêchant ainsi d'éliminer les cellules cancéreuses.

Afin d'obtenir des candidats moléculaires permettant d'expliquer cette distribution préférentielle dans les réseaux de matrice, nous nous sommes basés sur une analyse transcriptomique par puce Affymetrix réalisée sur des tumeurs MMTV-NeuNT exprimant ou non la TNC. Les résultats de cette analyse ont révélé que sur 47 gènes significativement dérégulés en présence de la TNC, 13 présentent une annotation liée au système immunitaire selon une analyse par Gene Ontology dont 2 chimiokines (CXCL12 et CCL21) décrites pour leur capacité à induire le chimiotactisme des lymphocytes T CD8^{+} (Bonacchi et al. 2003; Okabe 2005). Nous avons donc entrepris de valider cette signature immunitaire par RT-qPCR dans le modèle de greffe NT193, avec une attention particulière pour le CXCL12 et le CCL21. Les résultats ont montré que seulement la TNC produite par les cellules tumorales régule à la hausse l'expression des 2 chimiokines. Ces résultats ont également été confirmés au niveau protéique par des tests d'ELISA. La TNC ayant été décrite comme pouvant lier certains facteurs solubles comme le TGFβ, nous avons réalisé des analyses de spectrométrie de résonance plasmonique de surface pour savoir si la TNC est capable d'interagir avec le CXCL12 et le CCL21 (De Laporte et al. 2013). Les résultats ont démontré que la TNC peut lier *in vitro* les 2 chimiokines avec une forte affinité.

Nous nous sommes ensuite intéressés au pouvoir chimiotactique du CXCL12 et du CCL21 envers les lymphocytes T CD8^{+} en présence de TNC. Pour ce faire nous avons utilisé des chambres de migration dont les inserts ont été recouverts d'une couche matricielle (fibronectine (FN), TNC ou collagène IV (Col IV)). Pour évaluer la capacité de la TNC à agir comme une simple barrière mécanique à la migration des lymphocytes, nous avons recouvert la face supérieure de l'insert de la couche matricielle correspondante. A l'inverse, pour évaluer la capacité de la TNC à agir comme un substrat chemo-attracteur/adhésif, nous avons recouvert la face inférieure. Ces différents tests de migration ont montré qu'à l'inverse du CCL21, le CXCL12 est un puissant chemo-attracteur pour les lymphocytes CD8+. De plus, lorsque la couche de TNC est présente à la face inférieure de l'insert, il y a plus de cellules adhérentes à cette face en présence de CXCL12. Sachant que la TNC peut

lier le CXCL12, ces résultats montrent que la TNC peut retenir les lymphocytes CD8+ en présence du CXCL12.

Nous avons ensuite voulu savoir quelle serait la source de CXCL12 dans le modèle de greffe NT193. Sachant que la TNC produite par les cellules cancéreuses a précédemment montré *in vivo* un impact sur la production de CXCL12, nous sommes intéressés au sécrétome des cellules NT193. Un dosage protéique du milieu conditionné des cellules NT193 par ELISA a montré que les cellules sécrètent le CXCL12 et que cette expression est régulée à la hausse par la TNC endogène des cellules. Nous avons ensuite évalué la capacité de ce sécrétome à induire la migration des lymphocytes T CD8+ en utilisant le même procédé que précédemment décrit. Le milieu conditionné des cellules NT193 shC était capable d'induire la migration des lymphocytes ainsi que leur adhésion à la TNC. Afin de déterminer si c'est le CXCL12 présent dans le sécrétome qui engendrait ces effets, nous avons effectué ces expériences en présence de l'AMD3100, un inhibiteur non-peptidique du CXCR4 qui est le récepteur du CXCL12. En présence de l'inhibiteur, les effets liés au CXCL12 décrits précédemment sont abolis, confirmant ainsi qu'il s'agit bien du CXCL12 présent dans le sécrétome des cellules tumorales qui permet le chimiotactisme des lymphocytes T CD8+ et leur adhésion à la TNC.

Afin d'évaluer l'effet du chimiotactisme induit par le CXCL12 sur les lymphocytes T CD8+ *in vivo*, nous avons inhibé l'axe de signalisation CXCR4-CXCL12 par des injections péri-tumorale quotidienne de AMD3100 sur une durée de 5 semaines. Ceci a provoqué une régression tumorale plus précoce avec des tumeurs de plus petites tailles que le groupe contrôle à la fin de l'expérience. De plus, l'analyse histologique des tumeurs a révélé un afflux plus important de lymphocytes T CD8+ dans le lit tumoral des tumeurs traitées avec l'inhibiteur, s'accompagnant d'un index apoptotique plus important que le groupe contrôle.

Conclusion

En utilisant un nouveau modèle immunocompétent de greffe syngénique, nous avons montré que la TNC joue un rôle prépondérant dans la tumorigenèse mammaire, notamment en impactant l'infiltrat immunitaire. Ceci se traduit d'une part par l'induction d'un rejet tumoral à un stade précoce du développement tumoral. Ce rejet s'accompagne d'un fort infiltrat de lymphocytes T CD8+ et de la surexpression de gènes impliqués dans les voies de traitement et de présentation d'antigène. Ceci suggère que la TNC produite par les cellules cancéreuses serait reconnu par le système immunitaire comme un signal de danger ou DAMP comme cela avait préalablement été décrit dans la polyarthrite rhumatoïde. De plus, nous avons pu corréler cette signature de gènes avec un meilleur taux de survie chez des patientes avec des cancers du sein au stade 3. Ces résultats suggèrent donc que lors des phases précoces du développement tumoral, la TNC peut induire une réponse immunitaire anti-tumorale efficace. Toutefois, lors de la progression tumorale s'accompagnant d'une forte expression de la TNC, nous avons décrit que cette dernière pouvait corrompre la réponse immunitaire anti-tumorale. En effet, nos résultats montrent que la TNC peut séquestrer les lymphocytes T CD8+ dans des réseaux de matrice par l'intermédiaire du CXCL12. L'inhibition du récepteur CXCR4 *in vivo* provoque un rejet partiel et surtout précoce de la tumeur avec un afflux important de lymphocytes T CD8+. Ces résultats montrent que l'axe de signalisation CXCR4-CXCL12 est important dans la régulation de la migration des lymphocytes T cytotoxiques par la TNC au sein de la tumeur. A l'heure où les nouvelles immunothérapies font face à des échecs thérapeutiques en raison d'un infiltrat immunitaire insuffisante dans le lit tumoral, ces nouvelles données peuvent être mises à profit pour établir des thérapies synergiques permettant à la fois de libérer les cellules effectrices du système immunitaire du réseau de matrice et les activer pour mieux détruire les cellules cancéreuses.

II.   Contribution to manuscripts

- **Scientific articles**

1) **Combined action of host and tumor cell-derived Tenascin-C determines breast tumorigenesis.** (in preparation)

   Murdamoothoo D*, Sun Z*, Velázquez-Quesada I, Deligne C, Yilmaz A, Erne W, Cremel G, Dutreux F, Paul N, Mertz M, Van der Heyden M, Carapito R, Midwood K and Orend G+, * equal contribution, + corresponding authors

2) **Tenascin-C provides environmental cues that control macrophage phenotypes in cancer.** (in preparation)

   Deligne C*, **Murdamoothoo D***, Van der Heyden M, Orend G+ and Midwood K+, * equal contribution, + corresponding authors

3) **Tenascin-C promotes oral squamous cell carcinoma impacting immune cell infiltration.** (in preparation)

   Spenlé C*, Loustau T*, **Murdamoothoo D**, Bourdely P, Erne W, Burckel H, Mariotte A, Cremel G, Beghelli-de la Forest Divonne S, Sudaka A, Nouhen K, Schaub S, Rekima S, Georgel P, van der Heyden M, Noel G, Anjuère F3+, Van Obberghen-Schilling E+ and Orend G+, * equal contribution, + corresponding authors

4) **Role of Tenascin-C in promoting lung metastasis through impacting vascular invasions**. (submitted)

   Sun Z*, Velázquez-Quesada I*, **Murdamoothoo D**, Averous G, Ahowesso C, Yilmaz A, Erne W, Van der Heyden M, Spenlé C, Lefebvre O, Klein A, Oberndorfer F, Oszwald A, Bourdon C, Mangin P, Mathelin C, Deligne C, Midwood K, Chenard MP, Christofori G, Hussenet T, Kain R, Loustau T and Orend G+, * equal contribution, + corresponding authors

5) **Tenascin-C orchestrates tumor cell apoptosis by impacting TRAIL in cancer.** (in preparation)

   Erne W, **Murdamoothoo D**, Yilmaz A, Van der Heyden M, Cremel G, Lefebvre O, Orend G+

6) Sun, Z.*, Schwenzer, A.*, Rupp, T.*, **Murdamoothoo, D**., Vegliante, R., Lefebvre, O., Klein, A., Hussenet, T., and Orend, G. **(2017). Tenascin-C promotes tumor cell migration and metastasis through integrin α9β1 -mediated YAP inhibition. Cancer Research** canres.1597.2017.

7) Platet, N., Hinkel, I., Richert, L., **Murdamoothoo, D.**, Moufok-Sadoun, A., Vanier, M., Lavalle, P., Gaiddon, C., Vautier, D., Freund, J.-N., et al. (**2017**). **The tumor suppressor CDX2 opposes pro-metastatic biomechanical modifications of colon cancer cells through organization of the actin cytoskeleton. Cancer Letters** 386, 57–64.

8) Rupp, T., Langlois, B., Koczorowska, M.M., Radwanska, A., Sun, Z., Hussenet, T., Lefebvre, O., **Murdamoothoo, D**., Arnold, C., Klein, A., et al. (**2016**). **Tenascin-C Orchestrates Glioblastoma Angiogenesis by Modulation of Pro- and Anti-angiogenic Signaling. Cell Rep** 17, 2607–2619.

- **Chapters**

1) **Murdamoothoo, D.***, Schwenzer, A.*, Kant, J., Rupp, T., Marzeda, A., Midwood, K., and Orend, G. **(2018). Investigating cell-type specific functions of tenascin-C. In Methods in Cell Biology**, (Elsevier), pp. 401–428.

2) Giblin, S.P.*, **Murdamoothoo, D.***, Deligne, C.*, Schwenzer, A.*, Orend, G., and Midwood, K.S. **(2018). How to detect and purify tenascin-C. In Methods in Cell Biology,** (Elsevier), pp. 371–400.

- **Reviews**

1) **Impact of the tumor microenvironment on NKG2D immune checkpoint control in cancer.** (in preparation)

Murdamoothoo D., Carapito R., Bahram S., Orend G+.

III. Abbreviations

APC	Antigen presenting cell
APS	Antigen presenting signature
B2M	Beta-2-microglobulin
BEC	Blood endothelial cell
BRCA1	Breast cancer 1
BRCA2	Breast cancer 2
CAF	Cancer associated fibroblast
CART	chimeric antigen receptor T cell
CCL	C-C motif chemokine
CCR	C-C chemokine receptor
CD	Cluster of differentiation
CIITA	MHC class II transactivator
Col IV	Collagen IV
CSF1	Colony-stimulating factor-1
CSF-1R	Colony-stimulating factor-1 receptor
CSPG5	Chondroitin Sulfate Proteoglycan 5
CTGF	Connective tissue growth factor
CTL	Cytotoxic T lymphocytes
CTLA4	Cytotoxic T-lymphocyte-associated protein 4
CTSS	Cathepsin S
CXCL	C-X-C motif chemokine
CXCR	C-X-C chemokine receptor
DAMP	Danger associated molecular pattern
DC	Dendritic cell
DCIS	Ductal carcinomas in situ
DNA	Deoxyribonucleic acid
ECM	Extracellular matrix
EGF-L	Epidermal growth factor-like
EMT	Epithelial-to-mesenchymal transition
EndMT	Endothelial-to-mesenchymal transition

ER	Estrogen receptor
FAK	Focal adhesion kinase
FAP	Fibroblast activation protein
FGF	Fibroblast growth factor
FN	Fibronectin
FNIII	Fibronectin type-III
GBM	Glioblastoma
GTP	Guanosine triphosphate
HER2	Human epidermal growth factor receptor 2
HGF	Hepatocyte growth factor
HR	Hazard ratio
IFNγ	Interferon γ
IGF1	Insulin-like growth factor 1
IL	Interleukin
JNK	c-Jun N-terminal kinase
Kd	Dissociation constant
KLRC1	Killer cell lectin like receptor C 1
LEC	Lymphatic endothelial cell
LM	Laminin
LMγ2	Laminin γ2
LOX	Lysyl oxidase
MAP	Mitogen-activated protein
MCS	Mesenchymal stem cell
MDSC	Myeloid-derived suppressor cell
MHC	Major histocompatibility complex
MMP	Matrix metalloproteinase
MMTV	Mouse mammary tumor virus
mRNA	Messenger Ribonucleic acid
Mφ	Macrophage
NF-κB	Nuclear factor-kappa B
NK	Natural killer
NKT	Natural killer T cell
NOS2	Nitric oxide synthase 2

OS	Overall survival
OSCC	Oral Squamous Cell Carcinoma
PD-1	Programmed cell death protein 1 receptor
PDGF	Platelet-derived-growth factor
PDGFR	Platelet-derived-growth factor receptor
PD-L1	Programmed death-ligand 1
PDX	Patient-derived xenograft
PNET	Pancreatic neuroendocrine tumor
POSTN	Periostin
PR	Progesterone receptor
PyMT	polyomavirus middle T-antigen
RA	Rheumatoid arthritis
RFS	Relapse free survival
RhoA	Ras homolog gene family, member A
RNA	Ribonucleic acid
RNA seq	RNA sequencing
ROS	Reactive oxygen species
RPTPβζ	Receptor-type protein tyrosine phosphatase beta zeta
SDF1	Stromal cell-derived factor 1
SPR	Surface plasmon resonance
TAA	Tumor associated antigen
TAM	Tumor associated macrophage
TAP1	Antigen peptide transporter 1
TAP2	Antigen peptide transporter 2
TCR	T cell receptor
TGFβ	Transforming growth factor β
Th	T helper
TIL	Tumor infiltrating lymphocyte
TLR4	Toll-like receptor 4
TME	Tumor microenvironment
TMT	Tumor matrix track
TNBC	Triple negative breast cancers
TNC	Tenascin-C

TNCKO	Tenascin C knock out
TNFα	Tumor necrosis factor α
T_{reg}	Regulatory T cells
uPA	Urokinase plasminogen activator
VEGF-A	Vascular endothelial growth factor A
VEGF-C	Vascular endothelial growth factor C
VEGF-D	Vascular endothelial growth factor D
VEGFR2	Vascular endothelial growth factor receptor 2
VEGFR3	Vascular endothelial growth factor receptor 3
YAP	Yes activating protein
αSMA	α-smooth muscle actin

1. Introduction

Over the past fifty years, considerable advancement in the understanding of breast cancer biology has transformed the current landscape of the disease management. The new approaches include early diagnosis strategies to track the disease progression, implementation of breast-conserving surgery techniques whenever complete mastectomy can be avoided and development of targeted therapies antagonizing the hormonal pathway and the human epidermal growth factor receptor 2 (HER2/neu) signaling pathway (Sledge et al. 2014). Indeed, since the characterization of the steroid hormone receptors as critical prognostic markers in the 1960's, the advent of anti-estrogen therapies have been a major breakthrough in ER-positive breast cancer therapeutics and have even served as a paradigm for the development of targeted therapies in the oncology field (Baum et al. 1983; Ke and Shen 2017). In parallel, the development of the HER2-targeting monoclonal antibody Trastuzumab revolutionized the management of patients with metastatic breast cancer that overexpressed HER2 where it increased the clinical benefit of first-line chemotherapy (Slamon et al. 2001). Altogether, this improvement of breast cancer management has significantly contributed to a better prognosis for the patients with breast cancer, where death rates decreased by 39% since 1989 (DeSantis et al. 2017). Nevertheless, still too many patients are concerned by this disease as e.g. in 2017, 58 968 women were expected to be affected by breast cancer in France with 11833 dying from the disease (Jéhannin-Ligier et al. 2017). Breast cancer remains the most prevalent malignancy in women and the second most common cause of cancer-related death worldwide (Siegel, Miller, and Jemal 2017; Cardoso et al. 2012). There is therefore a strong need to better understand the molecular mechanisms underlying this disease to develop novel treatment strategies to further improve breast cancer patient survival.

For long, cancer research and particularly breast cancer research have been focusing on the transformation of normal somatic cells into malignant tumor cells due to genetic alterations of the tumor cells themselves. As a matter of fact, 5 out of the first 6 hallmarks of cancer that have been described almost 20 years ago now,

emphasized the ability of tumor cells to evade regulatory mechanisms and cell death while at the same time sustaining potent cell proliferation and invasion (Hanahan and Weinberg 2000). Yet, now established evidence shows that cancers are not just masses of neoplastic cells but also contain a significantly altered surrounding stroma (greek: mat to lie on) forming the tumor microenvironment (TME) (Balkwill, Capasso, and Hagemann 2012). The composition of the stroma representing itself as a particular tumor ecosystem in a 3D context and its persistent interaction with the tumor cells has profound effects on tumor growth and malignant progression. In fact, there exists a dynamic reciprocity between the proliferating tumor cells and the intricate stroma. The malignant cells not only respond to the stroma but also modulate their environment. So much, that in 2011, by revisiting the hallmarks of cancer, the authors included, after the vascular endothelial system, a second major interacting component of the TME, the immune system (Hanahan and Weinberg 2011) (**Fig 1**).
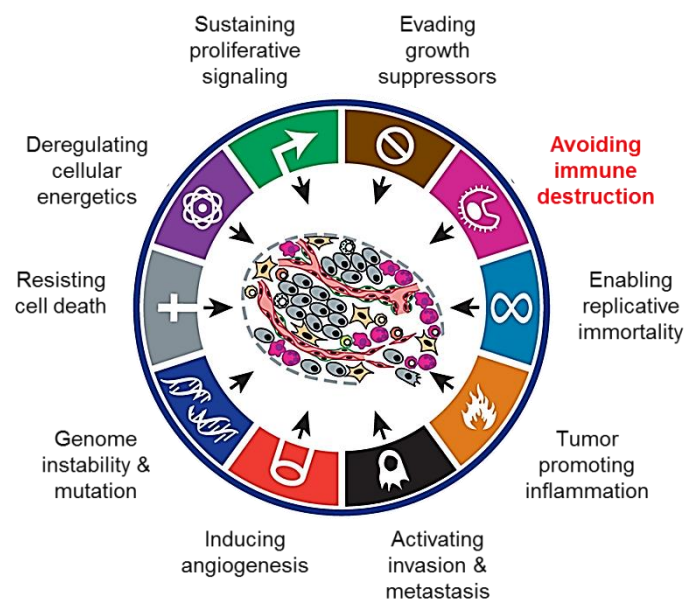

Figure 1: Next generation hallmarks of cancer. Apart from intrinsic characteristics of the malignant cells, the new hallmarks of cancer integrate the close interactions of the tumor cells with the immune compartment, a key component of the TME. Adapted from Hanahan and Weinberg (2011).

1.1. The Tumor Microenvironment

The tumor microenvironment (TME) is the ecosystem which defines the behavior of a developing cancer, not only by the genetic alterations of the malignant cells but also through their interaction with the surrounding milieu (Mbeunkui and Johann 2009). This dynamic and collaborative network includes the tumor cells, stromal cells such as fibroblasts, endothelial cells and infiltrating immune cells, soluble factors like cytokines and an intricate extracellular matrix (ECM) that does not only provide physical support but also actively participates in shaping the tumor ecosystem (Hanahan and Coussens 2012) (**Fig 2**). Over the last two decades the TME and its constituent stromal compartment have been the focus of numerous studies, deciphering their functional role in tumorigenesis and metastasis formation (Witz and Levy-Nissenbaum 2006; Hanahan and Coussens 2012). In breast cancer patients, several studies also highlight the importance of the TME. For instance, whole-genome analyses of breast cancer patients carrying the BRCA1/2 mutations suggested that the accumulation of genomic instability in the stromal compartment build up a TME that promotes genetic instability in the epithelial cells and therefore promotes transformation in these cells (Weber et al. 2006). Another study was based upon a retrospective cross-sectional analysis of DNA from the epithelium and stroma of 220 primary sporadic invasive breast carcinomas (Fukino et al. 2007). There, the authors looked for the relationship between genomic alterations (through loss of heterozygocity / allelic imbalance) and clinicopathological features. There were more correlations between the clinicopathological features and the genomic alterations in the stroma than in the epithelial cells, suggesting a major contribution of the stroma to the development of malignancies. Some aspects of the TME like angiogenesis and ECM remodeling have been recognized as relevant in tumor progression since a long time (J. Folkman 1971; Bissell, Hall, and Parry 1982). Yet, an integrated and comprehensive loco-spatial understanding of the TME and its evolution over time as well as the impact on the tumor cells is still missing.
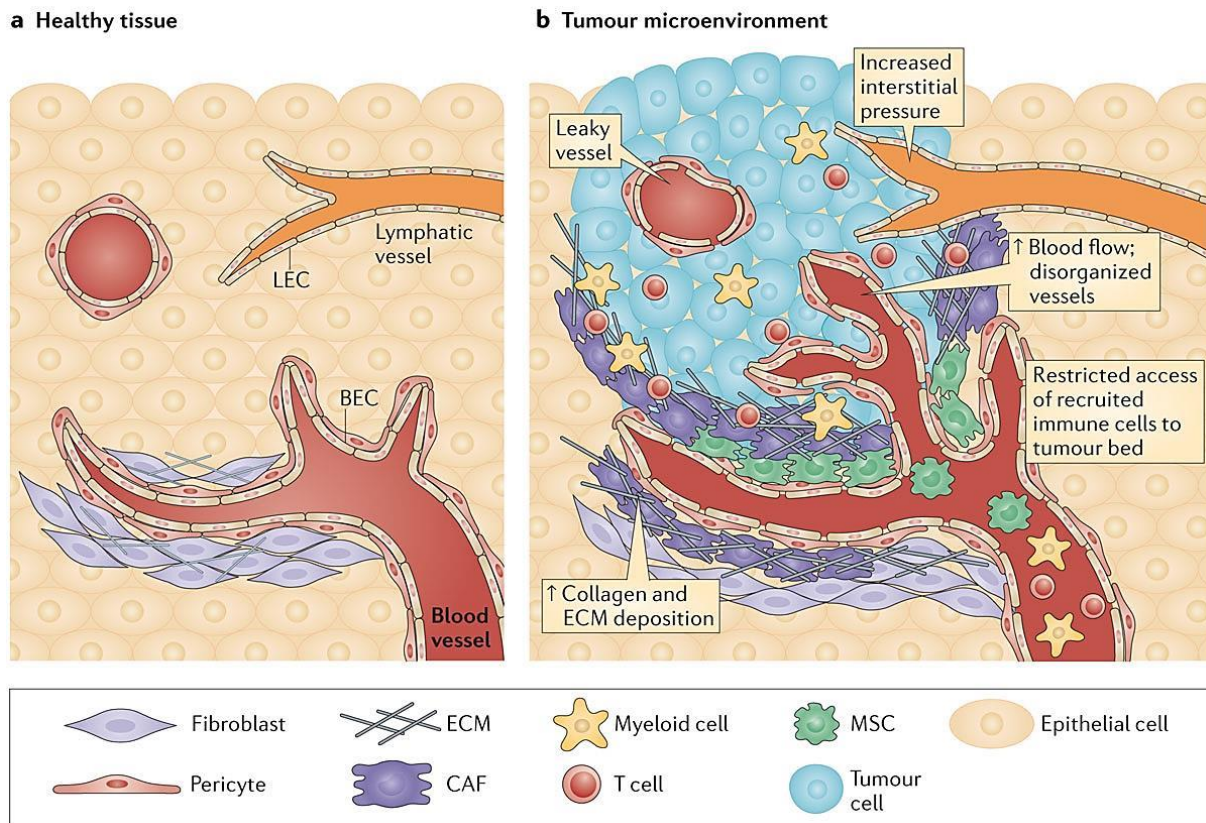
Figure 2: Changes in the tumor microenvironment upon tumor growth. (a) In physiological conditions, stromal cells, mainly fibroblasts, blood endothelial cells (BEC) and lymphatic endothelial cells (LEC) are present in interstitial spaces in the respective organs and help maintaining tissue homeostasis. (b) Upon tumor growth, the TME is remodeled, accompanied by an increase of infiltrating cells such as T cells, myeloid cells and cancer-associated fibroblasts (CAFs). Also, leaky blood vessels are formed. Finally, several extracellular matrix (ECM) molecules are massively expressed establishing novel ECM networks that are not present in the normal tissue (Turley, Cremasco, and Astarita 2015).

1.1.1. The cancer cells

The tumor cells are obviously a key player in cancer progression. They arise from the transformation of normal cells into malignant cells by genetic alterations in oncogenes and tumor suppressor genes which are accompanied by an altered gene expression not only affecting their own fate but also reprogramming their microenvironment. These cells are essentially characterized by the 10 hallmarks of cancer which are: sustaining proliferative signaling, evading growth suppressors, avoiding immune destruction, enabling replicative immortality, inducing tumor-

promoting inflammation, resisting cell death, inducing angiogenesis, activating invasion and metastasis, deregulating cellular energetics in favor of malignant cell proliferation and finally presence of genome instability and mutations (Hanahan and Weinberg 2011) (**Fig 1**).

Besides these general features, breast cancer cells are particularly characterized by an accumulation of multiple molecular alterations (Geyer et al. 2009; Simpson et al. 2005), some of which have subsequently been used as biomarkers for breast cancer classification (Rakha, Reis-Filho, and Ellis 2010). Among the main biomarkers routinely used for the characterization of breast cancers are the estrogen receptor (ER), the progesterone receptor (PR) and human epidermal growth factor receptor 2 (HER2). ER-positive tumors (ER+) accounts for 75% of all breast cancer types (Anderson et al. 2002). ER expression plays an important role in the breast carcinogenic process and its inhibition through selective ER antagonists or aromatase inhibitors still forms the backbone of breast cancer endocrine therapy (Early Breast Cancer Trialists' Collaborative Group 1988, 2015). On the other hand, the PR gene is regulated by estrogen. Therefore, its expression is considered to reflect an intact and functioning ER pathway (Horwitz, Koseki, and McGUIRE 1978). Even though in breast cancer, ER expression is considered as the main determinant of the patient's response to hormonal therapy, ER+/PR− tumors are generally less responsive than ER+/PR+ tumors to tamoxifen treatment (Bardou et al. 2003; Arpino et al. 2005).

Last but not least, HER2 is a key determinant in breast cancer prognosis. HER2 belongs to the tyrosine kinase receptor family and mediates cell survival and differentiation (Gschwind, Fischer, and Ullrich 2004). 15-25% of breast cancers are associated with an overexpression of HER2 and correlate with aggressive behavior of the malignant cells (Slamon et al. 2001). This particular characteristic of breast cancer cells gave rise to the development of a humanized monoclonal antibody directed against the extracellular domain of HER2, the Trastuzumab. Treatment with trastuzumab after adjuvant chemotherapy significantly improved disease-free survival among women with HER2-positive breast cancer (Piccart-Gebhart et al. 2005). On the other hand, these 3 biomarkers also define a group of cancer patients as triple-negative: ER-/PR-/HER2-. These patients comprise 10-15% of all breast cancers with

a relatively poor outcome since they don't respond to endocrine therapies nor to HER2-targeted therapies (Foulkes, Smith, and Reis-Filho 2010).

1.1.2. The stromal cells

As mentioned above, the stromal cells of the TME represent an integral part of the tumor. The stromal cells include mainly the endothelial cells, the cancer associated fibroblasts and the immune cells (Mueller and Fusenig 2004). There is an incessant still poorly understood crosstalk existing between these cells and the tumor cells that shapes tumor growth and metastasis formation. The relative contribution of these stromal cells to tumor growth will be presented here.

1.1.2.1. The endothelial cells

It is now well established that endothelial cells play a crucial role in tumor progression by generating novel support and dissemination routes as well as niches for cancer stem cells (Ping, Zhang, and Bian 2016). Tumors require the formation of a complex vascular network to meet the metabolic needs of the proliferating malignant cells. To grow beyond a size of 1-2mm in diameter, the tumor needs to induce angiogenesis (Judah Folkman 2003). This process requires the recruitment of vascular endothelial cells, pericytes (to cover the endothelial tubes to promote vessel integrity) and bone marrow-derived cells like macrophages, neutrophils and myeloid progenitors (Zumsteg and Christofori 2009). Apart from the recruitment of these cells, tumor vascularization is accompanied by an upregulation of soluble pro-angiogenic factors, as e.g. the vascular endothelial growth factor A (VEGF-A) that directly acts on the endothelial cells (Hanahan and Weinberg 2011). The *in vivo* pro-angiogenic response to VEGF-A is mainly mediated through signaling by its receptor VEGFR2 which leads to endothelial cell survival, proliferation and migration (Claesson-Welsh and Welsh 2013).

Together with blood endothelial cells, lymphatic endothelial cells (LEC) play also an important role in tumor progression and metastasis formation. Lymphatic vessels represent an alternate route for tumor cells to disseminate to different organs. Lymphangiogenesis in primary tumors is mediated by the soluble factors VEGF-C and VEGF-D that activate their receptor VEGFR3 (Joukov et al. 1996; Achen et al. 1998). Since the approval of the monoclonal antibody Bevacizumab as anti-angiogenic therapy in breast cancer in 2004 (recently retracted due to lack of

efficiency(Zambonin et al. 2017)), many more drugs have successfully been developed to target angiogenesis in tumor development with a mixed efficacy (Vasudev and Reynolds 2014; Al-Husein et al. 2012). A new paradigm is not the complete destruction of newly formed blood vessels but their normalization which would reduce vessel leakiness and would provide a good route for drug delivery (Stylianopoulos and Jain 2013).

1.1.2.2. Cancer associated fibroblasts (CAF)

The most abundant cell type in breast cancer stroma and in cancer stroma in general is the fibroblast. In early stages of tumorigenesis and upon activation, resident fibroblasts, differentiated into myofibroblasts, are able to inhibit tumor progression through gap junctions between the fibroblasts and through secretion of IL-6 (Cornil et al. 1991; Lu, Vickers, and Kerbel 1992). The origin of the CAFs in the TME is still debated. During tumor progression, it is hypothesized that the fibroblasts are corrupted by the tumor cells to being transformed into CAFs that exhibit myofibroblastic properties. Other studies suggest that CAFs result from endothelial-to-mesenchymal transition (EndMT) (Marsh, Pietras, and McAllister 2013). This hypothesis is supported by lineage-tracing experiments performed in a B16F10 melanoma mouse model and in a Rip1-Tag2 spontaneous neuroendocrine pancreatic carcinoma model that showed that CAFs derived from an endothelial origin (Zeisberg et al. 2007).

In the TME, CAFs are abundantly present and can be distinguished from normal resident fibroblasts by the upregulation of α-smooth actin (αSMA) and fibroblast activation protein (FAP) (Shiga et al. 2015). Accumulation of CAFs in the TME has often been correlated with bad prognosis in tumors like colorectal cancer (Tsujino et al. 2007). Furthermore, CAFs have been shown to support cell transformation and tumor growth. A key experiment has been performed by Olumi and colleagues where the authors grafted CAFs or normal fibroblasts together with non-tumorigenic immortalized prostatic epithelial cells. Only the CAFs promoted tumor formation yet the normal fibroblasts did not (Olumi et al. 1999). These results suggest pro-oncogenic properties of CAFs in the TME. This tumor-supporting role of CAFs has been described to be mediated by the secretion of soluble factors acting directly on the malignant cells. For example, CAFs secrete the hepatocyte growth factor (HGF)

and insulin-like growth factor 1 (IGF1) which support tumor cell proliferation (Willis, Dubois, and Borok 2006; Spaeth et al. 2009). CAFs can also secrete chemokines such as CXCL12 that can promote growth and survival of tumor cells (Orimo et al. 2005). Moreover, CAFs massively secrete ECM and ECM remodeling molecules which play an important role in tumor growth and dissemination. This aspect will be discussed in section 1.1.3.

1.1.2.3. Immune cells

The main physiological function of the immune cells is to maintain tissue homeostasis, protect against foreign pathogens and eradicate damaged or transformed cells. In the TME, the innate immune system (including macrophages, neutrophils, mast cells, dendritic cells and natural killer cells) and the adaptive immune system (T and B lymphocytes) interact with the tumor cells via a complex interaction network. Initially thought to mediate only an anti-tumor response, it is now accepted that immune cells can also contribute to tumor progression by establishing a state of chronic inflammation (Grivennikov, Greten, and Karin 2010). Over the last two decades, an increasing amount of data on tumor immunity has led to a radical change in the understanding of the tumor immune landscape (Sharma and Allison 2015). The crucial role of the infiltrating immune cells in the TME and the therapeutic implications will be addressed in more detail in section 1.3.

1.1.2.4. Other cell types

In breast cancer, stromal cells also include resident adipocytes. Until only recently, the adipocytes were considered as mere providers of energy for the surrounding tissue. However, there is now growing evidence that these cells can produce soluble factors like cytokines, growth factors such as leptin that can stimulate tumor progression through generating a pro-inflammatory microenvironment (Delort et al. 2015). Adipocytes have also been shown to increase tumor cell aggressiveness through secretion of IL-6 (Dirat et al. 2011). Furthermore, adipocytes can promote ovarian cancer metastasis to the omentum through IL-8 secretion (Nieman et al. 2011). Neuroendocrine cells present in the tumor microenvironment also interact with the tumor cells and can influence tumor progression. In prostate cancer, neurogenesis is correlated with tumor aggressiveness and recurrence (Ayala et al. 2008).

1.1.3. Extracellular matrix (ECM)

The extracellular matrix is a complex dynamic 3-dimensional network of macromolecular fibrous proteins and non-fibrous proteoglycans that are present in the stroma of all tissues. These ECM network can either be organized as thin meshes as in the basement membranes or as loose fibril-like structures in the interstitial matrix (Sorokin 2010). Initially thought to serve only as a physical scaffold, the ECM comprising large macromolecules like collagens, fibronectin, laminins and tenascins have been shown to affect cell behavior through regulation of cell shape, proliferation and gene transcription (Ghajar and Bissell 2008; Bissell, Hall, and Parry 1982). The interaction between the ECM and the cells is largely mediated by the integrins which are cell surface receptors interacting with the intracytoplasmic compartment and the cytoskeleton (Teti 1992). The integrins can also act as biomechanical sensors for the cells. Indeed, it is now clear that the stiffness and the topography of the ECM surrounding the cells regulate integrin-mediated signaling and subsequent cell behavior (Engler et al. 2006). The stiffness of the ECM is affected by the composition and the organization of the ECM molecules.

In the TME, the ECM undergoes a profound remodeling thereby establishing a pro-tumorigenic microenvironment (Hynes and Naba 2012). For instance, high deposit of ECM molecules like collagen is correlated with mammographically dense breast tissue, that is strongly associated with an increased risk of developing breast carcinoma (Boyd et al. 2001; Ursin et al. 2005). Moreover, *in vivo* studies assessing the role of ECM stiffening in a breast cancer model showed that lysyl oxidase (LOX)-mediated collagen crosslinking promotes focal adhesion formation and subsequent signaling involving PI3K thereby promoting tumor progression (Levental et al. 2009). Similarly, high expression of fibronectin by cancer cells in invasive breast cancer patients correlated with poor overall survival and disease-free survival (Bae et al. 2013). Matricellular proteins like tenascin-C (TNC) and periostin (POSTN) have also been shown to be highly expressed in metastatic niches where they contribute to tumor aggressiveness by multiple poorly understood mechanisms. What is known is that TNC and POSTN activated Notch and Wnt signaling, respectively in the tumor models (Oskarsson et al. 2011; Malanchi et al. 2011; Saupe et al., 2013).

High expression of ECM molecules in the TME is also often associated to high enzymatic modifications of the cancer matrix. The importance of LOX family has previously been described in collagen crosslinking, yet other ECM modifying enzymes have been studied for their respective roles in cancer progression. These enzymes involve the matrix metalloproteinases (MMPs), urokinase plasminogen activator (uPA) system and cathepsins (Oskarsson 2013). For example, MMPs have been described in facilitating tumor cell invasion through ECM degradation (Radisky and Radisky 2015). However, MMPs can also act directly on the tumor cells and trigger their invasiveness. In particular, it has been shown that MMP3 can trigger epithelial-to-mesenchymal transition (EMT), both *in vitro* and *in vivo* in breast cancer models, and to promote tumorigenicity (Sternlicht et al. 1999). In addition to the previous contributions of the ECM to tumor progression, it has been widely described that ECM molecules can bind soluble factors (Schultz and Wysocki 2009). These soluble factors include growth factors like vascular endothelial growth factor (VEGF), transforming growth factor β (TGFβ) and fibroblast growth factor (FGF) that have been described for their pro-tumorigenic properties respectively (Wijelath et al. 2006; Martino et al. 2013; Simian et al. 2001). Upon matrix remodeling these growth factors are potentially released in the TME and contribute to a pro-tumorigenic phenotype (Hynes 2009).

1.1.4. Soluble factors

Besides the growth factors aforementioned, the TME includes a plethora of soluble factors playing important roles in inflammation and tumor cell growth. These comprise cytokines and chemokines that can modulate cellular trafficking in the TME. These soluble factors can be secreted by the different cells present in the TME, including the tumor cells themselves (Chow and Luster 2014). Indeed, it has been described that melanoma cells can express several cytokines such as CXCL1, CXCL3, CXCL8, CCL2 and CCL5 that are implicated in tumor growth (Payne and Cornelius 2002). Tumor cells can also respond to the chemokines present in the TME. For instance in breast cancer, it has been described that tumor cells can upregulate their expression of CXCR4, the cognate receptor of CXCL12, thereby inducing chemotactic responses towards a CXCL12 gradient (Müller et al. 2001). This work laid the foundations for the implication of chemokines and their receptors in determining the metastatic destinations or homing of tumor cells. Among the cells

that are also impacted by the presence of cytokines in the TME are the immune cells. The loco-spatial expression gradient of soluble factors within the TME largely impact immune cell infiltration. For instance, high levels of CXCL9 and CXCL10 are associated with higher CD8+ T cell recruitment into the tumor and correlate with better prognosis in ovarian and colon cancer patients (Kryczek et al. 2009; Zhang et al. 2003; Pagès et al. 2005). On the opposite, CCL22 secreted by macrophages and tumor cells, recruits regulatory T (T_{reg}) cells, expressing the cognate receptor CCR4, into the TME thereby favoring tumor growth which correlated with poor prognosis in ovarian cancer patients (Curiel et al. 2004). In summary, omnipresent and acting as a reservoir of soluble factors, the ECM is in a prime position to orchestrate the crosstalk between tumor and stromal cells within the TME thereby regulating tumor progression.

1.2. Tenascin-C (TNC)

1.2.1. Structure and expression

TNC is a large extracellular matrix glycoprotein belonging to the tenascin family together with tenascin-R, tenascin-W and tenascin-X (Chiquet-Ehrismann and Tucker 2011). The name was inspired by the fact that tenascin-C is expressed at two sites under physiological conditions: in tendons ('tenere' to hold) and in embryonic tissue ('nasci' to be born) (Ehrismann, Chiquet, and Turner 1981; K. Midwood et al. 2016). The TNC molecule is composed of 6 huge monomers of approximately 300 kDa each. Each monomer is composed of a N-terminal assembly domain, followed by 14 ½ epidermal growth factor-like repeats (EGF-L), 8 constant and up to 9 alternatively spliced fibronectin type-III (FNIII) repeats and a C-terminal fibrinogen-like globular domain (**Fig 3**). In human TNC, FNIII 1-8 are conserved whereas the 9 additional repeats (A1-D) are alternatively spliced in or out providing up to 511 theoretical isoforms (K. Midwood et al. 2016).

The heptad repeats near the N-terminus can accommodate trimerization of the monomers. Subsequently, 2 trimers can assemble together and give rise to a hexamer. This hexameric form of TNC is the reason why TNC was initially named "hexabrachion". Due to its multimodular structure described previously, TNC is able to interact with a plethora of binding partners (**Fig 3**). These include other ECM molecules like fibronectin and perlecan as well as cell surface located receptors such as integrins and toll-like receptor 4 (TLR4) (Orend and Chiquet-Ehrismann 2006; K. Midwood et al. 2009)

TNC is highly expressed during embryonic development and its expression is restricted in the adult organs to some connective tissues like tendons, stem cell niches and reticular fibers in lymphoid organs. Furthermore, it is also expressed *de novo* during wound healing, mammary gland involution or in pathological conditions such as chronic inflammation and cancer. High expression of TNC in several types of cancer has been associated with poor prognosis (K. Midwood et al. 2016). These include melanoma, lung, head and neck and colorectal cancers respectively (Parekh et al. 2005; Wang et al. 2010; Emoto et al. 2001). Breast cancer is of no exception to

this. It has been observed in both animal models and breast cancer patients that there is a particularly high expression of TNC in the stroma as well as at the invasive fronts of the tumor (Mackie et al. 1987). This high TNC expression is associated with poor metastasis-free and overall survival in breast cancer patients (Oskarsson et al. 2011).
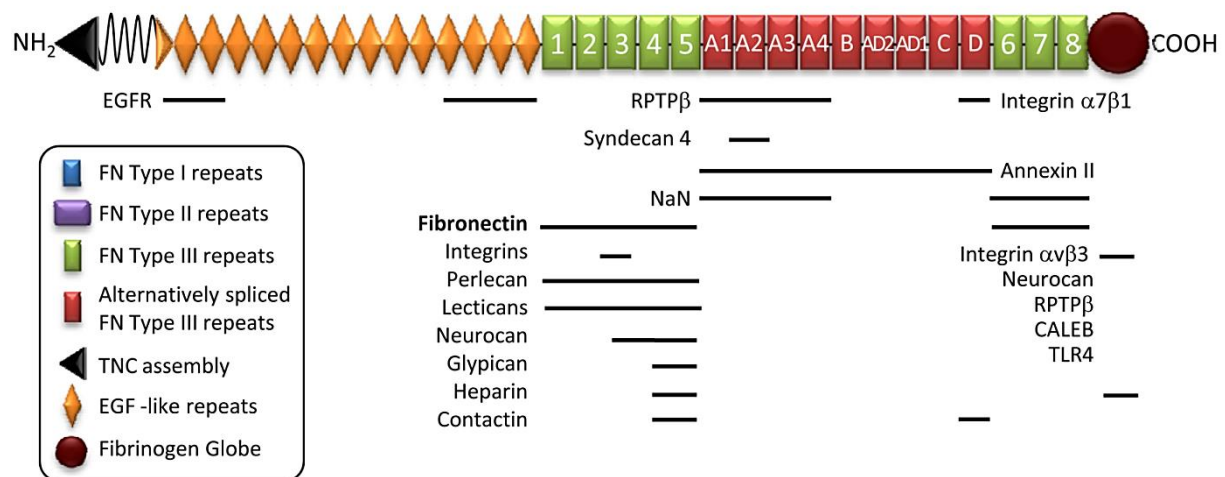
Figure 3: Structure of TNC and binding partners. TNC is a multimodular extracellular matrix glycoprotein whose monomer is composed of an oligomerization domain, epidermal growth factor-like repeats (EGF-L), fibronectin type-III (FNIII) repeats, and a fibrinogen like domain. Binding sites for interacting partners are shown (Van Obberghen-Schilling et al. 2011).

Expression of TNC in the TME can be regulated by various pro- and anti-inflammatory cytokines such as IFNγ, TNFα and interleukins (IL-1/4/6/8/13) (Orend and Chiquet-Ehrismann 2006). Growth factors such as EGF, TGFβ and CTGF and stress conditions such as hypoxia, mechanical stress and reactive oxygen species (ROS) can also induce TNC expression (Gebb and Jones 2003; Chiquet, Sarasa-Renedo, and Tunç-Civelek 2004; Yamamoto et al. 1999). Interestingly, while TNC has been described to induced by Ras/MAP kinase and Wnt signaling respectively, these signaling pathways can in turn drive TNC expression in the TME (Maschler et al. 2004; Beiter et al. 2005; Ruiz et al. 2004). Moreover, some transcription factors like NFκB and c-Jun have been reported to induce the transcription of the TNC gene (Orend and Chiquet-Ehrismann 2006). Whereas many triggers exist to induce TNC

only a few mechanism are known to downregulate TNC expression which include the transcription factor GATA and anti-inflammatory corticosteroids (Tucker and Chiquet-Ehrismann 2009).

1.2.2. TNC sources in the TME

As described previously, most solid tumors are accompanied by a high expression of TNC. Yet, this TNC expression is not homogeneously distributed in the TME. For instance, grade IV glioblastomas exhibited high TNC expression in perivascular regions (Herold-Mende et al. 2002). On the other hand, in breast tumors and melanomas, TNC is highly expressed at the invasive fronts in the primary tumor as well as at the metastatic site (**Fig 4**) (Mackie et al. 1987; Ilmonen et al. 2004; Oskarsson et al. 2011). This heterogeneous distribution suggests that TNC can be expressed by different compartments of the TME. Indeed, TNC can be expressed by both the stromal and the tumor cells during the different stages of tumor development.
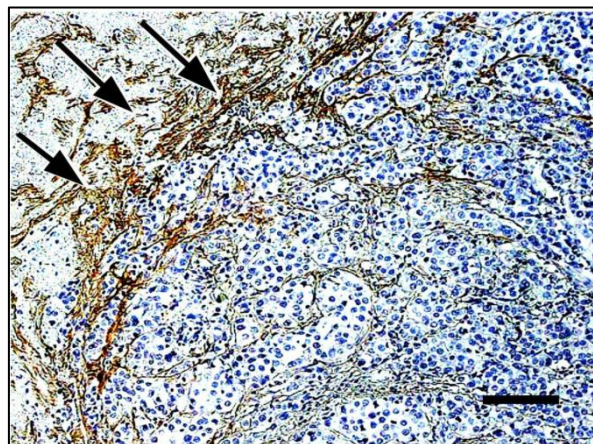
Figure 4: TNC expression in lung metastasis. Immunohistochemistry image showing the expression of TNC at the invasive front of lung metastasis from a breast cancer patient. Scale bar : 50 µm. (Oskarsson et al. 2011)

The cancer associated stroma is a major source of TNC (Mackie et al. 1987). More specifically, activated fibroblasts and myeloid cells are the main producers of TNC and their respective contributions deeply impact tumorigenesis. This has been nicely shown in a study where different classes of fibroblasts were eliminated *in vivo*. This

study showed that whereas αSMA positive cells were not expressing TNC in tumors, it was fibroblast-specific protein 1 (FSP1) positive cells mostly CAFs and myeloid cells that expressed TNC (O'Connell et al. 2011). In a breast cancer orthotopic grafting model, where 4T1 cells were injected into TNC wildtype and TNC knock out mice, less metastatic nodules were found in absence of TNC from the stroma. In addition, depletion of S100A4+ stromal cells (mainly fibroblasts) significantly decreased the level of expression of TNC at the metastatic site (O'Connell et al. 2011). Together these data suggest that TNC produced by S100A4+ stromal/myeloid cells are important for metastatic colonization. Another source of TNC in the TME is the endothelial cells. In physiological conditions, resting endothelial cells do not express TNC. However, in tumors, angiogenic tumor cells highly induce expression of TNC (Zagzag et al. 1996; Seaman et al. 2007; Langlois et al. 2014). Moreover, high perivascular expression of TNC in high grade brain tumors has been correlated with glioma recurrence in patients, suggesting that TNC impacts tumor progression through angiogenesis (Herold-Mende et al. 2002) as recently also shown in a stochastic tumor model (Langlois et al. 2014; Saupe et al. 2013). TNC has a janus function on endothelial cells where a direct contact with TNC causes cell rounding and anoikis (involving inhibition of YAP and prosurvival factors), yet this interaction also triggers endothelial cells to upregulate Wnt signaling (through inhibiting DKK1) and express high levels of FN that is assembled into a protective pericellular FN network coat around the TNC-exposed endothelial cells (Radwanska et al., 2017).

Besides the stromal compartment, tumor cells themselves may express high levels of TNC. This has been described in several studies and in different types of tumors including breast cancer, colon cancer and oral squamous cell carcinoma (T. Yoshida et al. 1997; Hanamura et al. 1997; Hindermann et al. 1999). In addition, immunohistochemical analysis and in situ hybridization carried out on human breast cancers revealed that TNC is expressed by both stromal cells and tumor epithelial cells and that tumor cell-derived TNC correlates with worsened survival (Ishihara et al. 1995). The elevated expression of TNC during tumor progression certainly impacts the different cellular components of the TME and this will be discussed in section 1.2.4.

1.2.3. TNC as ligand for cellular receptors

The main interactions between TNC and cells in the TME are mediated through integrins. They are a large family of cell surface receptors that bind to ECM molecules (Desgrosellier and Cheresh 2010). The interaction of integrins with ECM molecules gives rise to a number of intracellular signaling pathways involved in important cell functions like proliferation, differentiation and motility. The repertoire of integrins present at the surface of a particular cell will characterize the cellular response to a given matrix molecule. Likewise, TNC has been described to bind to several integrins such as α9β1, αVβ3 and α7β1 (**Fig 5**). For instance, immunohistochemical analyses of primary gastric and colorectal cancers have shown a co-localization of α9β1 integrin and TNC at the invasive fronts of the tumors (Gulubova and Vlaykova 2006). In an orthotopic breast cancer model, α9β1 integrin expressed by tumor cells promoted tumor growth and lymph node metastasis (Ota et al. 2014). Interestingly, in basal-like breast cancer patients, the only breast cancer subtype reported to express α9β1 integrin, the expression of the integrin was correlated to poor overall survival (Allen et al. 2011). Moreover, while plating of SV480 cells expressing α9β1 or αvβ3 integrins on recombinantly expressed TNC FNIII3 domain molecules resulted in an enhanced cell proliferation, treatment of tumor-derived cell lines with an αvβ3 antagonist showed an increase in the apoptotic index (Yokosaki et al. 1996; Taga et al. 2002). Integrin αvβ3 is also known to be expressed in various cell types including epithelial cells, fibroblasts and endothelial cells, suggesting the possibility that interaction of these cells with TNC in the TME could be mediated by these integrins (Toshimichi Yoshida, Akatsuka, and Imanaka-Yoshida 2015). In addition to integrins, TNC modulates syndecan-4 function either by competition or by binding (at least to a recombinantly expressed FNIIIA2 TNC domain molecule) thereby affecting cell adhesion and matrix contraction (K. S. Midwood et al. 2004; W. Huang et al. 2001; Orend et al. 2003). Other binding partners described for TNC are the receptor-type protein tyrosine phosphatase beta zeta (RPTPβζ), contactin, CSPG5 and glypican (K. Midwood et al. 2011) and the ganglioside GM1(Angelov et al. 1998).
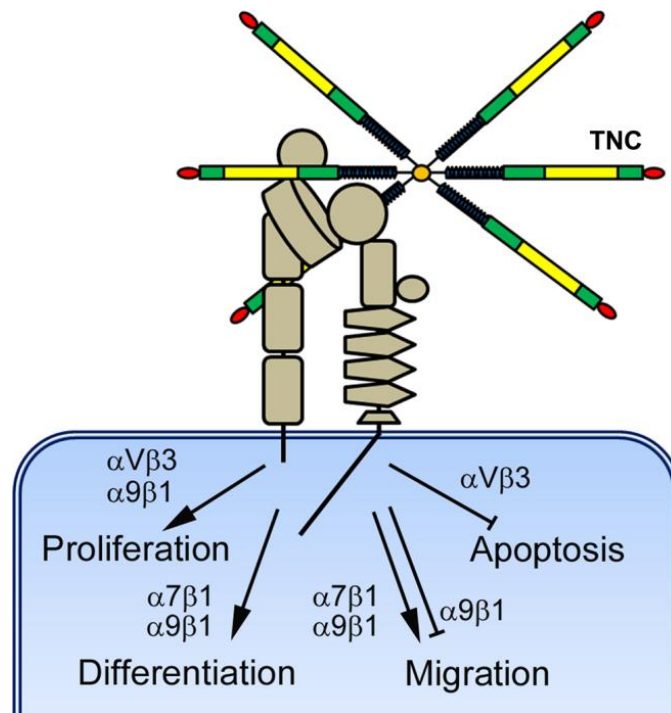
Figure 5: Integrins as TNC receptors in cancer. Through its interaction with specific integrins, TNC can influence cellular functions like proliferation, differentiation, migration and apoptosis (modified from Tucker and Chiquet-Ehrismann 2015).

1.2.4. TNC and pathological cell responses

1.2.4.1. Cell adhesion

Among the functional descriptions of TNC that have been reported, modulation of cell adhesion has been the first (Chiquet-Ehrismann et al. 1986). Depending on the cell lines studied, several mechanisms have been described for the antiadhesive or adhesion modulatory properties of TNC (Chiquet-Ehrismann and Tucker 2011). For example, adhesion of MDA-MB-231 breast carcinoma cells and T98G glioblastoma cells was compromised when cell were plated on a mixed substratum composed of FN and TNC. The authors identified the antiadhesive effect of TNC as a result of the binding of the molecule to FN through the 13th fibronectin type III repeat (FNIII13) of FN, thereby competing with syndecan-4 binding to the same site in FN (W. Huang et al. 2001). As a result of this interaction, Ras homolog gene family, member A (RhoA) and focal adhesion kinase (FAK) activities were compromised, modifying the actin cytoskeleton and downregulating focal adhesion formation (Wenk, Midwood, and Schwarzbauer 2000; Ruiz et al. 2004; Midwood and Schwarzbauer 2002; Lange et

al. 2007). The antiadhesive properties of TNC can also be modulated through external signaling pathways involving lysophosphatidic acid receptor (LPAR), platelet-derived-growth factor receptor (PDGFR) and endothelin receptors (Lange et al. 2007; Midwood et al. 2016). Since adhesion modulation is a known mechanism to impact cellular functions like proliferation and migration, TNC has also been widely investigated in this context.

1.2.4.2. Cell proliferation

In many malignant carcinomas, TNC expression co-localizes with Ki67 positively stained cells, suggesting that TNC could promote cell proliferation (Vollmer 1997). More specifically in breast cancer patients, high TNC expression was correlated to a high proliferation index in the tumor cells (Tsunoda et al. 2003). Cell culture experiments also demonstrated that TNC induces cell proliferation in several cancer cell lines, including MDA-MB-231 cells, and smooth muscle cells (Chiquet-Ehrismann et al. 1986; W. Huang et al. 2001; Orend and Chiquet-Ehrismann 2006). Through binding to the FNIII3 repeat of FN, TNC stimulates proliferation in tumor cells. Yet, not all cells respond in the same way to TNC. For instance, normal fibroblasts displayed proliferation inhibition in presence of TNC (Crossin 1991; Orend et al. 2003).

1.2.4.3. Cell migration and invasion

TNC has been described to induce cell migration in several cell types. These include tumor cells (Orend and Chiquet-Ehrismann 2006; Saupe et al. 2013; Tavazoie et al. 2008), fibroblasts (Wenk, Midwood, and Schwarzbauer 2000, 200; Tamaoki et al. 2005) and endothelial cells (Castellon et al. 2002; Rupp et al. 2016). The mechanisms through which TNC mediates cell migration and subsequent invasive properties are varied. For instance, in presence of TNC, pancreatic cancer cells displayed enhanced migration and invasion through the JNK/c-Jun signaling pathway (Cai et al. 2017). In osteosarcoma, *in vitro* and *in vivo* models, TNC was shown to promote tumor cell migration and metastasis formation by acting on the actin cytoskeleton through integrin α9β1-mediated yes activating protein (YAP) inhibition (Sun et al. 2017). Moreover, TNC has been described to promote breast cancer cells (MCF-7, T47D, MDA-MB-231 and MDA-MB-468) invasion through upregulation of MMPs and most notably MMP-13 (Hancox et al. 2009). Interestingly, the addition of

TNC to MCF-7 cells induced an EMT-like phenotype in the cells, accompanied by the delocalization of E-cadherin and β-catenin from the cell-cell contacts to the cytoplasm (Nagaharu et al. 2011). The TNC-induced EMT-like phenotype also correlated with FAK phosphorylation by SRC resulting in a loss of cell-cell adhesion and increased migration. Here, binding to αVβ6 and αVβ1 integrins appears to mediate the pro-migratory effect of TNC (Katoh et al. 2013).

1.3. Cancer immunity

Cancer is characterized by the unrestricted proliferation of cells accompanied by the accumulation of genetic alterations (Tian et al. 2011). These mutations generate neo-antigens at the surface of the malignant cells that can be detected by the immune system. Though widely accepted now, the establishment of the cancer immunity concept was the fruit of several age-old scientific contributions. The recognition of malignant cells by the immune cells was first postulated by Paul Ehrlich more than a century ago (Ehrlich 1909). He stated that the "organism's positive mechanisms" could restrain aberrant cells from becoming unusually common. After the first clear demonstrations of the capacity of tumor cells to elicit an immune response by Gross and Foley in 1953, notably with methylcholantrene-induced tumors, Thomas and Burnet formulated the immune surveillance theory (Foley 1953; M. Burnet 1957; F. M. Burnet 1970; Ribatti 2017). The authors hypothesized that neo-antigens at the surface of malignant cells could induce an immune response against the tumor cells.

1.3.1. The Cancer-Immunity cycle

In order to mediate an effective killing of tumor cells, the antitumor immune response exerts a series of stepwise events that Chen and Mellman have called the Cancer-Immunity Cycle (**Fig 6**) (Chen and Mellman 2013). The first step that initiates this cycle is the release of neo-antigen by the tumor cells as a result of an accumulation of mutations in the cell's genome. These tumor associated antigens (TAA) are then captured and processed by the antigen presenting cells (APC), mainly dendritic cells (DCs), and taken up to the lymphoid organs to be presented to the T cells through the MHC class I/II molecules. This gives rise to the priming and activation of the effector T cells directed against the cancer-specific antigens. This is a step of prime importance since it will determine the nature of the immune response to be triggered. Once activated, the effector T cells migrate towards their targeted tumor antigens through the blood stream to the tumor site. The immune cells then infiltrate the tumor bed and recognize the tumor cells through interaction of the T cell receptor (TCR) with the tumor antigens towards which the immune reactions have been initiated. Upon recognition of their targeted cells, the T cells mediate tumor cell killing through

secretion of cytokines and enzymes like granzyme B and perforin. Killing of the target cells also generates more TAA in the TME which feeds back the loop of the Cancer-Immunity Cycle.
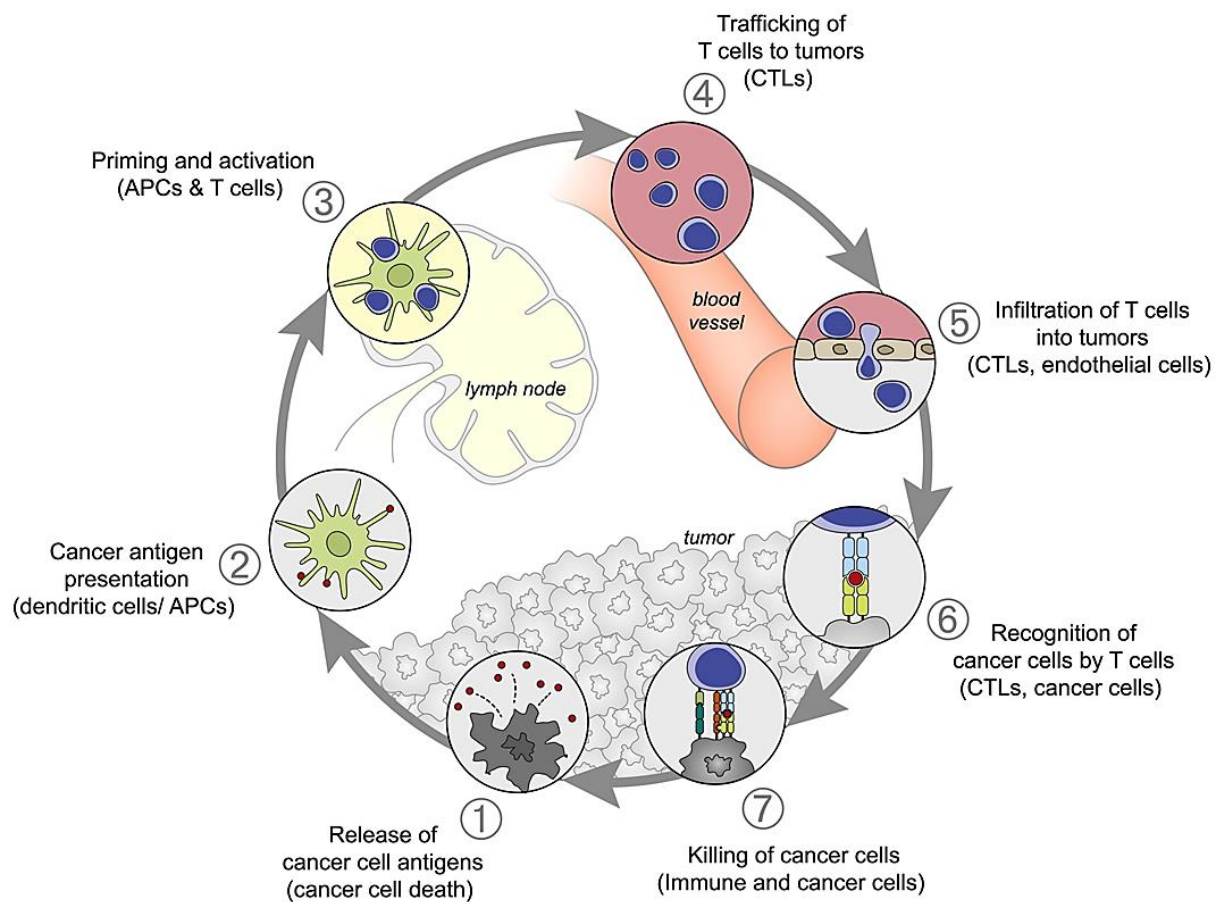
Figure 6: Cancer-Immunity Cycle. T cell-mediated killing of tumor cells happens through a cyclic process starting by the release of tumor associated antigens (TAA). These antigens are taken up by dendritic cells (DCs) and presented to the T cells for priming. The activated cells then migrate to the tumor cells and kill the target cells (Chen and Mellman 2013).

1.3.2. The cancer immunoediting concept

In 2001 a conclusive experiment carried out in Robert Schreiber's lab demonstrated that tumors formed in mice lacking an intact immune system were more immunogenic than tumors generated from immune competent hosts (Shankaran et al. 2001). This brought out the notion that the immune system not only protects the host against

tumor formation through the process of cancer immunosurveillance but can also modulate the immunogenicity of the malignant cells. This was the basis of the cancer immunoediting concept (Dunn et al. 2002; Schreiber, Old, and Smyth 2011).

The cancer immunoediting concept postulates that tumor development in an immunocompetent TME is the result of 3 distinct phases called "elimination", "equilibrium" and "escape", respectively. In the elimination phase, the developing tumor cells undergo killing through natural killer (NK) and T-cells (**Fig 7**). Tumor cells that are able to survive the elimination phase enter into a state of functional dormancy, the equilibrium phase (Mittal et al. 2014). Despite not being able to eradicate the malignant cells completely, the immune system is able to restrict their expansion and subsequent tumor progression. This has been shown to be mediated by the adaptive immune system involving IL-12 and IFNγ (Koebel et al. 2007).

Being at that stage under persistent selection pressure against the immune response, the malignant cells evolve to a less immunogenic phenotype and proceed to the escape phase. Tumor cell escape can happen through different mechanisms including decreased immune recognition and increased resistance to immune cell-mediated killing (Vesely et al. 2011; Dunn et al. 2002). For instance malignant cells can establish an immunosuppressive state in the TME through secretion of cytokines like TGFβ, induction of high infiltration of regulatory T cells (T_{reg}) and myeloid-derived suppressor cells (MDSCs) and expression of negative costimulatory molecules such as the Programmed death-ligand 1 (PD-L1) (Dunn, Old, and Schreiber 2004; Reiman et al. 2007; Schreiber, Old, and Smyth 2011).
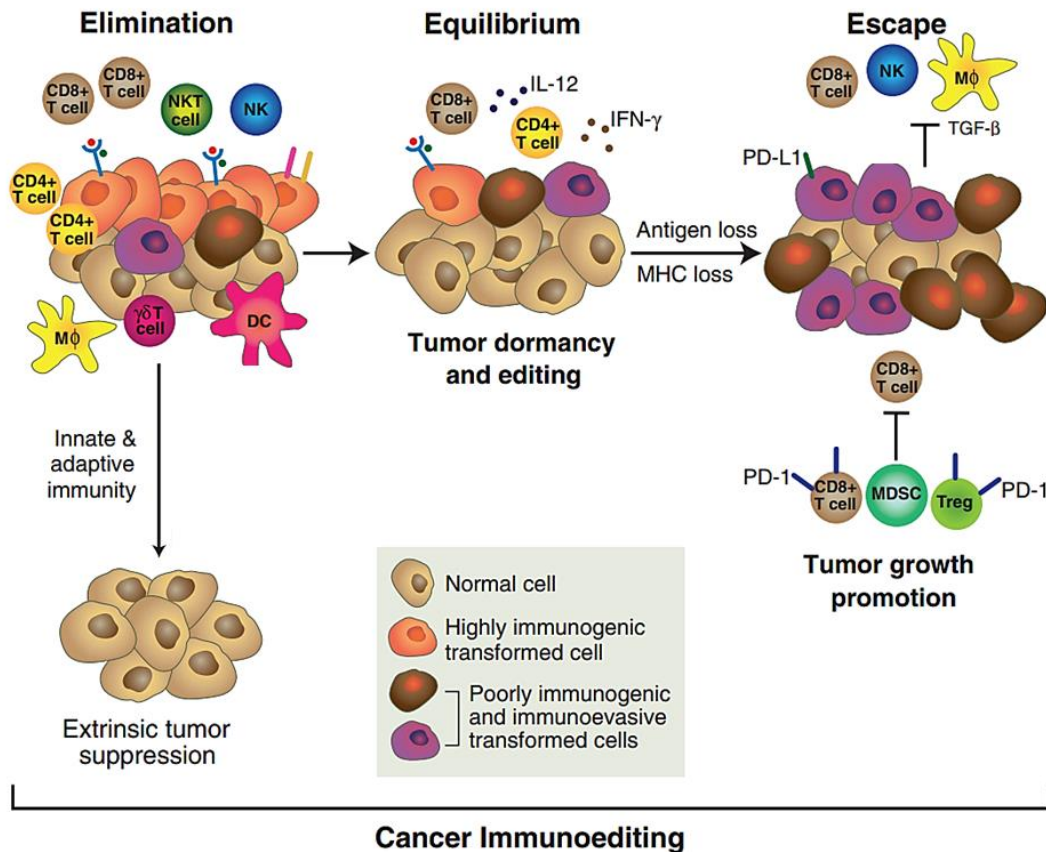
Figure 7: The cancer immunoediting concept. At early stages of tumorigenesis, malignant cells express tumor associated antigens (TAA) that are recognized by the immune system and initiate the cancer immunoediting process. During the elimination phase, an effective malignant cell killing is mediated by the innate and the adaptive immune system. Unsuccessful killing of some tumor cells results in the equilibrium phase where malignant cells undergo tumor dormancy and editing. The resultant tumor cells are no longer recognized by the immune cells and establish an immunosuppressive TME. This is the escape phase where tumor cells evade the immune system and cause tumor progression (Schreiber, Old, and Smyth 2011).

1.3.3. The tumor immune microenvironment in breast cancer

The immune infiltrates in different types of cancer are heterogeneous and subsequently the resultant immune response may vary according to the major immune cell types present in the TME. A prospective study of tumor tissues from breast cancer patients using polychromatic flow cytometry in combination with confocal immunofluorescence and immunohistochemical analysis of tissue sections showed that activated T lymphocytes were the major component of the immune cell

infiltrate in the tumor (Ruffell et al. 2012). Interestingly, when compared to normal breast tissue, infiltration of cells from the myeloid lineage was largely restricted.

1.3.3.1. Tumor infiltrating lymphocytes (TILs)

A major determinant of the successful control of the tumor expansion is the capacity of the T cells to infiltrate the tumor. The correlation between high levels of TILs in breast cancer and better prognosis in early stage breast cancer patients has now been confirmed in large cohorts of patients (Ali et al. 2014; Whitford, George, and Campbell 1992; Baxevanis et al. 1994). Furthermore, it has recently been shown that high levels of TILs predict response of breast cancer patients to neoadjuvant chemotherapy (Denkert et al. 2018). In this same study, increased TILs concentration in HER2-positive and triple negative breast cancers (TNBC) was associated with better patient's overall survival. On the contrary, in luminal-HER2-negative breast cancer, high T cell infiltration was correlated to worsened survival. These data suggest that apart from the concentration of TILs, the biology of the immune infiltrate needs particular attention.

TILs include essentially CD8+ cytotoxic T lymphocytes (CTLs) and CD4+ T helper (Th) cells. CTLs are one of the main effectors of the antitumor immune response. Upon activation of the TCR, they mediate tumor cells killing through release of granzymes, perforin and other cytotoxins that induce apoptosis. In a study based upon a cohort totaling more than 12000 breast cancer patients, it has been shown that the presence of CD8+ T cells in breast cancer tissue is associated with better overall survival in HER2-positive (both ER-negative and ER-positive) tumors (Ali et al. 2014). Yet, despite the presence of these effector T cells in the TME, the tumors do not regress, suggesting inhibitory mechanisms against the T cells response. An important mechanism is described where inhibitory checkpoints like PD-1 and cytotoxic T-lymphocyte-associated protein 4 (CTLA4) at the surface of the lymphocytes are upregulated and inhibit the CD8+ T cell response (Pardoll 2012). Activation of these pathways by the tumor cells suppresses the T cell antitumor response through inhibiting proliferation, survival and cytokine production of the T cells. Over the last decade, these checkpoint receptors have been of major interest and their implication in the development of novel anti-cancer therapeutics will be discussed later.

CD4+ T helper cells are also a major component of the antitumor immune response. The main subtypes of Th cells that have been described include Th1, Th2, Th17 and T_{reg} cells. Th1 induced pathways are mediated by secretion of IL-2, IL-12 and IFNγ to sustain the CTLs responses. On the other side, Th2 cells secrete cytokines like IL-13 and TGFβ, favoring tumor growth through inhibition of T cell-mediated immunity (Kalams and Walker 1998; Ellyard, Simson, and Parish 2007). It is therefore not surprising that Th1 and Th2 responses are inversely correlated, where the Th1 pathway is associated with lower risk of disease free survival in ER-negative breast cancer patients (Teschendorff et al. 2010). The role of Th17 cells in cancer immunity is less well studied. Yet, accumulating evidence suggests that intratumoral Th17 cell infiltration can be associated with both good and bad prognosis, depending on the cancer type (Guéry and Hugues 2015). Th17-derived cytokines can stimulate Th1 responses promoting antitumor responses as well as stimulating tumor promoting processes like angiogenesis (Numasaki et al. 2003). Finally, the function of T_{reg} is to maintain a balance between effective cell-mediated killing and suppression of autoimmune responses. In assessing the clinical significance of T_{reg} infiltrates in breast tumors, it was shown that T_{reg} density was higher in invasive breast carcinomas compared to ductal carcinomas in situ (DCIS) (Bates et al. 2006). In this same study, high T_{reg} infiltration was correlated to shorter relapse-free survival and overall survival of patients with invasive tumors. Moreover, it was shown in Alexander Rudensky's lab that breast tumor-infiltrating T_{reg}s exhibit a different phenotype as e.g. through upregulation of the chemokine receptor CCR8, than T_{reg}s found in normal tissues (Plitas et al. 2016).

1.3.3.2. Innate immune responses

Tumor-associated macrophages (TAMs) have been associated with both antitumor and pro-tumor responses (Allavena et al. 2008). This can be explained by the remarkable plasticity of the TAMs that can respond to the TME signal and adapt between an M1 and M2 phenotype (Murray et al. 2014; Biswas and Mantovani 2010). M1 macrophages have been described as pro-inflammatory cells which was accompanied by secretion of factors like IL-12, nitric oxide synthase 2 (NOS2) and tumor necrosis factor α (TNFα) and to mediate Th1 responses (Allavena et al. 2008). On the opposite, M2 macrophages have more an immunosuppressive phenotype as they secrete high levels of IL-10 and TGFβ. M2 macrophages also suppress Th1

responses and promote angiogenesis. Given the high plasticity of macrophages and the complex pool of cytokines in the TME, the clear-cut dichotomy between M1 and M2 phenotype is probably an oversimplification.

Macrophages are recruited into tumors after activation of the colony-stimulating factor-1 receptor (CSF-1R) by its ligands CSF1 or IL-34 (Chihara et al. 2010). In breast cancer, high levels of CCL2 have also been described to recruit macrophages (Qian et al. 2011; Soria and Ben-Baruch 2008). An early study looking for the clinical impact of infiltrating TAMs in breast cancer showed that a high density of TAMs correlated with poor disease-free survival and shorter overall survival (Leek et al. 1996). This was also associated with increased angiogenesis. Moreover, a recent meta-analysis study covering a total of 4 541 breast cancer patients also correlated the high density of TAMs to poor survival rates (Zhao et al. 2017). Interestingly, it was observed that TAMs infiltration was inversely correlated to CD8+ T cells infiltration in breast cancer patients and that a $CD68^{low}/CD4^{low}/CD8^{high}$ signature correlated with better response to neoadjuvant chemotherapy (DeNardo et al. 2011).

In addition to macrophages, NK cells are key players of the innate immune response in the TME. They are effector lymphocytes that can drive direct tumor cell killing without any previous sensitization (Herberman, Nunn, and Lavrin 1975). Similarly to CTLs, NK cells mediate target cell killing through secretion of perforin, granzymes and TNFα (Trapani and Smyth 2002). Over the last 20 years, several studies have put forward the fact that the density of NK cells infiltrating solid tumors such as colorectal carcinoma, gastric carcinoma and squamous cell lung carcinoma correlates with better prognosis for the patients (Coca et al. 1997; Takeuchi et al. 2001; Villegas et al. 2002). A recent study suggests that poor infiltration of NK cells into breast tumor tissue might be predictive for chemotherapy treatment failure (Mariel et al. 2018). Indeed in this study, tumor samples resistant to neoadjuvant chemotherapy displayed a decrease in gene expression of cell-surface receptors related to NK cells like killer cell lectin like receptor C 1-4 (KLRC1-4).

Dendritic cells (DCs) are a critical heterogeneous group of leukocytes that ensures the link between the innate and the adaptive immunity. They are the most effective antigen presenting cells (APCs) of the immune system and ensure effective T cell activation through interaction of CD40 expressed on DCs and its cognate ligand

expressed on T cells (Turnis and Rooney 2010; Nencioni et al. 2008). During tumor progression, the previous mechanisms can be hijacked in several ways like reduced uptake and processing of antigen and lowered expression of costimulatory molecules leading to a poor T cell activation (Ma et al. 2013). For instance, in a breast cancer model it has been shown that T cells interact with DCs at the margins of the tumor but yet they are not activated properly (Engelhardt et al. 2012). Furthermore, a previous study assessing the immunological function of DCs in breast cancer patients pointed out that peripheral and lymph nodal DCs were unable to induce a proper T cell response due to a lowered expression of the a major histocompatibility class II molecule (MCH II) as well as the costimulatory molecule CD86 (Satthaporn et al. 2004). Due to the recurring inefficient activation of T cells by DCs in several types of cancer, one strategy has been to develop DCs vaccines (Lee et al. 2002). Briefly, this consists of taking immature DCs from the patient and putting them in contact with the TAAs ex vivo, ensuring a proper processing and presentation of the TAA by the DCs. The latter are then injected back to the patient to elicit an efficient T cell response. A pilot study of the use of DCs vaccines in breast cancer patients displayed a successful CTLs response that lasted for more than 6 months (Brossart et al. 2000). Similar results were observed in a larger cohort of ER/PR double negative breast cancer patients (Qi et al. 2012).

1.3.3.3. The immune contexture

As described previously, each component of the immune system plays an important role either in tumor surveillance or in tumor progression. Up to now, the role of each immune subtype has been addressed separately. However, all these cells operate in the same TME, interacting dynamically with the tumor cells, and the ECM surrounding them. Putting back all these functional immune cells in the context of the TME is a concept that has been coined "immune contexture" (Fridman et al. 2012). Fridman and colleagues defined the immune contexture as the density, the composition, the functional state and the organization of the leukocyte infiltrates in the tumor. We can easily imagine that together with the total number of infiltrating leukocytes, the representation of each cellular subtype with their respective functional state will determine the net resulting effect on the proliferating tumors cells. However the localization of the immune infiltrates is also of prime importance. For instance a comprehensive analysis of a large cohort of colorectal cancers revealed that the

tumors were highly infiltrated with memory T cells and that this infiltration correlated with better disease-free survival as well as overall survival (Pagès et al. 2005). Again in colorectal cancer, it was observed that this high infiltration of T cells was not homogeneous all around the tumor but in fact was preferentially localized in the center and the invasive margin of the tumor nest, both localizations correlating with good prognosis (J. Galon 2006). The immune contexture can be used not only to predict clinical outcome in patients but also to predict response to therapies based upon the accessibility of each cellular subtype which is applied in the so called "immunoscore" (Fridman et al. 2012; Jérôme Galon et al. 2014, 2012; Angell and Galon 2013).

1.3.4. Immunomodulatory properties of TNC

TNC is known to be highly induced in context of inflammation and to enhance chronic inflammatory diseases such as rheumatoid arthritis. In this disease, TNC activated toll like receptor 4 (TLR4) in macrophages and induced expression of several pro-inflammatory cytokines like TNFα, IL-6 and IL-8 (Midwood et al. 2016, 2009b). A similar effect was also seen involving TNC and integrin α9β1 (Asano et al. 2014). Based on these and similar observations TNC is hypothesized to act as a danger associated molecular pattern (DAMP) molecule (Goh et al. 2010; Midwood et al. 2011). Moreover, TNC is highly expressed in areas rich in CD4+ T cells and activated DCs in the lymph nodes, suggesting a role of TNC in immunity (Chilosi et al. 1993; Ocklind et al. 1993; Udalova et al. 2011). Several studies have shown that TNC impact directly T cell behavior. In a bronchial asthma model using mice expressing TNC or not, it was documented that TNC upregulates expression of IL-5 and IL-13 (Nakahara et al. 2006). This was confirmed *in vitro* where TNC stimulated secretion of these cytokines as well as of IFNγ by spleen lymphocytes. In contrast, other studies assessing the impact of TNC *in vitro* showed that TNC was able to block T cell activation induced by a natural antigen or anti-CD3 antibodies co-immobilized with FN (Rüegg, Chiquet-Ehrismann, and Alkan 1989; Hemesath, Marton, and Stefansson 1994). This T cell inhibiting property of TNC has been mapped to the alternatively spliced region TnFnIII A-D, with the minimum motif essential for this activity being the TnFnIII A1A2 domains (Puente Navazo, Valmori, and Rüegg 2001). These studies suggested a potential immunosuppressive activity of TNC, which was further addressed by others.

Co-culture of TILs isolated from non-small cell lung cancer (NSCLC) with TNC decreased significantly their IFNγ secretion capacity (Parekh et al. 2005). In a recent study, Jachetti et al., (2015) used a prostate cancer model and observed that TNC inhibited T-cell proliferation and IFN-γ secretion also in this model. To further investigate the role of TNC in the interaction between cancer cells and T-cells, they used fluorescent live cell imaging in order to visualize the interactions during the first 4 hours of co-culture of prostate cancer stem like cells and CD8 T-cells upon silencing of TNC in the tumor cells. They observed that TNC significantly decreased the duration of contacts between the two cell types (Jachetti et al. 2015). Interestingly, the authors assessed whether TNC inhibits T-cell activation by blocking the cytoskeletal organization based on the literature about TNC showing that TNC suppresses Rho activation (Wenk, Midwood, and Schwarzbauer 2000; Woodside, Wooten, and McIntyre 1998). It was found that the actin polymerization of T-cells was inhibited when they were stimulated in presence of cancer cells expressing TNC or were directly stimulated with TNC, whereas in presence of cancer cells that were silenced for TNC, the actin polymerization was rescued in both CD4+ and CD8+ cells (Jachetti et al. 2015). The results suggest that TNC blocks actin polymerization in stimulated T-cells thus inhibiting their further proliferation.

Moreover, another study reported that high concentrations of TNC in glioma-associated blood vessels inhibits migration of T-cells, resulting in an accumulation of T cells in the peritumoral region (J.-Y. Huang et al. 2010). Silencing of TNC in glioma cells significantly increased the transmigration rate of Jurkat cells and CD3/CD28 activated T-cells. Interestingly, this study also suggests that TNC influences the T cells' morphology from a rough to an amoeba-like phenotype, which was associated with high migration.

2. Aims

High expression of the extracellular matrix molecule TNC correlates with worsened metastasis-free survival in breast cancer patients (Oskarsson et al. 2011). Moreover, expression of TNC by both stromal and cancer cells correlates with poor overall survival (Ishihara et al. 1995). As a fact, the immune system plays an important role in tumor progression and anti-cancer therapies. Despite some evidence for a role of TNC in tumor immunity, there is poor mechanistic insight how TNC impacts on breast cancer immunity, mainly due to the lack of relevant immunocompetent models.

In this thesis work, I used a novel orthotopic syngeneic breast cancer model that has been established by former members of the laboratory. This grafting model is based upon the stochastic MMTV-NeuNT breast cancer model (Muller et al. 1988). In this model a constitutively active form of the rat homologue of ErbB2 (neu) is expressed under the control of the mouse mammary tumor virus (MMTV) promoter, leading to spontaneous breast tumor formation and lung metastasis. The NT193 breast tumor cell line was established from a primary tumor of a MMTV-NeuNT mouse and its expression of TNC was engineered before grafting cells into syngeneic mice expressing or lacking the TNC protein. The resulting immunocompetent grafting breast cancer model was used to address:

Aim 1: Identify the cellular and molecular mechanisms of the impact of TNC on breast cancer progression.

Aim 2: Identify the role of tumor and host-derived TNC in breast tumor growth.

3. Manuscript

Combined action of host and tumor cell-derived Tenascin-C determines breast tumorigenesis

Devadarssen Murdamoothoo*[1], Zhen Sun*[1], Ines Velázquez-Quesada*[1], Claire Deligne[2], Alev Yilmaz[1], William Erne[1], Gérard Cremel[1], Annick Klein[1], Christiane Arnold[1], Fanny Wack[1], Fabien Dutreux[3], Nicodème Paul[3], Michel Mertz[1], Michael van der Heyden[1], Raphael Carapito[3,4], Kim Midwood[2] and Gertraud Orend[1]

* Equal contribution

Corresponding author : Gertraud Orend, INSERM U1109, ImmunoRhumatologie Moléculaire (IRM), Hôpital civil, Institut d'Hématologie et d'Immunologie, 1, Place de l'Hôpital, 67091 Strasbourg, France, phone (direct): 0033 (0) 3 68 85 39 96, gertraud.orend@inserm.fr, https://u1109.wordpress.com/tumor-micro-environment/

[1]Université Strasbourg, INSERM U1109, MN3T and The Tumor Microenvironment laboratory, Fédération de Médecine Translationnelle de Strasbourg (FMTS), Strasbourg, France

[2]Kennedy Institute of Rheumatology, Oxford University, Oxford, UK

[3] Laboratoire d'ImmunoRhumatologie Moléculaire, plateforme GENOMAX, INSERM UMR_S 1109, Faculté de Médecine, Fédération Hospitalo-Universitaire OMICARE, Fédération de Médecine Translationnelle de Strasbourg (FMTS), LabEx TRANSPLANTEX, Université de Strasbourg, Strasbourg, France.

[4] Service d'Immunologie Biologique, Plateau Technique de Biologie, Pôle de Biologie, Nouvel Hôpital Civil, Strasbourg, France.

3.1. Abstract

The extracellular matrix molecule tenascin-C (TNC) promotes tumor progression and metastasis by poorly understood mechanisms. We used a novel mammary gland tumor progression model based on a syngeneic orthotopic tumor cell grafting approach with engineered levels of TNC in the tumor cells and the host, respectively and, identified TNC as an important regulator of tumor growth. We document that TNC promotes the battle between tumor regression and growth, where combined expression of tumor cell- and host-derived TNC induces tumor cell rejection. Tumor cell-derived TNC may elicit regression by induction of an antigen presenting signature (APS) expressed by the host, which correlates with better breast cancer patient survival. Tumor-cell derived TNC also triggers CXCL12 expression, thereby causing trapping of CD8+ T cells in the surrounding TNC matrix tracks. TNC binds CXCL12, and combined TNC/CXCL12 attracts and immobilizes CD8+ T cells. Inhibition of the CXCL12 receptor CXCR4 causes tumor regression that is accompanied by massive infiltration of CD8+ T cells and cell death inside the tumor cell nests. Altogether, TNC-triggered CXCL12 signaling may dampen CD8+ T cell function where physical trapping of CD8+ T cells in the TNC matrix may have implications for immune cell therapies. Our results and new tumor model, offer novel opportunities for preclinical cancer research and therapy of cancer patients by triggering the "good" and blocking the "bad" actions of TNC. In particular, overcoming the immune suppressive action of TNC, through inhibition of CXCR4, could be a useful approach.

3.2. Introduction

The extracellular matrix (ECM) molecule tenascin-C (TNC) is a prominent component of the tumor microenvironment (TME) and is highly expressed in tumor tissue (Midwood et al. 2016). TNC plays multiple roles in cancer progression, as recently demonstrated in a stochastic pancreatic neuroendocrine tumor (PNET) model with abundant and no TNC. TNC was found to enhance survival, proliferation, invasion, angiogenesis and lung metastasis (Saupe et al. 2013). Also in breast cancer models, TNC was shown to play a role in promoting metastasis lung colonization (O'Connell et al. 2011; Oskarsson et al. 2011) (Sun et al., submitted).

Cancers are often characterized by an early inflammatory state, followed by an immune deserted TME which is weakly immunogenic, thus enhancing cancer progression (Teng et al. 2015; Zitvogel, Tesniere, and Kroemer 2006). The impact of the TME and in particular its ECM on tumor immunity is poorly known. As TNC is highly expressed in the TME, TNC may play a role in tumor immunity. Yet, only a few models are available to address the roles of TNC in tumor immunity and so far no model existed to address the roles of tumor cell and host-derived TNC on tumorigenesis in an immune competent host. Recently, TNC was shown to affect CD8+ T cells in a prostate cancer model (Jachetti et al. 2015), but how TNC affects CD8+ T cells *in vivo* is unknown. The possibility that TNC plays a role in tumor immunity is supported by its role as a danger associated molecular pattern (DAMP) molecule in other pathological conditions such as rheumatoid arthritis (RA) where TNC is highly expressed and aggravates the pathology (Midwood et al. 2009).

By using our novel immune competent tumor models we identified a janus role of TNC in tumorigenesis where TNC induces an antigen-presenting-signature (APS), thus explaining tumor rejection induced by TNC. TNC also generates an immuno-tolerogenic TME by upregulation of CXCL12 and trapping CD8+ T cells, thereby promoting tumor growth. The balance between these two actions of TNC may largely impact tumor growth. Both mechanisms offer novel targeting opportunities as high expression of the antigen-presenting-signature APS correlates with better survival of breast cancer patients. On the contrary, blocking CXCL12 signaling caused tumor regression which could be suitable in treatment of human cancer patients.

3.3. Results

The syngeneic NT193 orthotopic grafting model phenocopies the genetic MMTV-NeuNT model

We have established the cell line NT193 from a MMTV-NeuNT tumor (Arpel et al. 2016), and now show that NT193 cells induce a tumor that morphologically mimics the anatomy of the genetic tumor upon orthotopic engraftment in the surgically opened mammary gland of an immune competent female FVB mouse (**Fig. S1A**). NT193 cells are a pool of mostly epithelial cells (E-cadherin+) that express low levels of estrogen and progesterone, and persistent high levels of NeuNT (rat orthologue of ErbB2) in cultured cells and all grafted tumors, respectively (**Fig. S1B, S1C, S1E, S1F,** data not shown). Moreover, in NT193 tumors the stroma is similarly organized into tumor matrix tracks (TMT) surrounding tumor cell nests, compared to MMTV-NeuNT tumors (**Fig. S1G**). Like in other tumors, TNC is expressed together with fibronectin (FN), laminin (LM) and collagen IV (Col IV) in parallel aligned fibrillary networks (Spenlé et al. 2015). We have previously shown that NT193 tumor cells spontaneously metastasize to the lung (Sun et al., submitted), thus the NT193 grafting model mimics the genetic model anatomically and functionally.

The cellular source of TNC impacts tumor growth

To address the contribution of tumor cell-derived TNC, we knocked down (KD) TNC in NT193 cells by shRNA technology (**Fig. S1D**) and determined cell multiplicity in culture. No difference was noted between control NT193 cells and TNC KD cells (**Fig. S2A**). We already demonstrated that the TNC KD is preserved *in vivo* as NT193 shTNC cell-derived tumors express very little TNC (Sun et al., submitted). We previously noticed that all end stage tumors had a similar volume independent of

TNC expression. In contrast, we found that host-derived TNC promotes lung metastasis (Sun et al., submitted) suggesting that the cellular origin of TNC may impact tumor progression. Now we wanted to know whether host and/or tumor cell-derived TNC influenced the tumor growth kinetics. Therefore, we engrafted NT193 shC (sh control) and shTNC cells into a wildtype (WT) or TNC knockout (TNCKO) host and determined the tumor growth over 11 weeks. We observed that all engrafted cells induced tumors that grew exponentially in a TNCKO host similar to a WT host, except for shC cells (**Fig. 1A, B**). These cells were completely rejected after 28 days in half of the WT mice and shrank to a still palpable size in the other half of mice (**Fig. 1B, S2B**). The latter group of tumors started to regrow after 6 weeks and reached a comparable volume as all other tumors at the end of the experiment (**Fig. 1B, S2E**). Interestingly, neither shC cells were rejected in a TNCKO host, nor did shTNC cells experience regression in a WT host (**Fig. 1A, B**). These observations suggest that the cellular source of TNC matters and that combined expression of host- and tumor cell-derived TNC is necessary to trigger tumor cell rejection. We used nude mice, lacking B and T cells and, naturally expressing TNC, for engraftment and observed no rejection of shC cells, suggesting that through B and/or T cells TNC may impact tumor growth (**Fig. S2C**).

The observed tumor volumes may be due to a difference in apoptosis and/or proliferation which we determined by tissue staining for cleaved caspase 3 (Casp3) and Ki67, respectively. Indeed, apoptosis was highest and lowest in tumors of a WT host engrafted with shC cells (WT/shC) at 3 (early stage) and 11 weeks (late stage), respectively (**Fig. 1C-F, Fig. S2F**). Proliferation was slightly higher in WT/shC tumors compared to TNCKO/shC (**Fig. 1G-J, Fig. S2G**). Thus, tumor cell-derived TNC promotes apoptosis right upon engraftment, yet not anymore in the end stage tumors.

TNC induces an antigen-presenting-signature (APS) in the regressing tumors

As WT/shC (opposed to WT/shTNC) tumors showed the highest apoptosis and regressed (**S2D, F**), we considered that tumor cell-derived TNC may elicit an immune response. To gain insight into the underlying mechanism we performed a RNA seq analysis by comparing gene expression in KO/shC tumors versus KO/shTNC tumors. This analysis revealed 21 genes that according to the gene ontology classification have a function in antigen presentation and processing (**Fig. 2A, B, Tables S8, S11**). Using the Kegg pathway analysis for genes that are expressed by tumor cells in a TNC-dependent manner (KO/shC and KO/shTNC) revealed that TNC upregulates genes that are involved in many steps of antigen presentation including several MHCI and MHCII molecules (**Fig. 2D**). We confirmed high expression of ciita, ctss, b2m, cd74, tap1, tap2, cd4 and cd86 by qRTPCR in KO/shC tumors versus KO/shTNC (**Fig. 2C**). Except tap2, all these genes were also more expressed in WT/shC than in WT/shTNC tumors (**Fig. S3B**). This observation reveals that the identified APS signature is similarly regulated by tumor cell-derived TNC in both WT and TNCKO host. Thus induction of APS by TNC may explain regression of WT/shC tumors (**Fig. S3A, B**). The APS genes are known to be expressed by the host. Indeed expression of b2m, cd74 and cd4 was lower in shC tumors from a TNCKO host in comparison to a WT host (**Fig. S3C**). These results can explain the host contribution to regression of WT/shC tumor cells. Increasing antigen presentation may enhance the infiltration of cytotoxic T cells (CTL) in the tumor. In support of this hypothesis, we observed that the abundance of CD8+ T cells was much higher in early stage WT/shC (regression) than in WT/shTNC tumors (no regression) (**Fig. 2E, S3D**). CD8+ T cells were also more abundant in TNC-high (WT/shC) tumors compared to TNC-low (KO/shTNC)

tumors (**Fig. 2F, G**). Finally, expression of granzyme B and perforin, two molecules expressed by CTL and involved in execution of cytotoxicity (Froelich et al. 1996), correlated with TNC expression by the host and were higher in the condition of tumor regression (**Fig. 2H, I**). Altogether, APS expression, high CD8+ T cell abundance and strong expression of CTL execution markers correlate with high apoptosis in the TNC-high tumors and tumor regression (**Fig. 1C, D**). It is remarkable, that host and tumor cell-derived TNC are required for tumor regression which can be explained by tumor cells inducing APS genes in the host.

Next, we wanted to know whether the antigen presenting gene signature APS has relevance for human breast cancer. Therefore we performed a Kaplan Meier analysis comparing expression of 7-genes of the APS (CD4, CD74, B2m, CTSS, CIITA, TAP1, CD86) and stratified patients according to expression below or above the median. We noticed that expression above the median of these 7 genes correlates with better outcome in a cohort of 444 grade III breast cancer patients in particular for overall survival (OS, HR: 0.46 (0.27 – 0.79)) and relapse-free survival (RFS, HR: 0.49 (0.36 – 0.68)). This is not the case for grade I and II breast cancer patients (**Fig. 2J, S3E, F**). High expression of some genes alone already correlated with better OS and RFS, yet the significance was stronger when expression of the 7-genes was combined (lower HR and p values) (**Fig. S3G, H**).

Gene expression profiling reveals TNC induction of immune modulatory molecules

So far we have shown that combined expression of TNC in the host and the tumor cells triggers tumor regression presumably through induction of an antigen presenting signature and high CTL activity. Yet, around 6 weeks some of the regressed tumors

start to regrow and generate the most metastatic cancers (Sun et al., submitted). To get an unbiased insight into the underlying mechanisms for this surprising observation, we performed gene expression analysis by RNA sequencing of cultured NT193 cells and late stage NT193 tumors (WT/shC, WT/shTNC and KO/shC), and used Affymetrix chip analysis for MMTV-NeuNT tumors with WT and TNCKO genotypes (**Fig. 3A, B, C, D**). By using gene ontology classification we observed an impact of TNC on genes encoding molecules that regulate proliferation and cell cycle progression in NT193 cells that are more abundant in the TNC expressing cells (**Fig. 3A, S4A, B**). We also noted an immune modulatory signature in the grafted and genetic tumors (**Fig. 3B-D, Table S12-S14**). Upon comparison of the 50 most up- or down-regulated genes we noticed clear differences between TNC high and low conditions in NT193 cells (shC, sh2TNC) and tumors (WT/shC, KO/sh2TNC), and between NT193 tumors where the host is expressing (WT/shC, WT/sh2TNC) (**Fig. 3A-C**).

To get a broad overview of how TNC may affect tumor immunity, we compared general abundance of immune cells in MMTV-NeuNT and in NT193 tumors (WT/shC and WT/shTNC) by FACS analysis and observed an impact of TNC on macrophages, dendritic cells and CD8+ T cells, reducing their abundance (**Fig. 3E, F, S4F, G** and Deligne et al., in preparation).

As TNC has an impact on CD8+ T cell adhesion *in vitro* (Hauzenberger et al. 1999) and we saw an effect on the abundance of CD8+ T cells in the early stage NT193 tumors, we considered the possibility that TNC may impact the local distribution of immune cells. To address this hypothesis, we used immunofluorescence (IF) tissue staining of NT193 TNC-high (WT/shC) and TNC-low (KO/shTNC) tumors. We noticed that CD45+ leukocytes, F4/80+ macrophages, CD4+ T cells and CD11c+ dendritic

cells are present in TNC matrix and, inside the tumor cell nests. No obvious difference in localization was seen between groups of the late stage tumors (**Fig. S4C**). In contrast, CD8+ T cells were more abundant inside the TMT of TNC-high tumors in comparison to TNC-low tumors, accompanied by more CD8+ T cells infiltrating the tumor cell nests (**Fig. 3G, H, S4D-E**). Finally, expression of granzyme B and perforin was significantly lower in MMTV-NeuNT WT compared to TNCKO tumors and, in late stage TNC-high compared to TNC-low tumors indicating that TNC may lower CTL killing activity in the end stage tumors (**Fig. S6A-D**). Altogether, these results suggest a role of TNC in regulating CD8+ T cell function and loco-spatial distribution impacting their abundance inside the tumor cell nests.

TNC impacts CD8+ T cell adhesion and migration through CXCL12

We wanted to know how TNC impacts CD8+ T cells and looked for candidate molecules that are expressed in a TNC-dependent manner. We observed that the chemokine CXCL12 is upregulated by TNC in MMTV-NeuNT and NT193 tumors and, in cultured NT193 cells (**Fig. 3A, D, Table S3-8**). We confirmed TNC-associated CXCL12 expression at the mRNA (qRTPCR) and protein level (ELISA) in cultured NT193 cells (total lysate and conditioned medium (CM)) and in NT193 tumors (**Fig. 4A-D, Fig. S5A, B**). These experiments showed that CXCL12 is induced by TNC in the tumor cells in culture and also in the NT193 tumors in a tumor cell-dependent manner. As CXCL12 levels are similar in shC tumors, independent of the host, we conclude that this chemokine is predominantly expressed by the tumor cells *in vivo* which we confirmed by tissue staining where CXCL12 overlapped with CK8/18 (**Fig. 4E, F**). As TNC binds several soluble molecules (De Laporte et al. 2013; Martino et al. 2013), by surface plasmon resonance spectroscopy we addressed whether

CXCL12 binds TNC. Indeed, we observed considerable binding of CXCL12 to TNC with a Kd of 7,9 x 10^{-7} M, in a 35-fold lower range as to its receptor (Richter et al. 2014) (**Fig. 4G**).

As TNC can bind CXCL12, CXCL12 is induced by TNC in the tumors and CD8+ T cell abundance and localization is regulated by TNC, we considered that TNC may affect CD8+ T cell adhesion and migration. Therefore, we compared transwell migration towards TNC with that towards fibronectin (FN) and collagen IV (Col IV), by coating the ECM molecule on the lower surface of the insert, and then using described attraction-supporting concentrations of CXCL10 (a well-known chemoattractant (Liu et al., 2011)), CCL21 (another candidate molecule induced by TNC, **Fig. 3D**) and CXCL12. We counted floating cells in the lower well by FACS or, on the ECM coated lower surface upon paraformaldehyde (PFA) fixation (**Fig. S5C-F**). These experiments revealed, that CXCL12 and CXCL10 attracted more cells towards the lower well than CCL21 and, that TNC attracted significantly less cells to float in the lower well than FN and Col IV (**Fig. S5C, D**). By measuring the cells that were attached to the lower coated surface of the insert, TNC turned out to be the most adhesive, in particular in combination with CXCL12 (**Fig. S5E, F**). Combining the numbers of all cells, floating and adherent, TNC attracted the most cells, where CXCL12 was highly active as chemoattractant (**Fig. 4H**). Altogether, these results demonstrate that TNC/CXCL12 is attracting and binding CD8+ T cells which is in contrast to FN or Col IV that also attract CD8+ T cell, but do not immobilize them.

As TNC increases CXCL12 expression in NT193 cells (**Fig. 4C-F**) we asked whether the conditioned medium (CM) of shC cells has a similar effect as CXCL12. Therefore, we measured floating and adherent cells in the lower well towards CM derived from shC and shTNC cells, respectively. Indeed, only CM from shC cells attracted CD8+ T

cells and facilitated cell adhesion to TNC (**Fig. 4I, J, S5G, H**). To address whether this effect is due to CXCL12 we used AMD3100 to block CXCR4, a receptor for CXCL12 (Balabanian et al. 2005). Again, the cell attraction effect of the CM from shC cells was blocked and reveals that CXCL12 is the major CD8+ T cell attracting factor induced by TNC in the NT193 cells (**Fig. 4I, J, S5G, H**). This mechanism may be relevant in tumors where tissue staining revealed co-localization of CD8+ T cells with CXCL12 in the TNC matrix (**Fig. 4F**).

To address whether CXCL12 could impact tumor cell behavior *in vivo* we determined expression of the two receptors CXCR4 and CXCR7 by qRTPCR in cultured tumor cells and in the NT193 tumors. Both receptors are expressed in shC cells with comparable levels in cultured cells (**Fig. S5I**). Whereas CXCR7 expression was unaffected by TNC, CXCR4 levels were lower in shC compared to shTNC cells (**Fig. S5I**). Regulation of CXCR4 by TNC was also seen in NT193 tumors where CXCR4 levels were the lowest when tumor cells expressed TNC (**Fig. S5J**). In 48h cell culture experiments, shC and shTNC cell numbers increased similarly with and without CXCL12 (**Fig. S5K**). Altogether, these results suggest that CXCL12 may poorly affect the tumor cells *in vivo* but rather CD8+ T cells.

CXCR4 signaling regulates CD8+ T cell function *in vivo*

So far we have shown that TNC upregulates CXCL12, impacts CD8+ T cell adhesion and migration and, CD8+ T cell loco-spatial distribution within the tumor. Therefore, we considered that TNC-induced CXCL12 signaling may impact regrowth of WT/shC tumors. We investigated this possibility by treating WT/shC tumor mice with the CXCR4 antagonist AMD3100 starting 2 weeks after tumor cell engraftment and measured the tumor volume over the next 5 weeks. Indeed, the tumor volume

immediately dropped and tumors only slowly started to regrow. This was clearly different to control tumors that strongly expanded (**Fig. 5A, B**). As proliferation of NT193 cells is not affected by CXCL12 **(Fig. S5K)** and CXCR4 is lowered by TNC (**Fig. S5J**), AMD3100 may not directly target tumor cells but affect them through CD8+ T cells. In support, by tissue staining for TNC and CD8, we observed that upon AMD3100-treatment CD8+ T cells highly infiltrated the tumors which was accompanied by many cells stained for cleaved caspase 3, indicating massive tumor cell death (**Fig. 5C-H**). This resembled the early stage WT/shC tumor phenotype with highly infiltrated CD8+ T cells and tumor regression. These results suggest that inhibition of CXCR4 signaling overcomes the immune suppressive effect of TNC by increasing CD8+ T cell infiltration, activating immune surveillance and triggering tumor cell death.

In summary, our results have revealed two opposing activities of TNC in tumor immunity (**Fig. 5I)**, where TNC may act as "alarmin", inducing an antigen-presenting APS signature and triggering immune defense. In contrast, TNC may also corrupt tumor surveillance through induction of CXCL12 causing immune shielding of tumor cells by physically trapping CD8+ T cells in the TNC matrix. The balance between these opposing TNC activities may determine whether tumor cells get rejected or grow. This battle might be relevant in human breast cancer, where high expression of the antigen presenting APS signature correlates with better survival.

3.4. Discussion

Our study provides mechanistic insight in how TNC impacts tumor growth. TNC modulates immunity and in particular the temporal and spatial localization of CD8+ T cells. We describe a Janus role of TNC that is characterized by eliciting an immune response and, also corrupting immune surveillance. This dual role of TNC in tumor immunity has not been known so far and offers novel cancer targeting opportunities.

Tumor immunity is resurrecting as an important field in anti-cancer therapy where activation of immune checkpoint regulators is a promising approach to block tumor growth in some but not all patients (Sharma and Allison 2015). The response rates should be better. A more in-depth knowledge is necessary to comprehend the crosstalk of tumor cells with the immune system within the TME where the TME may counteract the immune checkpoint therapies. Until today this question was difficult to address as only a few models existed that allow to address how the TME, and in particular the tumor relevant ECM, impacts the evolution of an immune response during tumor onset and along tumor progression. Here, we have established a novel syngeneic orthotopic mammary gland grafting model where the impact of the tumor specific ECM on the evolution of tumor immunity can be analyzed thanks to growth of the grafted tumor cells into a tumor over many weeks.

Whereas initial experiments in a PyMT model expressing or lacking the TNC protein did not show a TNC-dependent effect on tumor growth nor lung metastasis (Talts et al. 1999), a few other models support a metastasis enhancing role of TNC. In the first stochastic PNET tumorigenesis model with engineered TNC expression, high TNC levels correlated with enhanced lung metastasis (Saupe et al. 2013). In immune compromised PDX (patient derived xenograft) tumors, using human breast cancer

cell lines (Oskarsson et al. 2011c; Minn et al. 2005), host-and tumor cell-derived TNC was shown to be important for colonization of intravenously injected tumor cells (Oskarsson et al. 2011). By grafting 4T1 cells into a syngeneic host expressing or lacking the TNC protein, the authors also observed that host TNC was involved in enhancing lung metastasis colonization (O'Connell et al. 2011). Now, by using the MMTV-NeuNT model expressing or lacking TNC and by applying the NT193 grafting model with engineered TNC levels, we have recently shown that again host-derived TNC plays a role in promoting lung parenchymal metastasis formation (Sun et al., submitted). Altogether, we demonstrate that the NT193 grafting model is a relevant surrogate model to recapitulate events driving tumor progression in the MMTV-NeuNT model. Here, we show that this model is also relevant to address evolution of tumor immunity.

We have thoroughly characterized our novel NT193 cell line derived from a MMTV-NeuNT tumor (Arpel et al. 2016) that upon orthotopic engraftment into the mammary epithelium of an immune competent mouse develops adenocarcinomas. In the tumors, the tumor cells remain epithelial and maintain expression of the (NeuNT) oncogene. This is opposed to a previously described MMTV-Neu model where expression of another ErbB ortholog got lost and cells underwent EMT which may have selected cells to grow (Kmieciak et al. 2007; Knutson et al. 2006). In the NT193 model we showed that over a period of 11 weeks tumor cells spontaneously disseminate and form lung metastasis (Sun et al., submitted). Moreover, the general organization of the arising NT193 adenocarcinomas is undistinguishable from MMTV-NeuNT tumors. Furthermore, ECM including TNC is arranged into tumor matrix

tracks (TMT) in the NT193 grafted tumors similar to MMTV-NeuNT tumors where we have described TMT for the first time in this model.

We engineered TNC expression in the NT193 tumor cells and noticed that upon engraftment the TNC KD is stable in the arising tumors (Sun et al., submitted). This model now allowed us to address cell type specific roles of TNC by using a WT or TNCKO host for engraftment of shC or shTNC cells. We observed that tumor cell and host-derived TNC have distinct effects on tumor growth. Unexpectedly, we observed a transient tumor regression or complete rejection, when both the host and the tumor cells expressed TNC. This was not seen when only the tumor cells or only the host expressed TNC. We described that tumor cell-derived TNC induced an antigen-presenting-signature APS in the host which could explain the combined actions of both TNC sources in tumor cell rejection.

Interestingly, high expression of an APS signature correlates with better survival of breast cancer patients which could have future diagnostic and therapeutic value. This result also reveals that antigen presentation in breast cancer might have therapeutic relevance which has not been known so far. In glioblastoma (GBM) patients, it was recently shown that antibodies against TNC correlate with a longer survival (Mock et al. 2015). Based on this observation, the company Immatics had developed an immunization protocol for GBM patients where antigenic peptides from TNC are included (reviewed in Spenlé et al. 2015). Our results suggest that a similar strategy might also be useful in grade III breast cancer patients. We further noticed that surgical wounding is essential to allow eliciting of an immune defense and to trigger tumor cell rejection as, no rejection was seen when NT193 shC cells were engrafted through the nipple (Deligne et al., in preparation). Maybe through wounding, the

immune system is alerted and innate immune cells can trigger a defense reaction before a strong negative feedback loop sets in to inactivate the innate immune response (Deligne et al., in preparation).

Certainly more work is needed to identify how TNC elicits an immune response. TNC may induce a neoantigen in NT193 cells or, TNC could act as TAA itself. To address whether TNC acts as TAA can be tested by immunization of a WT host with TNC and then monitoring growth of engrafted shC cells which should be rejected. If rejection is not increased, one or more molecules induced by TNC (in the shC cells) may serve as TAA. Candidate molecules may be present in the list of genes that are expressed in cultured shC cells but are lacking in shTNC cells. Analysis of our RNA seq data revealed a difference in FNIII domains of TNC molecules that are expressed by the host and the tumor cells (unpublished results), which suggests that a particular TNC sequence may be antigenic in this model. This intriguing possibility has to be investigated in more depth in the future. Also, it remains to be determined whether glycosylation or, citrullination of particular sites in TNC generates antigenic sites as antibodies against citrullinated TNC were identified in RA patients (Schwenzer et al. 2016). Also, cleavage of TNC may release cryptic antigenic sites (Midwood et al. 2016).

How does TNC act as alarmin or DAMP in cancer? From studies in RA patients it is known that TNC enhances expression of pro-inflammatory cytokines in the connective tissue of the joints through integrin α9β1 and TLR4 (Asano et al. 2014; Midwood et al. 2009) . Whether this is also the case in our model has to be

addressed. Our unpublished data suggest a role of TRL4 in TNC corrupting tumor immune surveillance in this model (Deligne et al., in preparation).

TNC may generate an immunotolerogenic TME by creating ECM-enriched tumor matrix tracks (TMT) that have previously been described in other tumors and were found to have structural and molecular similarities with reticular fibers in the thymus (Drumea-Mirancea et al. 2006; Spenlé et al. 2015; Midwood et al. 2009). In human and murine insulinoma and colon carcinoma we found fibroblasts inside the matrix tracks and, expression of characteristic ECM molecules such as FN, LMγ2, Col IV and TNC (Spenlé et al. 2015). It is remarkable that the expression of TNC in the adult organism is largely regulated and restricted to only a few sites such as some stem cell niches and noticeably, reticular fibers of lymphoid organs. The particular expression in reticular fibers could be meaningful as immune cell education is believed to occur in the reticular fibers (Fletcher et al., 2015). We had previously speculated that in tumors the genetic program for reticular fibers is turned on to trigger the formation of TMT (Midwood et al. 2009). TMT are bigger than reticular fibers, where a not yet identified exhaustive number of ECM molecules is arranged in aligned fibrillar arrays oriented parallel to the tumor cell nests (Spenlé et al. 2015). Interestingly, TNC is a very prominent component of these TMT that we have seen in insulinoma, colon carcinoma, glioblastoma and recently in head and neck squamous cell carcinomas (Spenlé et al. 2015; Rupp et al. 2016, Sun et al., submitted, Spenlé, Loustau et al., in prep). We now have shown that TMT are indeed formed in the NeuNT and NT193 tumors where ECM expression resembles those of other tumors (Spenlé et al. 2015) and considered that TMT in NT193 tumors may impact tumor immunity. Whereas we found leukocytes enriched in TMT of insulinomas, in NT193 tumors we found CD8+ T cells sequestered in the TMT. The function of these TMT

appears to be different in the absence of TNC, as we saw less CD8+ T cells residing in the TMT of tumors with low TNC expression. Instead, in the TNC-low tumors more CD8+ T cells entered the tumor cell nests which correlates with enhanced apoptosis and tumor regression.

One of the TNC-regulated genes was the chemokine CXCL12 that was upregulated at mRNA and protein level in tumors with high TNC as well as in the secretome of TNC expressing cells. CXCL12 was shown to regulate T lymphocyte migration (Okabe 2005b) through CXCR4 (CXCR7) (Balabanian et al. 2005) and, at low and high concentrations, acts as a chemoattractant or repellent (Poznansky et al. 2000). CXCL12 is also known to be an important player in TME-driven immune exclusion (Joyce and Fearon 2015). Thus, it is possible that through upregulation of CXCL12 by TNC tumor cells generate a CD8+ T cell repelling local milieu. Indeed, we showed that inhibition of CXCR4 with AMD3100 caused massive infiltration of CD8+ T cells into the tumors and their regression. As CXCL12 binds TNC we considered that TNC also impacts CD8+ T cells by attraction and immobilization. Indeed, our cell culture experiments confirmed that CXCL12 promotes attraction of CD8+ T cells towards TNC where cells adhered to the usually poorly adhesive TNC substratum, thereby causing their immobilization. Interestingly, CXCL12 is the major CD8+ T cell attraction factor induced by TNC in this model, as CM from shC cells attracted CD8+ T cells which was not the case with CM from shTNC cells. Moreover, this attraction was blocked upon inhibition of CXCR4. Thus, TNC may impact localization of CD8+ T cells away from the tumor cell nests by two mechanisms, first through induction of CXCL12 generating a CD8+ T cell repelling local milieu and second by sequestering CD8+ T cells inside the TMT, thereby keeping CD8+ T cells away from the tumor

cells. Whether TNC affects the cytotoxic function of CD8+ T cells is another important question that we did not address in depth here as this is shown in another manuscript (Deligne et al., in preparation). Our results suggest that TNC impairs CD8+ T cell functions at multiple levels. Apparently, CXCR4 signaling is instrumental for tumor growth as CXCR4 inhibition caused tumor regression. CD8+ T cells largely infiltrated the tumor cell nests where apoptosis is highly elevated. These results suggest that inhibition of CXCR4 signaling in CD8+ T cells causes their infiltration and, killing of tumor cells. Future experiments have to address the exact mechanism. Do the levels of CXCL12 indeed reach the CD8+ T cell repelling concentration in vivo? It remains also to be seen whether the killing activity of CD8+ T cells is increased upon CXCR4 inhibition. This could be relevant for immune checkpoint and CART cell therapies as TNC is highly expressed in established tumors. It is possible that restoration of immune checkpoints may be hampered by TNC physically sequestering CD8+ T cells away from the tumor cells. It is interesting to note that combining CXCR4 inhibition with PD-1 blockade enforced tumor regression (Zboralski et al. 2017), thereby potentially counteracting TNC. By orchestrating immune defense and immune evasion TNC may fine-tune tissue immunity. This may also be relevant in wound healing and inflammation thereby preventing overshooting of immune reactions that would lead to chronically inflamed or autoimmune conditions. In cancer this balance is obviously disturbed thereby promoting corruption of immune surveillance.

In summary, here we have established a powerful tumor grafting model that allowed us to shed light on the roles of TNC on the evolution of tumor immunity. TNC may locally orchestrate tumor and immune cell behavior where the cellular origin of TNC is important. Tumor cell-derived TNC triggers expression of an antigen-presenting-

signature APS in the host causing tumor cell rejection. Tumor cells also increase CXCL12 expression in a TNC dependent manner. Binding of CXCL12 to TNC generates an adhesive substratum for CD8+ T cells thereby sequestering them away from the tumor cells. An in-depth understanding of the balance between the "good" and "bad" actions of TNC in cancer may open novel opportunities for future targeting of cancer, thereby taking into account the temporal and loco-spatial organization of the TME.

3.5. Material and methods

Experimental mice

MMTV-NeuNT female mice in FVB/NCrl (provided by Gerhard Christofori, University of Basel, Switzerland) engineered to express a constitutive active form of the rat ortholog of ErbB2 (NeuNT) under the mouse mammary tumor virus promoter develop multifocal breast adenocarcinoma and lung metastasis (Muller et al. 1988b). TNC+/- mice in the 129/sv genetic background (provided by Reinhard Fässler, Max Planck Institute, Martinsried, Germany, Talts et al. 1999) were crossed consecutively for at least ten times with FVB/NCrl mice (Charles River) before crossing TNC+/- FVB mice with MMTV-NeuNT (FVB/NCrl) mice. All mice were housed and handled according to the guidelines of INSERM and the ethical committee of Alsace, France (CREMEAS) (Directive 2010/63/EU on the protection of animals used for scientific purposes).

To generate an orthotopic syngeneic model, FVB mice with TNC+/+ or TNC -/- genotypes were grafted with 10×10^6 NT193 cells (Arpel, et al., 2014) in the surgically opened left fourth mammary gland. Tumor growth was assessed by measuring the tumor sizes every 3 or 7 days with a Vernier caliper and tumor volume was determined using the following calculation V= (width)^2 x length/2. Tumor bearing mice were euthanized at indicated time points and breast tumors and lungs were processed for subsequent analyses: tissues were frozen in liquid nitrogen for protein and mRNA analysis or embedded in O.C.T (Sakura Finetek) and paraffin for immunostainings. To assess the role of CXCL12 in tumorigenesis, tumor-bearing mice (FVB/NCrl from Charles River) were treated with AMD3100 (Sigma) at 5 mg/kg/day in PBS. The CXCR4 inhibiting molecule was administered by peritumoral injection as from day 15 after NT193 cells engraftment up to 7 weeks.

FACS analysis

The tumor tissue was cut into small pieces (<5mm^3) and digested in PRMI medium supplemented with 5 % of inactivated fetal bovine serum, penicillin (10 000 U/ml), streptomycin (10 mg/ml), Liberase TM (500ug/ml) and DNAse (100ug/ml) for 30 minutes at 37°C under agitation. Cells were then separated through a 70µm cell strainer and counted. Surface staining was performed according to standard protocols and analysed with a LSR Fortessa machine (BD Biosciences, San Jose, CA, USA). Antibodies used were anti-CD8α-Pacific Blue, anti-CD45-PE-Cy7 and anti-CD3ε-Brillant Violet 785 from Biolegend. Dead cells were stained using Live/Dead Fixable yellow dead cell stain kit from Thermofisher. FlowJo was used for the data analysis.

Hematoxylin-Eosin staining (HE)

The paraffin embedded sections were dewaxed and rehydrated with 100% toluene (2 washes of 15 min) and 100%–70% alcohol (10 min each) before staining with hematoxylin (Surgipath) and eosin (Harris) according to standard protocols (ref) and embedding in Eukitt solution (Sigma).

Immunohistochemical staining (IHC)

Paraffin embedded sections (7 µm-thick) were rehydrated as described previously and antigen retrieval was performed by boiling in 10 mM pH 6 sodium citrate solution for 20 min. Cooled slides were then washed and incubated in peroxidase solution (0.6% H_2O_2 in methanol) for 30 min. Slides were washed and incubated with a blocking solution (5% normal goat serum in PBS) for 1 hour at room temperature to block non-specific binding sites. Avidin/biotin receptors were blocked by using the

avidin/biotin blocking kit as recommended by the manufacturer (Vector). Slides were incubated with the indicated primary antibody overnight at 4°C and then incubated with the corresponding biotin-coupled secondary antibody for 1 hour at room temperature. Peroxidase detection was performed using the Elite ABC system (VECTASTAIN) with DAB (Vector) as substrate. Finally, tissue was stained with hematoxylin, dehydrated and embedded in Eukitt solution (Sigma).

Immunofluorescence staining (IF)

O.C.T embedded tissue sections (7 µm-thick) were incubated with a blocking solution (5% normal goat serum in PBS) for 1 hour at room temperature before incubation with the indicated primary antibody overnight at 4°C. The slides were then washed and incubated with the corresponding fluorophore-coupled secondary antibody for 1 hour at room temperature. The list of the different antibodies used is given in **Table S1**. The slides were washed, stained with DAPI (Sigma) for 10 min at room temperature washed and embedded with FluorSave^{TM} Reagent (Calbiochem). The fluorescent signal was analyzed with a Zeiss Axio Imager Z2 microscope. The image acquisition setting (microscope, magnification, light intensity, exposure time) was kept constant per experiment and genetic conditions. Quantification of IF microscopic images was done by the ImageJ (National Institutes of Health) software using a constant threshold.

Fluorophore-labeled MTn12 antibody and IF

In order to be able to do costaining of TNC and immune cells on tissue sections, the MTn12 antibody was labeled with DyLight 488 as recommended by the manufacturer (Thermofisher). When using the DyLight 488-labeled MTn12 antibody, the previously described IF protocol was adapted as follows: after the incubation of the sections with

the secondary antibodies, the slides were washed and incubated with the DyLight 488-labeled MTn12 antibody for 3 hours at room temperature. The slides were then washed, DAPI stained and embedded as described above.

Real Time quantitative PCR (qPCR) analysis

Total RNA was prepared using TriReagent (Life Technologies) according to the manufacturer's instructions. RNA was treated with DNase I (Roche) at 0.5U/µg RNA. After DNase I inactivation, RNA was reverse transcribed (MultiScribe reverse transcriptase, Applied Biosystems) and qPCR was done on cDNA (diluted 1:5 in water) on a 7500 Real Time PCR machine (Applied Biosystems) using SYBR green reaction buffer or Taqman reaction buffer (Applied Biosystems). Data were normalized by using a Taqman mouse GAPDH endogenous control (4333764T, Life Technology) and fold induction was calculated using the comparative Ct method (-ddCt). Primers used for qPCR are listed in the **Table S2.**

Analysis of protein expression

Tissue or cell lysates were prepared in lysis buffer (50 mM Tris-HCl pH 7.6, 150 mM NaCl,1% NP-40, 0.5% sodium deoxycholate, 0.1% SDS) supplemented with protease inhibitor (Roche) and Phosphatase Inhibitor Cocktail (Santa Cruz). The protein concentration was determined by Bradford assay (BioRad). 20-30µg of protein lysate was loaded in precasted 4-20% gradient gels (BioRad), together with Laemmli buffer and separated by SDS-PAGE. The separated proteins were then transferred onto nitrocellulose membranes (BioRad) using the TransBlot Turbo™ Transfer system (Biorad). Nitrocellulose membranes were then blocked with 5 % Blocking-Grade blocker (Biorad) in 0.1% Tween-20 PBS and incubated with the primary (overnight at 4°C) and secondary antibodies (1 hour at RT) in 1.5 %

Blocking-Grade Blocker in 0.1 %Tween-20 PBS. Antibodies used are listed in **Table S1**. Protein bands were detected with the Amersham[TM] ECL[TM] Western Blotting detection reagent (GE Healthcare) or SuperSignal[TM] West Femto Maximum Sensitivity Substrate (ThermoFisher). CXCL12 expression was determined in tissue and protein lysates using the mouse CXCL12/SDF-1 alpha Quantikine ELISA Kit (R&D systems) according to the manufacturer's instructions.

Cell culture

The NT193 cell line has been previously established in the laboratory from a primary MMTV-NeuNT breast tumor (Arpel et al. 2014). NT193 cells were cultured in DMEM with 4.5 g/L glucose (GIBCO) supplemented with 10 % of fetal bovine serum (Invitrogen), penicillin (10 000 U/ml), streptomycin (10 mg/ml) (PenStrep, Dutscher) and Gentamicin (40µg/ml) (ThermoFischer). Cells were maintained at 37°C in a humidified atmosphere of 5 % CO_2. Silencing of TNC in these cells was done by short hairpin (sh) mediated gene expression knock down. Briefly, lentiviral particles shRNA vectors (Sigma) encoding specific shRNAs for the knock down of TNC were used: (sh1TNC: CCGGCCCGGAACTGA-ATATGGGATTCTCGAGAATCCCATATTCAGTTCCGGGTTTTTG, sh2TNC: C-CGGGCATCAACACAACCAGTCTAACTCGAGTTAGACTGGTTGTGTTGATGCTTT TTG). Lentiviral particles encoding a non-targeting shRNA vector were used as control (SHC202V, Sigma). The resulting transduced cells were selected with the previously described culture medium supplemented with 10 µg/ml puromycin (Thermofisher) and the selection pressure was kept in all *in vitro* experiments. To collect conditioned medium from NT193 cells, the cells were seeded in 10 cm cell culture dishes in previously described culture medium, starved at confluence in

DMEM with 4.5 g/L glucose for 48 hours at 37°C. The resulting conditioned medium was filtered at 0.22 µm and stored at -80°C for future use.

Cell multiplicity assay

Serum starved NT193 cells (both shC and shTNC) were plated into 96-well plates (5000/well with 6 replicates for each time point). Cells were treated with recombinant CXCL12 (500 ng/mL) (R&D Systems or not. MTS incorporation assay was done using the CellTiter 96 aqueous non-radioactive cell proliferation assay (Promega) after 4h, 24h, 48h when treated with CXCL12 and 24h, 48h, 72h, 96h when non-treated.

CD8^{+} T cells isolation

Spleens of sacrificed mice were isolated and cut into small pieces on a 70 µm filter with a syringe piston. After a wash with PBS, the red blood cells in the cell suspension were lysed with potassium ammonium chloride lysing buffer (Thermofisher). CD8+ T cells were sorted from the resulting cells by using the murine CD8a^{+} T Cell Isolation Kit (Miltenyi Biotec) according to the manufacturer's instructions. After each CD8+ T cell sorting, the purity of the isolated cells was assessed by FACS analysis (antibodies in Table S1).

CD8+ T cell migration assay

The CD8^{+} T cell migration assays were done in 5µm-pore size polycarbonate membrane transwells (Costar). The lower surface of the transwells were first coated with fibronectin (FN), TNC or collagen IV (Col IV) at a final concentration of 1 µg/cm^{2} and were incubated 1h at 37°C. The transwells were then washed with PBS and blocked with 1% BSA overnight at 4°C. The following day, the transwells were

washed and air-dried. The lower chambers of the transwells were filled with TexMACS medium (Miltenyi Biotec) containing chemokines as chemoattractant: CXCL12 (1 µg/mL), CCL21 (1 µg/mL) or CXCL10 (500µg/mL) (R&D Systems). To assess the migration of CD8+ T cells towards the secretome of the NT193 cells, conditioned medium from NT193 shC or shTNC cells was placed in the lower chamber. In order to block the chemotaxis of CD8+ T cells towards CXCL12, the cells were incubated for 1 hour at 37°C with AMD3100 (Sigma) at a concentration of 5 µg/mL in TexMACS medium before seeding in the upper chamber. After 5 hours of migration at 37°C, the medium in the lower chamber was collected and the number of migrated cells was counted by FACS.

CD8+ T cell adhesion assay

The CD8^{+} T cell adhesion assays were done with the same set up described in the migration experiment. After 5 hours of migration, the cells that were attached to the lower surface of the transwells, were fixed in 4% PFA and stained with DAPI. Pictures were taken and analyzed by the ImageJ software.

Surface Plasmon Resonance analysis

Surface plasmon resonance binding experiments were performed on a Biacore 2000 instrument (Biacore Inc.) at 25°C. TNC (Huang et al., 2001) was immobilized at high surface density (around 7000 resonance units) on an activated CM5 chip (Biacore Inc.) using a standard amine-coupling procedure according to the manufacturer's instruction. Soluble molecules were added at a concentration of 10 µg/mL in 10 mM sodium acetate, pH 5.0, and at a flow rate of 5 µL/min for 20 min before addition of 1 M ethanolamine. CXCL12 (from 0.6×10^{-7} M to 6×10^{-7} M) was added to the chip at pH 7.4 (10 mM HEPES, 150 mM sodium chloride, 0.005% (v/v) surfactant P20), at a flow

rate of 10 μL/min. A blank CM5 chip was used for background correction. 10 mM glycine, pH 2.0, at 100 μL/min for 1 min was used to regenerate the chip surface between two binding experiments. The dissociation constant (Kd) was determined using the 1:1 Langmuir association model as described by the manufacturer.

Gene expression analysis

RNA integrity for NT193 shControl and shTNC cells (2 samples per group) was assessed with the Agilent total RNA Pico Kit on a 2100 Bioanalyzer instrument (Agilent Technologies). Ribosomal RNA was depleted with the Low Input RiboMinus™ Eukaryote System v2 kit (ThermoFisher) following the manufacturer's instructions. The sequencing library was prepared with the Ion Total RNA-seq kit v2 (ThermoFisher) according to the manufacturer's instructions. The libraries were loaded two by two at a concentration of 20 pM on an Ion PI™ Chip using the Ion Chef Instrument (ThermoFisher). Finally, the sequencing was performed on an Ion Proton sequencer with the Ion PI™ Hi-Q™ Sequencing 200 Kit (ThermoFisher). The transcriptome data were processed by the RNASeqAnalysis plugin from the Torrent Suite Software 5.06. The approach is based on the Life Technologies Application note: "Transcriptome sequencing using the Ion Proton System". The reads are mapped on a two-step alignment scheme. They are first aligned to the reference genome (mm10) using STAR (Dobin et al. 2013) to find full mappings and the unmapped reads are mapped using the bowtie2 aligner to find partial mappings (Langmead and Salzberg 2012). The total reads mapped are finally available in BAM format for raw read counts extraction. Read counts are found by the htseq-count tool of the Python package HTSeq (Anders, Pyl, and Huber 2015). Differential analyses were performed by the DESEQ2 package of the Bioconductor framework (Love,

Huber, and Anders 2014). Up-regulated and down-regulated genes are selected based on the adjusted p-value cutoff 10%.

RNA from MMTV-NeuNT WT and TNCKO mammary tumors (3 samples per group) were used for the Microarray experiments, performed at the IGBMC Affymetrix Core Facility (Illkirch, France). Biotinylated single strand cDNA targets were prepared by using the Affymetrix GeneChip WT Terminal Labeling Kit (Affymetrix) according to manufacturer`s recommendations. Following fragmentation and end-labelling, 2 µg of cDNAs were hybridized for 16 hours at 45°C on GeneChip Human Gene 1.0 ST arrays (Affymetrix) interrogating 28.869 genes represented by approximately 27 probes spread across the full length of the gene. The chips were washed and stained in the GeneChip® Fluidics Station 450 (Affymetrix) and scanned with the GeneChip Scanner 3000 7G (Affymetrix) at a resolution of 0.7 µm. Raw data (.CEL Intensity files) were extracted from the scanned images using the Affymetrix GeneChip Command Console (AGCC) version 3.1. CEL files were further processed with Affymetrix Expression Console software version 1.1 to calculate probe set signal intensities using Robust Multi-array Average (RMA) algorithms with default settings. Deregulated gene expression analysis was performed using the PANTHER version 11 (Mi et al. 2017) and DAVID software (D. W. Huang, Sherman, and Lempicki 2009).

Patient survival data

Patient array data were obtained from and analyzed by Kaplan–Meier plotter tool (kmplot.com) as described elsewhere (Györffy et al. 2010). The cohort was split by median of corresponding gene expression ("High" and "Low," respectively). Analysis

was performed for overall survival and relapse-free survival in the cohort of breast cancer patients, stratified according to the tumor grade (Grade I, II, III).

Statistical analysis

Statistical analysis and graphical representations of data were done using GraphPad Prism software. The Agostino-Pearson normality test was used to confirm the normality of the data. The statistical difference of Gaussian data sets was analyzed using the Student unpaired two-tailed t test, with Welch's correction in case of unequal variances and, the one way ANOVA test followed by a Tukey's multiple comparison post-test was used for multiple data comparison. For data not following a Gaussian distribution, the permutation test was used and the one-way ANOVA test followed by the permutation multiple comparisons post-test was used for multiple data comparison. Graphs are represented as Mean +/- SEM unless stated otherwise. Contingency was analyzed using the chi-square test. p-values smaller than 0.05 were considered as significant (*, $p<0.05$, **, $p < 0.01$, ***, $p < 0.001$, ****, $p < 0.0001$).

Disclosure of potential conflict of interest

Authors contribution

DM, ZS and IVQ developed the genetic and orthotopic grafting model. DM, ZS, IVQ, CD, AY, TH, WE, GC, FD, NP, MM and MvH performed experiments, analyzed and interpreted the data. KM and RC critically reviewed the manuscript and interpreted data. DM and GO wrote the manuscript. GO conceptualized and supervised this study. Grants to GO and KM financed the study.

Acknowledgements

3.6. Figures

Figure 1

Figure 1. Tumor cell-derived TNC triggers tumor rejection in the TNC WT host.

(A,B) Tumor growth curves of the corresponding grafted NT193 cells in the TNC knock out **(A)** hosts (shC N=12, sh1TNC N=10, sh2TNC N=15) and wildtype hosts **(B)** (shC N=13, sh1TNC N=11, sh2TNC N=9) respectively. **(C-F)** Representative images of IF analysis from apoptosis in early stage tumors **(C)** and late stage tumors **(E)** assessed by cleaved caspase-3 staining and quantification in early stage **(D)** (N = 6 for each group) and late stage tumors **(F)** (N = 7 for each group) respectively. **(G-J)** Representative images of IF analysis from cell proliferation in early stage **(G)** and late stage tumors (I) by Ki67 staining and quantification in early stage **(H)** (N = 7 for each group) and late stage tumors **(I)** (N = 7 for each group) respectively. Scale bar: 50 µm.

Figure 2

A NT193 - early

B NT193 - early

KO/shC   KO/sh2TNC

C NT193 - early

KO/shC
KO/sh2TNC

D Antigen processing and presentation

E NT193 - early

F NT193 TNC-high   NT193 TNC-low

TNC
CD8
LM

G

H

I

J APS in breast cancer grade III

HR=0.49
P<0.00001

Low
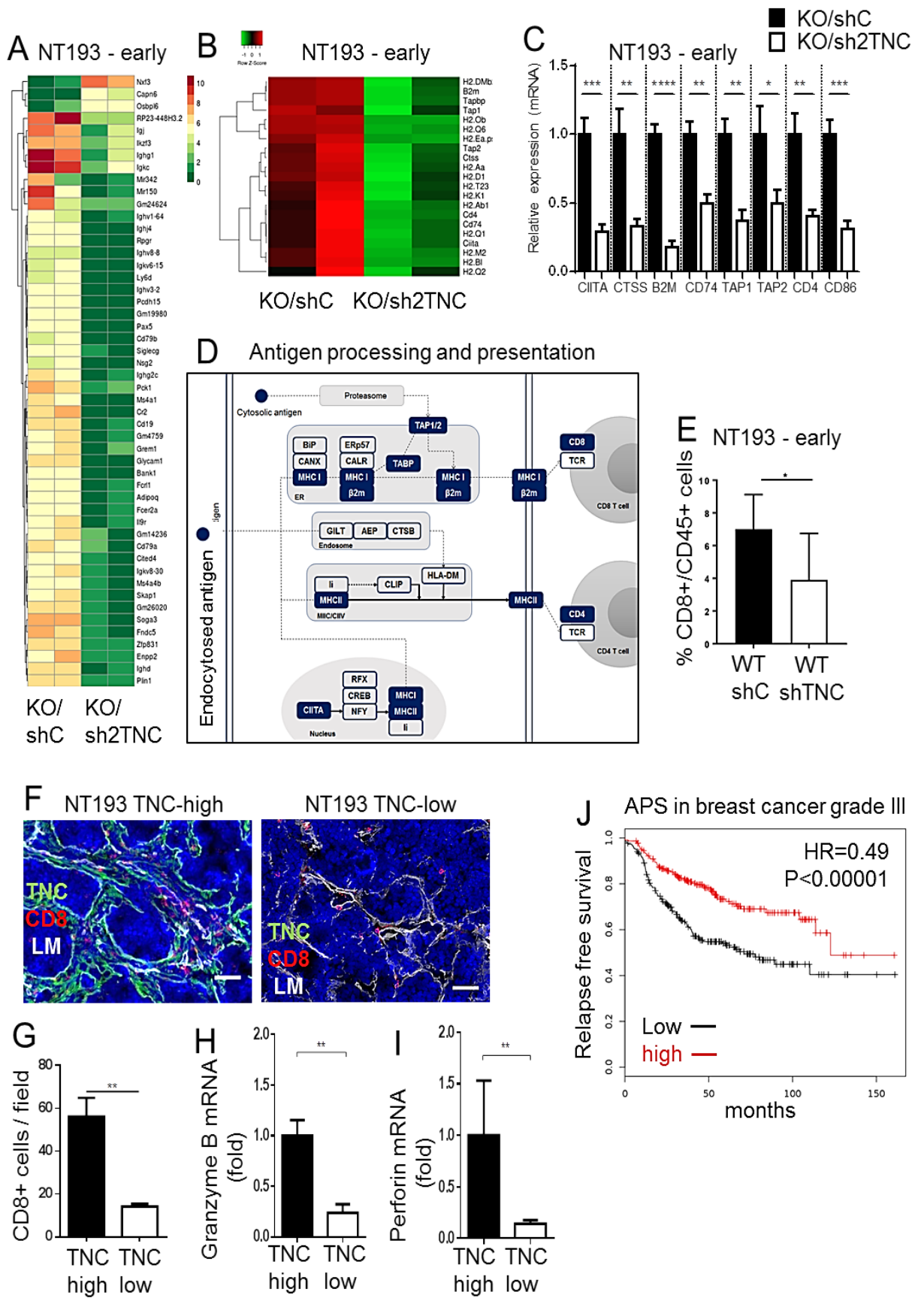
Figure 2. Tumor-derived TNC induces expression of an antigen presentation signature (APS) by the host. (A-C) Heatmap for the 50 most deregulated genes in early KO/shC and KO/sh2TNC tumors (N=2) and selection of 21 APS-related genes **(B)** of which 7 were investigated by qRTPCR (N=5) **(C). (D)** Kegg plot with representation of the molecules involved in antigen processing and presentation where TNC-induced molecules are marked. **(E)** FACS analysis of CD8+ and CD3+ cells, represented as % of all CD45+ cells in early WT/shC and WT/sh2TNC tumors (N=7). Mean +/- SD **(F, G)** Representative IF images **(F)** and quantification **(G)** of CD8+ T cell infiltration in early TNC-high (WT/shC) and TNC-low (KO/sh2TNC) tumors (N=5 tumors). **(H, I)** Expression of granzyme B and perforin in early TNC-high (WT/shC) and TNC-low (KO/sh2TNC) tumors by qRTPCR (TNC-high, N=5; TNC-low, N=6). **(J)** Kaplan Meier relapse free survival of breast cancer patients grade III (total of 444 patients) in correlation with expression of the APS signature below (n= 222 patients) or above the median (n= 222 patients). HR=0.49 (0.36 – 0.68), p<0.00001. Scale bar: 50µm

Figure 3

A — NT193 cells — shC / sh2TNC

B — NT193 late — WT/shC / WT/sh2TNC

C — NT193 late — WT/shC / KO/sh2TNC

D — MMTV-NeuNT — Row Z-Score — WT / TNCKO

E — NT193 - late — % CD8+/CD45+ cells — WT/shC, WT/shTNC — p=0.08

F — MMTV-NeuNT — % CD8+/CD45+ cells — WT, TNCKO — *

G — NT193 TNC-high — NT193 TNC-low — Late stage — TNC, CD8, LM

H — CD8+ cells (%) — Matrix, Tumor nest — TNC high, TNC low — *
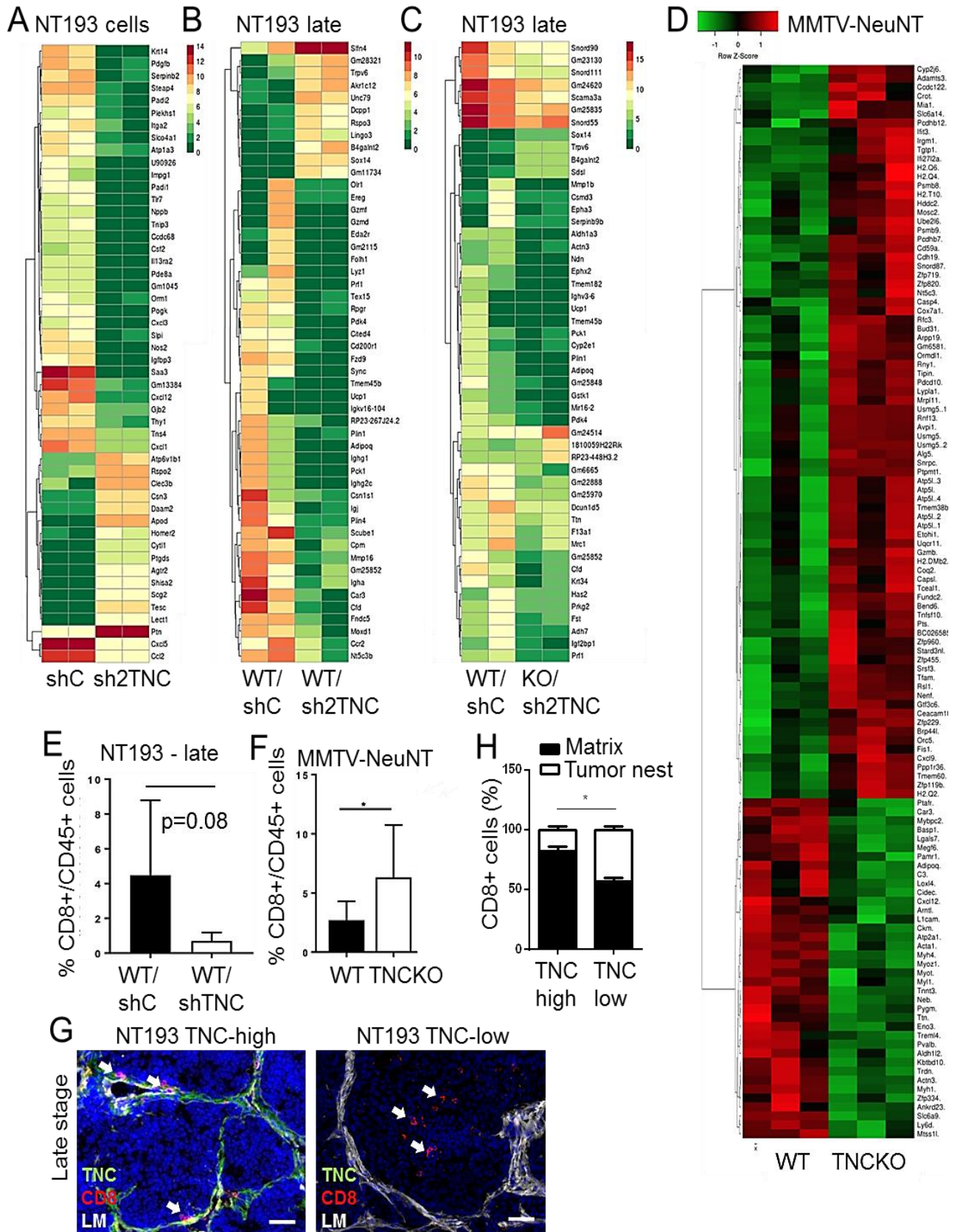
Figure 3. Differential gene expression and spatial distribution of CD8+ T cells in late stage tumors (A-B) Heatmaps showing expression of the 50 most deregulated genes **(A-C)** and all genes with a minimal fold change of 1.5 **(D)** in cultured NT193 shC and sh2TNC cells **(A),** late stage WT/shC and WT/sh2TNC tumors **(B)**, WT/shC and KO/sh2TNC tumor **(C)** (N=2) and MMTV-NeuNT WT and TNCKO tumors (N=3) **(D)**. **(E-F)** FACS analysis of CD8+ and CD3+ cells, represented as % of all CD45+ cells in late WT/shC (N=7) and WT/sh2TNC tumors (N=5) **(E)** and MMTV-NeuNT WT (N=11) and TNCKO tumors (N=5) **(F)**. Mean +/- SD **(G, H)** Loco-spatial distribution and abundance of CD8+ T cells in late stage TNC-high (WT/shC) and TNC-low (KO/sh2TNC) tumors upon IF staining **(G)** and quantification in matrix-rich areas and tumor cell nests, respectively **(H),** N=5 tumors, 3 slides, 8 random fields per tumor). Scale bar: 50 µm
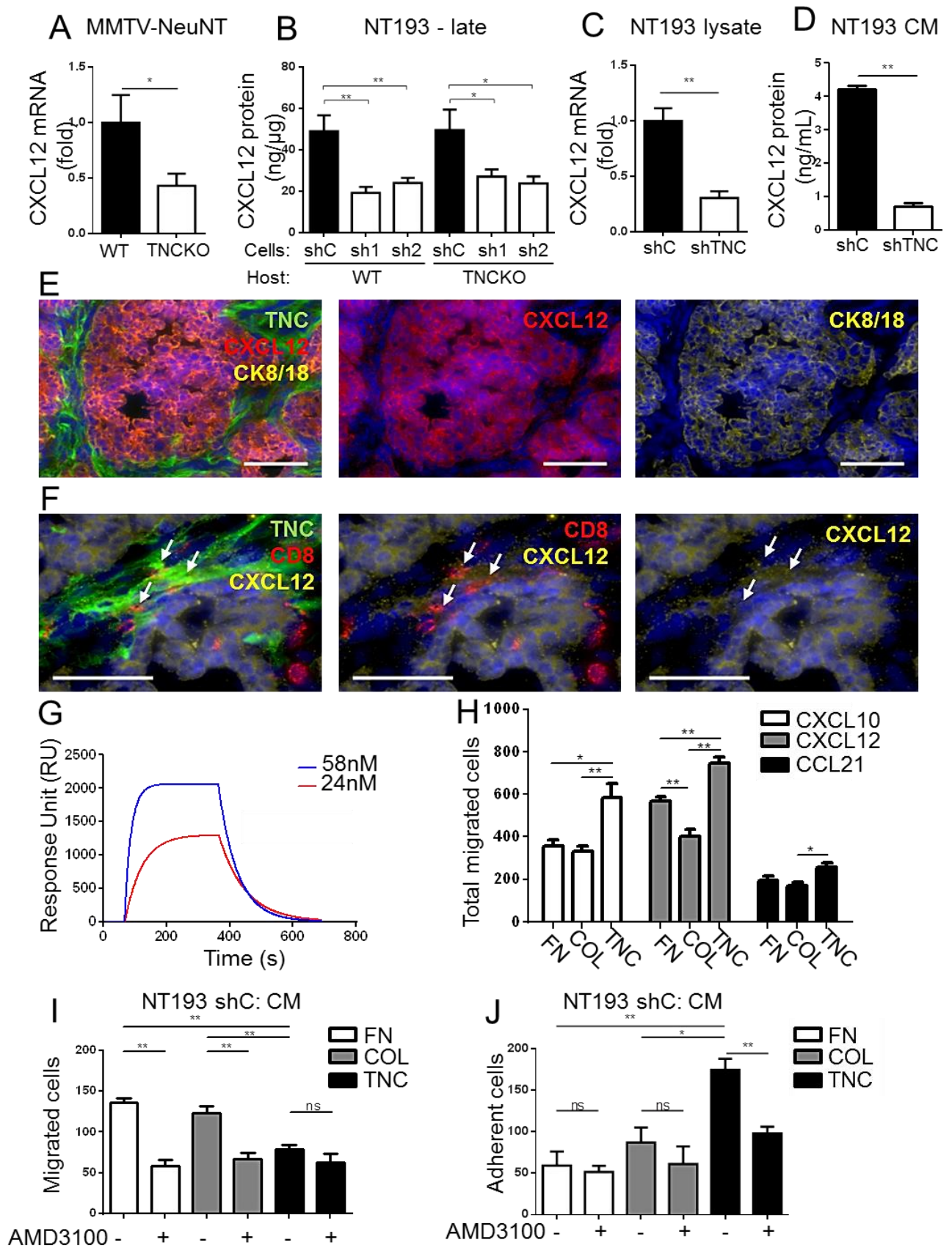
Figure 4

Figure 4. TNC-CXCL12 axis impacts CD8+ T cells (A-F) Expression of CXCL12 in MMTV-NeuNT (WT, N=13; TNCKO, N=6) **(A)** late stage NT193 tumors (N=7 for each group) **(B),** and in lysate (N=5) **(C)** and conditioned medium (CM) (N=6) **(D)** from cultured NT193 cells (N=5) as assessed by qRTPCR **(A-C)** and ELISA **(D)**. **(E, F)** Representative IF image of CXCL12 expression in a late stage WT/shC tumor. Arrow points at CD8+ T cells in close proximity to CXCL12 inside the TNC-rich TMT. Scale bars = 50 μm. **(G)** Surface plasmon resonance binding assay on chip-immobilized recombinant TNC with recombinant mouse CXCL12 at the indicated concentrations (KD: 7.9E-07M). **(H-J)** Boyden chamber transwell migration assays with ECM coating (FN, Col I, TNC) of the lower surface of the insert and the following chemoattractants, CXCL10, CXCL12, CCL21 **(H)** and CM from NT193 shC cells **(I, J)**. Floating **(I)** or adherent CD8+ T cells **(J)** or the sum of both **(H)** upon addition of AMD3100 **(I, J)** were assessed by FACS or, by counting upon fixation **(I, J)**, respectively (N=3 in duplicates).

Figure 5

A

Control
AMD3100

B

C Control   D AMD3100

TNC CD8   TNC CD8

E

F Control   G AMD3100

Cl.Casp3   Cl.Casp3

H

I

TNC
① ② DEATH ③
?

④ ⑤ ⑥ GROWTH ⑦

Surveillance
Escape
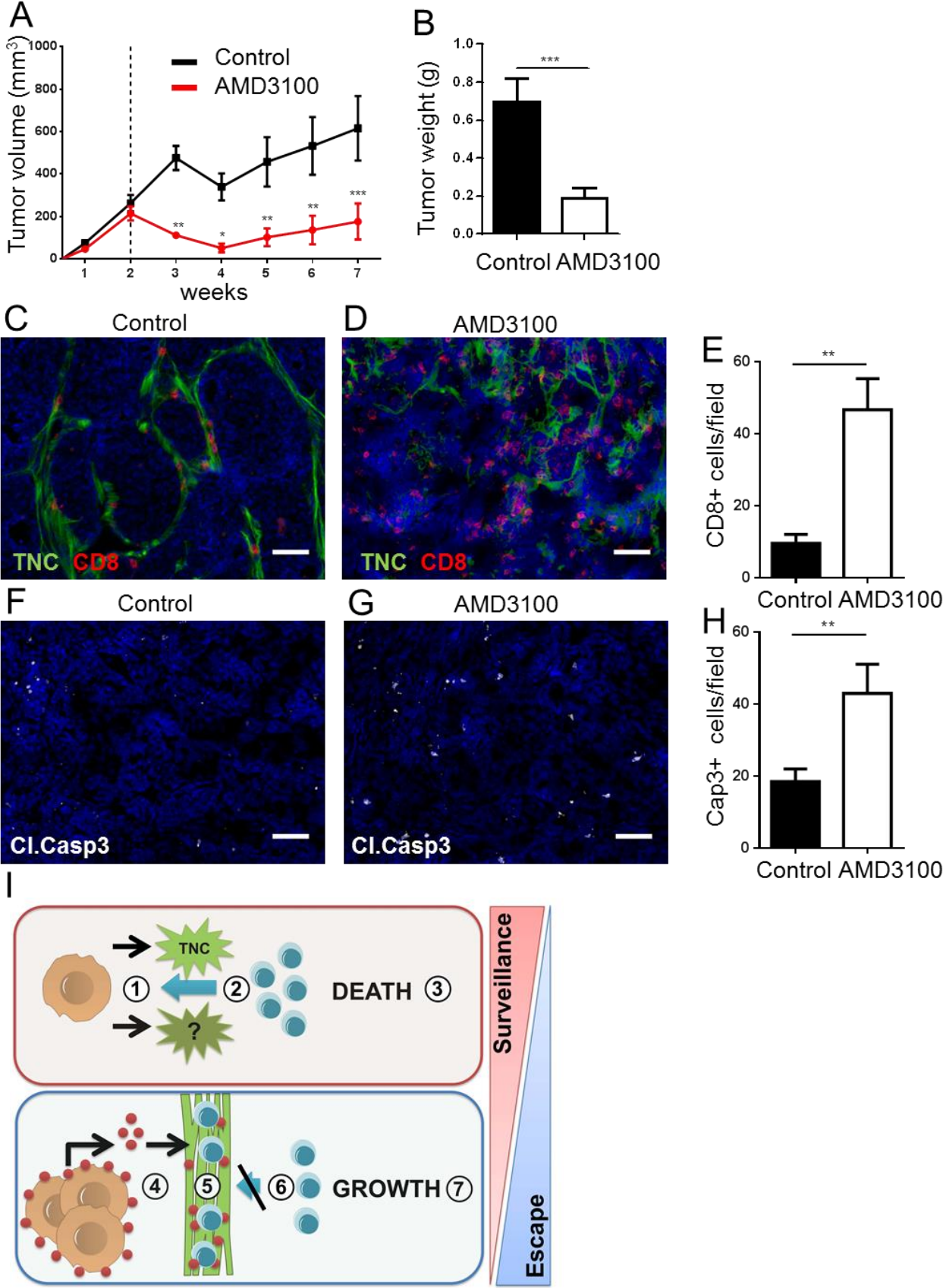
Figure 5. Inhibition of CXCR4 enhances tumor rejection. (A, B) Growth curve **(A)** and final volume **(B)** of WT/shC tumors upon treatment with AMD3100 (5mg/kg/day) or control solution for 5 weeks (N=20). **(C, D)** Representative IF images **(C, D, F, G)** and quantification of CD8+ T cells **(E)** and apoptosis (Cl. caspase 3) **(H)** in control and AMD3100 tumors (N=5). Scale bar: 50 µm. **(I)** Tumor cells express TNC or other molecules in a TNC-dependent manner (1.) that are recognized by the host and elicit expression of an antigen presenting signature APS, thereby presumably priming CD8+ T cells. These primed CD8+ T cells are recruited into the tumor epithelium where they kill the tumor cells (2.) thereby eliminating the cancer cells and providing successful immune surveillance (3.). Escapers proliferate and express CXCL12 in a TNC dependent manner. Here expression of CXCL12 induced by TNC in the tumor cells might be instrumental. High CXCL12 concentrations may generate a repellent shield for CD8+ T cells (4.). CXCL12 also binds to TNC in the tumor matrix tracks where it attracts CD8+ T cells and immobilizes them (5.), thereby preventing their entry into the tumor epithelial nests (6.). In consequence, tumor cells are protected from killing by CD8+ T cells and continue to thrive (7.) and, form metastasis as recently be shown (Sun et al.,submitted). In summary, TNC may be a critical player in orchestrating the balance between surveillance and escape.
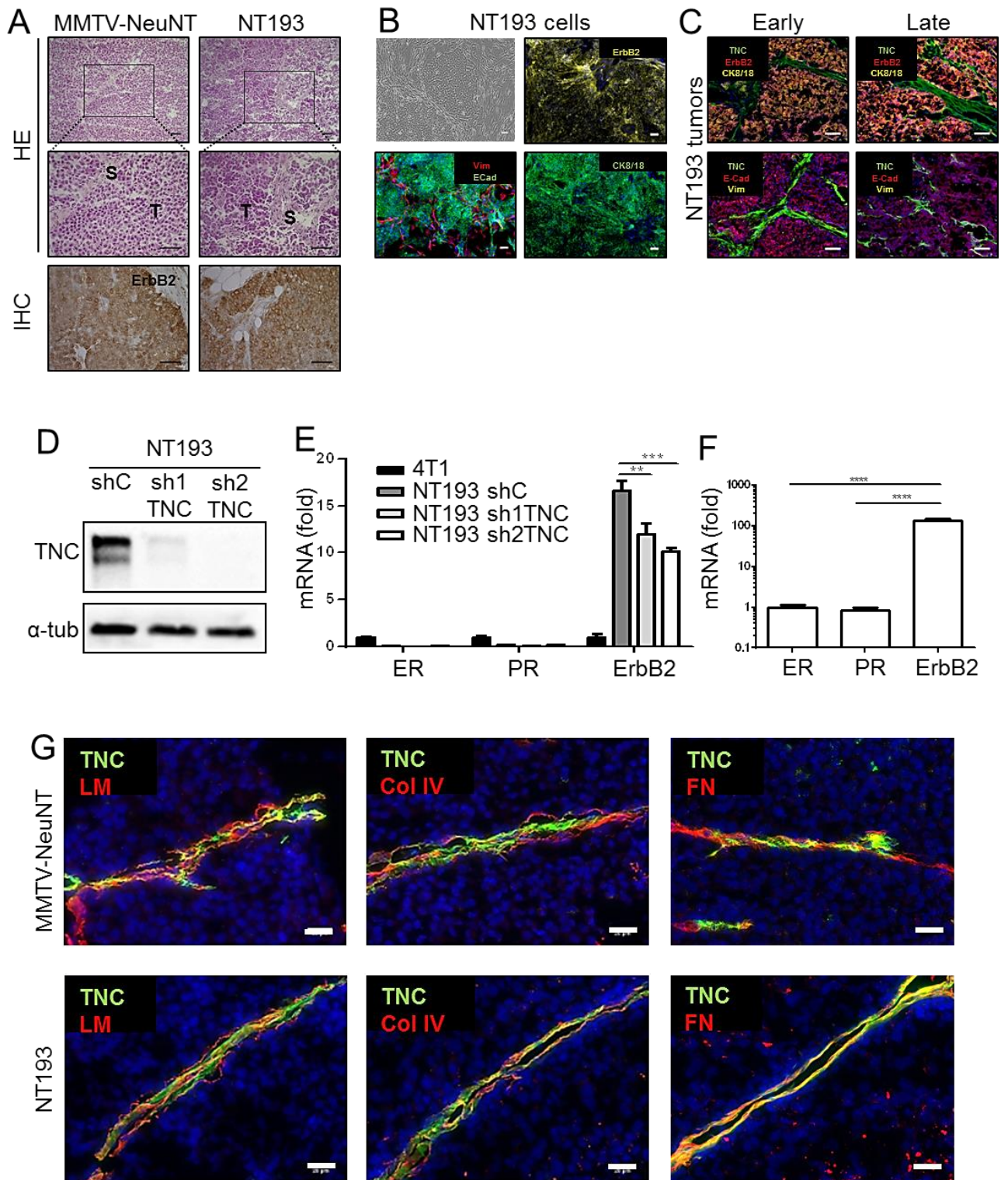
Figure S1

Figure S1. The NT193 orthotopic grafting model is a novel surrogate model to the MMTV-NeuNT model. (A) Comparative histological analysis of the NT193 grafted tumors and MMTV-NeuNT tumors by HE staining and IHC for ErbB2 expression, S: stroma and T: tumor nest. **(B)** Characterization of the NT193 cells by phase contrast and IF for ErbB2, vimentin, E-Cadherin and CK8/18 expression. **(C)** IF analysis of NT193 tumors for the corresponding markers shows that upon grafting, the NT193 cells generate epithelial tumors expressing ErbB2. This is the case both at the early stage and the late stage of tumor growth. **(D)** Immunoblot showing the knock down of TNC expression in NT193 cells with alpha tubulin as loading control. **(E)** Comparison between NT193 cells and 4T1 cells, an established triple negative cell line, at mRNA level shows that NT193 cells are ER⁻, PR⁻, and ErbB2⁺ (N=3). Knock down of TNC in the NT193 cells (sh1TNC and sh2TNC) shows lowered levels of ErbB2 compared to the control cells. **(F)** NT193 tumors express high level of ErbB2 and low levels of ER and PR at mRNA level (N=7). **(G)** Characterization of the tumor matrix tracks (TMT) in the MMTV-NeuNT and the NT193 tumors by IF for TNC, laminin, collagen IV and fibronectin. Scale bar: 50 µm.
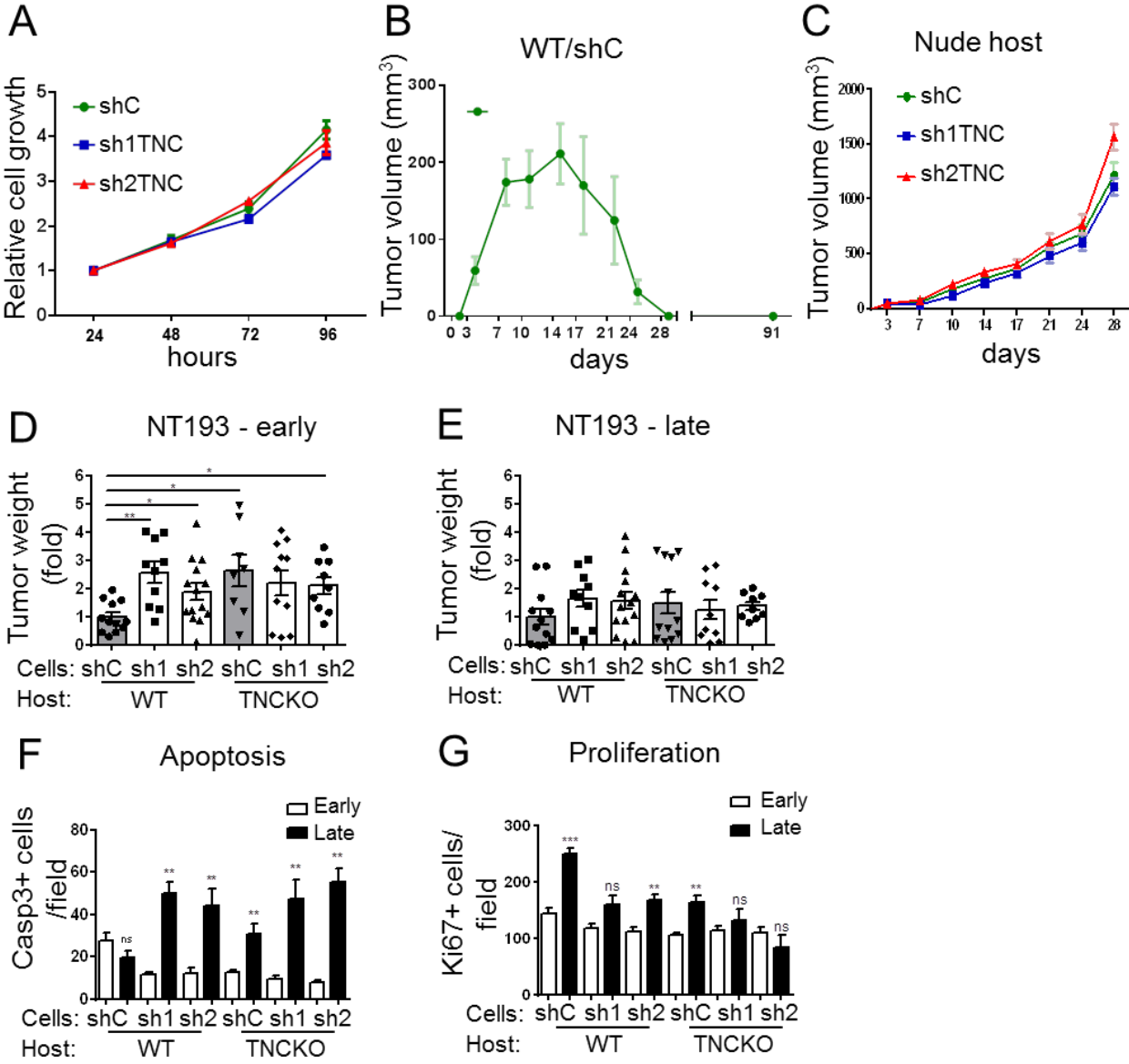
Figure S2

Figure S2. Characterization of NT193 tumors. (A) MTS multiplicity assay for NT193 cells upon lowered expression of TNC (n=9, 3 independent experiments). **(B)** Tumor growth curve for NT193 tumors that were completely rejected in the TNC WT host (n=11). **(C)** Tumor growth curves of NT193 cells injected into a nude host (n=7). **(D, E)** Relative tumor weight at early stage (3 weeks after tumor cell engraftment) and late stage (11 weeks after tumor cell engraftment) respectively, (early stage tumors: WT/shC, N = 12; WT/sh1TNC, N = 10; WT/sh2TNC, N = 14; KO/shC, N = 8; KO/sh1TNC, N = 11; KO/sh2TNC, N = 9, late stage tumors: WT/shC, N = 12; WT/sh1TNC, N = 10; WT/sh2TNC, N = 14; KO/shC, N = 12; KO/sh1TNC, N = 10; WT/sh2TNC, N = 9. **(F, G)** Comparative levels of cleaved caspase-3 and Ki67 levels in early and late stage tumors.

Figure S3
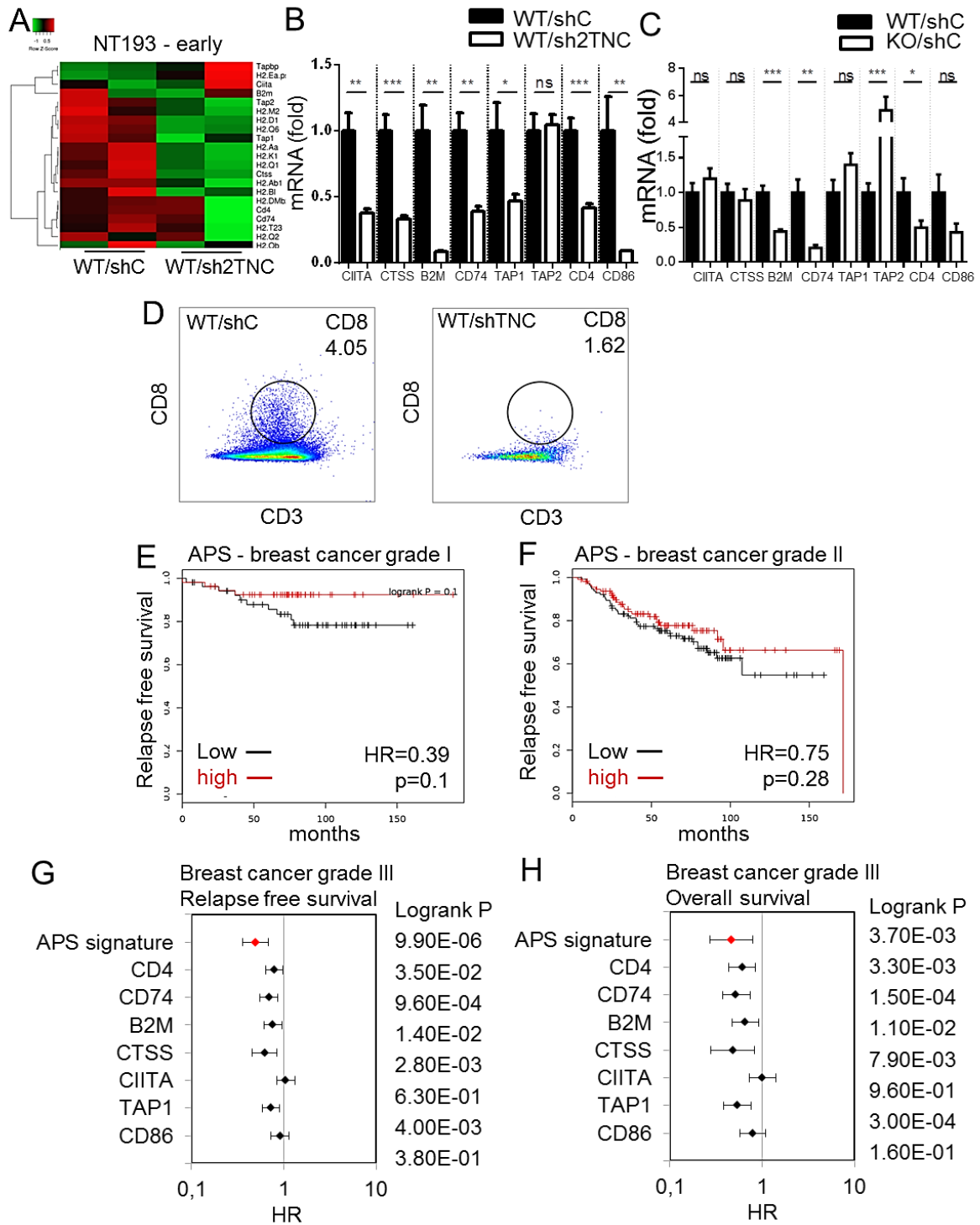
Figure S3. APS signature expression in murine tumors and breast cancer patients. (A-C) Heatmap representing expression of the antigen processing and presentation (APS)-related genes in early WT/shC and WT/sh2TNC tumors (N=2) and comparative expression of selected genes in the chosen tumor groups (N=5) (**B, C**). **(D)** Representative images of the FACS scatter plots of gated CD3+/CD8+ cells in early WT/shC and WT/sh2TNC tumors. **(E, F)** Kaplan Meier relapse free survival curves for expression of the APS signature below or above the median in breast cancer patients with grade I (N=108 patients, HR=0.39, p=0.1) and grade II (N= 227 patients, HR=0.75, p=0.28) tumors. **(G, H)** Forest plots showing the hazard ratios for expression of the APS signature (or single members of the signature) above the median in breast cancer grade III patients and, in correlation to relapse free **(F)** or overall survival **(G)**, revealing the best HR value for the APS signature.

Figure S4

A NT193 shC to sh2TNC: Upregulated genes

DNA metabolic process (GO:0006259)
sensory perception of stimulus (GO:0007606)
DNA replication (GO:0006260)
cellular process (GO:0009987)
chromosome segregation (GO:0007059)
DNA repair (GO:0006281)
cellular component movement (GO:0006928)
locomotion (GO:0040011)
cell proliferation (GO:0008283)
metabolic process (GO:0008152)

-log10 (p-value)

B NT193 shC to sh2TNC:Downregulated genes

sensory perception of stimulus (GO:0007606)
developmental process (GO:0032502)
cellular amino acid metabolic process (GO:0006520)
response to biotic stimulus (GO:0009607)
cellular component morphogenesis (GO:0032989)
defense response to bacterium (GO:0042742)
complement activation (GO:0006956)
B cell mediated immunity (GO:0019724)
immune response (GO:0006955)
cell adhesion (GO:0007155)

-log10 (p-value)

C Leucocytes   Macrophages   CD4 T cells   Dendritic cells

D NT193 TNC-high

E NT193 TNC-low

F WT/shC - late   WT/shTNC - late

G NeuNT-TNCKO   NeuNT-WT

Figure S4. Characterization of late stage NT193 tumors (A, B) Comparative gene ontology analysis of late stage WT/shC and WT/sh2TNC tumors showing the 10 most significantly enriched gene annotations. **(C, D)** Representative single **(C)** or mosaic **(D)** IF images of ECM and the indicated immune cells in late stage TNC-high (WT/shC) and TNC-low (KO/sh2TNC) tumors (N=5). White arrows point at CD8+ T cells present inside the tumor cell nest. Scale bar: 50 μm.
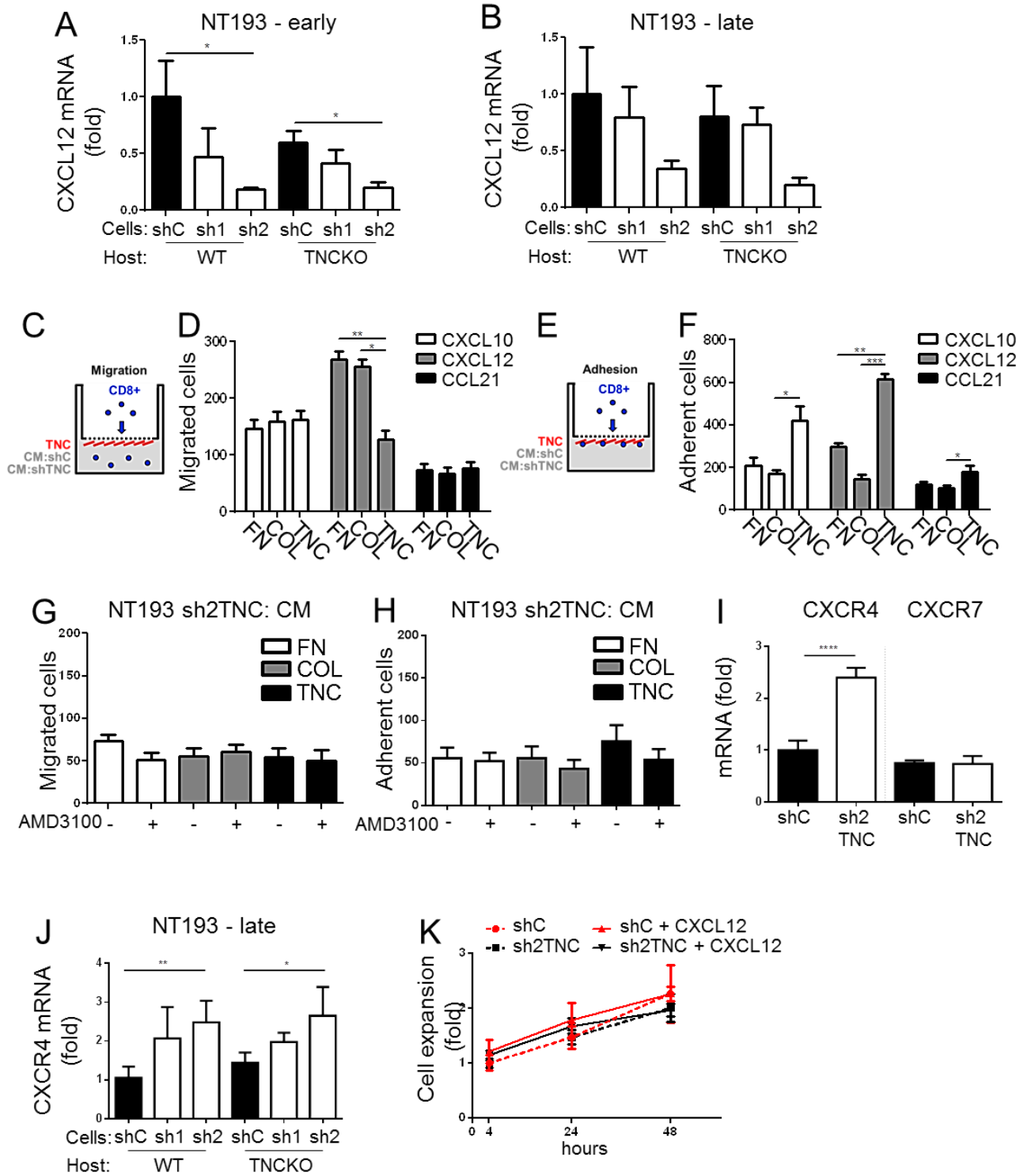
Figure S5

Figure S5. TNC upregulates expression of CXCL12 and impacts migration of CD8+ T cells towards a CXCL12 gradient. (A, B) Expression of CXCL12 in early (N=5) (A) and late (N=7) (B) NT193 tumors. **(C-H)** Boyden chamber transwell migration assays of CD8+ T cells towards the corresponding chemokine gradient (CXCL10, CXCL12, CCL21) **(D, E)** or CM from NT193:sh2TNC cells **(G, H)** and, coating of the lower side of the insert by FN, Coll I and TNC, respectively **(D, E)**. **(C, D)** schematic representation of the experimental setup to determine the attracted/floating and adherent cells towards a chemokine gradient (here depicted by CM). Assessment of floating cells (**C, D,G**) and adherent cells (**E, F, H**) (N=3 in duplicates). **(I, J)** Expression of CXCR4 (N=5) and CXCR7 (N=6) in cultured NT193 shC and sh2TNC cells **(I)** and in late stage NT193 tumors **(J)** by qRTPCR. **(K)** MTS multiplicity assay for NT193 shC and sh2TNC cells upon treatment with recombinant murine CXCL12 (N=3).

Figure S6
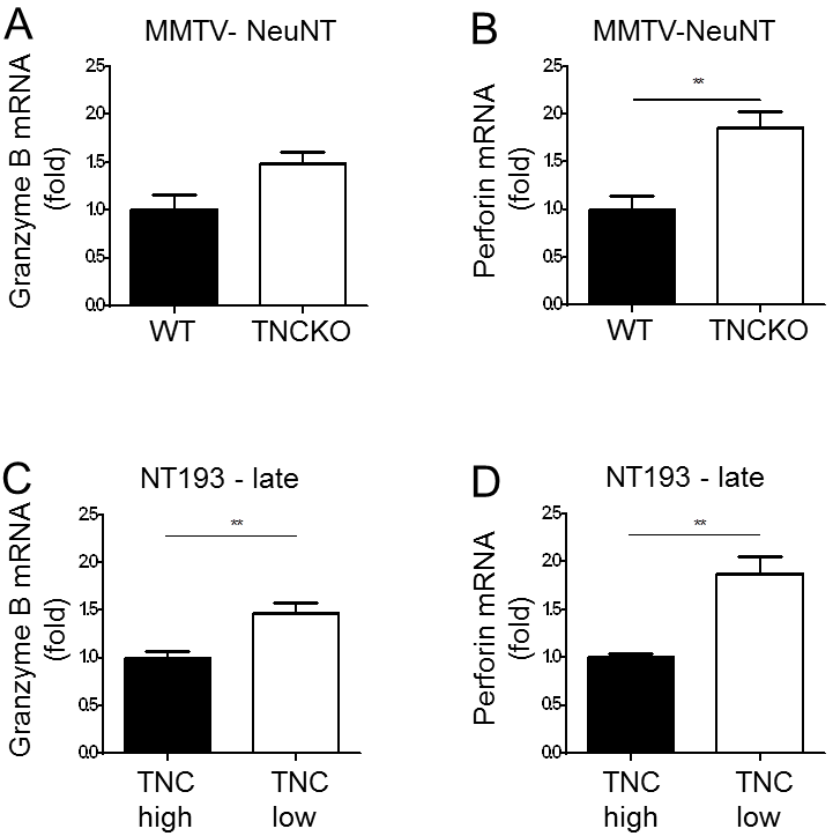
Figure S6. TNC dependent expression of cytotoxicity markers. Expression of granzyme B and perforin by qRTPCR in MMTV-NeuNT (WT, N = 5; TNCKO, N = 11) (A, B) and NT193 late stage TNC-high (WT/shC) and TNC-low (KO/sh2TNC) tumors (N=6) (C, D) by qRTPCR.

3.8. Supplementary tables

Table S1	List of antibodies				
Antigen	**Host**	**Antibody reference**	**Company**	**Dilution**	**Application**
TNC	Rat	(Aufderheide and Ekblom 1988)		2 µg/mL 0.4 µg/mL	IF WB
ErbB2	Rabbit	MA5-13675	ThermoFisher	1/50	IF
Cytokeratin CK8/18	Guinea pig	GP11	Progen	1/500	IF
Pan-laminin Ln6 7s	Rabbit	(Simo et al. 1992)		1/2000	IF
Collagen IV	Rabbit	(De Arcangelis et al. 1996)		1/200	IF
Fibronectin	Rabbit	F3648	Sigma	1/200	IF
E-cadherin	Rat	13-1900	Life technology	1/200	IF
Vimentin	Rabbit	2707-1	Epitomics	1/500	IF
α-tubulin	mouse	3873S	Cell signaling	1/2000	WB
Caspase-3 cleaved	Rabbit	9661	Cell signaling	1/500	IF
Ki-67	Rabbit	RM-9106	Thermofisher	1/600	IF
CD8a	Rat	550281	BD Pharmingen	1/400	IF
CD4	Rat	553727	BD Pharmingen	1/800	IF
CD45	Rat	550566	BD Pharmingen	1/500	IF
F4/80	Rat	MCA497G	AbD serotec	1/50	IF
CD11c	Guinea pig	550283	BD Pharmingen	1/50	IF
CXCL12	Rabbit	Ab9797	Abcam	1/1000	IF
CD8a	REAfinity Recombinant	130-109-248	Miltenyi Biotec	1/10	Flow cytometry
CD11c	REAfinity Recombinant	130-110-701	Miltenyi Biotec	1/50	Flow cytometry
CD4	REAfinity Recombinant	130-109-418	Miltenyi Biotec	1/10	Flow cytometry

Table S2. List of primers for RTqPCR

Gene	Forward primer (5' to 3')	Reverse primer (5' to 3')
ER	TTTCTGTCCAGCACCTTGAA	CCAGGAGCAGGTCATAGAGG
PR	GGTGGAGGTCGTACAAGCAT	CTCATGGGTCACCTGGAGTT
ErbB2	CCTGCCCTCTGAGACTGATG	CAAGTACTCGGGGGTTCTCCA
CIITA	CCCTGCGTGTGATGGATGTC	ATCTCAGACTGATCCTGGCAT
CTSS	CATTCCTCCTTCTTCTTCTAC	CCTTGETCACCAAAGTTAAGG
B2M	CCCCACTGAGACTGATACATACG	CGATCCCAGTAGACGGTCTTG
CD74	CAACGCGACCTCATCT	TGTTGCCGTACTTGGTAA
TAP1	GGACTTGCCTTGTTCCGAGAG	GCTGCCACATAACTGATAGCGA
TAP2	TGTATCTAGTCATACGGAGG	TATCCCCGTACATGTAAACC
CD86	ACAGAGAGACTATCAACCTG	GAATTCCAATCAGCTGAGAAC
Granzyme B	Taqman probe: Mm00442837_m1 Thermofisher	
Perforin	Taqman probe: Mm00812512_m1 Thermofisher	
CXCL12	Taqman probe: Mm00445553_m1 Thermofisher	
CXCR4	Taqman probe: Mm01996749_s1 Thermofisher	
CXCR7	Taqman probe: Mm00442837_m1 Thermofisher	

Table S3. Gene expression of NT193 shC and NT193 sh2TNC cells

RNA sequencing data, p-value <0.1, 50 most upregulated and 50 most downregulated genes, N = 2

Gene name	Log2 fold change	P value	padj
Saa3	9.39863765	1.51E-77	8.16E-74
Cxcl12	7.153371117	2.21E-50	4.46E-47
Krt14	6.889690074	1.44E-36	1.37E-33
Cxcl5	6.502533727	1.66E-89	2.68E-85
Steap4	6.248165654	1.38E-35	1.24E-32
Pdgfb	6.128383532	3.8E-33	2.79E-30
Serpinb2	5.920109667	1.86E-32	1.31E-29
Nos2	5.710887396	5.15E-25	2.38E-22
Padi2	5.577910018	6.37E-27	3.43E-24
Tns4	5.567321043	6.74E-46	9.9E-43
Pogk	5.368390202	4.47E-20	1.25E-17
Igfbp3	5.314731738	4.23E-21	1.37E-18
Cxcl1	5.244019495	3.07E-44	4.13E-41
Gjb2	5.125635668	2.17E-31	1.41E-28
Ccl2	5.068071509	1.62E-47	2.9E-44
Serpina3h	5.065659758	6.45E-51	1.49E-47
U90926	4.907715173	6.7E-16	1.29E-13
Thy1	4.880710438	6.35E-26	3.11E-23
Slco4a1	4.877155179	6.4E-19	1.59E-16
Slpi	4.803905442	5.98E-17	1.25E-14
Cxcl3	4.75424686	5.68E-15	9.27E-13
Tnc	4.715648115	4.19E-55	1.35E-51
Mmp3	4.593496226	1.02E-37	1.1E-34
Serpina3i	4.546413964	1.49E-34	1.15E-31
Atp1a3	4.534362701	2.06E-18	4.81E-16
Kcnn3	4.485197535	1.16E-17	2.6E-15

Tmem176b	4.456659166	3.11E-35	2.65E-32
Armcx4	4.442972183	2.67E-22	1E-19
Acap1	4.438714527	3.16E-17	6.71E-15
Mmp9	4.268628295	5.64E-23	2.4E-20
Klhdc8a	4.248934911	1.7E-15	3.09E-13
Stra6	4.238070222	8.16E-24	3.57E-21
Padi1	4.229427673	2.3E-12	2.66E-10
Itga2	4.177137739	3.28E-16	6.47E-14
Tnip3	4.169126714	3.39E-11	3.39E-09
Sod3	4.080621611	1.06E-36	1.07E-33
Lama3	4.072176543	8.99E-17	1.86E-14
Impg1	4.057481528	2.05E-10	1.75E-08
Ccdc68	4.053616554	1.47E-10	1.3E-08
Anxa8	3.980989005	6.27E-20	1.72E-17
Gria1	3.914980398	3.67E-13	4.95E-11
Bst1	3.893105957	2.58E-20	8.02E-18
Il13ra2	3.853183874	1.77E-09	1.26E-07
Epgn	3.831373897	1.59E-13	2.24E-11
Tlr7	3.817643962	9.43E-10	7.05E-08
Pde8a	3.811065211	2.78E-09	1.84E-07
Dapk1	3.80293621	6.63E-14	1E-11
Plekhs1	3.788679173	9.05E-11	8.17E-09
Slc16a2	3.771438654	2.76E-20	8.25E-18
Celsr1	3.767860636	1.92E-16	3.87E-14
Pik3r1	-0.740101131	0.014748	0.094116
Cpe	-0.740300379	0.01319	0.086535
Sash1	-0.745227273	0.013369	0.087423
Egfr	-0.746491969	0.012822	0.084945
Eef1a1	-0.748722012	0.014219	0.091587
Ndufb9	-0.761400241	0.013988	0.090413
Eps8	-0.762677013	0.014516	0.092896
Gas1	-0.762854031	0.010945	0.076393
Nt5dc2	-0.766239971	0.015742	0.098462

Cmtm4	-0.768919313	0.012142	0.082089
Eif4b	-0.769476577	0.010609	0.0745
Map1lc3b	-0.774286993	0.011586	0.079435
Pygb	-0.774490862	0.012245	0.082373
Cnn3	-0.775706546	0.010712	0.075108
Nacc2	-0.776289344	0.015747	0.098462
Nab2	-0.781348975	0.011117	0.077357
Cd82	-0.786478879	0.013315	0.087108
Cyb5r1	-0.789300945	0.012904	0.085316
Nedd4l	-0.794838894	0.013492	0.088047
Aldh1l2	-0.796145796	0.007151	0.056305
Neat1	-0.79702844	0.007721	0.059485
Cul7	-0.801448892	0.013513	0.08808
Asap1	-0.803380851	0.008363	0.063177
Idh2	-0.804059966	0.010665	0.074825
Cdk5rap3	-0.805242981	0.015724	0.098462
Gramd1b	-0.806515765	0.01278	0.084805
Tiam2	-0.813241879	0.009655	0.069893
Ppp1r12b	-0.813311678	0.010927	0.076298
Ppt1	-0.814144204	0.012364	0.083002
Oxct1	-0.81626631	0.00759	0.058962
Cdh11	-0.822805757	0.006642	0.053527
Rev3l	-0.823575364	0.009541	0.069318
Coq9	-0.823584538	0.012565	0.083793
Sh3d19	-0.825209065	0.010446	0.073606
Tbx15	-0.82629365	0.009395	0.068658
Meis1	-0.830464554	0.014405	0.09244
Tpt1-ps3	-0.83336779	0.013679	0.088909
Ssbp2	-0.834253916	0.01282	0.084945
Enpp2	-0.838432894	0.009917	0.07115
Txnip	-0.840139535	0.008752	0.065045
Tacc1	-0.842849297	0.005211	0.044401
Bsg	-0.843170432	0.015583	0.097901

Prdm5	-0.84363056	0.016036	0.09993
Lama4	-0.843874616	0.005985	0.049282
Marcks	-0.844037633	0.013974	0.090391
Coro7	-0.845046256	0.014879	0.094581
Prpf40b	-0.84513028	0.012405	0.083103
Rsrc1	-0.848133216	0.010233	0.072794
Trabd2b	-0.849518	0.013021	0.085774
Gba	-0.851301581	0.00874	0.065018

Table S4. Gene expression of late stage WT-shC and WT-sh2TNC tumors

RNA sequencing data, p-value <0.1, 50 most upregulated and 50 most downregulated genes, N = 2

Genename	Log2foldchange	pvalue	padj
Saa3	9.39863765	1.51E-77	8.16E-74
Cxcl12	7.153371117	2.21E-50	4.46E-47
Krt14	6.889690074	1.44E-36	1.37E-33
Cxcl5	6.502533727	1.66E-89	2.68E-85
Steap4	6.248165654	1.38E-35	1.24E-32
Pdgfb	6.128383532	3.8E-33	2.79E-30
Serpinb2	5.920109667	1.86E-32	1.31E-29
Nos2	5.710887396	5.15E-25	2.38E-22
Padi2	5.577910018	6.37E-27	3.43E-24
Tns4	5.567321043	6.74E-46	9.9E-43
Pogk	5.368390202	4.47E-20	1.25E-17
Igfbp3	5.314731738	4.23E-21	1.37E-18
Cxcl1	5.244019495	3.07E-44	4.13E-41
Gjb2	5.125635668	2.17E-31	1.41E-28
Ccl2	5.068071509	1.62E-47	2.9E-44
Serpina3h	5.065659758	6.45E-51	1.49E-47
U90926	4.907715173	6.7E-16	1.29E-13
Thy1	4.880710438	6.35E-26	3.11E-23
Slco4a1	4.877155179	6.4E-19	1.59E-16
Slpi	4.803905442	5.98E-17	1.25E-14
Cxcl3	4.75424686	5.68E-15	9.27E-13
Tnc	4.715648115	4.19E-55	1.35E-51
Mmp3	4.593496226	1.02E-37	1.1E-34
Serpina3i	4.546413964	1.49E-34	1.15E-31
Atp1a3	4.534362701	2.06E-18	4.81E-16
Kcnn3	4.485197535	1.16E-17	2.6E-15

Tmem176b	4.456659166	3.11E-35	2.65E-32
Armcx4	4.442972183	2.67E-22	1E-19
Acap1	4.438714527	3.16E-17	6.71E-15
Mmp9	4.268628295	5.64E-23	2.4E-20
Klhdc8a	4.248934911	1.7E-15	3.09E-13
Stra6	4.238070222	8.16E-24	3.57E-21
Padi1	4.229427673	2.3E-12	2.66E-10
Itga2	4.177137739	3.28E-16	6.47E-14
Tnip3	4.169126714	3.39E-11	3.39E-09
Sod3	4.080621611	1.06E-36	1.07E-33
Lama3	4.072176543	8.99E-17	1.86E-14
Impg1	4.057481528	2.05E-10	1.75E-08
Ccdc68	4.053616554	1.47E-10	1.3E-08
Anxa8	3.980989005	6.27E-20	1.72E-17
Gria1	3.914980398	3.67E-13	4.95E-11
Bst1	3.893105957	2.58E-20	8.02E-18
Il13ra2	3.853183874	1.77E-09	1.26E-07
Epgn	3.831373897	1.59E-13	2.24E-11
Tlr7	3.817643962	9.43E-10	7.05E-08
Pde8a	3.811065211	2.78E-09	1.84E-07
Dapk1	3.80293621	6.63E-14	1E-11
Plekhs1	3.788679173	9.05E-11	8.17E-09
Slc16a2	3.771438654	2.76E-20	8.25E-18
Celsr1	3.767860636	1.92E-16	3.87E-14
Pik3r1	-0.740101131	0.014748	0.094116
Cpe	-0.740300379	0.01319	0.086535
Sash1	-0.745227273	0.013369	0.087423
Egfr	-0.746491969	0.012822	0.084945
Eef1a1	-0.748722012	0.014219	0.091587
Ndufb9	-0.761400241	0.013988	0.090413
Eps8	-0.762677013	0.014516	0.092896
Gas1	-0.762854031	0.010945	0.076393
Nt5dc2	-0.766239971	0.015742	0.098462

Cmtm4	-0.768919313	0.012142	0.082089
Eif4b	-0.769476577	0.010609	0.0745
Map1lc3b	-0.774286993	0.011586	0.079435
Pygb	-0.774490862	0.012245	0.082373
Cnn3	-0.775706546	0.010712	0.075108
Nacc2	-0.776289344	0.015747	0.098462
Nab2	-0.781348975	0.011117	0.077357
Cd82	-0.786478879	0.013315	0.087108
Cyb5r1	-0.789300945	0.012904	0.085316
Nedd4l	-0.794838894	0.013492	0.088047
Aldh1l2	-0.796145796	0.007151	0.056305
Neat1	-0.79702844	0.007721	0.059485
Cul7	-0.801448892	0.013513	0.08808
Asap1	-0.803380851	0.008363	0.063177
Idh2	-0.804059966	0.010665	0.074825
Cdk5rap3	-0.805242981	0.015724	0.098462
Gramd1b	-0.806515765	0.01278	0.084805
Tiam2	-0.813241879	0.009655	0.069893
Ppp1r12b	-0.813311678	0.010927	0.076298
Ppt1	-0.814144204	0.012364	0.083002
Oxct1	-0.81626631	0.00759	0.058962
Cdh11	-0.822805757	0.006642	0.053527
Rev3l	-0.823575364	0.009541	0.069318
Coq9	-0.823584538	0.012565	0.083793
Sh3d19	-0.825209065	0.010446	0.073606
Tbx15	-0.82629365	0.009395	0.068658
Meis1	-0.830464554	0.014405	0.09244
Tpt1-ps3	-0.83336779	0.013679	0.088909
Ssbp2	-0.834253916	0.01282	0.084945
Enpp2	-0.838432894	0.009917	0.07115
Txnip	-0.840139535	0.008752	0.065045
Tacc1	-0.842849297	0.005211	0.044401
Bsg	-0.843170432	0.015583	0.097901

Prdm5	-0.84363056	0.016036	0.09993
Lama4	-0.843874616	0.005985	0.049282
Marcks	-0.844037633	0.013974	0.090391
Coro7	-0.845046256	0.014879	0.094581
Prpf40b	-0.84513028	0.012405	0.083103
Rsrc1	-0.848133216	0.010233	0.072794
Trabd2b	-0.849518	0.013021	0.085774
Gba	-0.851301581	0.00874	0.065018

Table S5. Gene expression of late stage WT-shC and KO-sh2TNC tumors

RNA sequencing data, p-value <0.1, 50 most upregulated and 25 most downregulated genes, N = 2

Genename	Log2foldchange	pvalue	padj
Cfd	3.902923	3.54E-08	4.77E-05
Aldh1a3	3.64824	1.32E-07	0.000119
Snora34	3.322463	1.12E-11	8.62E-08
Scarna3a	3.289446	2.05E-07	0.000166
Snord90	3.250772	1.66E-06	0.001158
Adh7	3.235122	5.4E-06	0.002568
Igf2bp1	3.184942	8.74E-06	0.003527
Prkg2	3.169095	1.92E-06	0.001282
Krt34	3.159725	9.8E-06	0.003822
Snord17	3.0924	4.07E-07	0.000312
Akr1c14	3.081198	3.03E-06	0.001855
Snord111	3.074667	3.92E-06	0.002074
Fst	3.060685	1.55E-05	0.005166
Pdk4	3.051571	1.69E-05	0.005524
Scarna6	2.948318	4.58E-06	0.002266
Cd200r1	2.934992	3.16E-06	0.00186
Snord87	2.901348	5.53E-06	0.002568
Dcun1d5	2.837775	4.84E-05	0.011594
Adam22	2.819852	4.55E-05	0.011252
F13a1	2.809306	7.12E-05	0.015827
Prf1	2.78798	5.96E-05	0.013644
Mir1955	2.782776	6.33E-06	0.002773
Mgat3	2.78001	4.43E-05	0.011252
Plin1	2.77372	0.000148	0.027675
Adipoq	2.714306	0.000205	0.029654
n-R5s122	2.711125	2.82E-05	0.008617

Gene	Value 1	Value 2	Value 3
Mir16-2	2.704402	0.000188	0.029654
Lpl	2.704007	1.58E-10	8.07E-07
Mmp13	2.693217	3.69E-06	0.002017
Scarna3b	2.666584	1.47E-05	0.005008
Abca8a	2.640221	4.62E-05	0.011252
Ttn	2.635373	0.000197	0.029654
Csmd3	2.574389	0.000445	0.049106
Rny1	2.572595	6.59E-12	8.62E-08
Hoxc8	2.543204	9.17E-05	0.019264
Snora2b	2.522576	9.97E-06	0.003822
Gstk1	2.517885	0.000551	0.054494
Snora7a	2.499019	0.000153	0.027675
Ccdc80	2.49833	1.53E-08	2.61E-05
Ephx2	2.49829	0.000647	0.059522
Scn7a	2.494671	5.41E-05	0.012763
Fabp4	2.4799	7.86E-05	0.016961
Actn3	2.476001	0.000689	0.062531
Has2	2.465093	0.000584	0.055963
n-R5s139	2.459577	0.000173	0.02953
Snord55	2.453238	0.000438	0.0487
Yap1	2.445397	0.000357	0.043408
Zfp521	2.444163	0.000111	0.021818
Hspb8	2.427201	0.00032	0.040509
Lrrk2	2.423052	4E-05	0.010757
Itgb4	-1.25564	0.001158	0.088274
Arhgef1	-1.31009	0.001165	0.088424
Tbc1d17	-1.37874	0.001243	0.092454
Lgals3	-1.38294	0.000409	0.047057
Psmb9	-1.39749	0.000868	0.073911
Samd10	-1.48962	0.000886	0.074331
Lsr	-1.49287	0.000199	0.029654
Gab1	-1.49294	0.000204	0.029654
H2-DMb2	-1.65654	0.001354	0.096795

0610011F06Rik	-1.70884	0.000381	0.045305
Eps8l1	-1.86903	9.75E-05	0.020203
Dbp	-1.87867	4.24E-05	0.011213
Hba-a1	-1.93878	0.00038	0.045305
Prkcz	-1.98268	0.000508	0.051607
Mir6236	-2.03939	0.000274	0.037156
Grik3	-2.06166	0.000207	0.029654
Snph	-2.08178	0.000304	0.040104
H2-K2	-2.23477	7.06E-06	0.003005
Cpsf4l	-2.3143	0.000783	0.068587
RP23-448H3.2	-2.62194	0.000182	0.029654
Trpv6	-2.6453	0.0002	0.029654
1810059H22Rik	-2.64594	0.00018	0.029654
Sdsl	-2.67944	0.000203	0.029654
Inpp5j	-2.75202	8.13E-06	0.003369
B4galnt2	-2.91915	5.64E-05	0.013092

Table S6 Gene expression of late stage WT-shC and KO-sh2TNC tumors

RNA sequencing data, p-value <0.1, 50 most upregulated and 50 most downregulated genes, N = 2

GeneName	log2FoldChange	pvalue	padj
Nxf3	4.782327	7.53E-52	1.19E-47
1500015O10Rik	4.411205	2.83E-25	7.47E-22
Capn6	4.11556	3.68E-21	5.83E-18
4930500J02Rik	3.987005	2.32E-21	4.09E-18
Ehd3	3.880178	1.09E-35	5.79E-32
Map7d2	3.678068	1.01E-14	8.89E-12
Akr1c12	3.668848	3.52E-20	5.08E-17
Unc79	3.49069	4.75E-19	5.38E-16
Rspo3	3.38613	3.5E-14	2.92E-11
Trp63	3.338888	1.42E-24	2.81E-21
Rragd	3.314198	4.06E-16	4.3E-13
Lingo3	3.079038	1.43E-10	6.68E-08
Podxl2	2.789925	6.53E-13	4.32E-10
Dok7	2.70964	2.08E-12	1.27E-09
St8sia1	2.686302	1.94E-13	1.34E-10
Gsdma3	2.666996	1.47E-08	4.08E-06
Rtn1	2.651851	4.76E-12	2.8E-09
Abcc12	2.642471	4.59E-08	1.01E-05
Nrxn1	2.595724	7.48E-12	4.24E-09
Peg3	2.564868	1.65E-13	1.19E-10
Galk1	2.532211	1.22E-09	4.32E-07
Dbt	2.516286	2.54E-09	8.39E-07
Clstn3	2.516018	8.75E-08	1.76E-05
Otoa	2.500053	1.43E-10	6.68E-08
Dcpp2	2.482226	5.87E-08	1.26E-05
A130023I24Rik	2.472544	4.24E-07	6.94E-05

Inha	2.400048	1E-07	1.96E-05
Slc22a8	2.398335	9.13E-07	0.000129
Epha3	2.380781	8.94E-07	0.000128
Gspt2	2.270234	7.01E-07	0.000105
Dcpp1	2.238826	8.74E-08	1.76E-05
Serping1	2.235031	2.25E-08	5.58E-06
Nxf7	2.183733	1.54E-07	2.78E-05
Zmym6	2.169536	1.44E-07	2.66E-05
Calml3	2.163131	5.67E-09	1.83E-06
Gpm6b	2.155951	2.02E-06	0.000257
Comp	2.155108	1.33E-07	2.51E-05
Sall2	2.147831	5.11E-11	2.61E-08
Prom1	2.144485	2.72E-08	6.47E-06
Hdac9	2.126506	1.78E-07	3.14E-05
Glrb	2.117231	1.32E-05	0.001217
Gsdma2	2.09534	1.58E-05	0.0014
Gtsf1l	2.093008	4.08E-06	0.000449
Scn5a	2.060925	1.91E-07	3.33E-05
Il12a	2.059011	2.45E-05	0.001969
Igkv14-111	2.057077	1.81E-08	4.86E-06
Zfp521	2.043601	1.14E-07	2.2E-05
Fgg	2.029045	2.94E-06	0.000354
Luzp2	2.019896	1.36E-05	0.00124
Chad	2.000075	4.16E-05	0.003146
Chp1	-0.76537	0.00236	0.075017
Myh9	-0.76907	0.000731	0.030827
Aars	-0.77161	0.002842	0.085713
Ssh3	-0.77575	0.003193	0.092761
Tcirg1	-0.79033	0.001151	0.043257
Trpm4	-0.79561	0.002062	0.067198
Surf4	-0.8038	0.001047	0.040814
Faim2	-0.81903	0.001509	0.053201
Osbpl3	-0.81909	0.000834	0.034191

Fbln2	-0.827	0.002854	0.085901
Wipi1	-0.83558	0.002467	0.076998
Smox	-0.83909	0.002917	0.087463
Tenc1	-0.84027	0.003512	0.09845
Cep170b	-0.84077	0.000455	0.020854
Lmna	-0.85976	0.00247	0.076998
Pcdhgb2	-0.86161	0.003104	0.091181
Orai1	-0.86629	0.001546	0.05389
Arhgef26	-0.87277	0.002961	0.088119
Neat1	-0.87352	0.001032	0.04038
Spns2	-0.87769	0.001924	0.063864
Btg1	-0.88175	0.000298	0.015444
Cldn3	-0.89115	0.000156	0.009257
Rab11fip5	-0.89629	0.002932	0.087753
Mcrs1	-0.89986	0.002124	0.06863
Pdlim7	-0.89987	0.00108	0.04167
Tmem63a	-0.90091	0.00031	0.01584
Cd59a	-0.90112	0.001938	0.064188
Nr4a1	-0.90406	0.000655	0.028179
Cdc25b	-0.90877	0.001825	0.061468
Mvp	-0.91139	0.001389	0.049952
Prr14	-0.92169	0.001536	0.053795
Rps6kb2	-0.92641	0.003185	0.092721
Baz1a	-0.92697	0.001153	0.043257
Fhod1	-0.92912	0.001821	0.061457
AI846148	-0.93283	0.002455	0.07688
Igsf8	-0.93537	0.00081	0.033569
Zfp36l2	-0.9415	0.00324	0.093503
Pdlim5	-0.95046	0.000245	0.013284
Tap1	-0.95945	0.000378	0.018517
Bcl2l1	-0.96005	0.002521	0.077957
Abca7	-0.97044	0.003307	0.094855
Agfg2	-0.97137	0.002416	0.076056

Arhgef16	-0.97207	0.001137	0.043257
1700037H04Rik	-0.98462	0.002836	0.085683
Baiap2	-0.98484	0.000154	0.009201
Epn3	-0.98609	0.002003	0.065529
Ssr2	-0.98652	0.002956	0.088119
Ephb4	-0.98956	3.19E-05	0.002495
Matn2	-0.99043	0.001544	0.05389
Bcar1	-0.99273	0.000444	0.020664

Table S7. Gene expression of MMTV-NeuNT TNC WT and TNC KO tumors

Gene profiling, p-value <0.05, upregulated genes : FC > 1.5, downregulated genes : FC<0.67, N = 3

Gene Name	fold change	p-value
Myl1	4.306427	0.037067
Car3	3.823795	0.011999
Acta1	3.542491	0.009477
Atp2a1	3.23413	0.005609
Ckm	2.779926	0.003915
Myh4	2.434557	0.000764
Trdn	2.122104	0.004477
Lgals7	1.991338	0.005973
Pvalb	1.943118	0.013342
C3	1.933223	0.030531
Myh1	1.916339	0.002974
Neb	1.864235	0.007296
Ttn	1.86169	0.031816
Arntl	1.845573	0.034453
Adipoq	1.827656	0.028892
Aldh1l2	1.793551	0.042536
Actn3	1.787349	0.006973
Basp1	1.781559	0.01139
Cidec	1.763181	0.030952
Ly6d	1.723905	0.008942
Treml4	1.721668	0.042997
Myot	1.711343	0.024934
Tnnt3	1.694148	0.009523
Pygm	1.666728	0.035201
Ptafr	1.662204	0.02479
L1cam	1.654507	0.035527

Mtss1l	1.636479	0.01327
Pamr1	1.609094	0.033586
Myoz1	1.6049	0.002738
Slc6a9	1.603903	0.002174
Ankrd23	1.603234	0.03663
Eno3	1.594889	0.022113
Zfp334	1.561029	0.037268
Mybpc2	1.541567	0.003739
Loxl4	1.530589	0.044732
Kbtbd10	1.512636	0.012493
Megf6	1.504314	0.016282
Cxcl12	1.494626	0.040517
Rnf13	0.665679	0.035053
Bud31	0.665075	0.022959
Zfp719	0.664658	0.031959
Uqcr11	0.663535	0.037836
H2-DMb2	0.663304	0.043547
1810035L17Rik	0.661014	0.028921
Adamts3	0.6606	0.00871
4930420K17Rik	0.660574	0.021619
B230307C23Rik	0.659809	0.03016
Mosc2	0.659618	0.040543
Cdh19	0.658898	0.018816
Zfp820	0.656642	0.032888
Cd59a	0.6533	0.000752
H2-Q2	0.652239	0.048309
Hddc2	0.650521	0.036789
Fis1	0.6505	0.033802
Orc5	0.649939	0.010316
Avpi1	0.648424	0.034725
2810047C21Rik1	0.646438	0.043102
1810013D10Rik	0.646438	0.025499
Ptpmt1	0.645511	0.046777

Zfp119b	0.645085	0.014716
Atp5l	0.64494	0.049363
Slc6a14	0.644872	0.037944
Gtf3c6	0.644433	0.02153
Tmem60	0.643592	0.012806
Gm6581	0.643567	0.004667
Stard3nl	0.643052	0.040909
Capsl	0.637697	0.028367
3110052M02Rik	0.635966	0.001211
Coq2	0.635862	0.022556
Tceal1	0.634815	0.016322
Nt5c3	0.634399	0.048495
Atp5l	0.633038	0.044854
Arpp19	0.632942	0.013873
H2-Q4	0.632858	0.049011
Rfc3	0.632735	0.018377
Mrpl11	0.631807	0.019335
0610009D07Rik	0.631706	0.044019
Nenf	0.630896	0.01591
Pts	0.630025	0.039559
Rsl1	0.629193	0.017796
Brp44l	0.62851	0.02389
Alg5	0.627882	0.019004
Atp5l	0.627694	0.031777
Ppp1r36	0.625472	0.019345
Snord87	0.62499	0.031056
Lypla1	0.624445	0.011886
Usmg5	0.623904	0.045895
Atp5l	0.622645	0.045595
Pcdhb12	0.621653	0.028195
Zfp455	0.620817	0.047118
Rnu2-10 // Rnu2-10 // Rnu2-10 // Rnu2-10 // Rnu2-10	0.620367	0.035363

H2-Q6	0.620251	0.033787
Pcdhb7	0.615595	0.005492
Crot	0.613973	0.02248
Rnu2-10 // Rnu2-10 // Rnu2-10 // Rnu2-10 // Rnu2-10 // Rnu2-10	0.611696	0.034924
Snrpc	0.611199	0.031496
Usmg5	0.604841	0.038175
Rnu2-10 // Rnu2-10 // Rnu2-10 // Rnu2-10 // Rnu2-10 // Rnu2-10	0.604596	0.039253
Rnu2-10 // Rnu2-10 // Rnu2-10 // Rnu2-10 // Rnu2-10 // Rnu2-10	0.604596	0.039253
Rnu2-10 // Rnu2-10 // Rnu2-10 // Rnu2-10 // Rnu2-10 // Rnu2-10	0.604596	0.039253
Rnu2-10 // Rnu2-10 // Rnu2-10 // Rnu2-10 // Rnu2-10 // Rnu2-10	0.604596	0.039253
Atp5l	0.600938	0.0387
Usmg5	0.594582	0.024745
Gm13235 // Gm13235 // Gm13235	0.593095	0.007131
Gm13235 // Gm13235 // Gm13235	0.593095	0.007131
Zfp229	0.590708	0.032097
BC026585	0.584944	0.013068
H2-T10	0.583018	0.043437
Rnu2-10 // Rnu2-10 // Rnu2-10 // Rnu2-10 // Rnu2-10	0.582095	0.029497
Ormdl1	0.579867	0.042961
Psmb9	0.578594	0.033675
Bend6	0.577169	0.011552
Tfam	0.576949	0.026785
Etohi1	0.576563	0.034996
Ccdc122	0.57421	0.022729
Psmb8	0.571896	0.018297
Ceacam10	0.570288	0.04479
Zfp960	0.569107	0.040252

Tipin	0.568007	0.048938
Gm10509	0.560049	0.000821
Gm10509	0.556079	0.009861
Gm7285	0.550153	0.039751
Cyp2j6	0.545942	0.011705
Cox7a1	0.54357	0.031935
Srsf3	0.533844	0.043622
Tmem38b	0.521442	0.04487
Cxcl9	0.521123	0.028954
Casp4	0.512671	0.02039
Ube2l6	0.512112	0.047497
Mia1	0.502461	0.023091
Pdcd10	0.49807	0.012915
Fundc2	0.495796	0.003917
Tnfsf10	0.495444	0.014626
Irgm1	0.484378	0.038173
6720489N17Rik	0.467381	0.016201
Gzmb	0.446219	0.040239
Rny1	0.391509	0.039101
Tgtp1	0.369274	0.037981
Gm12250	0.347129	0.047339
Ifi27l2a	0.341212	0.006045
Ifit3	0.332339	0.022433
I830012O16Rik	0.295353	0.037745

Table S8. Gene expression of early stage KO-shC and KO-sh2TNC tumors

RNA sequencing data, p-value <0.1, 50 most upregulated and 50 most downregulated genes

GeneName	log2FoldChange	pvalue	padj
Soga3	4.974722	1.35E-31	2.26E-27
Cr2	4.66075	7.29E-24	3.04E-20
Fndc5	4.427587	5.9E-23	1.97E-19
Cd19	4.093622	2.14E-18	2.23E-15
Ms4a1	3.966162	1.95E-16	1.55E-13
Ighd	3.8585	1.08E-16	9.01E-14
Glycam1	3.64805	8.56E-14	4.25E-11
Atp2a3	3.622823	5.57E-20	1.33E-16
Plin1	3.574527	1.95E-14	1.06E-11
Enpp2	3.419972	1.64E-13	6.85E-11
Skap1	3.412422	1.2E-12	4.05E-10
Zfp831	3.390016	2.41E-13	9.35E-11
Igkv8-30	3.366326	6.49E-12	1.97E-09
Dnah8	3.245777	5.33E-16	3.86E-13
Mmp3	3.225534	8.01E-20	1.67E-16
Mmp16	3.218418	2.47E-19	4.12E-16
Bank1	3.205099	1.15E-10	2.43E-08
Ighg2c	3.152484	1.44E-10	3E-08
Pck1	3.137237	2.48E-11	6.16E-09
Ttn	3.074721	1.69E-14	9.73E-12
Prkcq	3.067823	1.08E-11	3.09E-09
Car3	3.058731	8.18E-19	9.74E-16
Pax5	3.034193	1.3E-09	2.18E-07
Sell	3.014942	1.02E-10	2.24E-08
Ms4a4b	2.991239	1.79E-09	2.89E-07
Itk	2.95074	2.96E-11	6.94E-09

Il9r	2.940194	2.85E-09	4.54E-07
Cd6	2.869695	7.41E-10	1.31E-07
Il27ra	2.866832	5.64E-10	1.04E-07
RP23-448H3.2	2.861077	1.06E-08	1.45E-06
Fcrl1	2.804937	1.84E-08	2.32E-06
mt-Ts2	2.794961	2.02E-18	2.23E-15
Fcer2a	2.788472	2.52E-08	3.06E-06
Cd79b	2.784876	2.91E-08	3.44E-06
Grem1	2.775607	2.02E-08	2.49E-06
Itgb7	2.771844	8.36E-10	1.47E-07
Pogk	2.764924	2.01E-19	3.72E-16
Adipoq	2.751886	2.75E-08	3.28E-06
Ikzf3	2.750856	6.69E-10	1.21E-07
Ighv3-2	2.736129	5.17E-08	5.78E-06
mt-Tp	2.718786	2.75E-13	1.04E-10
Cited4	2.699686	5.02E-08	5.65E-06
Pcdh15	2.681679	9.41E-08	9.56E-06
Cd79a	2.663046	7.42E-08	7.74E-06
Snord85	2.646641	3.67E-19	5.28E-16
Cd37	2.640986	1.15E-10	2.43E-08
Traf3ip3	2.639993	9.5E-11	2.11E-08
Cd2	2.589652	1.5E-07	1.41E-05
Gimap3	2.582825	5.11E-09	7.4E-07
Mir342	2.573055	3.01E-07	2.61E-05
Eef1a1	-0.52231	0.004642	0.07385
Erbb3	-0.52794	0.006132	0.09119
Nhsl1	-0.54158	0.005599	0.085627
Clstn1	-0.55718	0.005424	0.083486
Pkp4	-0.56347	0.005885	0.088707
Itpr1	-0.57091	0.004731	0.075048
Eif5a	-0.5716	0.004001	0.066231
Dock9	-0.57919	0.004391	0.070931

Lphn3	-0.58639	0.004545	0.072572
Rpl6	-0.58918	0.004893	0.077174
Rpl18a	-0.59109	0.004417	0.071151
Galnt3	-0.59508	0.005412	0.083486
Acox2	-0.59834	0.00624	0.092242
Col16a1	-0.60104	0.005306	0.082207
Rpl5	-0.60478	0.004357	0.070725
Ncl	-0.60618	0.006908	0.098182
Hdac11	-0.6102	0.006347	0.093471
Ppia	-0.61881	0.002777	0.050412
Slc7a5	-0.62389	0.006241	0.092242
Sel1l	-0.62533	0.001109	0.02474
Txndc5	-0.62882	0.002467	0.046109
Otub1	-0.62931	0.006641	0.096272
Gpr126	-0.62967	0.004398	0.070974
Hgsnat	-0.63477	0.006622	0.096081
Neo1	-0.63571	0.001913	0.037554
Rab11fip4	-0.6366	0.003743	0.063025
Tmed10	-0.6377	0.004057	0.067097
Esrp2	-0.64227	0.004373	0.070909
Copz1	-0.64451	0.00438	0.070931
Rpl36a	-0.64933	0.006772	0.096991
Srsf3	-0.6501	0.002371	0.044654
Pdcd4	-0.65307	0.006739	0.096597
Gnl3l	-0.65714	0.0022	0.042065
Aldoa	-0.66287	0.002526	0.047023
Copg2	-0.66665	0.005383	0.083169
Esyt3	-0.67675	0.004668	0.074187
Lars	-0.6785	0.003053	0.054179
Eid1	-0.68088	0.001728	0.034884
Ctcf	-0.68175	0.004288	0.069886
Phgdh	-0.69082	0.006968	0.09895
Taf1d	-0.69302	0.00573	0.087006

Serpine2	-0.69479	0.004525	0.072332
Atl2	-0.69548	0.006032	0.090006
Cdk14	-0.69689	0.003892	0.064554
Fry	-0.70189	0.002617	0.048159
Kif16b	-0.70253	0.002174	0.04166
Tubb6	-0.70356	0.006212	0.091971
Eif1a	-0.70784	0.003818	0.063868
Slc29a1	-0.70901	0.000198	0.006244
Morf4l1	-0.71005	0.005452	0.08385

Table S9. Gene expression of early stage WT-shC and WT-sh2TNC tumors

RNA sequencing data, p-value <0.1, 50 most upregulated and 50 most downregulated genes, N = 2

GeneName	log2FoldChange	pvalue	padj
Soga3	3.625839	4.02E-27	1.54E-23
Fndc5	3.181018	9.68E-23	2.47E-19
Pogk	2.485018	1.25E-16	2.74E-13
Dpp10	2.303031	6.59E-15	1.01E-11
Ehhadh	2.016389	6.5E-09	3.32E-06
Nt5c3b	1.92826	1.03E-09	6.25E-07
BC021891	1.900109	6.91E-09	3.42E-06
Cited4	1.871005	8.28E-08	3.02E-05
Pck1	1.806114	1.8E-07	5.4E-05
Pcdhb11	1.804422	1.72E-07	5.27E-05
Rnf207	1.798574	2.69E-07	6.87E-05
Thrsp	1.731021	6.39E-07	0.000141
Cyp2f2	1.711923	1.53E-07	4.89E-05
Zfp518a	1.665057	2.69E-07	6.87E-05
B4galnt3	1.656278	1.74E-06	0.000325
Plekha6	1.627588	5.23E-08	2.01E-05
Ptpru	1.607093	4.01E-08	1.58E-05
H2-Q6	1.590465	1.06E-09	6.25E-07
Btn2a2	1.587586	5.36E-06	0.000821
Tacstd2	1.576446	1.83E-06	0.000339
Fam208a	1.499988	2.2E-07	6.31E-05
Nrtn	1.416212	1.9E-06	0.000342
Gnao1	1.407243	2.05E-07	6.04E-05
9330159F19Rik	1.383475	7.15E-05	0.006901
Csn1s1	1.379278	7.99E-05	0.00745

Pcdhb13	1.369864	6.51E-05	0.006478
Mir6236	1.348581	8.93E-08	3.11E-05
Dnajc22	1.345651	0.000106	0.009242
B3galt5	1.336431	2.28E-06	0.000401
Chic1	1.334113	0.000107	0.00929
Gas6	1.331636	1.49E-08	6.72E-06
Arhgap4	1.325416	1.57E-06	0.000301
Mmp16	1.311686	8.33E-05	0.007693
RP23-247F18.3	1.303844	0.000149	0.012014
Car6	1.268888	7.2E-05	0.006901
Arsg	1.26719	4.01E-05	0.004296
Pcdhb14	1.265808	0.000113	0.009528
Crlf1	1.261436	0.00011	0.009414
Hexa	1.256344	2.22E-07	6.31E-05
Arnt2	1.246277	0.00017	0.013532
Pcdhb12	1.24577	0.000356	0.022896
Lrrc75b	1.243992	2.39E-06	0.000411
Fn3k	1.236046	0.000374	0.023498
L1cam	1.233444	0.000408	0.024459
Armcx6	1.230761	0.000373	0.023498
Mmp3	1.229634	0.000178	0.013948
Car12	1.227175	0.000387	0.024013
Mfsd4	1.224224	0.000179	0.013948
Bmf	1.208651	3.04E-06	0.000507
Ttc39c	1.196132	0.000495	0.028211
Mfge8	-0.57427	0.002582	0.095836
Myo7a	-0.57853	0.002603	0.096381
Nudt4	-0.60433	0.001649	0.069652
Gnai2	-0.60529	0.002691	0.097859
Tmed10	-0.61869	0.002154	0.084905
Dusp4	-0.63656	0.002318	0.089365
Sema5a	-0.64194	0.001485	0.064668
Cttnbp2nl	-0.64314	0.00191	0.079117

Myadm	-0.65048	0.002287	0.088998
Etv5	-0.65462	0.000761	0.039952
Lamb1	-0.6581	0.002016	0.081757
Zfp36l1	-0.65868	0.002694	0.097859
Fryl	-0.66097	0.000656	0.035296
Stac2	-0.66778	0.001247	0.057219
Gys1	-0.68759	0.001266	0.057918
mt-Nd5	-0.68874	0.002528	0.0946
Adcy7	-0.68959	0.001458	0.064027
Ly6e	-0.70488	0.000358	0.022896
Col4a2	-0.70521	0.000273	0.018873
Rpl10a-ps1	-0.70658	0.002284	0.088998
Ncl	-0.70804	0.001043	0.050035
Snora68	-0.70991	0.001939	0.079463
Gpc4	-0.71347	0.001016	0.049299
Ptbp1	-0.71429	0.000359	0.022896
Gorasp2	-0.71937	0.00039	0.024049
Pgk1	-0.72185	0.000604	0.033189
Rplp2	-0.72251	0.001547	0.066784
Lcn2	-0.72906	0.000153	0.012253
Agpat1	-0.74211	0.001463	0.064098
Cx3cl1	-0.74418	0.000927	0.045826
Ptma	-0.74644	0.00232	0.089365
P4ha1	-0.75291	0.001925	0.079126
Sept11	-0.75294	0.001899	0.078888
Abhd2	-0.75359	0.000408	0.024459
Lama4	-0.75514	0.001035	0.049906
Atp6v0c	-0.75837	0.002481	0.093907
Ier3	-0.7615	0.000484	0.027989
Myc	-0.76232	0.00178	0.07477
Rny3	-0.76913	0.000255	0.018094
Nrarp	-0.76981	0.002522	0.0946
Tubb6	-0.77136	0.002016	0.081757

Ctgf	-0.77184	0.002364	0.090422
Kdm3a	-0.77344	0.000289	0.019496
Gpi1	-0.77777	0.000439	0.025882
Zyx	-0.77918	0.000401	0.024225
Hk2	-0.78112	0.000573	0.031714
Zfand2a	-0.79739	0.001111	0.052257
Tuba4a	-0.79785	0.000239	0.017033
Etv4	-0.7981	0.001312	0.058969
Dag1	-0.79921	2.73E-05	0.003102

Table S10. Gene expression of early stage WT-shC and KO-sh2TNC tumors

RNA sequencing profiling, p-value <0.1, 50 most upregulated and 50 most downregulated genes, N = 2

GeneName	log2FoldChange	pvalue	padj
Fndc5	4.58642	2.59E-43	2.73E-40
Soga3	4.414497	1.23E-39	8.55E-37
Mmp16	3.919085	5.78E-57	1.4E-53
Pogk	3.04537	4.08E-44	4.96E-41
Ehhadh	2.780499	1.51E-14	2.39E-12
BC021891	2.647785	2.72E-21	7.33E-19
Efemp2	2.532649	3.96E-17	8.24E-15
9330159F19Rik	2.484396	2.18E-11	2.15E-09
Nt5c3b	2.478791	3.44E-25	1.35E-22
RP24-212P5.2	2.30298	1.72E-12	1.97E-10
Dpp10	2.222111	3.17E-26	1.4E-23
Slc2a9	2.172606	3.08E-21	8.15E-19
Rpgr	2.10133	4.38E-08	2.21E-06
Mks1	2.085582	4.38E-08	2.21E-06
Car6	2.032001	2.7E-12	2.89E-10
RP23-389J8.3	2.026442	7.83E-11	7E-09
Rnf207	2.020555	2.93E-08	1.56E-06
Pcdhb13	2.008547	1.47E-07	6.56E-06
Mir6236	1.989502	4.03E-40	2.94E-37
Khdrbs3	1.97923	4.36E-16	7.94E-14
Gas6	1.947406	5.17E-24	1.84E-21
Adig	1.946402	8.99E-09	5.2E-07
Pck1	1.897842	6.63E-07	2.42E-05
Pcdhb11	1.884528	7.47E-08	3.53E-06
Chic1	1.878485	7.29E-08	3.46E-06
Nrtn	1.877583	4.9E-12	5.17E-10

Btn2a2	1.87684	5.02E-07	1.84E-05
Armcx6	1.773207	3.47E-06	0.000102
Mmp3	1.699443	8.98E-09	5.2E-07
Akip1	1.69593	9.31E-06	0.000238
Plxdc1	1.693679	8.2E-06	0.000213
Gvin1	1.689115	6.99E-08	3.35E-06
Tacstd2	1.681804	6.71E-08	3.24E-06
Sync	1.680915	9.31E-06	0.000238
Fn3k	1.657291	3.72E-06	0.000109
L1cam	1.650273	6.74E-06	0.000181
Scube1	1.647711	1.7E-05	0.000395
Fam208a	1.638585	9.2E-11	8.03E-09
Car12	1.631882	3.75E-06	0.000109
Pgm5	1.629496	2.18E-05	0.000473
Rps13-ps1	1.623614	2.23E-06	7.05E-05
Col6a5	1.615461	1.03E-05	0.000257
Mfsd4	1.608039	3.4E-07	1.36E-05
Snx22	1.60352	4.44E-09	2.79E-07
Per2	1.601995	2.36E-14	3.59E-12
Hexa	1.594837	9.87E-17	2E-14
Zfp518a	1.583349	1.37E-06	4.53E-05
H3f3a-ps2	1.57033	3.01E-05	0.000623
Cilp	1.554622	2.49E-18	5.59E-16
Ptpru	1.527146	1.97E-14	3.05E-12
Wnt5a	-0.50053	0.011513	0.072113
Gabpa	-0.50095	0.002799	0.024819
AI597479	-0.50125	0.01466	0.085005
Mtx3	-0.50171	0.006872	0.049913
Usp22	-0.50181	0.000211	0.00315
Atp8b1	-0.50317	0.003112	0.027148
Clu	-0.50425	3.78E-05	0.000761
Mkl1	-0.50575	0.00667	0.048733
Arf4	-0.50635	0.001841	0.017917

Mbd6	-0.50847	0.015771	0.089696
Eef1a1	-0.50915	1.57E-05	0.000368
Ldha	-0.50969	0.000321	0.0044
Atf7ip	-0.50995	0.000119	0.001973
Cdk5rap2	-0.51158	0.009927	0.06482
Lamtor1	-0.51172	0.007378	0.052569
Srcap	-0.51224	3.65E-05	0.00074
Pigs	-0.51226	0.002335	0.021572
Aldoa	-0.51248	1.74E-05	0.0004
Gpr125	-0.51274	0.000654	0.007798
Bcl9	-0.51369	0.001119	0.012182
Etv3	-0.51416	0.001473	0.015191
Fbln2	-0.51534	0.001247	0.013274
Irf2	-0.51543	0.00314	0.027357
C2cd5	-0.51636	0.000119	0.001971
Polr2b	-0.51658	0.001734	0.017214
Hadha	-0.51742	0.000122	0.002003
Arglu1	-0.51767	0.002881	0.0254
Rft1	-0.51864	0.005522	0.042296
Ubap2l	-0.51912	0.000126	0.002046
Isg20l2	-0.51998	0.004838	0.038216
Slc35b2	-0.52008	0.001759	0.017398
Cdc42ep1	-0.52077	0.00297	0.026072
Ppap2b	-0.5208	0.000669	0.007952
Nap1l1	-0.5213	0.01089	0.069409
Snw1	-0.5219	0.002971	0.026072
Hivep1	-0.5227	0.002908	0.025583
Lrrk1	-0.52334	0.00054	0.006645
Atn1	-0.52374	0.001269	0.013436
Tada2b	-0.52399	0.013587	0.080543
Sh3bp2	-0.52441	0.010024	0.065232
Rad23b	-0.52525	0.001631	0.01648
Prrg4	-0.52606	0.015412	0.088275

Sema6a	-0.52735	0.000922	0.010357
Fgd1	-0.52749	0.008626	0.058617
Tbc1d9	-0.52789	0.006994	0.050548
Nav1	-0.52812	0.014456	0.084187
Nrarp	-0.52836	0.013032	0.078368
Ddx24	-0.52859	0.000742	0.008713
Rbp7	-0.52862	0.006517	0.047915
Gpc4	-0.52952	0.000938	0.010514

Table S11. Gene ontology analysis of upregulated genes in early stage KO-shC and KO-sh2TNC tumors

GO biological process	Fold enrichment	p-value	FDR
Antigen processing and presentation of endogenous peptide antigen via MHC class I via ER pathway, tap-dependent (GO:0002485)	34,62	4,13E-04	1,04E-02
Antigen processing and presentation of endogenous peptide antigen via MHC class I via ER pathway (Go:0002484)	34,62	4,13E-04	1,03E-02
Negative regulation of dendritic cell apoptotic process (GO:2000669)	34,62	3,94E-05	1,32E-03
T cell activation via T cell receptor contact with antigen bound to MHC molecule on antigen presenting cell (GO:0002291)	34,62	4,13E-04	1,03E-02
Antigen processing and presentation of endogenous peptide antigen via MHC class I (GO:0019885)	29,68	6,94E-07	3,23E-05
T cell chemotaxis (Go:0010818)	27,7	6,93E-05	2,14E-03
Regulation of immunological synapse formation (GO:2000520)	25,97	7,08E-04	1,62E-02
Positive regulation of cd8-positive, alpha-beta T cell differentiation (GO:0043378)	25,97	7,08E-04	1,62E-02
Regulation of dendritic cell apoptotic process (GO:2000668)	24,73	1,15E-05	4,43E-04
Positive regulation of gamma-delta T cell differentiation (GO:0045588)	23,08	1,13E-04	3,36E-03

Table S12. Relapse-free survival in grade III breast cancer patients and expression of candidate genes

Gene name	Hazard ratio	Log rank p
APS	0.49 (0.36 – 0.68)	9,90E-06
CD4	0,79 (0.64 – 0.98)	3,50E-02
CD74	0,69 (0.55 – 0.86)	9,60E-04
B2M	0,76 (0.61 – 0.95)	1,40E-02
CTSS	0,62 (0.45 – 0.85)	2,80E-03
CIITA	1,05 (0.85 – 1.31)	6,30E-01
TAP1	0,72 (0.58 – 0.9)	4,00E-03
CD86	0,91 (0.73 – 1.13)	3,80E-01

Table S13. Overall survival in grade III breast cancer patients and expression of candidate genes

Gene name	Hazard ratio	Log rank p
APS	0.46 (0.27 – 0.79)	3,70E-03
CD4	0,79 (0.64 – 0.98)	3,30E-03
CD74	0,69 (0.55 – 0.86)	1,50E-04
B2M	0,76 (0.61 – 0.95)	1,10E-02
CTSS	0,62 (0.45 – 0.85)	7,90E-03
CIITA	1,05 (0.85 – 1.31)	9,60E-01
TAP1	0,72 (0.58 – 0.9)	3,00E-04
CD86	0,91 (0.73 – 1.13)	1,60E-01

4. Discussion and perspectives

TNC is a large ECM glycoprotein which is largely expressed during embryonic development. However, its expression in the adult organism is restricted to some tissues such as tendons, some stem cell niches and reticular fibers of lymphoid organs. However, TNC is expressed *de novo* during wound healing and pathological situations like inflammation and cancer. High expression of TNC correlates with poor prognosis in several cancer types such as melanoma and colorectal cancer (Midwood et al. 2016). In breast cancer, high TNC expression is associated with poor metastasis-free survival and overall survival (Oskarsson et al. 2011). Furthermore, it has previously been shown that in the TME, TNC can be expressed by both the stromal and the cancer cells and that tumor cell-derived TNC correlates with poor survival in breast patients (Ishihara et al. 1995). Despite these significant clinical observations, how exactly TNC impacts breast tumor progression is largely unknown.

In order to address this question, we developed a novel orthotopic, syngeneic and immunocompetent breast cancer model (NT193 model) with engineered levels of TNC in both the host and the tumor cells. This allowed us to study the impact of host- and tumor cell-derived TNC on breast cancer progression and lung metastasis formation. Our results showed that host-derived TNC promotes a higher metastatic burden as well as tumor cells survival (Appendix I, Sun et al, submitted). *In vitro*, TNC increases cell migration through the induction of an EMT-like phenotype that is relevant *in vivo* as we see more EMT like changes and enhanced breaching into the lung parenchyma in TNC expressing conditions. Supported by observations in the transgenic MMTV-NeuNT breast cancer model we demonstrated that TNC promotes tumor cell extravasation to the lung parenchyma where promoting cellular plasticity is an important mechanism (Appendix I, Sun et al, submitted).

We also demonstrated that the NT193 syngeneic model is an important model to investigate the impact of TNC on the evolution of an immune response towards engrafted tumor cells. Our results show clearly two phases and a previously unknown janus role of TNC in tumor immunity. In a first phase, tumor cells express TNC which triggers expression of an antigen presenting signature (APS) by the host that

enforces infiltration of CD8+ T cells into the tumor nests and subsequent tumor cell death and tumor rejection. In a second phase, applying to the escapers, high expression of TNC and organization in matrix tracks, corrupts the CD8+ T cell-mediated immune response. We identified CXCL12/CXCR4 signaling as an important downstream TNC triggered mechanism that leads to biochemical and physical shielding of the tumor cell nests from the CD8+ T cell attack.

4.1. The NT193 grafting model recapitulating the MMTV-NeuNT transgenic model is a valid novel preclinical breast cancer model

Research using breast cancer models has been instrumental in generating new insights into the mechanisms underpinning tumor progression. One of the significant transgenic mice used in breast cancer research is the MMTV-NeuNT model (Muller et al. 1988). These mice express an activated form of the rat homologue of the HER2 oncogene (neu) specifically in the mammary epithelium. The main significance of this model is that it mimics the progression phase of HER2+ breast cancers that are characterized by an overexpression of HER2. HER2 plays a major role in mammary carcinogenesis of about 15-25% of breast cancer patients (Yarden 2001). In the original MMTV-Neu model, approximately 50% of mice develop multifocal breast tumors with a latency of 5 to 8 months and, around 30% of the tumor-bearing mice develop lung metastases (Muller et al. 1988). Despite the fact that this model develops spontaneously breast tumors that progress into lung metastasis, the long kinetics is a problem for preclinical research and in particular drug testing. On the other side the long kinetics may better mimic the events that occur in human cancer and in particular may allow establishing a relevant TME.

In the laboratory, we developed a syngeneic orthotopic immunocompetent grafting model as a surrogate for the MMTV-NeuNT model. This was done by isolating a tumor cell line (NT193 cells) from the primary tumor of a MMTV-NeuNT mouse (Arpel et al. 2016). Upon grafting of NT193 cells in the surgically opened mammary fat pad of a syngeneic FVB/NCrl host, breast tumors develop in a fraction of mice that spontaneously form lung metastasis after 11-14 weeks. Histological analysis of the resulting tumors revealed that the NT193 tumors are indistinguishable from the MMTV-NeuNT tumors. An in-depth characterization of the NT193 tumors shows that the tumors display an epithelial phenotype, a sustained expression of ErbB2 and an

organization of the tumor matrix as matrix tracks as we have seen in the MMTV-NeuNT tumors. We concluded that the novel grafting model is a good substitute for the transgenic mouse model.

In comparison with other models, the NT193 model presents some advantages. For example the EO771 triple negative syngeneic (C57BL/6 host) grafting model is poorly metastatic. In contrast, the NT193 model spontaneously develops lung metastasis with features seen in the genetic model that are highly relevant for human cancer. In the NT193 model vascular invasions are formed as precursors of parenchymal metastasis (Casey, Laster, and Ross 1951, Appendix I, Sun et al., submitted). The 4T1 syngeneic (BALB/c host) grafting model is highly metastatic. Yet, these cells are so aggressive that early events in the primary tumor cannot be investigated. This applies in particular to the aspect of immune surveillance (Lelekakis et al. 1999; Aslakson and Miller 1992). A similar drawback is seen with the PyMT syngeneic grafting model (C57Bl6 and FVB host) that is similarly aggressive as the 4T1 model (Yang et al. 2017). Tumor grafting models from a MMTV-Neu tumor have previously been established but were discarded because the tumor cells underwent EMT *in vivo* and therefore could not well be compared to the epithelial tumors of the stochastic model (Santisteban et al. 2009). We had established the NT193 cell line from another MMTV model where the cells express a constitutively active version of the rat ErbB2 molecule, NeuNT. The NeuNT contains a point mutation that generates an amino acid substitution (Val-Glu) in the transmembrane domain of the protein, leading to constant ligand-independent dimerization of the receptor (Bargmann, Hung, and Weinberg 1986; Weiner et al. 1989). The NT193 cells are plastic in cell culture where the majority of cells is epithelial (only E-cadherin positive) and the minority is mesenchymal (only vimentin positive). For engraftment we used this pool of cells and observed that all arising tumors were epithelial as they only expressed E-cadherin but not vimentin.

Another aspect that has to be considered is the local milieu where the tumor cells are engrafted. In most studies cells are injected through the nipple or directly into the mammary fat pad. Both approaches have a drawback because the tumor cells are not placed in their proper microenvironment, meaning directly into the mammary epithelium. Therefore, we had surgically opened the mammary gland for engraftment

of the NT193 cells thereby enhancing the chances to place the cells in contact with the mammary epithelium. Tissue wounding may have also another impact on early events of immune surveillance. By engraftment of a massive number of tumor cells (in the range of 10^6 or more) the poor number of circulating immune cells will not be able to stage an immune response. Therefore, usually tumor penetrance in the applied grafting models is 100%. Upon tissue wounding, the immune system is already alerted and more immune cells may be primed to stage a defense against the tumor cells upon grafting. Indeed, this seems to be the case, as only 50% of mice develop tumors upon engraftment of NT193 cells and those tumors that are not rejected experience a transient slowdown in their growth. Indeed wounding is important for tumor rejection to occur in this model as without wounding, namely by engraftment through the nipple no tumor rejection is seen (Deligne et al., in preparation). Altogether, this wounding approach allowed us to establish the novel NT193 syngeneic orthotopic grafting model with a kinetics that allows developing a proper TME that promotes spontaneous metastasis to the lung. Most importantly, this model is the first to allow addressing the evolution of tumor immunity.

4.2. Tumor cell-derived TNC impacts tumor growth in the WT hosts

TNC can be expressed by both the tumor cells and the stromal cells in the TME. The high expression of TNC by the tumor cells has been correlated with shorter relapse-free survival, low lymph-node metastasis-free survival and poor overall survival in breast cancer patients (Ishihara et al. 1995). Since TNC expression is also associated to shorter lung metastasis-free survival in breast cancer, the impact of TNC on lung metastasis formation has been addressed in an immunocompromised mouse model (Oskarsson et al. 2011). In an elegant study using cells where TNC could be turned off at a given point upon injection, the authors found that tumor cell-derived TNC is important for survival until the host expresses TNC at the metastatic site in the lung. However one drawback of this study is that it lacks a functional immune system so that a potential impact of TNC on tumor immunity could not be addressed. Now, by using the NT193 model with engineered levels of TNC in the host and in the tumor cells, respectively, we were able to assess the impact of TNC derived from each cellular compartment on tumor progression and metastasis formation in an immunocompetent setting. Most importantly, the TNC knockdown by shRNA was stable *in vivo* and tumors induced by shTNC had very low TNC levels in

a TNCKO host. Therefore, we could well mimic MMTV-NeuNT tumors with high and no TNC in the NT193 grafting model.

We observed that when shC cells were grafted into a WT host they were totally or partially rejected as from the third week following engraftment. Interestingly, this was not observed when we grafted shTNC cells in the WT host, suggesting that tumor cell-derived TNC is involved in the tumor rejection process. Although TNC levels were reduced in WT/shTNC tumors there was still some TNC present, but apparently this did not elicit tumor rejection. On the contrary, injection of shC cells into a TNCKO host did not lead to tumor rejection either. Again, IF staining revealed some residual TNC expression in the tumors, but apparently this TNC did not induce tumor rejection. These experiments imply that the cellular origin of the TNC in the TME matters and that host-derived TNC is to some points different from tumor cell-derived TNC. Most importantly, these results also suggest that combined expression of TNC by the host and by the tumor cells is important to stage a rejection. Our further detailed analysis indeed provides an explanation for this conundrum (see below).

There are several possibilities for differences between host- and tumor cell-derived TNC. These include post-transcriptional alterations such as alternative splicing occurring inside the FNIII repeats (Giblin and Midwood 2015). To date around 100 alternatively spliced isoforms have been described compared to the theoretical 511 expected. Interestingly, our in silico analysis of the RNAseq data from the early stage NT193 tumors in the WT host revealed differences in TNC splice isoforms expressed by the host (WR/shTNC) or the tumor cells (KO/shC). We identified 5 isoforms where only one was specific for tumor cells. Interestingly, this isoform is the only one that contained a C domain of TNC. It is intriguing to speculate that this domain may have antigenic properties which have to be followed up in the future.

Structural differences in TNC can also be due to post-translational modifications. These include glycosylation and citrullination (Giblin and Midwood 2015; Schwenzer et al. 2016). For instance, in the RNAseq data comparison of early phase WT tumors, we observed a 2.5-fold higher expression of the peptidylarginine deiminase type IV (PAD4) in WT/shC versus WT/shTNC tumors. PAD4 is one of the enzymes that citrullinates proteins. Citrullinated proteins have been described to be significantly increased at sites of inflammation (Kinloch et al. 2008). In particular citrullinated TNC

was detected in blood from rheumatoid arthritis (RA) patients. Also circulating antibodies in blood of these patients detected the citrullinated FBG domain of TNC suggesting that indeed citrullinated TNC may be antigenic (Schwenzer et al. 2016). It remains to be seen whether other domains of TNC than the FBG globe can be citrullinated, in particular the C domain that was expressed by the tumor cells in our model. Also, future studies should address whether TNC is citrullinated in cancer which is unknown but an intriguing possibility. The NT193 model might be suitable to address this question. Given the higher expression of PAD4, it is possible that citrullination contributes to the observed tumor cell rejection phenotype in our model.

4.3. Tumor cell-derived TNC upregulates an antigen presentation signature (APS) in the host

Since tumor-cell derived TNC triggered a tumor rejection response in the early tumor phase, we speculated that this could be the result of an active tumor cell killing by the immune system rather than a decrease of proliferation of the tumor cells. We therefore injected the NT193 shC cells in a nude host, lacking B and T cells, and observed no tumor rejection. These data show that the adaptive immune system is implicated in the rejection process. To have some more insight about the mechanisms underpinning the tumor rejection, we analyzed the RNAseq data. We compared gene expression in KO/shC and KO/shTNC tumors. A gene ontology analysis showed that one of the most enriched GO terms with 21 genes was the antigen processing and presentation group of molecules. For instance these genes include tap1 and tap2 which are ATP-dependent transporters involved in the translocation of antigenic peptides from the cytosol to the endoplasmic reticulum (Blum, Wearsch, and Cresswell 2013). This observation suggested that TNC expressed by the tumor cells may elicit an immune response either by directly acting as antigen or by inducing molecules that are recognized by the immune system as antigens. Interestingly, although these 21 genes were upregulated in KO/shC tumors, these tumors did not get rejected. Next, we asked whether these genes would also be upregulated in the conditions where tumors regressed. And indeed also in WT/shC tumors these genes are upregulated (in comparison to WT/shTNC). We confirmed increased expression of 7 of these genes (ciita, ctss, b2m, cd74, tap1, cd4 and cd86) in WT/shC and KO/shC tumors and, coined them antigen-presenting-signature APS. These molecules as e.g. CD4 or CD86 are expressed by the host and

may explain why only in a WT host tumor cells were rejected. To investigate this possibility in more detail, we compared WT/shC with KO/shC tumors where the KO host is unable to induce tumor rejection. Indeed, three of the APS genes B2M, CD4 and CD86 were reduced in the KO/shC tumors. Altogether, this analysis revealed that tumor cells express molecules in a TNC dependent manner that trigger an immune response in a WT host where TNC expressed by the host is important to trigger an antigen-presenting-signature APS. Whether TNC itself is an antigen in these tumors is an intriguing possibility. It is possible that similar to RA where TNC was recognized as a danger-associated molecule (DAMP) TNC may have a similar function in tumors (Midwood et al. 2009). In regard of this information, we propose that TNC would be perceived by the immune system as an alarmin that would trigger the anti-tumor immune response. This is consistent with our data showing that in the WT hosts, expression of tumor cell-derived TNC is associated to high influx of CD8+ T cells, high mRNA levels of granzyme B and perforin, high apoptosis and tumor rejection and smaller tumors. However, how TNC triggers the anti-tumor immune response still needs to be investigated in the future.

We wanted to know whether the APS induced by TNC has any relevance for human breast cancer patients. Therefore, we analyzed the expression of the APS genes in publicly available breast cancer expression and survival data. Indeed, expression of the APS above the mean correlated with longer relapse-free and better overall survival in grade III breast cancer patients, but not in grade I or grade II patients. To understand why this correlation only applies in grade III but not in grade I and grade II patients we investigated in publicly available databases the level of expression TNC. We observed that the levels of expression of TNC were not different from grade I to grade III. To understand the clinical significance of the APS, we should therefore better stratify the patients according to their expression of hormonal receptors or HER2.

In summary, our results obtained in the NT193 tumor model revealed an unexpected function of TNC in cancer by eliciting an immune response where we have identified a group of molecules coined antigen-presenting-signature (APS) that can identify patients with better survival. This information could be useful for patient stratification and choice of therapy as well as for the design of an immunization protocol to elicit this APS. In this context it is interesting to note that recognition as TAA apparently

applies in glioblastoma (GBM) patients (Mock et al. 2015). Based on these observations the company Immatics had established an immunization protocol for GBM patients where they included peptides derived from the TNC sequence. It is urgent to determine which sequence in TNC is potentially antigenic in breast cancer or which molecules are induced by TNC that are antigenic. These molecules could be included in an immunization formula for breast cancer patients.

4.4. TNC impacts CD8+ T cell localization

Another main advantage of the NT193 model is that it allows monitoring different stages of tumor progression and in particular evolution of tumor immunity. As we discussed previously, expression of tumor-cell derived TNC in the WT host triggered tumor rejection. While 50% of the tumors were completely rejected, the other tumors regressed in size. As from the sixth week onwards the regressed tumors started to proliferate again, with their sizes matching those of the unrejected tumors (WT/shTNC) at the endpoint of the experiment. It can be noted that when we assessed lung metastasis formation in this same experiment, the metastatic burden was highest in the group of WT/shC mice that originally had experienced tumor regression. This was accompanied by the highest proliferation index and the lowest apoptotic index at the endstage of the experiment. These results are consistent with the immunoediting concept described by Robert Schreiber (Schreiber, Old, and Smyth 2011). A potential scenario is that early, tumor cell-derived TNC is seen as a danger molecule by the immune system and defensive immune cells readily invade the tumor to kill the tumor cells. Then a battle between the proliferating tumor cells and the killing immune cells, presumably the CD8+ T cells, follows. This process leads to tumor rejection in half on the cases and, in the other half potentially an immunoediting mechanism. In the not rejected tumors, cells may become more aggressive and invisible for the defensive immune cells, and/ or the immune cells turn into tumor-supportive ones. Altogether, this might be the reason why the metastatic burden was highest in this group of tumor mice.

Yet, how the tumor cells evade the anti-tumor response was still to be characterized. We therefore analyzed the immune infiltration in the NT193 tumors both by FACS analysis (Deligne et al. in preparation) and by immunostaining. This was assessed in NT193 tumors expressing high or low levels of TNC (WT/shC versus WT/shTNC).

148

We observed an impact of TNC on macrophages, dendritic cells and CD8+ T cells, with TNC reducing their abundance (Deligne ez al., in preparation). Interestingly, immunofluorescence analysis of these late phase tumors for infiltrating immune cells showed that the spatial distribution of CD8+ T cells was different, which was not the case for other immune cells such as CD4+, CD11c+, F4/80+ cells that all were present inside the tumor cell nests and the stroma. We found that CD8+ T cells were enriched preferentially in the tumor matrix tracks rather than in the tumor cell nests. This was accompanied by a decrease of granzyme B and perforin at mRNA level and higher apoptosis levels, suggesting that the CD8+ T cells might get inhibited by trapping in the TNC-enriched matrix and other mechanisms such as impaired priming (Deligne et al., in preparation).

As we have described in the introduction, the immune contexture addressing the localization of immune cells inside the tumor plays an essential role in determining the efficiency on anti-tumor immune responses as well as immunotherapy outcome (Fridman et al. 2012). In our NT193 model we describe the trapping of CD8+ T cells in TNC-enriched matrix tracks thereby keeping these immune cells physically away from the tumor cells. This observation matches the so called immune-exclusion tumor phenotype where immune cells are present but unable to penetrate into the tumor "parenchyma" where the latter term means tumor cell nests (Chen and Mellman 2017; Hegde, Karanikas, and Evers 2016). Interestingly, this interaction between TNC and immune cells has also been observed in another tumor model developed in the laboratory. Indeed, in a carcinogen-induced tongue OSCC tumor model, we have seen that in a WT host CD45+ leukocytes and most notably CD11c+ DCs were restricted to the TNC-enriched matrix tracks, while in the TNCKO tumors these cells invaded the tumor nests and killed the tumor cells (Appendix II, Spenle, Loustau et al., in preparation). These data strongly support our hypothesis that TNC plays an important role in positioning immune cells of the innate (CD11c+ cells in the OSCC model) and adaptive immune system (CD8+T cells in the NT193 model) inside the stromal areas thereby blocking their contact with the tumor cells. This mechanism could explain tumor progression by TNC. How TNC could do that we have investigated in some detail (see below).

.

4.5. TNC impacts CD8+ T cell adhesion and migration through CXCL12

In order to understand the mechanisms through which TNC impacts CD8+ T cells, we used the RNA seq data from the NT193 end stage tumors as well as the gene profiling data from the MMTV-NeuNT tumors. We observed that CXCL12 is increased in both tumor models in those tumors that express high levels of TNC. This we also saw in cultured NT193 cells where TNC induced mRNA levels and secretion of CXCL12. Interestingly, this chemokine has got some attention in the past and has been associated with the immune-excluded tumor phenotype (Chen and Mellman 2017).

CXCL12 is a highly pleiotropic chemokine that has been described to be involved in a variety of biological processes through interaction with its receptors CXCR4 and CXCR7 (Bleul et al. 1996; Balabanian et al. 2005). High expression of CXCL12 by bone marrow stromal cells is a prerequisite for maturation of B cells through enhanced attraction of hematopoietic stem cells to the bone marrow microenvironment (Egawa et al. 2001). In a landmark study, it was convincingly shown that through high expression of CXCR4 in breast cancer cells, CXCL12 regulates the homing of metastatic cells to the lymph nodes and the lungs (Müller et al. 2001). This concept was supported in many studies for different cancer types later on (Burger and Kipps 2006). Apart from the widely described metastasis promoting potential of CXCL12, this chemokine has also been reported to promote tumor cell proliferation and invasion as well as angiogenesis (Orimo et al. 2005; Liang et al. 2005). As TNC also impacts invasion, metastasis and endothelial cell abundance in the NT193 model (Sun et al., in prep), it will be interesting to see whether CXCL12 also plays a role in these particular phenotypes that are increased by TNC (Sun et al., submitted).

In the NT193 model, we showed that tumor cells were a main source of CXCL12 inside the tumor cell nests. We also assessed the receptor expression and observed that unlike CXCR7, the expression of CXCR4 was decreased by TNC. Altogether, these data suggest that in the presence of TNC the tumor cells establish a CXCL12-enriched microenvironment that probably does not directly affect the tumor cells. Inspired by work from De Laporte et al. (2013), who showed that TNC binds many soluble molecules, we investigated potential binding of CXCL12 to TNC and indeed

found such an interaction. This interaction was 35-fold weaker than that of CXCL12 with CXCR4. This may indicate that in tumor matrix tracks CXCL12 is exchanged between TNC and CXCR4, thereby attracting CD8+ T cells. It is also possible that a ternary complex is formed between TNC, CXCL12 and CXCR4, thereby facilitating adhesion of CD8+ T cells to the usually non-adhesive TNC substratum. Through which domain TNC binds CXCL12 and whether this is glycosylation dependent remains to be determined as many interactions with CXCL12 are gycosylation dependent (Huskens et al. 2007). Previously, it was reported that CXCL12 binding to a biomimetic film enhanced CXCL12-induced signaling in breast cancer cells by locally enhancing the signaling strength of CXCL12 (X. Q. Liu et al. 2017). It is intriguing to speculate that TNC mimics the role of the biomimetic film thereby enhancing CXCR4-CXCL12 signaling.

Since CD8+ T cells are localized in the TNC matrix tracks together with CXCL12, we hypothesized that through CXCL12 TNC may attract and immobilize CD8+ T cells. Indeed, we demonstrated, in cell migration assays, that the TNC/CXCL12 complex enhanced CD8+ T cell migration and adhesion. This could be reversed by inhibition of CXCR4 with the inhibitory drug AMD3100. Furthermore, inhibition of the CXCR4-CXCL12 axis *in vivo* induced tumor regression. At the endpoint of the experiment, the AM3100 treated tumors were smaller and highly infiltrated by CD8+ T cells accompanied by a higher apoptotic index than the control group. These data suggest that upon inhibition of the CXCR4-CXCL12 signaling axis, CD8+ T cells are enforced in their tumor cell killing activity. How this works remains to be determined. These results also suggest that CXCL12 expressed by the tumor cells may have a repellent activity as was previously shown in another model (Zboralski et al. 2017), thereby excluding CD8+ cells from the tumor cell nests. Thus CXCL12 expressed by the tumor cells in a TNC dependent manner may expel CD8+ T cells from the tumor cell nests and redirect them into the matrix tracks where they get stuck on TNC.

Previous *in vitro* studies assessing the impact of TNC on T cell function suggested that TNC blocks T cell activity (Rüegg, Chiquet-Ehrismann, and Alkan 1989; Jachetti et al. 2015). Our collaborators in Oxford indeed observed that also in the NT193 model CD8+ T cells were affected by TNC, as they were poorly primed. Macrophages were skewed into a M2 phenotype and DC were poorly activated which impacted on CD8+ T cell proliferation that was reduced by TNC. This involved TLR4

and PDL-1 as inhibition of both signaling reverted CD8+ T cell activities (Deligne et al., in preparation).

It is possible that a combined high expression of TNC together with CXCL12 may render tumors poorly responsive to immune checkpoint therapies. Infiltration of CD8+ T cells into the tumor cell nests is critical for successful antitumor immune surveillance, which is positively correlated with a better clinical outcome (Fridman et al. 2012; Naito et al. 1998). In a glioblastoma model, TNC has already been associated to T cell exclusion at the tumor periphery (J.-Y. Huang et al. 2010). Furthermore, in a pancreatic ductal adenocarcinoma model, it has been shown that inhibition of the CXCR4-CXCL12 axis resulted in the accumulation of T cells in the tumor which synergized with the response to an anti PD-L1 antibody (Feig et al. 2013). More recently, similar results were obtained in a murine colorectal cancer model where combined AMD3100 treatment and anti PD-L1 therapy lead to tumor regression (Zboralski et al. 2017). Together with our data, these observations suggest that high TNC and CXCL12 expression in breast cancer patients could be used to predict response efficacy to immune checkpoint therapies. We propose that these therapies are poorly effective in the presence of TNC because TNC would trap reactivated T cells (upon anti-PDL1 treatment or CART transfer). We suggest that preventing sequestration of CD8+ T cells in the TNC containing matrix tracks by inhibition of CXCR4 would enhance anti-PDL1 treatment efficiency. Here, our novel NT193 model could be highly relevant for investigating combinatorial treatment regimens targeting immune checkpoints and other relevant signaling such as CXCR4.

5. Summary

In summary, here we have established a powerful tumor grafting model that allowed us to shed light on the roles of TNC on the evolution of tumor immunity (**Fig 8**) and lung metastasis formation (Sun et al., submitted). TNC may locally orchestrate tumor and immune cell behavior where the cellular origin of TNC is important. Tumor cell-derived TNC triggers expression of an antigen-presenting-signature APS in the host causing tumor cell rejection. Tumor cells also increase CXCL12 expression in a TNC dependent manner. Binding of CXCL12 to TNC generates an adhesive substratum for CD8+ T cells thereby sequestering them away from the tumor cells. An in-depth understanding of the balance between the "good" and the "bad" actions of TNC in cancer may open novel opportunities for future targeting of cancer, thereby taking into account the temporal and loco-spatial organization of the TME. Our results provide a molecular grasp on the diffuse term of immune contexture and place TNC as a central player.
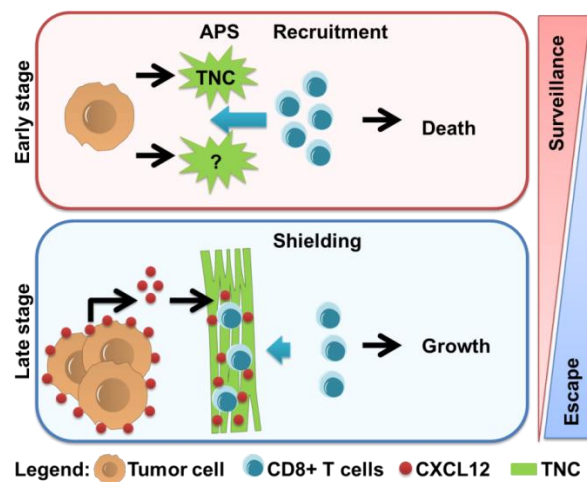
Figure 8: Summary figure illustrating the dual role of TNC during tumor progression. TNC produced by the tumor cells, induces an antigen presenting signature (APS) that triggers CD8+ T cell infiltration and subsequent tumor cell death. TNC also induces tumor cells to express and secrete CXCL12 which binds to the TNC-enriched tumor matrix tracks and attracts CD8+ T cells that are sequestered in the tumor matrix tracks. Thus, the tumor cells are shielded from the CD8+ T cells, and continue to grow. The balance between these two events determines whether tumor cells get rejected as seen at the early phase in the NT193 model, or continue to thrive and metastasize as seen upon escape from immune surveillance evident in the end stage tumors.

6. References

Achen, M. G., M. Jeltsch, E. Kukk, T. Mäkinen, A. Vitali, A. F. Wilks, K. Alitalo, and S. A. Stacker. 1998. "Vascular Endothelial Growth Factor D (VEGF-D) Is a Ligand for the Tyrosine Kinases VEGF Receptor 2 (Flk1) and VEGF Receptor 3 (Flt4)." *Proceedings of the National Academy of Sciences of the United States of America* 95 (2): 548–53.

Al-Husein, Belal, Maha Abdalla, Morgan Trepte, David L. DeRemer, and Payaningal R. Somanath. 2012. "Antiangiogenic Therapy for Cancer: An Update." *Pharmacotherapy: The Journal of Human Pharmacology and Drug Therapy* 32 (12): 1095–1111. https://doi.org/10.1002/phar.1147.

Ali, H. R., E. Provenzano, S.-J. Dawson, F. M. Blows, B. Liu, M. Shah, H. M. Earl, et al. 2014. "Association between CD8+ T-Cell Infiltration and Breast Cancer Survival in 12,439 Patients." *Annals of Oncology: Official Journal of the European Society for Medical Oncology* 25 (8): 1536–43. https://doi.org/10.1093/annonc/mdu191.

Allavena, Paola, Antonio Sica, Cecilia Garlanda, and Alberto Mantovani. 2008. "The Yin-Yang of Tumor-Associated Macrophages in Neoplastic Progression and Immune Surveillance." *Immunological Reviews* 222 (April): 155–61. https://doi.org/10.1111/j.1600-065X.2008.00607.x.

Allen, Michael D., Reza Vaziri, Michael Green, Claude Chelala, Adam R. Brentnall, Sally Dreger, Sabarinath Vallath, et al. 2011. "Clinical and Functional Significance of α9β1 Integrin Expression in Breast Cancer: A Novel Cell-Surface Marker of the Basal Phenotype That Promotes Tumour Cell Invasion." *The Journal of Pathology* 223 (5): 646–58. https://doi.org/10.1002/path.2833.

Anders, S., P. T. Pyl, and W. Huber. 2015. "HTSeq--a Python Framework to Work with High-Throughput Sequencing Data." *Bioinformatics* 31 (2): 166–69. https://doi.org/10.1093/bioinformatics/btu638.

Anderson, William F., Nilanjan Chatterjee, William B. Ershler, and Otis W. Brawley. 2002. "Estrogen Receptor Breast Cancer Phenotypes in the Surveillance, Epidemiology, and End Results Database." *Breast Cancer Research and Treatment* 76 (1): 27–36. https://doi.org/10.1023/A:1020299707510.

Angell, Helen, and Jérôme Galon. 2013. "From the Immune Contexture to the Immunoscore: The Role of Prognostic and Predictive Immune Markers in Cancer." *Current Opinion in Immunology* 25 (2): 261–67. https://doi.org/10.1016/j.coi.2013.03.004.

Angelov, D. N., M. Walther, M. Streppel, O. Guntinas-Lichius, W. F. Neiss, R. Probstmeier, and P. Pesheva. 1998. "Tenascin-R Is Antiadhesive for Activated Microglia That Induce Downregulation of the Protein after Peripheral Nerve Injury: A New Role in Neuronal Protection." *The Journal of Neuroscience: The Official Journal of the Society for Neuroscience* 18 (16): 6218–29.

Arpel, Alexia, Coralie Gamper, Caroline Spenlé, Aurore Fernandez, Laurent Jacob, Nadège Baumlin, Patrice Laquerriere, Gertraud Orend, Gérard Crémel, and Dominique Bagnard. 2016. "Inhibition of Primary Breast Tumor Growth and Metastasis Using a Neuropilin-1 Transmembrane Domain Interfering Peptide." *Oncotarget* 7 (34). https://doi.org/10.18632/oncotarget.10101.

Arpino, Grazia, Heidi Weiss, Adrian V. Lee, Rachel Schiff, Sabino De Placido, C. Kent Osborne, and Richard M. Elledge. 2005. "Estrogen Receptor–Positive, Progesterone Receptor–Negative Breast Cancer: Association With Growth Factor Receptor Expression and Tamoxifen Resistance." *JNCI: Journal of the National Cancer Institute* 97 (17): 1254–61. https://doi.org/10.1093/jnci/dji249.

Asano, Tsuyoshi, Norimasa Iwasaki, Shigeyuki Kon, Masashi Kanayama, Junko Morimoto, Akio Minami, and Toshimitsu Uede. 2014. "α9β1 Integrin Acts as a Critical Intrinsic Regulator of Human Rheumatoid Arthritis." *Rheumatology (Oxford, England)* 53 (3): 415–24. https://doi.org/10.1093/rheumatology/ket371.

Aslakson, C. J., and F. R. Miller. 1992. "Selective Events in the Metastatic Process Defined by Analysis of the Sequential Dissemination of Subpopulations of a Mouse Mammary Tumor." *Cancer Research* 52 (6): 1399–1405.

Aufderheide, E., and P. Ekblom. 1988. "Tenascin during Gut Development: Appearance in the Mesenchyme, Shift in Molecular Forms, and Dependence on Epithelial-Mesenchymal Interactions." *The Journal of Cell Biology* 107 (6 Pt 1): 2341–49.

Ayala, G. E., H. Dai, M. Powell, R. Li, Y. Ding, T. M. Wheeler, D. Shine, et al. 2008. "Cancer-Related Axonogenesis and Neurogenesis in Prostate Cancer." *Clinical Cancer Research* 14 (23): 7593–7603. https://doi.org/10.1158/1078-0432.CCR-08-1164.

Bae, Young Kyung, Aeri Kim, Min Kyoung Kim, Jung Eun Choi, Su Hwan Kang, and Soo Jung Lee. 2013. "Fibronectin Expression in Carcinoma Cells Correlates with Tumor Aggressiveness and Poor Clinical Outcome in Patients with Invasive Breast Cancer." *Human Pathology* 44 (10): 2028–37. https://doi.org/10.1016/j.humpath.2013.03.006.

Balabanian, Karl, Bernard Lagane, Simona Infantino, Ken Y. C. Chow, Julie Harriague, Barbara Moepps, Fernando Arenzana-Seisdedos, Marcus Thelen, and Françoise Bachelerie. 2005. "The Chemokine SDF-1/CXCL12 Binds to and Signals through the Orphan Receptor RDC1 in T Lymphocytes." *The Journal of Biological Chemistry* 280 (42): 35760–66. https://doi.org/10.1074/jbc.M508234200.

Balkwill, F. R., M. Capasso, and T. Hagemann. 2012. "The Tumor Microenvironment at a Glance." *Journal of Cell Science* 125 (23): 5591–96. https://doi.org/10.1242/jcs.116392.

Bardou, Valerie-Jeanne, Grazia Arpino, Richard M. Elledge, C. Kent Osborne, and Gary M. Clark. 2003. "Progesterone Receptor Status Significantly Improves

Outcome Prediction Over Estrogen Receptor Status Alone for Adjuvant Endocrine Therapy in Two Large Breast Cancer Databases." *Journal of Clinical Oncology* 21 (10): 1973–79. https://doi.org/10.1200/JCO.2003.09.099.

Bargmann, Cornelia I., Mien-Chie Hung, and Robert A. Weinberg. 1986. "Multiple Independent Activations of the Neu Oncogene by a Point Mutation Altering the Transmembrane Domain of p185." *Cell* 45 (5): 649–57. https://doi.org/10.1016/0092-8674(86)90779-8.

Bates, Gaynor J., Stephen B. Fox, Cheng Han, Russell D. Leek, José F. Garcia, Adrian L. Harris, and Alison H. Banham. 2006. "Quantification of Regulatory T Cells Enables the Identification of High-Risk Breast Cancer Patients and Those at Risk of Late Relapse." *Journal of Clinical Oncology: Official Journal of the American Society of Clinical Oncology* 24 (34): 5373–80. https://doi.org/10.1200/JCO.2006.05.9584.

Baum, M., D. M. Brinkley, J. A. Dossett, K. McPherson, J. S. Patterson, R. D. Rubens, F. G. Smiddy, et al. 1983. "Improved Survival among Patients Treated with Adjuvant Tamoxifen after Mastectomy for Early Breast Cancer." *Lancet (London, England)* 2 (8347): 450.

Baxevanis, C. N., G. V. Dedoussis, N. G. Papadopoulos, I. Missitzis, G. P. Stathopoulos, and M. Papamichail. 1994. "Tumor Specific Cytolysis by Tumor Infiltrating Lymphocytes in Breast Cancer." *Cancer* 74 (4): 1275–82.

Beiter, Katharina, Elke Hiendlmeyer, Thomas Brabletz, Falk Hlubek, Angela Haynl, Claudia Knoll, Thomas Kirchner, and Andreas Jung. 2005. "β-Catenin Regulates the Expression of Tenascin-C in Human Colorectal Tumors." *Oncogene* 24 (55): 8200–8204. https://doi.org/10.1038/sj.onc.1208960.

Bissell, Mina J., H.Glenn Hall, and Gordon Parry. 1982. "How Does the Extracellular Matrix Direct Gene Expression?" *Journal of Theoretical Biology* 99 (1): 31–68. https://doi.org/10.1016/0022-5193(82)90388-5.

Bissell, Mina J, and William C Hines. 2011. "Why Don't We Get More Cancer? A Proposed Role of the Microenvironment in Restraining Cancer Progression." *Nature Medicine* 17 (3): 320–29. https://doi.org/10.1038/nm.2328.

Biswas, Subhra K., and Alberto Mantovani. 2010. "Macrophage Plasticity and Interaction with Lymphocyte Subsets: Cancer as a Paradigm." *Nature Immunology* 11 (10): 889–96. https://doi.org/10.1038/ni.1937.

Bleul, C. C., M. Farzan, H. Choe, C. Parolin, I. Clark-Lewis, J. Sodroski, and T. A. Springer. 1996. "The Lymphocyte Chemoattractant SDF-1 Is a Ligand for LESTR/Fusin and Blocks HIV-1 Entry." *Nature* 382 (6594): 829–33. https://doi.org/10.1038/382829a0.

Blum, Janice S., Pamela A. Wearsch, and Peter Cresswell. 2013. "Pathways of Antigen Processing." *Annual Review of Immunology* 31: 443–73. https://doi.org/10.1146/annurev-immunol-032712-095910.

Bonacchi, Andrea, Ilaria Petrai, Raffaella M. S. Defranco, Elena Lazzeri, Francesco Annunziato, Eva Efsen, Lorenzo Cosmi, et al. 2003. "The Chemokine CCL21 Modulates Lymphocyte Recruitment and Fibrosis in Chronic Hepatitis C." *Gastroenterology* 125 (4): 1060–76.

Bonnans, Caroline, Jonathan Chou, and Zena Werb. 2014. "Remodelling the Extracellular Matrix in Development and Disease." *Nature Reviews Molecular Cell Biology* 15 (12): 786–801. https://doi.org/10.1038/nrm3904.

Boyd, N. F., L. J. Martin, J. Stone, C. Greenberg, S. Minkin, and M. J. Yaffe. 2001. "Mammographic Densities as a Marker of Human Breast Cancer Risk and Their Use in Chemoprevention." *Current Oncology Reports* 3 (4): 314–21.

Brossart, P., S. Wirths, G. Stuhler, V. L. Reichardt, L. Kanz, and W. Brugger. 2000. "Induction of Cytotoxic T-Lymphocyte Responses in Vivo after Vaccinations with Peptide-Pulsed Dendritic Cells." *Blood* 96 (9): 3102–8.

Burger, Jan A., and Thomas J. Kipps. 2006. "CXCR4: A Key Receptor in the Crosstalk between Tumor Cells and Their Microenvironment." *Blood* 107 (5): 1761–67. https://doi.org/10.1182/blood-2005-08-3182.

Burnet, F. M. 1970. "The Concept of Immunological Surveillance." *Progress in Experimental Tumor Research* 13: 1–27.

Burnet, M. 1957. "Cancer; a Biological Approach. I. The Processes of Control." *British Medical Journal* 1 (5022): 779–86.

Cai, Jun, Shaoxia Du, Hui Wang, Beibei Xin, Juan Wang, Wenyuan Shen, Wei Wei, Zhongkui Guo, and Xiaohong Shen. 2017. "Tenascin-C Induces Migration and Invasion through JNK/C-Jun Signalling in Pancreatic Cancer." *Oncotarget* 8 (43): 74406–22. https://doi.org/10.18632/oncotarget.20160.

Cardoso, F., N. Harbeck, L. Fallowfield, S. Kyriakides, E. Senkus, and on behalf of the ESMO Guidelines Working Group. 2012. "Locally Recurrent or Metastatic Breast Cancer: ESMO Clinical Practice Guidelines for Diagnosis, Treatment and Follow-Up." *Annals of Oncology* 23 (suppl 7): vii11-vii19. https://doi.org/10.1093/annonc/mds232.

Casey, A. E., W. R. Laster, and G. L. Ross. 1951. "Sustained Enhanced Growth of Carcinoma EO771 in C57 Black Mice." *Proceedings of the Society for Experimental Biology and Medicine. Society for Experimental Biology and Medicine (New York, N.Y.)* 77 (2): 358–62.

Castellon, Raquel, Sergio Caballero, Hamdi K. Hamdi, Shari R. Atilano, Annette M. Aoki, Roy W. Tarnuzzer, M. Cristina Kenney, Maria B. Grant, and Alexander V. Ljubimov. 2002. "Effects of Tenascin-C on Normal and Diabetic Retinal Endothelial Cells in Culture." *Investigative Ophthalmology & Visual Science* 43 (8): 2758–66.

Chen, Daniel S., and Ira Mellman. 2017. "Elements of Cancer Immunity and the Cancer–immune Set Point." *Nature* 541 (7637): 321–30. https://doi.org/10.1038/nature21349.

Chen, Daniel S., and Ira Mellman. 2013. "Oncology Meets Immunology: The Cancer-Immunity Cycle." *Immunity* 39 (1): 1–10. https://doi.org/10.1016/j.immuni.2013.07.012.

Chihara, T., S. Suzu, R. Hassan, N. Chutiwitoonchai, M. Hiyoshi, K. Motoyoshi, F. Kimura, and S. Okada. 2010. "IL-34 and M-CSF Share the Receptor Fms but Are Not Identical in Biological Activity and Signal Activation." *Cell Death and Differentiation* 17 (12): 1917–27. https://doi.org/10.1038/cdd.2010.60.

Chilosi, M., M. Lestani, A. Benedetti, L. Montagna, S. Pedron, A. Scarpa, F. Menestrina, S. Hirohashi, G. Pizzolo, and G. Semenzato. 1993. "Constitutive Expression of Tenascin in T-Dependent Zones of Human Lymphoid Tissues." *The American Journal of Pathology* 143 (5): 1348–55.

Chiquet, Matthias, Ana Sarasa-Renedo, and Vildan Tunç-Civelek. 2004. "Induction of Tenascin-C by Cyclic Tensile Strain versus Growth Factors: Distinct Contributions by Rho/ROCK and MAPK Signaling Pathways." *Biochimica et Biophysica Acta (BBA) - Molecular Cell Research* 1693 (3): 193–204. https://doi.org/10.1016/j.bbamcr.2004.08.001.

Chiquet-Ehrismann, Ruth, Eleanor J. Mackie, Carolyn A. Pearson, and Teruyo Sakakura. 1986. "Tenascin: An Extracellular Matrix Protein Involved in Tissue Interactions during Fetal Development and Oncogenesis." *Cell* 47 (1): 131–39. https://doi.org/10.1016/0092-8674(86)90374-0.

Chiquet-Ehrismann, Ruth, and Richard P. Tucker. 2011. "Tenascins and the Importance of Adhesion Modulation." *Cold Spring Harbor Perspectives in Biology* 3 (5). https://doi.org/10.1101/cshperspect.a004960.

Chow, M. T., and A. D. Luster. 2014. "Chemokines in Cancer." *Cancer Immunology Research* 2 (12): 1125–31. https://doi.org/10.1158/2326-6066.CIR-14-0160.

Claesson-Welsh, L., and M. Welsh. 2013. "VEGFA and Tumour Angiogenesis." *Journal of Internal Medicine* 273 (2): 114–27. https://doi.org/10.1111/joim.12019.

Coca, S., J. Perez-Piqueras, D. Martinez, A. Colmenarejo, M. A. Saez, C. Vallejo, J. A. Martos, and M. Moreno. 1997. "The Prognostic Significance of Intratumoral Natural Killer Cells in Patients with Colorectal Carcinoma." *Cancer* 79 (12): 2320–28.

Cornil, I., D. Theodorescu, S. Man, M. Herlyn, J. Jambrosic, and R. S. Kerbel. 1991. "Fibroblast Cell Interactions with Human Melanoma Cells Affect Tumor Cell Growth as a Function of Tumor Progression." *Proceedings of the National Academy of Sciences of the United States of America* 88 (14): 6028–32.

Crossin, K. L. 1991. "Cytotactin Binding: Inhibition of Stimulated Proliferation and Intracellular Alkalinization in Fibroblasts." *Proceedings of the National Academy of Sciences of the United States of America* 88 (24): 11403–7.

Curiel, Tyler J, George Coukos, Linhua Zou, Xavier Alvarez, Pui Cheng, Peter Mottram, Melina Evdemon-Hogan, et al. 2004. "Specific Recruitment of

Regulatory T Cells in Ovarian Carcinoma Fosters Immune Privilege and Predicts Reduced Survival." *Nature Medicine* 10 (9): 942–49. https://doi.org/10.1038/nm1093.

De Arcangelis, A., P. Neuville, R. Boukamel, O. Lefebvre, M. Kedinger, and P. Simon-Assmann. 1996. "Inhibition of Laminin Alpha 1-Chain Expression Leads to Alteration of Basement Membrane Assembly and Cell Differentiation." *The Journal of Cell Biology* 133 (2): 417–30.

De Laporte, Laura, Jeffrey J. Rice, Federico Tortelli, and Jeffrey A. Hubbell. 2013. "Tenascin C Promiscuously Binds Growth Factors via Its Fifth Fibronectin Type III-like Domain." *PloS One* 8 (4): e62076. https://doi.org/10.1371/journal.pone.0062076.

Delort, Laetitia, Adrien Rossary, Marie-Chantal Farges, Marie-Paule Vasson, and Florence Caldefie-Chézet. 2015. "Leptin, Adipocytes and Breast Cancer: Focus on Inflammation and Anti-Tumor Immunity." *Life Sciences* 140 (November): 37–48. https://doi.org/10.1016/j.lfs.2015.04.012.

DeNardo, David G., Donal J. Brennan, Elton Rexhepaj, Brian Ruffell, Stephen L. Shiao, Stephen F. Madden, William M. Gallagher, et al. 2011. "Leukocyte Complexity Predicts Breast Cancer Survival and Functionally Regulates Response to Chemotherapy." *Cancer Discovery* 1 (1): 54–67. https://doi.org/10.1158/2159-8274.CD-10-0028.

Denkert, Carsten, Gunter von Minckwitz, Silvia Darb-Esfahani, Bianca Lederer, Barbara I. Heppner, Karsten E. Weber, Jan Budczies, et al. 2018. "Tumour-Infiltrating Lymphocytes and Prognosis in Different Subtypes of Breast Cancer: A Pooled Analysis of 3771 Patients Treated with Neoadjuvant Therapy." *The Lancet. Oncology* 19 (1): 40–50. https://doi.org/10.1016/S1470-2045(17)30904-X.

DeSantis, Carol E., Jiemin Ma, Ann Goding Sauer, Lisa A. Newman, and Ahmedin Jemal. 2017. "Breast Cancer Statistics, 2017, Racial Disparity in Mortality by State: Breast Cancer Statistics, 2017." *CA: A Cancer Journal for Clinicians* 67 (6): 439–48. https://doi.org/10.3322/caac.21412.

Desgrosellier, Jay S., and David A. Cheresh. 2010. "Integrins in Cancer: Biological Implications and Therapeutic Opportunities." *Nature Reviews. Cancer* 10 (1): 9–22. https://doi.org/10.1038/nrc2748.

Dirat, B., L. Bochet, M. Dabek, D. Daviaud, S. Dauvillier, B. Majed, Y. Y. Wang, et al. 2011. "Cancer-Associated Adipocytes Exhibit an Activated Phenotype and Contribute to Breast Cancer Invasion." *Cancer Research* 71 (7): 2455–65. https://doi.org/10.1158/0008-5472.CAN-10-3323.

Dobin, Alexander, Carrie A. Davis, Felix Schlesinger, Jorg Drenkow, Chris Zaleski, Sonali Jha, Philippe Batut, Mark Chaisson, and Thomas R. Gingeras. 2013. "STAR: Ultrafast Universal RNA-Seq Aligner." *Bioinformatics* 29 (1): 15–21. https://doi.org/10.1093/bioinformatics/bts635.

Drumea-Mirancea, Mihaela, Johannes T. Wessels, Claudia A. Müller, Mike Essl, Johannes A. Eble, Eva Tolosa, Manuel Koch, et al. 2006. "Characterization of a Conduit System Containing Laminin-5 in the Human Thymus: A Potential Transport System for Small Molecules." *Journal of Cell Science* 119 (Pt 7): 1396–1405. https://doi.org/10.1242/jcs.02840.

Dunn, Gavin P., Allen T. Bruce, Hiroaki Ikeda, Lloyd J. Old, and Robert D. Schreiber. 2002. "Cancer Immunoediting: From Immunosurveillance to Tumor Escape." *Nature Immunology* 3 (11): 991–98. https://doi.org/10.1038/ni1102-991.

Dunn, Gavin P., Lloyd J. Old, and Robert D. Schreiber. 2004. "The Immunobiology of Cancer Immunosurveillance and Immunoediting." *Immunity* 21 (2): 137–48. https://doi.org/10.1016/j.immuni.2004.07.017.

Early Breast Cancer Trialists' Collaborative Group. 1988. "Effects of Adjuvant Tamoxifen and of Cytotoxic Therapy on Mortality in Early Breast Cancer." *New England Journal of Medicine* 319 (26): 1681–92. https://doi.org/10.1056/NEJM198812293192601.

Egawa, T., K. Kawabata, H. Kawamoto, K. Amada, R. Okamoto, N. Fujii, T. Kishimoto, Y. Katsura, and T. Nagasawa. 2001. "The Earliest Stages of B Cell Development Require a Chemokine Stromal Cell-Derived Factor/Pre-B Cell Growth-Stimulating Factor." *Immunity* 15 (2): 323–34.

Ehrismann, R., M. Chiquet, and D. C. Turner. 1981. "Mode of Action of Fibronectin in Promoting Chicken Myoblast Attachment. Mr = 60,000 Gelatin-Binding Fragment Binds Native Fibronectin." *The Journal of Biological Chemistry* 256 (8): 4056–62.

Ehrlich, P. 1909. "Über den jetzigen Stand der Chemotherapie." *Berichte der deutschen chemischen Gesellschaft* 42 (1): 17–47. https://doi.org/10.1002/cber.19090420105.

Ellyard, J. I., L. Simson, and C. R. Parish. 2007. "Th2-Mediated Anti-Tumour Immunity: Friend or Foe?" *Tissue Antigens* 70 (1): 1–11. https://doi.org/10.1111/j.1399-0039.2007.00869.x.

Emoto, K., Y. Yamada, H. Sawada, H. Fujimoto, M. Ueno, T. Takayama, K. Kamada, A. Naito, S. Hirao, and Y. Nakajima. 2001. "Annexin II Overexpression Correlates with Stromal Tenascin-C Overexpression: A Prognostic Marker in Colorectal Carcinoma." *Cancer* 92 (6): 1419–26.

Engelhardt, John J., Bijan Boldajipour, Peter Beemiller, Priya Pandurangi, Caitlin Sorensen, Zena Werb, Mikala Egeblad, and Matthew F. Krummel. 2012. "Marginating Dendritic Cells of the Tumor Microenvironment Cross-Present Tumor Antigens and Stably Engage Tumor-Specific T Cells." *Cancer Cell* 21 (3): 402–17. https://doi.org/10.1016/j.ccr.2012.01.008.

Engler, Adam J., Shamik Sen, H. Lee Sweeney, and Dennis E. Discher. 2006. "Matrix Elasticity Directs Stem Cell Lineage Specification." *Cell* 126 (4): 677–89. https://doi.org/10.1016/j.cell.2006.06.044.

Feig, Christine, James O. Jones, Matthew Kraman, Richard J. B. Wells, Andrew Deonarine, Derek S. Chan, Claire M. Connell, et al. 2013. "Targeting CXCL12 from FAP-Expressing Carcinoma-Associated Fibroblasts Synergizes with Anti-PD-L1 Immunotherapy in Pancreatic Cancer." *Proceedings of the National Academy of Sciences of the United States of America* 110 (50): 20212–17. https://doi.org/10.1073/pnas.1320318110.

Fitzmaurice, Christina, Daniel Dicker, Amanda Pain, Hannah Hamavid, Maziar Moradi-Lakeh, Michael F. MacIntyre, Christine Allen, et al. 2015. "The Global Burden of Cancer 2013." *JAMA Oncology* 1 (4): 505. https://doi.org/10.1001/jamaoncol.2015.0735.

Fletcher, Anne L., Sophie E. Acton, and Konstantin Knoblich. 2015. "Lymph Node Fibroblastic Reticular Cells in Health and Disease." *Nature Reviews. Immunology* 15 (6): 350–61. https://doi.org/10.1038/nri3846.

Foley, E. J. 1953. "Antigenic Properties of Methylcholanthrene-Induced Tumors in Mice of the Strain of Origin." *Cancer Research* 13 (12): 835–37.

Folkman, J. 1971. "Tumor Angiogenesis: Therapeutic Implications." *The New England Journal of Medicine* 285 (21): 1182–86. https://doi.org/10.1056/NEJM197111182852108.

Folkman, Judah. 2003. "Fundamental Concepts of the Angiogenic Process." *Current Molecular Medicine* 3 (7): 643–51.

Foulkes, William D., Ian E. Smith, and Jorge S. Reis-Filho. 2010. "Triple-Negative Breast Cancer." *New England Journal of Medicine* 363 (20): 1938–48. https://doi.org/10.1056/NEJMra1001389.

Frantz, C., K. M. Stewart, and V. M. Weaver. 2010. "The Extracellular Matrix at a Glance." *Journal of Cell Science* 123 (24): 4195–4200. https://doi.org/10.1242/jcs.023820.

Fridman, Wolf Herman, Franck Pagès, Catherine Sautès-Fridman, and Jérôme Galon. 2012. "The Immune Contexture in Human Tumours: Impact on Clinical Outcome." *Nature Reviews Cancer* 12 (4): 298–306. https://doi.org/10.1038/nrc3245.

Froelich, C. J., K. Orth, J. Turbov, P. Seth, R. Gottlieb, B. Babior, G. M. Shah, R. C. Bleackley, V. M. Dixit, and W. Hanna. 1996. "New Paradigm for Lymphocyte Granule-Mediated Cytotoxicity. Target Cells Bind and Internalize Granzyme B, but an Endosomolytic Agent Is Necessary for Cytosolic Delivery and Subsequent Apoptosis." *The Journal of Biological Chemistry* 271 (46): 29073–79.

Fukino, Koichi, Lei Shen, Attila Patocs, George L. Mutter, and Charis Eng. 2007. "Genomic Instability Within Tumor Stroma and Clinicopathological Characteristics of Sporadic Primary Invasive Breast Carcinoma." *JAMA* 297 (19): 2103. https://doi.org/10.1001/jama.297.19.2103.

Galon, J. 2006. "Type, Density, and Location of Immune Cells Within Human Colorectal Tumors Predict Clinical Outcome." *Science* 313 (5795): 1960–64. https://doi.org/10.1126/science.1129139.

Galon, Jérôme, Bernhard Mlecnik, Gabriela Bindea, Helen K. Angell, Anne Berger, Christine Lagorce, Alessandro Lugli, et al. 2014. "Towards the Introduction of the 'Immunoscore' in the Classification of Malignant Tumours." *The Journal of Pathology* 232 (2): 199–209. https://doi.org/10.1002/path.4287.

Galon, Jérôme, Franck Pagès, Francesco M. Marincola, Helen K. Angell, Magdalena Thurin, Alessandro Lugli, Inti Zlobec, et al. 2012. "Cancer Classification Using the Immunoscore: A Worldwide Task Force." *Journal of Translational Medicine* 10 (October): 205. https://doi.org/10.1186/1479-5876-10-205.

Gebb, Sarah A. L., and Peter Lloyd Jones. 2003. "Hypoxia and Lung Branching Morphogenesis." *Advances in Experimental Medicine and Biology* 543: 117–25.

Geyer, Felipe C., Maria A. Lopez-Garcia, Maryou B. Lambros, and Jorge S. Reis-Filho. 2009. "Genetic Characterization of Breast Cancer and Implications for Clinical Management." *Journal of Cellular and Molecular Medicine* 13 (10): 4090–4103. https://doi.org/10.1111/j.1582-4934.2009.00906.x.

Ghajar, Cyrus M., and Mina J. Bissell. 2008. "Extracellular Matrix Control of Mammary Gland Morphogenesis and Tumorigenesis: Insights from Imaging." *Histochemistry and Cell Biology* 130 (6): 1105–18. https://doi.org/10.1007/s00418-008-0537-1.

Giblin, Sean P, and Kim S Midwood. 2015. "Tenascin-C: Form versus Function." *Cell Adhesion & Migration* 9 (1–2): 48–82. https://doi.org/10.4161/19336918.2014.987587.

Goh, Fui G., Anna M. Piccinini, Thomas Krausgruber, Irina A. Udalova, and Kim S. Midwood. 2010. "Transcriptional Regulation of the Endogenous Danger Signal Tenascin-C: A Novel Autocrine Loop in Inflammation." *Journal of Immunology (Baltimore, Md.: 1950)* 184 (5): 2655–62. https://doi.org/10.4049/jimmunol.0903359.

Grivennikov, Sergei I., Florian R. Greten, and Michael Karin. 2010. "Immunity, Inflammation, and Cancer." *Cell* 140 (6): 883–99. https://doi.org/10.1016/j.cell.2010.01.025.

Gschwind, Andreas, Oliver M. Fischer, and Axel Ullrich. 2004. "The Discovery of Receptor Tyrosine Kinases: Targets for Cancer Therapy." *Nature Reviews Cancer* 4 (5): 361–70. https://doi.org/10.1038/nrc1360.

Guéry, Leslie, and Stéphanie Hugues. 2015. "Th17 Cell Plasticity and Functions in Cancer Immunity." *BioMed Research International* 2015: 1–11. https://doi.org/10.1155/2015/314620.

Gulubova, Maya, and Tatyana Vlaykova. 2006. "Immunohistochemical Assessment of Fibronectin and Tenascin and Their Integrin Receptors alpha5beta1 and

alpha9beta1 in Gastric and Colorectal Cancers with Lymph Node and Liver Metastases." *Acta Histochemica* 108 (1): 25–35. https://doi.org/10.1016/j.acthis.2005.12.001.

Györffy, Balazs, Andras Lanczky, Aron C. Eklund, Carsten Denkert, Jan Budczies, Qiyuan Li, and Zoltan Szallasi. 2010. "An Online Survival Analysis Tool to Rapidly Assess the Effect of 22,277 Genes on Breast Cancer Prognosis Using Microarray Data of 1,809 Patients." *Breast Cancer Research and Treatment* 123 (3): 725–31. https://doi.org/10.1007/s10549-009-0674-9.

Hanahan, Douglas, and Lisa M. Coussens. 2012. "Accessories to the Crime: Functions of Cells Recruited to the Tumor Microenvironment." *Cancer Cell* 21 (3): 309–22. https://doi.org/10.1016/j.ccr.2012.02.022.

Hanahan, Douglas, and Robert A Weinberg. 2000. "The Hallmarks of Cancer." *Cell* 100 (1): 57–70. https://doi.org/10.1016/S0092-8674(00)81683-9.

Hanahan, Douglas, and Robert A. Weinberg. 2011. "Hallmarks of Cancer: The Next Generation." *Cell* 144 (5): 646–74. https://doi.org/10.1016/j.cell.2011.02.013.

Hanamura, N., T. Yoshida, E. Matsumoto, Y. Kawarada, and T. Sakakura. 1997. "Expression of Fibronectin and Tenascin-C mRNA by Myofibroblasts, Vascular Cells and Epithelial Cells in Human Colon Adenomas and Carcinomas." *International Journal of Cancer* 73 (1): 10–15.

Hancox, Rachael A, Michael D Allen, Deborah L Holliday, Dylan R Edwards, Caroline J Pennington, David S Guttery, Jacqueline A Shaw, Rosemary A Walker, J Howard Pringle, and J Louise Jones. 2009. "Tumour-Associated Tenascin-C Isoforms Promote Breast Cancer Cell Invasion and Growth by Matrix Metalloproteinase-Dependent and Independent Mechanisms." *Breast Cancer Research* 11 (2). https://doi.org/10.1186/bcr2251.

Hauzenberger, D., P. Olivier, D. Gundersen, and C. Rüegg. 1999. "Tenascin-C Inhibits beta1 Integrin-Dependent T Lymphocyte Adhesion to Fibronectin through the Binding of Its fnIII 1-5 Repeats to Fibronectin." *European Journal of Immunology* 29 (5): 1435–47.

Hegde, P. S., V. Karanikas, and S. Evers. 2016. "The Where, the When, and the How of Immune Monitoring for Cancer Immunotherapies in the Era of Checkpoint Inhibition." *Clinical Cancer Research* 22 (8): 1865–74. https://doi.org/10.1158/1078-0432.CCR-15-1507.

Hemesath, T. J., L. S. Marton, and K. Stefansson. 1994. "Inhibition of T Cell Activation by the Extracellular Matrix Protein Tenascin." *Journal of Immunology (Baltimore, Md.: 1950)* 152 (11): 5199–5207.

Herberman, R. B., M. E. Nunn, and D. H. Lavrin. 1975. "Natural Cytotoxic Reactivity of Mouse Lymphoid Cells against Syngeneic Acid Allogeneic Tumors. I. Distribution of Reactivity and Specificity." *International Journal of Cancer* 16 (2): 216–29.

Herold-Mende, Christel, Margareta M. Mueller, Mario M. Bonsanto, Horst Peter Schmitt, Stefan Kunze, and Hans-Herbert Steiner. 2002. "Clinical Impact and Functional Aspects of Tenascin-C Expression during Glioma Progression." *International Journal of Cancer* 98 (3): 362–69.

Hindermann, W., A. Berndt, L. Borsi, X. Luo, P. Hyckel, D. Katenkamp, and H. Kosmehl. 1999. "Synthesis and Protein Distribution of the Unspliced Large Tenascin-C Isoform in Oral Squamous Cell Carcinoma." *The Journal of Pathology* 189 (4): 475–80. https://doi.org/10.1002/(SICI)1096-9896(199912)189:4<475::AID-PATH462>3.0.CO;2-V.

Horwitz, Kathryn B., Yoshihiro Koseki, and William L. McGUIRE. 1978. "Estrogen Control of Progesterone Receptor in Human Breast Cancer: Role of Estradiol and Antiestrogen*." *Endocrinology* 103 (5): 1742–51. https://doi.org/10.1210/endo-103-5-1742.

Huang, Da Wei, Brad T Sherman, and Richard A Lempicki. 2009. "Systematic and Integrative Analysis of Large Gene Lists Using DAVID Bioinformatics Resources." *Nature Protocols* 4 (1): 44–57. https://doi.org/10.1038/nprot.2008.211.

Huang, Jyun-Yuan, Yu-Jung Cheng, Yu-Ping Lin, Huan-Ching Lin, Chung-Chen Su, Rudy Juliano, and Bei-Chang Yang. 2010. "Extracellular Matrix of Glioblastoma Inhibits Polarization and Transmigration of T Cells: The Role of Tenascin-C in Immune Suppression." *Journal of Immunology (Baltimore, Md.: 1950)* 185 (3): 1450–59. https://doi.org/10.4049/jimmunol.0901352.

Huang, W., R. Chiquet-Ehrismann, J. V. Moyano, A. Garcia-Pardo, and G. Orend. 2001. "Interference of Tenascin-C with Syndecan-4 Binding to Fibronectin Blocks Cell Adhesion and Stimulates Tumor Cell Proliferation." *Cancer Research* 61 (23): 8586–94.

Huskens, Dana, Katrien Princen, Michael Schreiber, and Dominique Schols. 2007. "The Role of N-Glycosylation Sites on the CXCR4 Receptor for CXCL-12 Binding and Signaling and X4 HIV-1 Viral Infectivity." *Virology* 363 (2): 280–87. https://doi.org/10.1016/j.virol.2007.01.031.

Hynes, R. O. 2009. "The Extracellular Matrix: Not Just Pretty Fibrils." *Science* 326 (5957): 1216–19. https://doi.org/10.1126/science.1176009.

Hynes, R. O., and A. Naba. 2012. "Overview of the Matrisome--An Inventory of Extracellular Matrix Constituents and Functions." *Cold Spring Harbor Perspectives in Biology* 4 (1): a004903–a004903. https://doi.org/10.1101/cshperspect.a004903.

Ilmonen, S., T. Jahkola, J. P. Turunen, T. Muhonen, and S. Asko-Seljavaara. 2004. "Tenascin-C in Primary Malignant Melanoma of the Skin." *Histopathology* 45 (4): 405–11. https://doi.org/10.1111/j.1365-2559.2004.01976.x.

Ishihara, A., T. Yoshida, H. Tamaki, and T. Sakakura. 1995. "Tenascin Expression in Cancer Cells and Stroma of Human Breast Cancer and Its Prognostic

Significance." *Clinical Cancer Research: An Official Journal of the American Association for Cancer Research* 1 (9): 1035–41.

Jachetti, Elena, Sara Caputo, Stefania Mazzoleni, Chiara Svetlana Brambillasca, Sara Martina Parigi, Matteo Grioni, Ignazio Stefano Piras, et al. 2015. "Tenascin-C Protects Cancer Stem-like Cells from Immune Surveillance by Arresting T-Cell Activation." *Cancer Research* 75 (10): 2095–2108. https://doi.org/10.1158/0008-5472.CAN-14-2346.

Jéhannin-Ligier, Karine, Emmanuelle Dantony, Nadine Bossard, Florence Molinié, Gautier Defossez, Laëtitia Daubisse-Marliac, Patricia Delafosse, Laurent Remontet, and Zoé Uhry. 2017. "Projection de L'incidence et de La Mortalité Par Cancer En France Métropolitaine En 2017." Saint-Maurice: Santé publique France. http://www.e-cancer.fr/Expertises-et-publications/Catalogue-des-publications/Projection-de-l-incidence-et-de-la-mortalite-en-France-metropolitaine-en-2017-Rapport-technique.

Joukov, V., K. Pajusola, A. Kaipainen, D. Chilov, I. Lahtinen, E. Kukk, O. Saksela, N. Kalkkinen, and K. Alitalo. 1996. "A Novel Vascular Endothelial Growth Factor, VEGF-C, Is a Ligand for the Flt4 (VEGFR-3) and KDR (VEGFR-2) Receptor Tyrosine Kinases." *The EMBO Journal* 15 (2): 290–98.

Joyce, J. A., and D. T. Fearon. 2015. "T Cell Exclusion, Immune Privilege, and the Tumor Microenvironment." *Science* 348 (6230): 74–80. https://doi.org/10.1126/science.aaa6204.

Kalams, S. A., and B. D. Walker. 1998. "The Critical Need for CD4 Help in Maintaining Effective Cytotoxic T Lymphocyte Responses." *The Journal of Experimental Medicine* 188 (12): 2199–2204.

Katoh, D., K. Nagaharu, N. Shimojo, N. Hanamura, M. Yamashita, Y. Kozuka, K. Imanaka-Yoshida, and T. Yoshida. 2013. "Binding of αvβ1 and αvβ6 Integrins to Tenascin-C Induces Epithelial-Mesenchymal Transition-like Change of Breast Cancer Cells." *Oncogenesis* 2 (August): e65. https://doi.org/10.1038/oncsis.2013.27.

Ke, Xing, and Lisong Shen. 2017. "Molecular Targeted Therapy of Cancer: The Progress and Future Prospect." *Frontiers in Laboratory Medicine* 1 (2): 69–75. https://doi.org/10.1016/j.flm.2017.06.001.

Kinloch, Andrew, Karin Lundberg, Robin Wait, Natalia Wegner, Ngee Han Lim, Albert J. W. Zendman, Tore Saxne, Vivianne Malmström, and Patrick J. Venables. 2008. "Synovial Fluid Is a Site of Citrullination of Autoantigens in Inflammatory Arthritis." *Arthritis and Rheumatism* 58 (8): 2287–95. https://doi.org/10.1002/art.23618.

Kmieciak, Maciej, Keith L. Knutson, Catherine I. Dumur, and Masoud H. Manjili. 2007. "HER-2/Neu Antigen Loss and Relapse of Mammary Carcinoma Are Actively Induced by T Cell-Mediated Anti-Tumor Immune Responses." *European Journal of Immunology* 37 (3): 675–85. https://doi.org/10.1002/eji.200636639.

Knutson, Keith L., Hailing Lu, Brad Stone, Jennifer M. Reiman, Marshall D. Behrens, Christine M. Prosperi, Ekram A. Gad, Arianna Smorlesi, and Mary L. Disis. 2006. "Immunoediting of Cancers May Lead to Epithelial to Mesenchymal Transition." *Journal of Immunology (Baltimore, Md.: 1950)* 177 (3): 1526–33.

Koebel, Catherine M., William Vermi, Jeremy B. Swann, Nadeen Zerafa, Scott J. Rodig, Lloyd J. Old, Mark J. Smyth, and Robert D. Schreiber. 2007. "Adaptive Immunity Maintains Occult Cancer in an Equilibrium State." *Nature* 450 (7171): 903–7. https://doi.org/10.1038/nature06309.

Kryczek, I., M. Banerjee, P. Cheng, L. Vatan, W. Szeliga, S. Wei, E. Huang, et al. 2009. "Phenotype, Distribution, Generation, and Functional and Clinical Relevance of Th17 Cells in the Human Tumor Environments." *Blood* 114 (6): 1141–49. https://doi.org/10.1182/blood-2009-03-208249.

Lange, Katrin, Martial Kammerer, Monika E. Hegi, Stefan Grotegut, Antje Dittmann, Wentao Huang, Erika Fluri, et al. 2007. "Endothelin Receptor Type B Counteracts Tenascin-C-Induced Endothelin Receptor Type A-Dependent Focal Adhesion and Actin Stress Fiber Disorganization." *Cancer Research* 67 (13): 6163–73. https://doi.org/10.1158/0008-5472.CAN-06-3348.

Langlois, Benoit, Falk Saupe, Tristan Rupp, Christiane Arnold, Michaël van der Heyden, Gertraud Orend, and Thomas Hussenet. 2014. "AngioMatrix, a Signature of the Tumor Angiogenic Switch-Specific Matrisome, Correlates with Poor Prognosis for Glioma and Colorectal Cancer Patients." *Oncotarget* 5 (21): 10529–45. https://doi.org/10.18632/oncotarget.2470.

Langmead, Ben, and Steven L Salzberg. 2012. "Fast Gapped-Read Alignment with Bowtie 2." *Nature Methods* 9 (4): 357–59. https://doi.org/10.1038/nmeth.1923.

Lee, Andrew W, Tuan Truong, Kara Bickham, Jean-Francois Fonteneau, Marie Larsson, Ida Da Silva, Selin Somersan, Elaine K Thomas, and Nina Bhardwaj. 2002. "A Clinical Grade Cocktail of Cytokines and PGE2 Results in Uniform Maturation of Human Monocyte-Derived Dendritic Cells: Implications for Immunotherapy." *Vaccine* 20 (December): A8–22. https://doi.org/10.1016/S0264-410X(02)00382-1.

Leek, R. D., C. E. Lewis, R. Whitehouse, M. Greenall, J. Clarke, and A. L. Harris. 1996. "Association of Macrophage Infiltration with Angiogenesis and Prognosis in Invasive Breast Carcinoma." *Cancer Research* 56 (20): 4625–29.

Lelekakis, M., J. M. Moseley, T. J. Martin, D. Hards, E. Williams, P. Ho, D. Lowen, et al. 1999. "A Novel Orthotopic Model of Breast Cancer Metastasis to Bone." *Clinical & Experimental Metastasis* 17 (2): 163–70.

Levental, Kandice R., Hongmei Yu, Laura Kass, Johnathon N. Lakins, Mikala Egeblad, Janine T. Erler, Sheri F. T. Fong, et al. 2009. "Matrix Crosslinking Forces Tumor Progression by Enhancing Integrin Signaling." *Cell* 139 (5): 891–906. https://doi.org/10.1016/j.cell.2009.10.027.

Liang, Zhongxing, Younghyoun Yoon, John Votaw, Mark M. Goodman, Larry Williams, and Hyunsuk Shim. 2005. "Silencing of CXCR4 Blocks Breast Cancer Metastasis." *Cancer Research* 65 (3): 967–71.

Liu, Mingli, Shanchun Guo, and Jonathan K. Stiles. 2011. "The Emerging Role of CXCL10 in Cancer (Review)." *Oncology Letters* 2 (4): 583–89. https://doi.org/10.3892/ol.2011.300.

Liu, Xi Qiu, Laure Fourel, Fabien Dalonneau, Rabia Sadir, Salome Leal, Hugues Lortat-Jacob, Marianne Weidenhaupt, Corinne Albiges-Rizo, and Catherine Picart. 2017. "Biomaterial-Enabled Delivery of SDF-1α at the Ventral Side of Breast Cancer Cells Reveals a Crosstalk between Cell Receptors to Promote the Invasive Phenotype." *Biomaterials* 127 (May): 61–74. https://doi.org/10.1016/j.biomaterials.2017.02.035.

Love, Michael I, Wolfgang Huber, and Simon Anders. 2014. "Moderated Estimation of Fold Change and Dispersion for RNA-Seq Data with DESeq2." *Genome Biology* 15 (12). https://doi.org/10.1186/s13059-014-0550-8.

Lu, C., M. F. Vickers, and R. S. Kerbel. 1992. "Interleukin 6: A Fibroblast-Derived Growth Inhibitor of Human Melanoma Cells from Early but Not Advanced Stages of Tumor Progression." *Proceedings of the National Academy of Sciences of the United States of America* 89 (19): 9215–19.

Ma, Yang, Galina V. Shurin, Zhu Peiyuan, and Michael R. Shurin. 2013. "Dendritic Cells in the Cancer Microenvironment." *Journal of Cancer* 4 (1): 36–44. https://doi.org/10.7150/jca.5046.

Mackie, E. J., R. Chiquet-Ehrismann, C. A. Pearson, Y. Inaguma, K. Taya, Y. Kawarada, and T. Sakakura. 1987. "Tenascin Is a Stromal Marker for Epithelial Malignancy in the Mammary Gland." *Proceedings of the National Academy of Sciences of the United States of America* 84 (13): 4621–25.

Malanchi, Ilaria, Albert Santamaria-Martínez, Evelyn Susanto, Hong Peng, Hans-Anton Lehr, Jean-Francois Delaloye, and Joerg Huelsken. 2011. "Interactions between Cancer Stem Cells and Their Niche Govern Metastatic Colonization." *Nature* 481 (7379): 85–89. https://doi.org/10.1038/nature10694.

Mariel, Garcia-Chagollan, Carranza-Torres Irma Edith, Carranza-Rosales Pilar, Guzmán-Delgado Nancy Elena, Ramírez-Montoya Humberto, Martínez-Silva María Guadalupe, Mariscal-Ramirez Ignacio, et al. 2018. "Expression of NK Cell Surface Receptors in Breast Cancer Tissue as Predictors of Resistance to Antineoplastic Treatment." *Technology in Cancer Research & Treatment* 17 (January): 153303381876449. https://doi.org/10.1177/1533033818764499.

Marsh, Timothy, Kristian Pietras, and Sandra S. McAllister. 2013. "Fibroblasts as Architects of Cancer Pathogenesis." *Biochimica et Biophysica Acta (BBA) - Molecular Basis of Disease* 1832 (7): 1070–78. https://doi.org/10.1016/j.bbadis.2012.10.013.

Martino, M. M., P. S. Briquez, A. Ranga, M. P. Lutolf, and J. A. Hubbell. 2013. "Heparin-Binding Domain of Fibrin(ogen) Binds Growth Factors and Promotes

Tissue Repair When Incorporated within a Synthetic Matrix." *Proceedings of the National Academy of Sciences* 110 (12): 4563–68. https://doi.org/10.1073/pnas.1221602110.

Maschler, Sabine, Stefan Grunert, Adriana Danielopol, Hartmut Beug, and Gerhard Wirl. 2004. "Enhanced Tenascin-C Expression and Matrix Deposition during Ras/TGF-β-Induced Progression of Mammary Tumor Cells." *Oncogene* 23 (20): 3622–33. https://doi.org/10.1038/sj.onc.1207403.

Mbeunkui, Flaubert, and Donald J. Johann. 2009. "Cancer and the Tumor Microenvironment: A Review of an Essential Relationship." *Cancer Chemotherapy and Pharmacology* 63 (4): 571–82. https://doi.org/10.1007/s00280-008-0881-9.

Mi, Huaiyu, Xiaosong Huang, Anushya Muruganujan, Haiming Tang, Caitlin Mills, Diane Kang, and Paul D. Thomas. 2017. "PANTHER Version 11: Expanded Annotation Data from Gene Ontology and Reactome Pathways, and Data Analysis Tool Enhancements." *Nucleic Acids Research* 45 (D1): D183–89. https://doi.org/10.1093/nar/gkw1138.

Midwood, Kim, Matthias Chiquet, Richard P. Tucker, and Gertraud Orend. 2016. "Tenascin-C at a Glance." *Journal of Cell Science* 129 (23): 4321–27. https://doi.org/10.1242/jcs.190546.

Midwood, Kim, Thomas Hussenet, Benoit Langlois, and Gertraud Orend. 2011. "Advances in Tenascin-C Biology." *Cellular and Molecular Life Sciences* 68 (19): 3175–99. https://doi.org/10.1007/s00018-011-0783-6.

Midwood, Kim S., Matthias Chiquet, Richard P. Tucker, and Gertraud Orend. 2016. "Tenascin-C at a Glance." *Journal of Cell Science* 129 (23): 4321–27. https://doi.org/10.1242/jcs.190546.

Midwood, Kim S., and Jean E. Schwarzbauer. 2002. "Tenascin-C Modulates Matrix Contraction via Focal Adhesion Kinase- and Rho-Mediated Signaling Pathways." *Molecular Biology of the Cell* 13 (10): 3601–13. https://doi.org/10.1091/mbc.e02-05-0292.

Midwood, Kim S., Leyla V. Valenick, Henry C. Hsia, and Jean E. Schwarzbauer. 2004. "Coregulation of Fibronectin Signaling and Matrix Contraction by Tenascin-C and Syndecan-4." *Molecular Biology of the Cell* 15 (12): 5670–77. https://doi.org/10.1091/mbc.e04-08-0759.

Midwood, Kim, Sandra Sacre, Anna M. Piccinini, Julia Inglis, Annette Trebaul, Emma Chan, Stefan Drexler, et al. 2009. "Tenascin-C Is an Endogenous Activator of Toll-like Receptor 4 That Is Essential for Maintaining Inflammation in Arthritic Joint Disease." *Nature Medicine* 15 (7): 774–80. https://doi.org/10.1038/nm.1987.

Minn, Andy J., Yibin Kang, Inna Serganova, Gaorav P. Gupta, Dilip D. Giri, Mikhail Doubrovin, Vladimir Ponomarev, William L. Gerald, Ronald Blasberg, and Joan Massagué. 2005. "Distinct Organ-Specific Metastatic Potential of

Individual Breast Cancer Cells and Primary Tumors." *Journal of Clinical Investigation* 115 (1): 44–55. https://doi.org/10.1172/JCI22320.

Mittal, Deepak, Matthew M. Gubin, Robert D. Schreiber, and Mark J. Smyth. 2014. "New Insights into Cancer Immunoediting and Its Three Component Phases--Elimination, Equilibrium and Escape." *Current Opinion in Immunology* 27 (April): 16–25. https://doi.org/10.1016/j.coi.2014.01.004.

Mock, Andreas, Rolf Warta, Christoph Geisenberger, Ralf Bischoff, Alexander Schulte, Katrin Lamszus, Volker Stadler, et al. 2015. "Printed Peptide Arrays Identify Prognostic TNC Serumantibodies in Glioblastoma Patients." *Oncotarget* 6 (15): 13579–90. https://doi.org/10.18632/oncotarget.3791.

Mueller, Margareta M., and Norbert E. Fusenig. 2004. "Friends or Foes — Bipolar Effects of the Tumour Stroma in Cancer." *Nature Reviews Cancer* 4 (11): 839–49. https://doi.org/10.1038/nrc1477.

Müller, Anja, Bernhard Homey, Hortensia Soto, Nianfeng Ge, Daniel Catron, Matthew E. Buchanan, Terri McClanahan, et al. 2001. "Involvement of Chemokine Receptors in Breast Cancer Metastasis." *Nature* 410 (6824): 50–56. https://doi.org/10.1038/35065016.

Muller, W. J., E. Sinn, P. K. Pattengale, R. Wallace, and P. Leder. 1988. "Single-Step Induction of Mammary Adenocarcinoma in Transgenic Mice Bearing the Activated c-Neu Oncogene." *Cell* 54 (1): 105–15.

Murray, Peter J., Judith E. Allen, Subhra K. Biswas, Edward A. Fisher, Derek W. Gilroy, Sergij Goerdt, Siamon Gordon, et al. 2014. "Macrophage Activation and Polarization: Nomenclature and Experimental Guidelines." *Immunity* 41 (1): 14–20. https://doi.org/10.1016/j.immuni.2014.06.008.

Nagaharu, Keiki, Xinhui Zhang, Toshimichi Yoshida, Daisuke Katoh, Noriko Hanamura, Yuji Kozuka, Tomoko Ogawa, Taizo Shiraishi, and Kyoko Imanaka-Yoshida. 2011. "Tenascin C Induces Epithelial-Mesenchymal Transition–Like Change Accompanied by SRC Activation and Focal Adhesion Kinase Phosphorylation in Human Breast Cancer Cells." *The American Journal of Pathology* 178 (2): 754–63. https://doi.org/10.1016/j.ajpath.2010.10.015.

Naito, Y., K. Saito, K. Shiiba, A. Ohuchi, K. Saigenji, H. Nagura, and H. Ohtani. 1998. "CD8+ T Cells Infiltrated within Cancer Cell Nests as a Prognostic Factor in Human Colorectal Cancer." *Cancer Research* 58 (16): 3491–94.

Nakahara, Hiroki, Esteban C. Gabazza, Hajime Fujimoto, Yoichi Nishii, Corina N. D'Alessandro-Gabazza, Nelson E. Bruno, Takehiro Takagi, et al. 2006. "Deficiency of Tenascin C Attenuates Allergen-Induced Bronchial Asthma in the Mouse." *European Journal of Immunology* 36 (12): 3334–45. https://doi.org/10.1002/eji.200636271.

Nencioni, Alessio, Frank Grünebach, Susanne M. Schmidt, Martin R. Müller, Davide Boy, Franco Patrone, Alberto Ballestrero, and Peter Brossart. 2008. "The Use of Dendritic Cells in Cancer Immunotherapy." *Critical Reviews in*

Oncology/Hematology 65 (3): 191–99. https://doi.org/10.1016/j.critrevonc.2007.10.002.

Nieman, Kristin M, Hilary A Kenny, Carla V Penicka, Andras Ladanyi, Rebecca Buell-Gutbrod, Marion R Zillhardt, Iris L Romero, et al. 2011. "Adipocytes Promote Ovarian Cancer Metastasis and Provide Energy for Rapid Tumor Growth." *Nature Medicine* 17 (11): 1498–1503. https://doi.org/10.1038/nm.2492.

Numasaki, Muneo, Jun-ichi Fukushi, Mayumi Ono, Satwant K. Narula, Paul J. Zavodny, Toshio Kudo, Paul D. Robbins, Hideaki Tahara, and Michael T. Lotze. 2003. "Interleukin-17 Promotes Angiogenesis and Tumor Growth." *Blood* 101 (7): 2620–27. https://doi.org/10.1182/blood-2002-05-1461.

Ocklind, G., J. Talts, R. Fässler, A. Mattsson, and P. Ekblom. 1993. "Expression of Tenascin in Developing and Adult Mouse Lymphoid Organs." *The Journal of Histochemistry and Cytochemistry: Official Journal of the Histochemistry Society* 41 (8): 1163–69. https://doi.org/10.1177/41.8.7687262.

O'Connell, J. T., H. Sugimoto, V. G. Cooke, B. A. MacDonald, A. I. Mehta, V. S. LeBleu, R. Dewar, et al. 2011a. "VEGF-A and Tenascin-C Produced by S100A4+ Stromal Cells Are Important for Metastatic Colonization." *Proceedings of the National Academy of Sciences* 108 (38): 16002–7. https://doi.org/10.1073/pnas.1109493108.

Okabe, S. 2005. "Stromal Cell-Derived Factor-1 /CXCL12-Induced Chemotaxis of T Cells Involves Activation of the RasGAP-Associated Docking Protein p62Dok-1." *Blood* 105 (2): 474–80. https://doi.org/10.1182/blood-2004-03-0843.

Olumi, A. F., G. D. Grossfeld, S. W. Hayward, P. R. Carroll, T. D. Tlsty, and G. R. Cunha. 1999. "Carcinoma-Associated Fibroblasts Direct Tumor Progression of Initiated Human Prostatic Epithelium." *Cancer Research* 59 (19): 5002–11.

Orend, Gertraud, and Ruth Chiquet-Ehrismann. 2006. "Tenascin-C Induced Signaling in Cancer." *Cancer Letters* 244 (2): 143–63. https://doi.org/10.1016/j.canlet.2006.02.017.

Orend, Gertraud, Wentao Huang, Monilola A. Olayioye, Nancy E. Hynes, and Ruth Chiquet-Ehrismann. 2003. "Tenascin-C Blocks Cell-Cycle Progression of Anchorage-Dependent Fibroblasts on Fibronectin through Inhibition of Syndecan-4." *Oncogene* 22 (25): 3917–26. https://doi.org/10.1038/sj.onc.1206618.

Orimo, Akira, Piyush B. Gupta, Dennis C. Sgroi, Fernando Arenzana-Seisdedos, Thierry Delaunay, Rizwan Naeem, Vincent J. Carey, Andrea L. Richardson, and Robert A. Weinberg. 2005. "Stromal Fibroblasts Present in Invasive Human Breast Carcinomas Promote Tumor Growth and Angiogenesis through Elevated SDF-1/CXCL12 Secretion." *Cell* 121 (3): 335–48. https://doi.org/10.1016/j.cell.2005.02.034.

Oskarsson, Thordur. 2013. "Extracellular Matrix Components in Breast Cancer Progression and Metastasis." *The Breast* 22 (August): S66–72. https://doi.org/10.1016/j.breast.2013.07.012.

Oskarsson, Thordur, Swarnali Acharyya, Xiang H-F Zhang, Sakari Vanharanta, Sohail F Tavazoie, Patrick G Morris, Robert J Downey, Katia Manova-Todorova, Edi Brogi, and Joan Massagué. 2011. "Breast Cancer Cells Produce Tenascin C as a Metastatic Niche Component to Colonize the Lungs." *Nature Medicine* 17 (7): 867–74. https://doi.org/10.1038/nm.2379.

Ota, Daichi, Masashi Kanayama, Yutaka Matsui, Koyu Ito, Naoyoshi Maeda, Goro Kutomi, Koichi Hirata, et al. 2014. "Tumor-α9β1 Integrin-Mediated Signaling Induces Breast Cancer Growth and Lymphatic Metastasis via the Recruitment of Cancer-Associated Fibroblasts." *Journal of Molecular Medicine (Berlin, Germany)* 92 (12): 1271–81. https://doi.org/10.1007/s00109-014-1183-9.

Pagès, Franck, Anne Berger, Matthieu Camus, Fatima Sanchez-Cabo, Anne Costes, Robert Molidor, Bernhard Mlecnik, et al. 2005. "Effector Memory T Cells, Early Metastasis, and Survival in Colorectal Cancer." *New England Journal of Medicine* 353 (25): 2654–66. https://doi.org/10.1056/NEJMoa051424.

Pardoll, Drew M. 2012. "The Blockade of Immune Checkpoints in Cancer Immunotherapy." *Nature Reviews Cancer* 12 (4): 252–64. https://doi.org/10.1038/nrc3239.

Parekh, Kalpaj, Sabarinathan Ramachandran, Joel Cooper, Darell Bigner, Alexander Patterson, and T. Mohanakumar. 2005. "Tenascin-C, over Expressed in Lung Cancer down Regulates Effector Functions of Tumor Infiltrating Lymphocytes." *Lung Cancer* 47 (1): 17–29. https://doi.org/10.1016/j.lungcan.2004.05.016.

Payne, Aimee S., and Lynn A. Cornelius. 2002. "The Role of Chemokines in Melanoma Tumor Growth and Metastasis." *Journal of Investigative Dermatology* 118 (6): 915–22. https://doi.org/10.1046/j.1523-1747.2002.01725.x.

Piccart-Gebhart, Martine J., Marion Procter, Brian Leyland-Jones, Aron Goldhirsch, Michael Untch, Ian Smith, Luca Gianni, et al. 2005. "Trastuzumab after Adjuvant Chemotherapy in HER2-Positive Breast Cancer." *New England Journal of Medicine* 353 (16): 1659–72. https://doi.org/10.1056/NEJMoa052306.

Ping, Yi-Fang, Xia Zhang, and Xiu-Wu Bian. 2016. "Cancer Stem Cells and Their Vascular Niche: Do They Benefit from Each Other?" *Cancer Letters* 380 (2): 561–67. https://doi.org/10.1016/j.canlet.2015.05.010.

Plitas, George, Catherine Konopacki, Kenmin Wu, Paula D. Bos, Monica Morrow, Ekaterina V. Putintseva, Dmitriy M. Chudakov, and Alexander Y. Rudensky. 2016. "Regulatory T Cells Exhibit Distinct Features in Human Breast Cancer." *Immunity* 45 (5): 1122–34. https://doi.org/10.1016/j.immuni.2016.10.032.

Poznansky, M. C., I. T. Olszak, R. Foxall, R. H. Evans, A. D. Luster, and D. T. Scadden. 2000. "Active Movement of T Cells Away from a Chemokine." *Nature Medicine* 6 (5): 543–48. https://doi.org/10.1038/75022.

Puente Navazo, M. D., D. Valmori, and C. Rüegg. 2001. "The Alternatively Spliced Domain TnFnIII A1A2 of the Extracellular Matrix Protein Tenascin-C

Suppresses Activation-Induced T Lymphocyte Proliferation and Cytokine Production." *Journal of Immunology (Baltimore, Md.: 1950)* 167 (11): 6431–40.

Qi, Chun-Jian, Yong-Ling Ning, Ye-Shan Han, Hai-Yan Min, Heng Ye, Yu-Lan Zhu, and Ke-Qing Qian. 2012. "Autologous Dendritic Cell Vaccine for Estrogen Receptor (ER)/Progestin Receptor (PR) Double-Negative Breast Cancer." *Cancer Immunology, Immunotherapy* 61 (9): 1415–24. https://doi.org/10.1007/s00262-011-1192-2.

Qian, Bin-Zhi, Jiufeng Li, Hui Zhang, Takanori Kitamura, Jinghang Zhang, Liam R. Campion, Elizabeth A. Kaiser, Linda A. Snyder, and Jeffrey W. Pollard. 2011. "CCL2 Recruits Inflammatory Monocytes to Facilitate Breast-Tumour Metastasis." *Nature* 475 (7355): 222–25. https://doi.org/10.1038/nature10138.

Radisky, Evette S., and Derek C. Radisky. 2015. "Matrix Metalloproteinases as Breast Cancer Drivers and Therapeutic Targets." *Frontiers in Bioscience (Landmark Edition)* 20 (June): 1144–63.

Rakha, Emad A., Jorge S. Reis-Filho, and Ian O. Ellis. 2010. "Combinatorial Biomarker Expression in Breast Cancer." *Breast Cancer Research and Treatment* 120 (2): 293–308. https://doi.org/10.1007/s10549-010-0746-x.

Reiman, Jennifer M., Maciej Kmieciak, Masoud H. Manjili, and Keith L. Knutson. 2007. "Tumor Immunoediting and Immunosculpting Pathways to Cancer Progression." *Seminars in Cancer Biology* 17 (4): 275–87. https://doi.org/10.1016/j.semcancer.2007.06.009.

Ribatti, Domenico. 2017. "The Concept of Immune Surveillance against Tumors. The First Theories." *Oncotarget* 8 (4): 7175–80. https://doi.org/10.18632/oncotarget.12739.

Richter, Rudolf, Andrea Jochheim-Richter, Felicia Ciuculescu, Katarina Kollar, Erhard Seifried, Ulf Forssmann, Dennis Verzijl, et al. 2014. "Identification and Characterization of Circulating Variants of CXCL12 from Human Plasma: Effects on Chemotaxis and Mobilization of Hematopoietic Stem and Progenitor Cells." *Stem Cells and Development* 23 (16): 1959–74. https://doi.org/10.1089/scd.2013.0524.

Rüegg, C. R., R. Chiquet-Ehrismann, and S. S. Alkan. 1989. "Tenascin, an Extracellular Matrix Protein, Exerts Immunomodulatory Activities." *Proceedings of the National Academy of Sciences of the United States of America* 86 (19): 7437–41.

Ruffell, Brian, Alfred Au, Hope S. Rugo, Laura J. Esserman, E. Shelley Hwang, and Lisa M. Coussens. 2012. "Leukocyte Composition of Human Breast Cancer." *Proceedings of the National Academy of Sciences of the United States of America* 109 (8): 2796–2801. https://doi.org/10.1073/pnas.1104303108.

Ruiz, Christian, Wentao Huang, Monika E. Hegi, Katrin Lange, Marie-France Hamou, Erika Fluri, Edward J. Oakeley, Ruth Chiquet-Ehrismann, and Gertraud Orend. 2004. "Growth Promoting Signaling by Tenascin-C [Corrected]." *Cancer Research* 64 (20): 7377–85. https://doi.org/10.1158/0008-5472.CAN-04-1234.

Rupp, Tristan, Benoit Langlois, Maria M. Koczorowska, Agata Radwanska, Zhen Sun, Thomas Hussenet, Olivier Lefebvre, et al. 2016. "Tenascin-C Orchestrates Glioblastoma Angiogenesis by Modulation of Pro- and Anti-Angiogenic Signaling." *Cell Reports* 17 (10): 2607–19. https://doi.org/10.1016/j.celrep.2016.11.012.

Santisteban, Marta, Jennifer M. Reiman, Michael K. Asiedu, Marshall D. Behrens, Aziza Nassar, Kimberly R. Kalli, Paul Haluska, et al. 2009. "Immune-Induced Epithelial to Mesenchymal Transition in Vivo Generates Breast Cancer Stem Cells." *Cancer Research* 69 (7): 2887–95. https://doi.org/10.1158/0008-5472.CAN-08-3343.

Satthaporn, Sukchai, Adrian Robins, Wichai Vassanasiri, Mohamed El-Sheemy, Jibril A. Jibril, David Clark, David Valerio, and Oleg Eremin. 2004. "Dendritic Cells Are Dysfunctional in Patients with Operable Breast Cancer." *Cancer Immunology, Immunotherapy: CII* 53 (6): 510–18. https://doi.org/10.1007/s00262-003-0485-5.

Saupe, Falk, Anja Schwenzer, Yundan Jia, Isabelle Gasser, Caroline Spenlé, Benoit Langlois, Martial Kammerer, et al. 2013. "Tenascin-C Downregulates Wnt Inhibitor Dickkopf-1, Promoting Tumorigenesis in a Neuroendocrine Tumor Model." *Cell Reports* 5 (2): 482–92. https://doi.org/10.1016/j.celrep.2013.09.014.

Schreiber, R. D., L. J. Old, and M. J. Smyth. 2011. "Cancer Immunoediting: Integrating Immunity's Roles in Cancer Suppression and Promotion." *Science* 331 (6024): 1565–70. https://doi.org/10.1126/science.1203486.

Schultz, Gregory S., and Annette Wysocki. 2009. "Interactions between Extracellular Matrix and Growth Factors in Wound Healing." *Wound Repair and Regeneration* 17 (2): 153–62. https://doi.org/10.1111/j.1524-475X.2009.00466.x.

Schwenzer, Anja, Xia Jiang, Ted R. Mikuls, Jeffrey B. Payne, Harlan R. Sayles, Anne-Marie Quirke, Benedikt M. Kessler, et al. 2016. "Identification of an Immunodominant Peptide from Citrullinated Tenascin-C as a Major Target for Autoantibodies in Rheumatoid Arthritis." *Annals of the Rheumatic Diseases* 75 (10): 1876–83. https://doi.org/10.1136/annrheumdis-2015-208495.

Seaman, Steven, Janine Stevens, Mi Young Yang, Daniel Logsdon, Cari Graff-Cherry, and Brad St Croix. 2007. "Genes That Distinguish Physiological and Pathological Angiogenesis." *Cancer Cell* 11 (6): 539–54. https://doi.org/10.1016/j.ccr.2007.04.017.

Shankaran, V., H. Ikeda, A. T. Bruce, J. M. White, P. E. Swanson, L. J. Old, and R. D. Schreiber. 2001. "IFNgamma and Lymphocytes Prevent Primary Tumour Development and Shape Tumour Immunogenicity." *Nature* 410 (6832): 1107–11. https://doi.org/10.1038/35074122.

Sharma, P., and J. P. Allison. 2015. "The Future of Immune Checkpoint Therapy." *Science* 348 (6230): 56–61. https://doi.org/10.1126/science.aaa8172.

Shiga, Kazuyoshi, Masayasu Hara, Takaya Nagasaki, Takafumi Sato, Hiroki Takahashi, and Hiromitsu Takeyama. 2015. "Cancer-Associated Fibroblasts: Their Characteristics and Their Roles in Tumor Growth." *Cancers* 7 (4): 2443–58. https://doi.org/10.3390/cancers7040902.

Siegel, Rebecca L., Kimberly D. Miller, and Ahmedin Jemal. 2017. "Cancer Statistics, 2017." *CA: A Cancer Journal for Clinicians* 67 (1): 7–30. https://doi.org/10.3322/caac.21387.

Simian, M., Y. Hirai, M. Navre, Z. Werb, A. Lochter, and M. J. Bissell. 2001. "The Interplay of Matrix Metalloproteinases, Morphogens and Growth Factors Is Necessary for Branching of Mammary Epithelial Cells." *Development (Cambridge, England)* 128 (16): 3117–31.

Simo, P., F. Bouziges, J. C. Lissitzky, L. Sorokin, M. Kedinger, and P. Simon-Assmann. 1992. "Dual and Asynchronous Deposition of Laminin Chains at the Epithelial-Mesenchymal Interface in the Gut." *Gastroenterology* 102 (6): 1835–45.

Simpson, Peter T, Jorge S Reis-Filho, Theodora Gale, and Sunil R Lakhani. 2005. "Molecular Evolution of Breast Cancer." *The Journal of Pathology* 205 (2): 248–54. https://doi.org/10.1002/path.1691.

Slamon, Dennis J., Brian Leyland-Jones, Steven Shak, Hank Fuchs, Virginia Paton, Alex Bajamonde, Thomas Fleming, et al. 2001. "Use of Chemotherapy plus a Monoclonal Antibody against HER2 for Metastatic Breast Cancer That Overexpresses HER2." *New England Journal of Medicine* 344 (11): 783–92. https://doi.org/10.1056/NEJM200103153441101.

Sledge, George W., Eleftherios P. Mamounas, Gabriel N. Hortobagyi, Harold J. Burstein, Pamela J. Goodwin, and Antonio C. Wolff. 2014. "Past, Present, and Future Challenges in Breast Cancer Treatment." *Journal of Clinical Oncology* 32 (19): 1979–86. https://doi.org/10.1200/JCO.2014.55.4139.

Soria, Gali, and Adit Ben-Baruch. 2008. "The Inflammatory Chemokines CCL2 and CCL5 in Breast Cancer." *Cancer Letters* 267 (2): 271–85. https://doi.org/10.1016/j.canlet.2008.03.018.

Sorokin, Lydia. 2010. "The Impact of the Extracellular Matrix on Inflammation." *Nature Reviews. Immunology* 10 (10): 712–23. https://doi.org/10.1038/nri2852.

Spaeth, Erika L., Jennifer L. Dembinski, A. Kate Sasser, Keri Watson, Ann Klopp, Brett Hall, Michael Andreeff, and Frank Marini. 2009. "Mesenchymal Stem Cell Transition to Tumor-Associated Fibroblasts Contributes to Fibrovascular Network Expansion and Tumor Progression." Edited by Mikhail V. Blagosklonny. *PLoS ONE* 4 (4): e4992. https://doi.org/10.1371/journal.pone.0004992.

Spenlé, Caroline, Isabelle Gasser, Falk Saupe, Klaus-Peter Janssen, Christiane Arnold, Annick Klein, Michael van der Heyden, et al. 2015. "Spatial Organization of the Tenascin-C Microenvironment in Experimental and Human

Cancer." *Cell Adhesion & Migration* 9 (1–2): 4–13. https://doi.org/10.1080/19336918.2015.1005452.

Sternlicht, Mark D, Andre Lochter, Carolyn J Sympson, Bing Huey, Jean-Philippe Rougier, Joe W Gray, Dan Pinkel, Mina J Bissell, and Zena Werb. 1999. "The Stromal Proteinase MMP3/Stromelysin-1 Promotes Mammary Carcinogenesis." *Cell* 98 (2): 137–46. https://doi.org/10.1016/S0092-8674(00)81009-0.

Stylianopoulos, Triantafyllos, and Rakesh K. Jain. 2013. "Combining Two Strategies to Improve Perfusion and Drug Delivery in Solid Tumors." *Proceedings of the National Academy of Sciences of the United States of America* 110 (46): 18632–37. https://doi.org/10.1073/pnas.1318415110.

Sun, Zhen, Anja Schwenzer, Tristan Rupp, Devadarssen Murdamoothoo, Rolando Vegliante, Olivier Lefebvre, Annick Klein, Thomas Hussenet, and Gertraud Orend. 2017. "Tenascin-C Promotes Tumor Cell Migration and Metastasis through Integrin α9β1 -Mediated YAP Inhibition." *Cancer Research*, December, canres.1597.2017. https://doi.org/10.1158/0008-5472.CAN-17-1597.

Taga, Takashi, Atsushi Suzuki, Ignacio Gonzalez-Gomez, Floyd H. Gilles, Monique Stins, Hiroyuki Shimada, Lora Barsky, Kenneth I. Weinberg, and Walter E. Laug. 2002. "Alpha v-Integrin Antagonist EMD 121974 Induces Apoptosis in Brain Tumor Cells Growing on Vitronectin and Tenascin." *International Journal of Cancer* 98 (5): 690–97.

Takeuchi, H., Y. Maehara, E. Tokunaga, T. Koga, Y. Kakeji, and K. Sugimachi. 2001. "Prognostic Significance of Natural Killer Cell Activity in Patients with Gastric Carcinoma: A Multivariate Analysis." *The American Journal of Gastroenterology* 96 (2): 574–78. https://doi.org/10.1111/j.1572-0241.2001.03535.x.

Talts, J. F., G. Wirl, M. Dictor, W. J. Muller, and R. Fässler. 1999. "Tenascin-C Modulates Tumor Stroma and Monocyte/Macrophage Recruitment but Not Tumor Growth or Metastasis in a Mouse Strain with Spontaneous Mammary Cancer." *Journal of Cell Science* 112 (Pt 12) (June): 1855–64.

Tamaoki, Masashi, Kyoko Imanaka-Yoshida, Kazuto Yokoyama, Tomohiro Nishioka, Hiroyasu Inada, Michiaki Hiroe, Teruyo Sakakura, and Toshimichi Yoshida. 2005. "Tenascin-C Regulates Recruitment of Myofibroblasts during Tissue Repair after Myocardial Injury." *The American Journal of Pathology* 167 (1): 71–80. https://doi.org/10.1016/S0002-9440(10)62954-9.

Tavazoie, Sohail F., Claudio Alarcón, Thordur Oskarsson, David Padua, Qiongqing Wang, Paula D. Bos, William L. Gerald, and Joan Massagué. 2008. "Endogenous Human microRNAs That Suppress Breast Cancer Metastasis." *Nature* 451 (7175): 147–52. https://doi.org/10.1038/nature06487.

Teng, Michele W. L., Jerome Galon, Wolf-Herman Fridman, and Mark J. Smyth. 2015. "From Mice to Humans: Developments in Cancer Immunoediting." *The*

Journal of Clinical Investigation 125 (9): 3338–46. https://doi.org/10.1172/JCI80004.

Teschendorff, Andrew E., Sergio Gomez, Alex Arenas, Dorraya El-Ashry, Marcus Schmidt, Mathias Gehrmann, and Carlos Caldas. 2010. "Improved Prognostic Classification of Breast Cancer Defined by Antagonistic Activation Patterns of Immune Response Pathway Modules." *BMC Cancer* 10 (November): 604. https://doi.org/10.1186/1471-2407-10-604.

Teti, A. 1992. "Regulation of Cellular Functions by Extracellular Matrix." *Journal of the American Society of Nephrology: JASN* 2 (10 Suppl): S83-87.

Tian, Tianhai, Sarah Olson, James M. Whitacre, and Angus Harding. 2011. "The Origins of Cancer Robustness and Evolvability." *Integrative Biology: Quantitative Biosciences from Nano to Macro* 3 (1): 17–30. https://doi.org/10.1039/c0ib00046a.

Trapani, Joseph A., and Mark J. Smyth. 2002. "Functional Significance of the Perforin/Granzyme Cell Death Pathway." *Nature Reviews. Immunology* 2 (10): 735–47. https://doi.org/10.1038/nri911.

Tsujino, T., I. Seshimo, H. Yamamoto, C. Y. Ngan, K. Ezumi, I. Takemasa, M. Ikeda, M. Sekimoto, N. Matsuura, and M. Monden. 2007. "Stromal Myofibroblasts Predict Disease Recurrence for Colorectal Cancer." *Clinical Cancer Research* 13 (7): 2082–90. https://doi.org/10.1158/1078-0432.CCR-06-2191.

Tsunoda, Takatsugu, Hiroyasu Inada, Ilunga Kalembeyi, Kyoko Imanaka-Yoshida, Mirei Sakakibara, Ray Okada, Koji Katsuta, Teruyo Sakakura, Yuichi Majima, and Toshimichi Yoshida. 2003. "Involvement of Large Tenascin-C Splice Variants in Breast Cancer Progression." *The American Journal of Pathology* 162 (6): 1857–67. https://doi.org/10.1016/S0002-9440(10)64320-9.

Tucker, Richard P., and Ruth Chiquet-Ehrismann. 2009. "The Regulation of Tenascin Expression by Tissue Microenvironments." *Biochimica Et Biophysica Acta* 1793 (5): 888–92. https://doi.org/10.1016/j.bbamcr.2008.12.012.

Turley, Shannon J., Viviana Cremasco, and Jillian L. Astarita. 2015. "Immunological Hallmarks of Stromal Cells in the Tumour Microenvironment." *Nature Reviews. Immunology* 15 (11): 669–82. https://doi.org/10.1038/nri3902.

Turnis, Meghan E, and Cliona M Rooney. 2010. "Enhancement of Dendritic Cells as Vaccines for Cancer." *Immunotherapy* 2 (6): 847–62. https://doi.org/10.2217/imt.10.56.

Udalova, Irina A., Michaela Ruhmann, Scott J. P. Thomson, and Kim S. Midwood. 2011. "Expression and Immune Function of Tenascin-C." *Critical Reviews in Immunology* 31 (2): 115–45.

Ursin, Giske, Linda Hovanessian-Larsen, Yuri R Parisky, Malcolm C Pike, and Anna H Wu. 2005. "Greatly Increased Occurrence of Breast Cancers in Areas of Mammographically Dense Tissue." *Breast Cancer Research* 7 (5). https://doi.org/10.1186/bcr1260.

Van Obberghen-Schilling, Ellen, Richard P. Tucker, Falk Saupe, Isabelle Gasser, Botond Cseh, and Gertraud Orend. 2011. "Fibronectin and Tenascin-C: Accomplices in Vascular Morphogenesis during Development and Tumor Growth." *The International Journal of Developmental Biology* 55 (4–5): 511–25. https://doi.org/10.1387/ijdb.103243eo.

Vasudev, Naveen S., and Andrew R. Reynolds. 2014. "Anti-Angiogenic Therapy for Cancer: Current Progress, Unresolved Questions and Future Directions." *Angiogenesis* 17 (3): 471–94. https://doi.org/10.1007/s10456-014-9420-y.

Vesely, Matthew D., Michael H. Kershaw, Robert D. Schreiber, and Mark J. Smyth. 2011. "Natural Innate and Adaptive Immunity to Cancer." *Annual Review of Immunology* 29 (1): 235–71. https://doi.org/10.1146/annurev-immunol-031210-101324.

Villegas, Francisco R., Santiago Coca, Vicente G. Villarrubia, Rodrigo Jiménez, María Jesús Chillón, Javier Jareño, Marcos Zuil, and Luis Callol. 2002. "Prognostic Significance of Tumor Infiltrating Natural Killer Cells Subset CD57 in Patients with Squamous Cell Lung Cancer." *Lung Cancer (Amsterdam, Netherlands)* 35 (1): 23–28.

Vollmer, Günter. 1997. "Biologic and Oncologic Implications of Tenascin-C/Hexabrachion Proteins." *Critical Reviews in Oncology/Hematology* 25 (3): 187–210. https://doi.org/10.1016/S1040-8428(97)00004-8.

Wang, Zhuomin, Bo Han, Zhuang Zhang, Jian Pan, and Hui Xia. 2010. "Expression of Angiopoietin-like 4 and Tenascin C but Not Cathepsin C mRNA Predicts Prognosis of Oral Tongue Squamous Cell Carcinoma." *Biomarkers: Biochemical Indicators of Exposure, Response, and Susceptibility to Chemicals* 15 (1): 39–46. https://doi.org/10.3109/13547500903261362.

Weber, Frank, Lei Shen, Koichi Fukino, Attila Patocs, George L. Mutter, Trinidad Caldes, and Charis Eng. 2006. "Total-Genome Analysis of BRCA1/2-Related Invasive Carcinomas of the Breast Identifies Tumor Stroma as Potential Landscaper for Neoplastic Initiation." *The American Journal of Human Genetics* 78 (6): 961–72. https://doi.org/10.1086/504090.

Weiner, D. B., J. Liu, J. A. Cohen, W. V. Williams, and M. I. Greene. 1989. "A Point Mutation in the Neu Oncogene Mimics Ligand Induction of Receptor Aggregation." *Nature* 339 (6221): 230–31. https://doi.org/10.1038/339230a0.

Wenk, M. B., K. S. Midwood, and J. E. Schwarzbauer. 2000. "Tenascin-C Suppresses Rho Activation." *The Journal of Cell Biology* 150 (4): 913–20.

Whitford, P., W. D. George, and A. M. Campbell. 1992. "Flow Cytometric Analysis of Tumour Infiltrating Lymphocyte Activation and Tumour Cell MHC Class I and II Expression in Breast Cancer Patients." *Cancer Letters* 61 (2): 157–64.

Wijelath, E. S., S. Rahman, M. Namekata, J. Murray, T. Nishimura, Z. Mostafavi-Pour, Y. Patel, Y. Suda, M. J. Humphries, and M. Sobel. 2006. "Heparin-II Domain of Fibronectin Is a Vascular Endothelial Growth Factor-Binding Domain: Enhancement of VEGF Biological Activity by a Singular Growth

Factor/Matrix Protein Synergism." *Circulation Research* 99 (8): 853–60. https://doi.org/10.1161/01.RES.0000246849.17887.66.

Willis, B. C., RM Dubois, and Z Borok. 2006. "Epithelial Origin of Myofibroblasts during Fibrosis in the Lung." *Proceedings of the American Thoracic Society* 3 (4): 377–82. https://doi.org/10.1513/pats.200601-004TK.

Witz, Isaac P., and Orlev Levy-Nissenbaum. 2006. "The Tumor Microenvironment in the Post-PAGET Era." *Cancer Letters* 242 (1): 1–10. https://doi.org/10.1016/j.canlet.2005.12.005.

Woodside, D. G., D. K. Wooten, and B. W. McIntyre. 1998. "Adenosine Diphosphate (ADP)-Ribosylation of the Guanosine Triphosphatase (GTPase) Rho in Resting Peripheral Blood Human T Lymphocytes Results in Pseudopodial Extension and the Inhibition of T Cell Activation." *The Journal of Experimental Medicine* 188 (7): 1211–21.

Yamamoto, K., Q. N. Dang, S. P. Kennedy, R. Osathanondh, R. A. Kelly, and R. T. Lee. 1999. "Induction of Tenascin-C in Cardiac Myocytes by Mechanical Deformation. Role of Reactive Oxygen Species." *The Journal of Biological Chemistry* 274 (31): 21840–46.

Yang, Yuan, Howard H. Yang, Ying Hu, Peter H. Watson, Huaitian Liu, Thomas R. Geiger, Miriam R. Anver, et al. 2017. "Immunocompetent Mouse Allograft Models for Development of Therapies to Target Breast Cancer Metastasis." *Oncotarget* 8 (19): 30621–43. https://doi.org/10.18632/oncotarget.15695.

Yarden, Y. 2001. "Biology of HER2 and Its Importance in Breast Cancer." *Oncology* 61 Suppl 2: 1–13. https://doi.org/10.1159/000055396.

Yokosaki, Y., H. Monis, J. Chen, and D. Sheppard. 1996. "Differential Effects of the Integrins alpha9beta1, alphavbeta3, and alphavbeta6 on Cell Proliferative Responses to Tenascin. Roles of the Beta Subunit Extracellular and Cytoplasmic Domains." *The Journal of Biological Chemistry* 271 (39): 24144–50.

Yoshida, T., E. Matsumoto, N. Hanamura, I. Kalembeyi, K. Katsuta, A. Ishihara, and T. Sakakura. 1997. "Co-Expression of Tenascin and Fibronectin in Epithelial and Stromal Cells of Benign Lesions and Ductal Carcinomas in the Human Breast." *The Journal of Pathology* 182 (4): 421–28. https://doi.org/10.1002/(SICI)1096-9896(199708)182:4<421::AID-PATH886>3.0.CO;2-U.

Yoshida, Toshimichi, Tatsuya Akatsuka, and Kyoko Imanaka-Yoshida. 2015. "Tenascin-C and Integrins in Cancer." *Cell Adhesion & Migration* 9 (1–2): 96–104. https://doi.org/10.1080/19336918.2015.1008332.

Zagzag, D., D. R. Friedlander, J. Dosik, S. Chikramane, W. Chan, M. A. Greco, J. C. Allen, K. Dorovini-Zis, and M. Grumet. 1996. "Tenascin-C Expression by Angiogenic Vessels in Human Astrocytomas and by Human Brain Endothelial Cells in Vitro." *Cancer Research* 56 (1): 182–89.

Zambonin, Valentina, Alessandro De Toma, Luisa Carbognin, Rolando Nortilli, Elena Fiorio, Veronica Parolin, Sara Pilotto, et al. 2017. "Clinical Results of Randomized Trials and 'Real-World' Data Exploring the Impact of Bevacizumab for Breast Cancer: Opportunities for Clinical Practice and Perspectives for Research." *Expert Opinion on Biological Therapy* 17 (4): 497–506. https://doi.org/10.1080/14712598.2017.1289171.

Zboralski, Dirk, Kai Hoehlig, Dirk Eulberg, Anna Frömming, and Axel Vater. 2017. "Increasing Tumor-Infiltrating T Cells through Inhibition of CXCL12 with NOX-A12 Synergizes with PD-1 Blockade." *Cancer Immunology Research* 5 (11): 950–56. https://doi.org/10.1158/2326-6066.CIR-16-0303.

Zeisberg, E. M., S. Potenta, L. Xie, M. Zeisberg, and R. Kalluri. 2007. "Discovery of Endothelial to Mesenchymal Transition as a Source for Carcinoma-Associated Fibroblasts." *Cancer Research* 67 (21): 10123–28. https://doi.org/10.1158/0008-5472.CAN-07-3127.

Zhang, Lin, Jose R. Conejo-Garcia, Dionyssios Katsaros, Phyllis A. Gimotty, Marco Massobrio, Giorgia Regnani, Antonis Makrigiannakis, et al. 2003. "Intratumoral T Cells, Recurrence, and Survival in Epithelial Ovarian Cancer." *New England Journal of Medicine* 348 (3): 203–13. https://doi.org/10.1056/NEJMoa020177.

Zhao, Xixi, Jingkun Qu, Yuchen Sun, Jizhao Wang, Xu Liu, Feidi Wang, Hong Zhang, et al. 2017. "Prognostic Significance of Tumor-Associated Macrophages in Breast Cancer: A Meta-Analysis of the Literature." *Oncotarget* 8 (18): 30576–86. https://doi.org/10.18632/oncotarget.15736.

Zitvogel, Laurence, Antoine Tesniere, and Guido Kroemer. 2006. "Cancer despite Immunosurveillance: Immunoselection and Immunosubversion." *Nature Reviews Immunology* 6 (10): 715–27. https://doi.org/10.1038/nri1936.

Zumsteg, Adrian, and Gerhard Christofori. 2009. "Corrupt Policemen: Inflammatory Cells Promote Tumor Angiogenesis." *Current Opinion in Oncology* 21 (1): 60–70. https://doi.org/10.1097/CCO.0b013e32831bed7e.

Appendix I

Role of Tenascin-C in promoting lung metastasis through impacting vascular invasions

Zhen Sun[1-4&*], Inés Velázquez-Quesada[1-4*], Devadarssen Murdamoothoo[1-4], Gerlinde Averous[5], Constance Ahowesso[1-4], Alev Yilmaz[1-4], William Erne[1-4], Michael van der Heyden[1-4], Caroline Spenlé[1-4], Olivier Lefebvre[1-4], Annick Klein[1-4], Felicitas Oberndorfer[6], Andre Oszwald[6], Catherine Bourdon[7], Pierre Mangin[7], Carole Mathelin[8], Claire Deligne[9], Kim Midwood[9], Marie-Pierre Chenard[5], Gerhard Christofori[10], Thomas Hussenet[1-4], Renate Kain[6], Thomas Loustau[1-4] and Gertraud Orend[1-4#]

Running title: Through impacting vascular invasions tenascin-C increases metastasis

* equal contribution

correspondence:

Gertraud Orend, gertraud.orend@inserm.fr, Phone: +33 (0) 3 68 85 39 96, current address : Institut d'Hématologie et d'Immunologie, Hôpital Civil, 4 rue Kirschleger, 67085 Strasbourg Cedex

& Current address: 1. Tongji Cancer Research Institute, Tongji Hospital, Tongji Medical College in Huazhong University of Science and Technology, Wuhan, Hubei, China. 2. Department of Gastrointestinal Surgery, Tongji Hospital, Tongji Medical College in Huazhong University of Science and Technology, Wuhan, Hubei, China.

[1] INSERM U1109 - MN3T, The Microenvironmental Niche in Tumorigenesis and Targeted Therapy and, the Tumor Microenvironment group

[2] Université de Strasbourg, Strasbourg, France

[3] LabEx Medalis, Université de Strasbourg, France

[4] Fédération de Médecine Translationnelle de Strasbourg (FMTS), Strasbourg, France

[5] Department of Pathology, University Hospital Strasbourg, Strasbourg, France

[6] Department of Pathology, Medical University of Vienna (MUW), Vienna, Austria

[7] Etablissement Français du Sang, INSERM U949, Strasbourg, France

[8] Department of breast diseases and surgery, Strasbourg University Hospital, Strasbourg, France

[9] Kennedy Institute of Rheumatology, University of Oxford, Oxford, UK

[10] Department Medicine, University Basel, Basel, Switzerland

Abstract

Metastasis is a major cause of death in patients with cancer. The extracellular matrix molecule tenascin-C is a known promoter of metastasis but how is poorly understood. We used a transgenic murine MMTV-NeuNT model of metastasis, and a syngeneic orthotopic breast cancer model derived thereof, with spontaneous metastasis to the lung. Both models were engineered to control tenascin-C expression levels. We found that tenascin-C promotes tumor onset and metastasis and demonstrate that tenascin-C comprises a key component of vascular invasions in blood vessels at sites of metastatic invasion. We reveal that vascular invasions are organized clusters of platelet associated proliferating tumor cells with epithelial characteristics, that are surrounded by Fsp1+ cells, a layer of matrix and a monolayer of endothelial cells. We show that host tenascin-C promotes the development of the ensheathing endothelial cell coat around the intravascular tumor cell nest, increases platelet abundance, tumor cell survival and epithelial plasticity, and breaching of tumor cells into the lung parenchyma. This phenotype correlated with increased survival and migration of cultured tumor cells through tenascin-C-induced plasticity. Our results are relevant for human cancer, where vascular invasions are a sign of worsened prognosis. We document that in tumor blood vessels vascular invasions express tenascin-C and have an endothelial cell coat which is in contrast to lymphatic vessels that lack these traits. This information may be useful for stratification of cancer patients and provides tenascin-C blockade as a potential strategy to specifically targeting vascular invasions in blood vessels for preventing tumor spread.

Introduction

Despite earlier diagnosis and improved treatment a high number of cancer patients die due to cancer-related complications, tumor recurrence and, most frequently, metastasis [1]. Therefore, a better knowledge of the mechanisms of metastasis is required. The tumor microenvironment (TME) comprising tumor and stromal cells, soluble factors and extracellular matrix (ECM) promotes metastasis [2]. An important ECM molecule that enhances metastasis is tenascin-C (TNC) [3]. TNC plays multiple roles in cancer, as recently demonstrated in a stochastic pancreatic neuroendocrine tumor (PNET) model with abundant and no TNC, where TNC was found to enhance survival, proliferation, invasion, angiogenesis and, lung metastasis [4]. Also in breast cancer models, TNC was shown to play a role in promoting metastasis lung colonization [5,6]. Yet, whether TNC is also involved in earlier steps of metastasis before tumor cells enter the lung parenchyma was unknown. An important step represents escape of tumor cells from the primary tumor and homing to distant organs where vascular invasions are described as precursors of parenchymal lung metastasis. Vascular invasions are clusters of tumor cells in the primary tumor or in vessels of organs with metastasis. They are known since a long time and correlate with thromboembolism and worsened cancer patient survival [7–9]. Targeting vascular invasions may offer novel anti-cancer targeting opportunities yet, little was known about their cellular and molecular composition, which we had investigated here.

We generated MMTV-NeuNT mice [10] that lack TNC (TNCKO) [11] and compared tumor onset and lung metastasis with that in WT tumor mice. We observed that TNC accelerates tumor onset and increases lung metastasis. By grafting tumor cells, derived from the same model [12] , expressing abundant or low TNC into the mammary gland of immune competent syngeneic mice that do or do not express TNC, we identified

host-derived TNC as a component of vascular invasions, promoting parenchymal metastasis. In the MMTV-NeuNT model we describe vascular invasions as platelet associated nests of proliferating tumor cells, within blood vessels of the lung, where the tumor cells are surrounded by a layer of TNC and other ECM molecules and, a luminal endothelial monolayer. We demonstrate that in vascular invasions, TNC increases platelet abundance and endothelialization and, enhances tumor cell survival, plasticity and, breaching into the lung parenchyma. Similarly, tumor cells survive and migrate more in vitro upon TNC-induced plasticity. This insight may offer opportunities for targeting cancers with frequent vascular invasions found in blood vessels, such as we have documented for renal cell carcinoma (RCC), hepatocellular carcinoma (HCC) and PNET that, like the murine model, present a luminal endothelial monolayer ensheathing and TNC expression. In contrast, vascular invasions of lymphatic vessels, that we have seen in breast cancer and pancreatic adenocarcinomas lack these traits. Thus blockade of TNC actions could be a potential strategy to specifically targeting vascular invasions in blood vessels for preventing tumor spread to the lung.

Results

Tenascin-C accelerates tumor onset

We generated compound MMTV-NeuNT tumor mice lacking TNC (TNCKO) by breeding and compared tumorigenesis with mice expressing wildtype (WT) levels of TNC. By immunoblotting and immunofluorescence staining of primary tumors we found TNC expressed in tumor matrix tracks (TMT) (**Fig. S1A**) as previously shown in other cancers [13]. No TNC protein was found in *Tnc* knockout (TNCKO) tumors (**Fig. S1A, B**). We compared tumor latency and observed that in WT mice, tumors were first palpable at 135 days. Sixty days later, all mice had developed tumors. Tumor latency was largely delayed in TNCKO mice where tumors were first palpable at 175 days (**Fig. 1A**). As described in this model [10], all mice developed multiple tumors. Mice were sacrificed 3 months after first tumor palpation. No difference in tumor burden between genotypes was noted (**Fig. 1B**).

Tenascin-C enhances lung metastasis

We assessed lung metastasis by a stereological analysis [14] of the left and biggest lung lobe and noticed no difference in the number of metastasis between tumor mice expressing TNC or not (**Fig. 1C, D**). Yet, we found a higher metastatic index in WT mice indicated by a bigger lung metastatic surface (**Fig. 1E**). As vascular invasions have been described in MMTV-Neu mice as indicator of tumor spread [15], we used immunohistochemistry and immunofluorescence to analyze the vascular invasions in more detail. First, we observed vascular invasions to be present in blood vessels of the lung (**Fig. 1C, F**). Surface measurement revealed that vascular invasions are bigger in WT than in TNCKO mice (**Fig. 1F, G**). Reduced proliferation and/or increased apoptosis may account for this observation which we addressed by staining for cleaved caspase-3

and Ki67. We noticed that cleaved caspase-3+ cells are less abundant in WT than in TNCKO vascular invasions, suggesting that TNC promotes survival (**Fig. 1H, I**). It is remarkable that some tumor cells within the intravascular tumor cell nests proliferate, yet there was no difference in the number of Ki67+ cells between tumor mice expressing or lacking TNC (**Fig. 1J, K**). Similar to cells in the vascular invasions, also in parenchymal metastasis TNC did not influence cell proliferation but enhanced survival (**Fig. S1C-F**). In summary, these observations suggest that TNC promotes cancer cell survival in vascular invasions present in blood vessels and, in parenchymal metastasis which could explain the observed higher metastatic burden of WT tumor mice.

Host TNC impacts survival in vascular invasions and enhances lung metastasis

We wanted to know whether TNC from the tumor cells or the stroma promotes metastasis. Therefore, we established a syngeneic orthotopic grafting model by using NT193 cells that we had established from a MMTV-NeuNT tumor [12]. We engineered NT193 cells to downregulate *Tnc* by shRNA technology and, grafted cells into the mammary gland of a WT and TNCKO host, respectively. We confirmed *Tnc* knockdown in the cultured cells and in tumors by immunoblotting and immunofluorescence analysis, respectively (**Fig. S2A-C**). We noticed that NT193 tumors develop spontaneously lung metastasis including vascular invasions. As for the MMTV-NeuNT model, with the changing levels of TNC expression we found no difference in tumor burden (**Fig. S2D**) nor the incidence of lung metastasis (**Fig. 2A**). Yet, we noticed that the lung metastatic surface of shControl (shC) cell-derived tumors was bigger in WT than in TNCKO mice. Moreover, irrespective of the cell genotype, there was a tendency towards more metastasis in the WT than in the TNCKO host (**Fig. 2B**). Next, we determined the surface and found that vascular invasions derived from shC tumor cells were significantly bigger in a WT host than in a TNCKO host (**Fig. 2C**). Assessing survival and proliferation by

tissue staining revealed that some cells in the vascular invasions proliferate, yet independent of TNC which is similar to the transgenic MMTV-NeuNT model (**Fig. 2D, E**). In contrast, we saw the lowest apoptosis index when shC cells were grafted into a WT host in comparison to a TNCKO host (**Fig. 2F, G**). Altogether, these results identify host derived TNC as important component for enhancing survival of tumor cells in the vascular invasions.

Vascular invasions residing in blood vessels are nests of tumor cells surrounded by a layer of stromal cells expressing TNC

As our results suggest a role of TNC in vascular invasions, we characterized them by hematoxylin/eosin (HE) staining and immunofluorescence analysis. We found vascular invasions in blood vessels of the lung where they eventually occluded the vessel lumen and sometimes had a necrotic center (**Fig. 3A-C, S3A-C**). We wanted to know whether vascular invasions express TNC and saw abundant TNC at the periphery yet not within the ErbB2+ tumor cell clusters (**Fig. 3B-D**).

To assess the cellular origin of TNC in the vascular invasions of the grafting model, we stained for TNC together with αSMA. We found αSMA to be expressed in the lung vessel wall yet not in the vascular invasions. Upon grafting of shC cells we noticed that the vascular invasions expressed TNC when cells were grafted into a WT host. This was not the case when cells were grafted into a TNCKO host (**Fig. 3C, S3D**). As Fsp1+ cells were described as source of TNC in another breast cancer model [5], we asked whether these cells potentially express TNC in the vascular invasions. Indeed, we observed an overlap of TNC with the Fsp1 staining suggesting that Fsp1+ cells are a likely source of TNC in the MMTV-NeuNT model (**Fig. 3D**). A similar result was obtained in the grafting model, where the Fsp1 signal largely co-localized with TNC (**Fig. 3E**). Together, these results suggest that Fsp1-expressing cells are likely candidates to express TNC in the vascular

invasions in both models, also demonstrating similarities between the genetic and the grafting model.

Vascular invasions contain platelets and are surrounded by an endothelial cell monolayer which is influenced by TNC

As very little was known about the cellular and ECM composition of vascular invasions, we used multi-channel immunofluorescence staining for epithelial/tumor cells (CK8/18, ErbB2), endothelial cells (CD31), platelets (CD41, RAM1), leukocytes (CD45), fibronectin (FN) and laminin (LM) in sequential lung tissue sections. We observed that in all vascular invasions tumor cells, homogenously expressing ErbB2 and CK8/18, formed a tightly packed tumor cell cluster or nest that was enveloped by a layer of Fsp1+ cells and distinct layers of TNC, LM and FN that surrounded platelets inside the tumor cell cluster (**Fig. 4A** panel a-f). Endothelial cells were present at the luminal side of the vascular invasion as a monolayer, characterized by flat endothelial cell nuclei (**Fig. 4A** panel b and e**, S4A, B**). Neither FN, LM, TNC nor endothelial cells nor platelets or fibroblasts were found within the tumor cell nest but at the rim (**Fig. 4A**). Moreover, leukocytes were not associated with the vascular invasions but were present at the basal side of the vessel wall facing the lung parenchyma (**Fig. 4A** panel c). Furthermore, vascular invasions of the NT193 model resembled those of the MMTV-NeuNT model, expressing TNC and displaying a core of proliferating tumor cells and a layer composed of fibroblasts and endothelial cells (**Fig. 3C, E, Fig. S4B, C**).

Since vascular invasions were also present in lung vessels of TNCKO mice, we asked whether TNC had any impact on their organization. Staining for LM, FN, Fsp1 and αSMA did not reveal differences between genotypes, suggesting that TNC does not impact the formation of vascular invasions (**Fig. 3C, 4B, D**). Staining for CD31 revealed an

endothelial monolayer around the tumor cell nests in both models (**Fig. 4A, S4B**). Yet, we noticed more intact endothelial layers around the tumor nests in WT as compared to TNCKO mice (**Fig. 4B, C**). We also observed a continuum between the endothelial layers of the vascular invasion and the lung vessel wall (**Fig. 4A,** panel b and e).

Vascular invasions are known to be associated with vessel occlusion due to thromboembolism where platelets are instrumental [16]. By staining for CD41 and RAM1 (recognizing Gp1b [17]), respectively, we found platelets inside the vascular invasions. Moreover, platelets were surrounded by LM and the endothelial monolayer (**Fig. 4A, D, S4C, D**). We also noticed an overlap of CD41 and TNC expression suggesting that platelets may also be a source of TNC as was seen in another tumor model [18] (**Fig. S4E**). By quantification of CD41 we found less platelets in vascular invasions of TNCKO than in WT mice suggesting a potential role of TNC in platelet attachment as previously described in a thrombosis model [19] (**Fig. 4E**). Altogether, our detailed analysis allows us to deduce the organization of vascular invasions (**Fig. 4F**) as a CK8/18+ and ErbB2+ tumor cell cluster of proliferating tumor cells with local accumulation of platelets inside the tumor embolus. Moreover, the tumor cell nest is enveloped by distinct layers of stromal cells. Whereas Fsp1+ cells are in vicinity to the tumor cell nest and are a likely source of TNC, an endothelial monolayer is present at the luminal rim of the tumor embolus which is not in contact with TNC.

TNC promotes extravasation of tumor cells from vascular invasions into the lung parenchyma

Vascular invasions were described as precursors of parenchymal metastasis in one of the MMTV-Neu models [15]. We made a similar observation now in the MMTV-NeuNT model, where the relative abundance of parenchymal metastasis increased over time (**Fig. S5A**). When we compared the ratio of vascular invasions to parenchymal

metastasis between genotypes of MMTV-NeuNT mice we found more parenchymal metastasis in lungs of WT mice (**Fig. 5A**). Similarly, in the NT193 grafting model we saw more parenchymal metastasis when shC cells were grafted in a WT host compared to a TNCKO host. In addition, parenchymal metastasis in the WT host was lower when shTNC were grafted, suggesting that also tumor cell derived TNC may be relevant (**Fig. 5B**). Interestingly, whereas at the site of extravasation TNC appears to be absent (**Fig. 3B**), in the parenchymal metastasis TNC is expressed at the border and in matrix tracks (**Fig. S5B-E**). Altogether, these results suggest that TNC plays a role in progression of vascular invasions into parenchymal metastasis. In addition, TNC may also be relevant in the metastatic outgrowth by promoting survival as had been seen in another tumor model [6].

Plastic phenotype in TNC-expressing vascular invasions, in parenchymal metastasis and, in cultured tumor cells

Since vascular invasions are described as precursors of parenchymal metastasis, the question arises how tumor cells enter the lung parenchyma. In particular, epithelial-to-mesenchymal (EMT)-like cellular plasticity could be a relevant mechanism as described in another MMTV-Neu model [15]. Therefore, we investigated expression of EMT markers, such as E-cadherin and vimentin. We observed vimentin+ cells inside the tumor cell nests. We also observed tumor cells leaving the vascular invasions and invading the parenchymal lung tissue (**Fig. 3B, 4A, 5D**). While all tumor cells inside the vascular invasions expressed CK8/18, E-cadherin and ErbB2, some cells also co-expressed vimentin (**Fig. 5D**). This phenotype is reminiscent of cells undergoing epithelial plasticity, presumably promoting collective invasion into the parenchymal tissue (**Fig. 3B, 5D**). By quantification we noticed more vimentin-expressing cells within WT than in TNCKO vascular invasions (**Fig. 5C, S6**). Similarly, we also observed CK8/18+/vimentin+ cells

inside the parenchymal metastasis indicating a mixed epithelial/mesenchymal phenotype upon breaching/intravasation (**Fig. S5D, E**).

TNC was previously shown to promote an EMT-like plasticity in cellular models [20,21]. Therefore, we asked whether in our model TNC may induce cellular plasticity. We treated NT193 cells with TNC in monolayer or spheroid cultures and observed loss of E-cadherin and gain of vimentin expression by immunofluorescence, quantitative reverse transcription PCR (qPCR) and immunoblotting (**Fig. 5F,G, S5F,G**). We noticed increased mRNA levels of several EMT markers, such as *Snail*, *Slug*, *Zeb1*, *Vimentin*, *Pai-1*, *Mmp9* and *Tnc* itself upon treatment with TNC. On the contrary, mRNA levels of *E-cadherin* were found reduced, suggesting that TNC induces EMT in cultured NT193 cells (**Fig. S5G**). As we observed platelets residing inside the vascular invasions and, platelets are known to express TNC, and can induce an EMT [18], we considered a potential role of platelets in EMT in our models. In cultured tumor cells, we found that platelets indeed induced an EMT, since E-cadherin levels were decreased and vimentin expression was increased (**Fig. S5H**). Next, we asked what consequences a TNC-induced EMT has for the cells. We used a cellular wound closure and Boyden chamber migration assay and observed increased migration of NT193 cells upon addition of TNC (**Fig. 5H-J**). Since EMT can enhance tumor cell survival resistance against toxic reagents [22], we determined staurosporine-induced apoptosis by a caspase-3/7 activity assay and observed that pre-treatment of NT193 cells with TNC for 24 hours reduces apoptosis (**Fig. 5K**). In summary, our results show that TNC induces an EMT phenotype in the NT193 model. Also, TNC-induced plasticity promotes cell migration and apoptosis resistance against staurosporine. These mechanisms could be relevant for enhancing tumor cell survival inside the vascular invasions and their breaching.

Vascular invasions within blood vessels of human carcinomas present an endothelial monolayer and TNC expression

Vascular invasions in the primary tumor comprise an important prognostic tool and can occur in blood and lymphatic vessels [8,23]. To address whether vascular invasions in human carcinomas express TNC, similar to our models, we investigated tissue from several human cancers with and without recorded presence of lymph and or blood vessel invasions by sequential staining for TNC, CD31, podoplanin and platelet marker CD61 (**Table S1**). We observed that tumor cells had infiltrated veins in renal cell carcinoma (RCC), hepatocellular carcinoma (HCC) and pancreatic neuroendocrine tumors (PNET) (**Fig. 6A-C, S7A, B**). We noted that vascular invasons in blood vessels expressed TNC at both, the site of vessel wall invasion and the free rim exposed to the vessel lumen. Moreover, the vascular invasions were surrounded by a luminal endothelial monolayer. In bigger vascular invasions, TNC was also detected inside the body of the tumor embolus (**Fig. 6A, C, S7A-C**). Platelets may play a role as we could find a blood thrombus disrupting the endothelial layer and forming a "cap" on a vascular invason with prominent TNC staining (**Fig. 6C**). In pancreatic ductal adenocarcinoma (PDAC) and invasive mammary carcinomas (MaCa), we found that tumor cells had invaded lymphatic vessels as vessels stained for the lymphatic endothelial cell marker podoplanin (**Fig. S8A, B, Table S1**). Lymphovascular invasions in MaCa were present in all subtypes and appeared often as floating cell clusters (**Fig. S8B, Table S2**). Upon an unbiased search in MaCa (1/12) and the corresponding lung metastases (5/12) we observed vascular invasions in lymphatic vessels of both the primary tumor and the lung tissue. TNC was expressed in the vessel wall and the tumor tissue, however the tumor cell nests within the lymphatic vessels did not express TNC, were not covered by an endothelial cell layer, nor did they show signs of a thrombotic reaction (**Fig. S8A, B, Table S2**). To our knowledge, these results demonstrate for the first time differences in cellular and matrix composition

between vascular invasions of blood and lymphatic vessels. We conclude, that as in the murine metastasis models, vascular invasions in blood vessels of human cancers express TNC and are enclosed by an endothelial monolayer, which may offer novel diagnostic and targeting opportunities.

Discussion

It is well established that the tumor stroma plays an important role in enhancing tumor malignancy [2]. Moreover, the ECM molecule TNC which is abundantly expressed in cancer tissue enhances metastasis by incompletely understood mechanisms [3,4,6,24]. To address the roles of TNC in metastasis, we have compared NeuNT (ErbB2)-driven breast cancer lung metastasis in a genetic and a novel syngeneic orthotopic breast cancer model derived thereof with high TNC to that with no or low TNC, respectively where (in related models) tumor cells are found in vascular invasions of the lung vasculature [10,15]. We have observed that TNC increases tumor onset and lung metastasis, with a particular role of host-derived TNC in enhancing survival and, an EMT-like plasticity in the vascular invasions. Indeed, in cultured NT193 tumor cells we demonstrate that TNC induces EMT, migration and survival. It was known that cellular plasticity promotes metastasis in another MMTV-Neu model [15]. Now, our data suggest an important role of TNC in promoting cellular plasticity of the MMTV-NeuNT model which may account for enhanced cell survival and, progression of vascular invasions into parenchymal metastasis, thus elevating total metastasis burden by TNC.

The presence of vascular invasions correlates with thromboembolism and metastasis[23,25]. As our data (MMTV-NeuNT) and results from others in MMTV-Neu NDL mice [15], suggest that vascular invasions precede parenchymal metastasis, targeting vascular invasions could be effective in reducing overall metastasis. Indeed, inhibiting TGFβ signaling [15] or ErbB2 [12] reduced parenchymal metastasis in MMTV-Neu models by blocking breaching of cells from the vascular invasions into the lung parenchyma. Currently applied technology for detection of circulating tumor cells is focused on single cells or small tumor cell clusters in blood vessels and will miss vascular invasions [26]. Little was known about

the cellular composition and molecular characteristics which altogether would be important to exploit vascular invasions for prognosis or therapy [23,25]. We have bridged this gap by extensive tissue analysis of vascular invasions in our murine tumor models and in human cancers. First, we have found that vascular invasions in blood vessels and lymphatic vessels are different. Second, we report that within blood vessels, vascular invasions are organized as tightly packed clusters of proliferating tumor cells. Importantly, despite some cells with mesenchymal markers, all tumor cells express epithelial markers and have tight junctions which may contribute to synoikis, a junctional adhesion-associated survival mechanism [27]. We further find that the tumor cell nests are enveloped by Fsp1+ cells and a luminal endothelial monolayer, with FN and LM between the two cell layers (**Fig. 7**). In vascular invasions TNC is co-localized with platelets and Fsp1+ cells, supporting a potential role in TNC expression, as seen in other tumor models [5,18]. Our data are novel as until now a role of TNC (and in particular stromal cell derived TNC) before breaching was unknown. Although Fsp1+ cells had previously been shown to be important for metastasis, presumably by secreting TNC and VEGFA [5], yet their presence in vascular invasions was unknown. Our results enforce them as candidates for anti-mestastasis therapy.

We observed that endothelialization of vascular invasions is the rule in the MMTV-NeuNT model opposed to other Neu models, where vascular invasions were not apparent except in compound MMTV-NeuYD/VEGFA mice [28]. We observed that the proportion of parenchymal metastasis decreased when the endothelial layer was impaired, which happened in the absence of TNC, altogether presenting novel information and, pointing at an important role of this endothelial layer in metastasis. Several concepts for the formation of vascular invasions have been proposed where endothelial cells may play an active role [29–31]. Transdifferentiation of tumor cells into endothelial cells is a possibility [30],

as TNC was shown to promote transdifferentiation of neuroblastoma cells into endothelial cells [32]. We consider this possibility in our model unlikely as the endothelial cell layer is a contiguous monolayer and we do not see expression of ErbB2 in the endothelial cells. Budding from the tumor vasculature [31] may also not be a major source of vascular invasions as we do not see αSMA+ cells underneath the endothelial layer. Upon release into the circulation by budding, platelets would get in contact with the tumor cells at the outside of the tumor embolus. Yet, we see platelets inside the tumor cell nests beneath the endothelial layer. The prominent location deep inside argues for an early role of platelets in the formation of vascular invasions. Lapis and co-workers [29] proposed an endothelialization mechanism where wrapping of endothelial cells around tumor cells is initiated upon contact of tumor cells with the vasculature. A contiguous monolayer of endothelial cells around the vascular invasions that we observed in the murine model and in human cancers is supportive of this hypothesis. A pro-angiogenic function of TNC that we have seen in two other tumor models is also supportive [4,33]. In addition, we have detected eventual endothelial layer interruptions which is reminiscent of a glimpse on in-situ endothelialization. Bone marrow-derived endothelial progenitor cells (EPC) potentially also play a role in this process, as they promote metastasis by contributing to the angiogenic switch and outgrowth of metastasis [34]. Previously, it has been shown that EPC recruitment to the lesion was higher in an ischemia model in mice that express TNC as compared to mice lacking TNC expression [35]. We have further observed that TNC has an impact on the endothelial monolayer of the vascular invasions, since this layer is found interrupted or missing in the absence of TNC. Apparently, there are many possibilities of how TNC promotes endothelial monolayer formation around the tumor cell nests which remains to be determined in the future.

Our results are relevant for human cancers with vascular invasions in blood vessels such as RCC, HCC and PNET. We suggest that these patients may benefit from an anti-angiogenic drug treatment since these vascular invasions express TNC and have a luminal endothelial monolayer. Anti-angiogenic treatment (mostly in conjunction with other anti-cancer chemotherapies) is already applied in patients with RCC, HCC and PNET [36] thus, potentially indeed targeting vascular invasions. In support, we have seen a reduced metastasis burden in conditions where the endothelial monolayer around the vascular invasions is disrupted (TNCKO mice). Hence, TNC expression and endothelial ensheathing of vascular invasions in tumor biopsies could be used to stratify patients that may benefit from an anti-angiogenic drug treatment, maybe in combination with serum biomarkers that currently are exploited for prediction of anti-angiogenic treatment efficacy for metastatic renal cell carcinoma [37]. In contrast to vascular invasions in blood vessels, we have found that lymphatic invasions (observed in MaCa and PDAC) do not exhibit an endothelial layer nor TNC expression. Therefore our prediction is that MaCa and PDAC patients may poorly benefit from an anti-angiogenic treatment. Indeed, using the anti-angiogenic antibody bevacizumab/Avastin for treating advanced breast cancer patients has lost approval by the FDA due to the lack of a benefit for the patient [38,39].

Altogether our study has provided novel insights into the multiple roles of TNC in lung metastasis which provide novel diagnostic and targeting opportunities (**Fig. 7**). As only few relevant syngeneic orthotopic cancer models are available, our novel grafting model may be valuable for future metastasis inhibition studies targeting TNC and other molecules.

Methods

Detailed information about material and methods can be found in the Supplemental Material and Methods section.

Human cancer tissue

Two independent cohorts of human tissue from cancer patients were analyzed derived from the Medical University of Vienna/General Hospital Vienna (MUW) and the Hôpital Universitaire de Strasbourg Hautepierre (HUS). Mammary carcinoma (MaCa), MaCa lung metastasis, renal cell carcinoma (RCC), hepatocellular carcinoma (HCC) and pancreatic neuroendocrine tumor (PNET) tissue was histologically and immunologically analyzed with specific antibodies against TNC, Factor VIII, CD31, CD34, podoplanin (D2-40) or platelets (CD61). Ethical approval has been granted. Detailed information can be found in **Table S1-S3** and in the Supplementary Methods section. Results are summarized in **Table S2**.

Mouse models and tissue preparation

MMTV-NeuNT female mice (FVB/NCrl background), TNC +/+ and TNC-/- were obtained from crossing MMTV-NeuNT mice [10] provided by Gerhard Christofori (University of Basel, Switzerland) with TNC +/- mice donated by Reinhard Fässler [11]. Mice were housed and handled according to the guidelines of INSERM and the ethical committee of Alsace, France (CREMEAS). Syngeneic breast tumors were obtained by injecting 10^7 NT193 cells into the fourth mammary gland of FVB/NCrl mice (one side). Mice were euthanized at indicated time points and breast tumors and lungs were snap frozen in liquid nitrogen for western blot and qPCR or embedded in O.C.T. (Sakura Finetek) or in paraffin for

histological analysis and immunostaining. Stereological analysis of lung metastasis was performed as previously published [40]. Quantification of TNC staining intensity was scored [41]. Details are provided in the Supplementary Methods section.

Cell culture and in vitro assays

NT193 cells derived from a MMTV-NeuNT primary tumor [12] were cultured in DMEM medium. NT193 sublines, control (SHC202V) and TNC knockdown (KD) (sh1: TRCN0000312137; sh2: TRCN0000312138) were obtained by transduction using lentiviral particles with shRNA vectors (Sigma-Aldrich) and were maintained under constant selection pressure. Overnight serum-starved cells were incubated with recombinant TNC (purified as described in [42]) or with platelets. In vitro quantification of Caspase 3/7 activity was performed according to the manufacturer's instructions (Promega). Cellular wound healing assays were performed on non-proliferating, highly confluent NT193 cultures and relative wound closure was determined upon treatment for 24 hours. Transwell migration towards 10% FCS was assessed upon prior treatment of NT193 cells with TNC for 24 hours. Assessment of gene expression was done by quantitative reverse transcription polymerase chain reaction (qPCR) using the indicated primers (**Table S4**). Full information is included in the Supplementary Methods section.

Statistical analysis

The GraphPad Prism software (version 6) was used for graphical representations of data and statistical analysis to assess the significance of observed differences. All parametric (unpaired Student t-test with Welch's correction in case of unequal variance) and non-parametric tests (Mann-Whitney) were performed in a two-tailed fashion. To compare the proportion of vascular invasions and parenchymal metastases, Fisher's exact test or Chi-

square test was used. Mean ± SEM. p values < 0.05 were considered as statistically significant (*$p < 0.05$; **$p < 0.01$; ***$p < 0.001$; ****$p < 0.0001$).

Disclosure of potential conflict of interest

Authors contribution

Acknowledgements

References

1. Talmadge, J. E. & Fidler, I. J. AACR Centennial Series: The Biology of Cancer Metastasis: Historical Perspective. *Cancer Res.* **70,** 5649–5669 (2010).

2. Bissell, M. J. & Hines, W. C. Why don't we get more cancer? A proposed role of the microenvironment in restraining cancer progression. *Nat. Med.* **17,** 320–329 (2011).

3. Midwood, K. S., Chiquet, M., Tucker, R. P. & Orend, G. Tenascin-C at a glance. *J Cell Sci* **129,** 4321–4327 (2016).

4. Saupe, F. *et al.* Tenascin-C Downregulates Wnt Inhibitor Dickkopf-1, Promoting Tumorigenesis in a Neuroendocrine Tumor Model. *Cell Rep.* **5,** 482–492 (2013).

5. O'Connell, J. T. *et al.* VEGF-A and Tenascin-C produced by S100A4+ stromal cells are important for metastatic colonization. *Proc. Natl. Acad. Sci.* **108,** 16002–16007 (2011).

6. Oskarsson, T. *et al.* Breast cancer cells produce tenascin C as a metastatic niche component to colonize the lungs. *Nat. Med.* **17,** 867–874 (2011).

7. Kyriazi, V. Breast cancer as an acquired thrombophilic state. *J. Breast Cancer* **15,** 148–156 (2012).

8. Mandalà, M. & Tondini, C. Adjuvant therapy in breast cancer and venous thromboembolism. *Thromb. Res.* **130 Suppl 1,** S66-70 (2012).

9. Soerjomataram, I., Louwman, M. W. J., Ribot, J. G., Roukema, J. A. & Coebergh, J. W. W. An overview of prognostic factors for long-term survivors of breast cancer. *Breast Cancer Res. Treat.* **107,** 309–330 (2008).

10. Muller, W. J., Sinn, E., Pattengale, P. K., Wallace, R. & Leder, P. Single-step induction of mammary adenocarcinoma in transgenic mice bearing the activated c-neu oncogene. *Cell* **54,** 105–115 (1988).

11. Talts, J. F., Wirl, G., Dictor, M., Muller, W. J. & Fässler, R. Tenascin-C modulates tumor stroma and monocyte/macrophage recruitment but not tumor growth or metastasis in a mouse strain with spontaneous mammary cancer. *J. Cell Sci.* **112 (Pt 12),** 1855–1864 (1999).

12. Arpel, A. *et al.* Transmembrane Domain Targeting Peptide Antagonizing ErbB2/Neu Inhibits Breast Tumor Growth and Metastasis. *Cell Rep.* **8,** 1714–1721 (2014).

13. Spenlé, C. *et al.* Spatial organization of the tenascin-C microenvironment in experimental and human cancer. *Cell Adhes. Migr.* **9,** 4–13 (2015).

14. Nielsen, B. S. *et al.* A Precise and Efficient Stereological Method for Determining Murine Lung Metastasis Volumes. *Am. J. Pathol.* **158,** 1997–2003 (2001).

15. Siegel, P. M., Shu, W., Cardiff, R. D., Muller, W. J. & Massagué, J. Transforming growth factor β signaling impairs Neu-induced mammary tumorigenesis while promoting pulmonary metastasis. *Proc. Natl. Acad. Sci.* **100,** 8430–8435 (2003).

16. Meikle, C. K. S. *et al.* Cancer and Thrombosis: The Platelet Perspective. *Front. Cell Dev. Biol.* **4,** (2017).

17. Mangin, P. H. *et al.* Identification of five novel 14-3-3 isoforms interacting with the GPIb-IX complex in platelets. *J. Thromb. Haemost.* **7,** 1550–1555 (2009).

18. Labelle, M., Begum, S. & Hynes, R. O. Direct Signaling between Platelets and Cancer Cells Induces an Epithelial-Mesenchymal-Like Transition and Promotes Metastasis. *Cancer Cell* **20,** 576–590 (2011).

19. Schaff, M. *et al.* Novel Function of Tenascin-C, a Matrix Protein Relevant to Atherosclerosis, in Platelet Recruitment and Activation Under Flow. *Arterioscler. Thromb. Vasc. Biol.* **31,** 117–124 (2011).

20. Nagaharu, K. *et al.* Tenascin-C Induces Epithelial-Mesenchymal Transition–Like Change Accompanied by SRC Activation and Focal Adhesion Kinase Phosphorylation in Human Breast Cancer Cells. *Am. J. Pathol.* **178,** 754–763 (2011).

21. Xu, J., Lamouille, S. & Derynck, R. TGF-β-induced epithelial to mesenchymal transition. *Cell Res.* **19,** 156–172 (2009).

22. Singh, A. & Settleman, J. EMT, cancer stem cells and drug resistance: an emerging axis of evil in the war on cancer. *Oncogene* **29,** 4741–4751 (2010).

23. Kane, R. D., Hawkins, H. K., Miller, J. A. & Noce, P. S. Microscopic pulmonary tumor emboli associated with dyspnea. *Cancer* **36,** 1473–1482 (1975).

24. Dandachi, N. *et al.* Co-expression of tenascin-C and vimentin in human breast cancer cells indicates phenotypic transdifferentiation during tumour progression: correlation with histopathological parameters, hormone receptors, and oncoproteins. *J. Pathol.* **193,** 181–189 (2001).

25. Winterbauer, R., Elfenbein, B. & Ball, W. Incidence and clinical significance of tumor embolization to the lungs - ScienceDirect. (1968). Available at: https://www.sciencedirect.com/science/article/pii/0002934368900442?_rdoc=1&_fmt =high&_origin=gateway&_docanchor=&md5=b8429449ccfc9c30159a5f9aeaa92ffb. (Accessed: 10th April 2018)

26. Aceto, N. *et al.* Circulating Tumor Cell Clusters Are Oligoclonal Precursors of Breast Cancer Metastasis. *Cell* **158,** 1110–1122 (2014).

27. Shen, X. & Kramer, R. H. Adhesion-mediated squamous cell carcinoma survival through ligand-independent activation of epidermal growth factor receptor. *Am. J. Pathol.* **165,** 1315–1329 (2004).

28. Oshima, R. G. *et al.* Angiogenic acceleration of Neu induced mammary tumor progression and metastasis. *Cancer Res.* **64,** 169–179 (2004).

29. Lapis, K., Paku, S. & Liotta, L. A. Endothelialization of embolized tumor cells during metastasis formation. *Clin. Exp. Metastasis* **6,** 73–89 (1988).

30. Mahooti, S. *et al.* Breast carcinomatous tumoral emboli can result from encircling lymphovasculogenesis rather than lymphovascular invasion. *Oncotarget* **1,** 131–147 (2010).

31. Sugino, T. *et al.* An Invasion-Independent Pathway of Blood-Borne Metastasis. *Am. J. Pathol.* **160,** 1973–1980 (2002).

32. Pezzolo, A. *et al.* Oct-4+/Tenascin C+ neuroblastoma cells serve as progenitors of tumor-derived endothelial cells. *Cell Res.* **21,** 1470–1486 (2011).

33. Rupp, T. *et al.* Tenascin-C Orchestrates Glioblastoma Angiogenesis by Modulation of Pro- and Anti-angiogenic Signaling. *Cell Rep.* **17,** 2607–2619 (2016).

34. Gao, D. *et al.* Endothelial Progenitor Cells Control the Angiogenic Switch in Mouse Lung Metastasis. *Science* **319,** 195–198 (2008).

35. Ballard, V. L. T. *et al.* Vascular tenascin-C regulates cardiac endothelial phenotype and neovascularization. *FASEB J.* **20,** 717–719 (2006).

36. Rajabi, M. & Mousa, S. The Role of Angiogenesis in Cancer Treatment. *Biomedicines* **5,** 34 (2017).

37. Tran, H. T. *et al.* Prognostic or predictive plasma cytokines and angiogenic factors for patients treated with pazopanib for metastatic renal-cell cancer: a retrospective analysis of phase 2 and phase 3 trials. *Lancet Oncol.* **13,** 827–837 (2012).

38. Vasudev, N. S. & Reynolds, A. R. Anti-angiogenic therapy for cancer: current progress, unresolved questions and future directions. *Angiogenesis* **17,** 471–494 (2014).

39. Zambonin, V. *et al.* Clinical results of randomized trials and 'real-world' data exploring the impact of Bevacizumab for breast cancer: opportunities for clinical practice and perspectives for research. *Expert Opin. Biol. Ther.* **17,** 497–506 (2017).

40. Nielsen, S., Guo, Z., Johnson, C. M., Hensrud, D. D. & Jensen, M. D. Splanchnic lipolysis in human obesity. *J. Clin. Invest.* **113,** 1582–1588 (2004).

41. Shi, M. *et al.* Tenascin-C induces resistance to apoptosis in pancreatic cancer cell through activation of ERK/NF-κB pathway. *Apoptosis* **20,** 843–857 (2015).

42. Huang, W., Chiquet-Ehrismann, R., Moyano, J. V., Garcia-Pardo, A. & Orend, G. Interference of tenascin-C with syndecan-4 binding to fibronectin blocks cell adhesion and stimulates tumor cell proliferation. *Cancer Res.* **61,** 8586–8594 (2001).

Figures
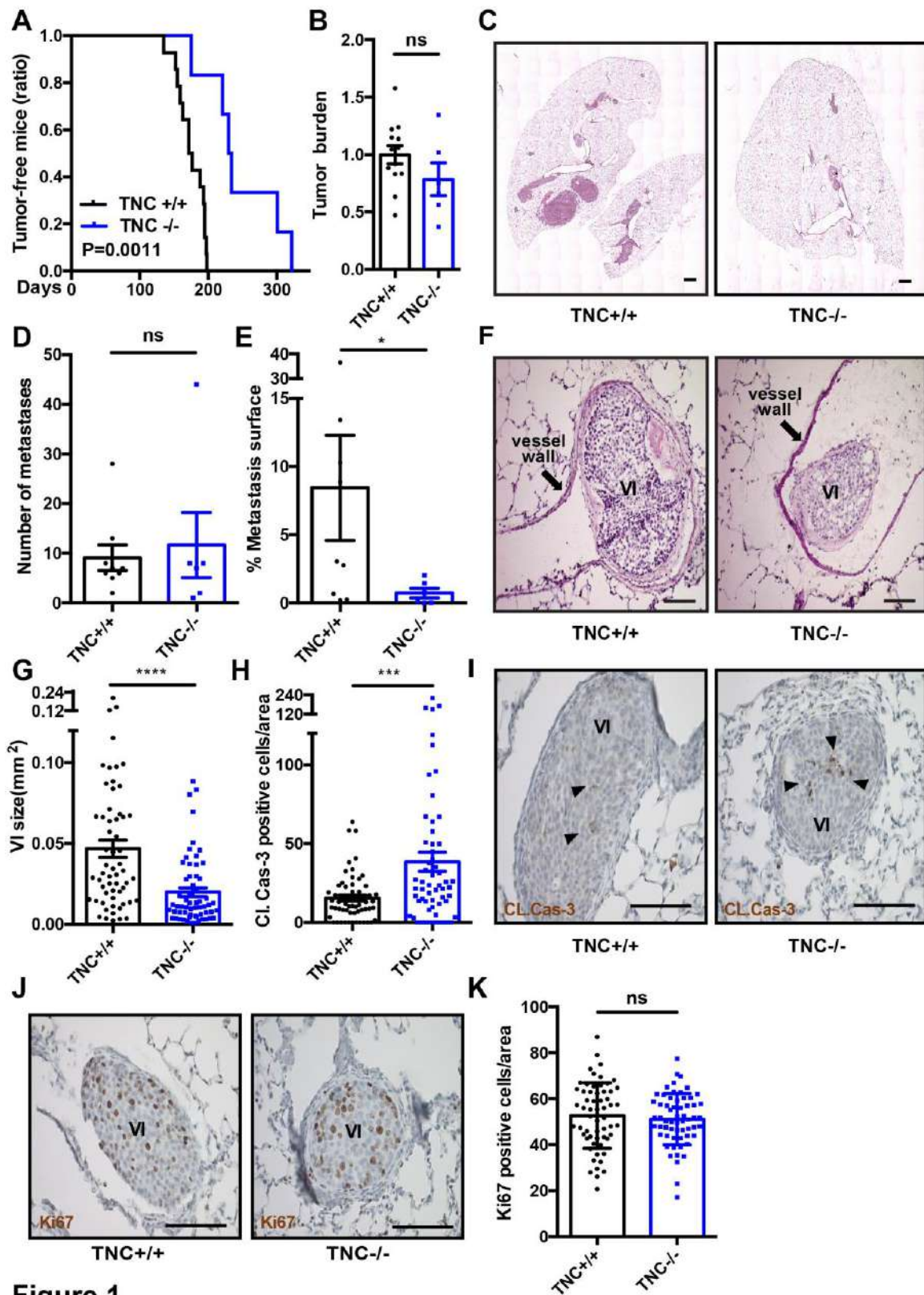
Figure 1

Figure 1. Reduced lung metastasis in the absence of TNC in MMTV-NeuNT mice

(A) Ratio of tumor-free mice is shown for MMTV-NeuNT tumor mice with two (TNC +/+, N = 13 mice) and no (TNC -/-, N = 6) TNC alleles. The absence of TNC significantly delays tumor latency (TNC +/+ versus TNC -/-, p = 0.0011; Log-rank tests). **(B)** Tumor burden of TNC-/- tumor mice (N = 6) was determined and normalized to the mean tumor weight of the control group (TNC +/+, N = 13). **(C)** Representative HE images of lung metastasis from MMTV-NeuNT mice (TNC +/+ and TNC -/-) that had been sacrificed 3 months after tumor detection. Scale bar: 1000 μm. **(D, E)** Number of lung metastases **(D)** and of the cumulated metastatic burden (metastatic area normalized to total lung area) **(E)** in lungs of TNC +/+ (N = 9) and TNC -/- (N = 6) mice. **(F, G)** HE stained lung tissue was used for size determination of vascular invasions (VI) (TNC +/+: N = 6 mice, n = 59 VI; TNC -/-: N = 6 mice, n = 60 VI). Scale bar: 100 μm. **(H-K)** Immunohistochemical (IHC) analysis for cleaved caspase-3 (Cl. Cas-3) **(I)** and Ki67 **(J)** in VI (TNC +/+, N = 6 mice, n = 59 VI; TNC -/-, N = 6 mice, n = 60 VI). Dots represent number of apoptotic **(H)** and proliferative cells **(K)** in VI per area (0.1 mm^2), respectively. Arrowhead denotes cleaved caspase-3 positive apoptotic cell **(I)**. Scale bar: 100 μm. Mean ± SEM.
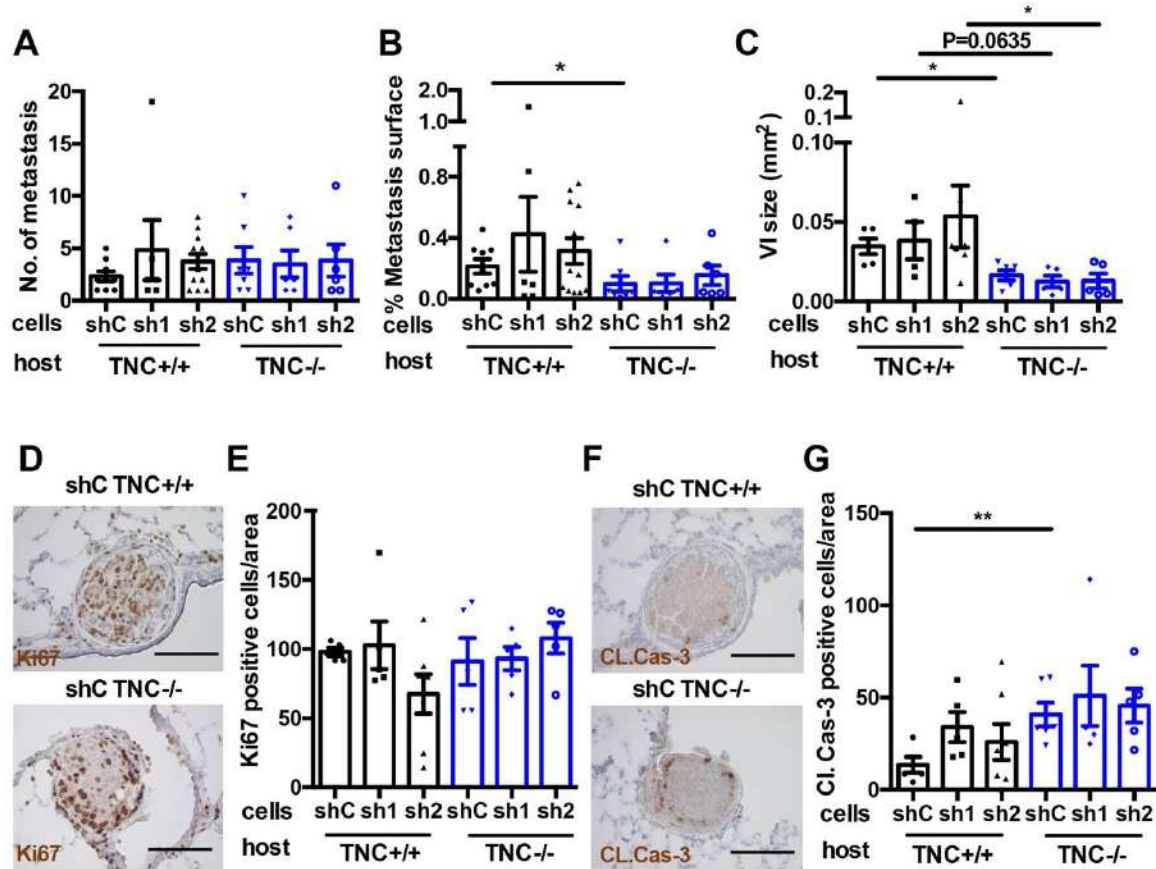
Figure 2. Host derived tenascin-C promotes lung metastasis in NT193 grafted tumor mice **(A-C)** Quantification of the number of lung metastases **(A)**, cumulated metastatic burden (metastatic area normalized to total lung area) **(B)** and size of vascular invasions (VI) **(C)** in lungs of TNC+/+ and TNC-/- FVB hosts 3.5 months after engraftment of NT193 sh control (shC), sh1TNC and sh2TNC cells (shC in TNC +/+ mice (N = 5); sh1TNC in TNC +/+ mice (N = 4); sh2TNC in TNC +/+ mice (N = 7); shC in TNC -/- mice (N = 6); sh1TNC in TNC -/- mice (N = 5); sh2TNC in TNC -/- mice (N = 5)). **(D-G)** IHC analysis for Ki-67 **(D)** and cleaved caspase-3 (Cl. Cas-3) **(F)** in vascular invasions of lungs from NT193 engrafted mice. Dots represent proliferative **(E)** and apoptotic cells in vascular invasions **(G)** per 0.1 mm^2, respectively. Scale bar: 100 µm. Mean ± SEM.
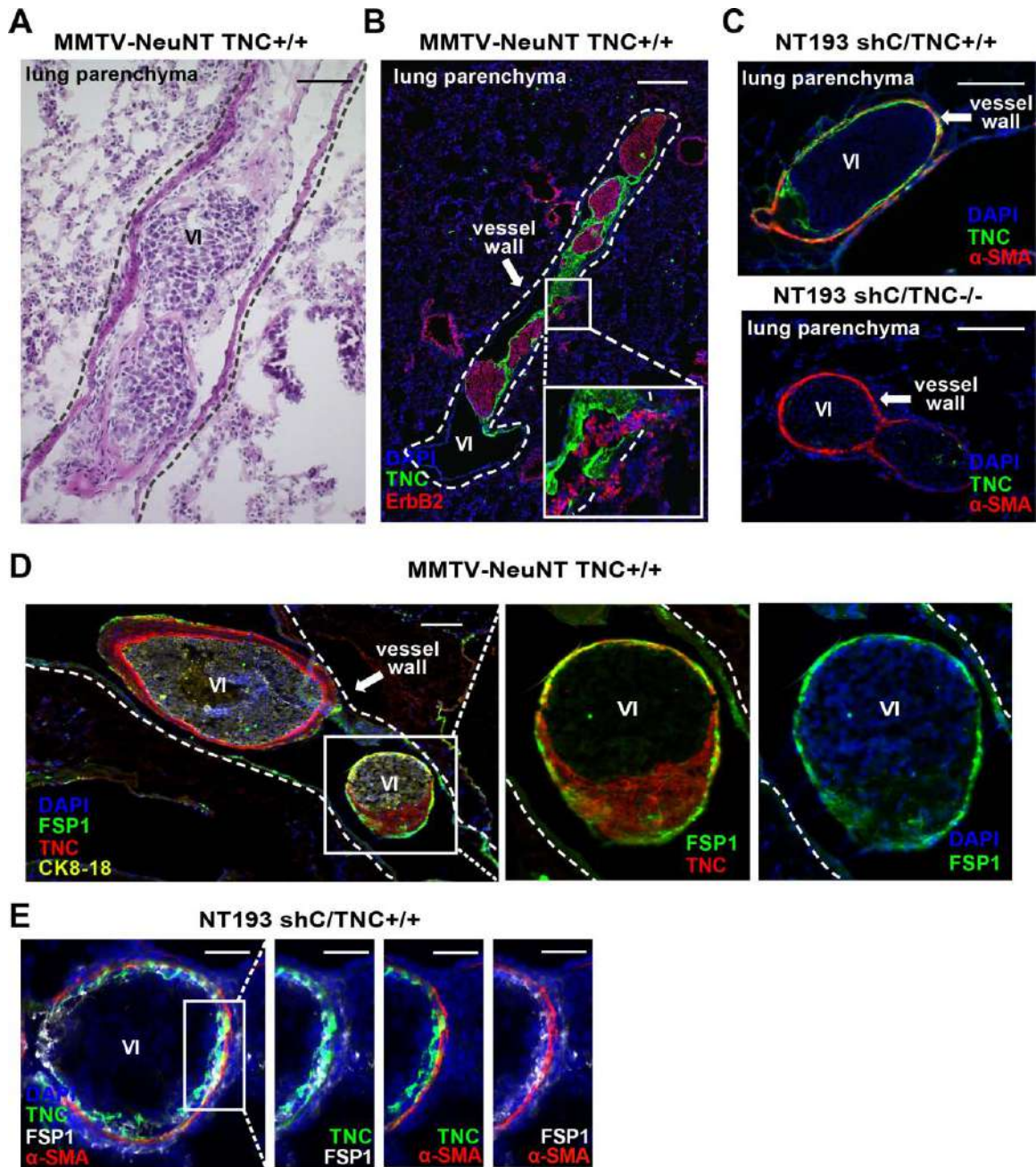
Figure 3

Figure 3. TNC expression in vascular invasions (A, B) Representative images of vascular invasions (VI) in MMTV-NeuNT/TNC+/+ lungs upon HE and IF staining for the indicated molecules. **(A)** is an adjacent section of the image shown in panel B and in **Fig.**

S3A. A dotted line is drawn along the vessel wall. **(B)** Note that TNC (green) is expressed around tumor cells (red, ErbB2). Cell nuclei stained with DAPI. Scale bar: 100 µm **(A)**, 500 µm **(B)**. **(C)** Representative IF images for TNC (green) in lung vascular invasions of tumor cell grafts of NT193 shC cells in a TNC+/+ and TNC-/- host. αSMA staining (red) marks blood vessels. Note, that TNC is expressed in vascular invasions of shC cells engrafted in a TNC+/+ host, yet not in a TNC-/- host. Scale bar: 100 µm. **(D, E)** Representative IF images for FSP1+ cells and TNC in vascular invasions of MMTV-NeuNT/TNC+/+ **(D)** and NT193 lung tissue **(E)**. Scale bar: 100 µm **(D)**, 50 µm **(E)**. White square represents area of higher magnification.

A MMTV-NeuNT TNC+/+

a — vessel wall, lung parenchyma, VI — DAPI, TNC, LM, CK8-18

b — vessel wall, VI — DAPI, CD31, LM, CK8-18

c — vessel wall, VI — DAPI, CD45, LM, CK8-18

d — vessel wall, VI — DAPI, TNC, FN, CK8-18

e — vessel wall, VI — DAPI, CD31, FN, CK8-18

f — vessel wall, VI — DAPI, CD41, LM, CK8-18

B MMTV-NeuNT TNC+/+   MMTV-NeuNT TNC-/-

DAPI, LM, CD31, CK8-18

DAPI, CD31

D MMTV-NeuNT TNC+/+ MMTV-NeuNT TNC-/-

DAPI, LM, CD41, CK8-18

C

CD31 coated VI
non-CD31 coated VI

Proportion

*

TNC+/+   TNC-/-
VI No. n=27   n=9

E

CD41 area / VI area

*

TNC+/+   TNC-/-
VI No. n=26   n=9

F

CD45
CD41
VI
CK8/18

CD31
CD31
LM/FN
TNC/FSP1

Blood vessel

Lung parenchyma

Figure 4

214

Figure 4. Organization of vascular invasions in blood vessels (A) Representative images of immunostainings for ECM molecules and cellular markers in vascular invasions (VI) of lung tissue from MMTV-NeuNT/TNC+/+ (**A, B, D**) and MMTV-NeuNT/TNC-/- mice (**B, D**). The empty arrows point at narrowing of endothelial layers reminiscent of fusion of the endothelial layers derived from the lung vasculature and the vascular invasions. White squares in each panel delineate the field shown at higher magnification. In panel **A**(c) arrows point at CD45+ cells. Scale bar: 100 µm. **(B)** Representative images of endothelial cells. Arrows point at the endothelial monolayer of the vascular invasions. The empty arrow points at the blood vessel wall. Scale bar: 100 µm. **(C)** Proportion of vascular invasions (VI) with and without a CD31 layer for each genotype (TNC +/+ N = 6 mice, n = 27 VI; TNC -/-, N = 4 mice, n = 8 VI). **(D)** Representative images of platelets (CD41+) together with LM. Scale bar: 200 µm. **(E)** Platelet abundance (CD41+ area normalized to area of the VI), TNC +/+, N = 6 mice, n = 26 VI; TNC -/-, N = 4 mice, n = 9 VI. Mean ± SEM. **(F)** Scheme depicting the composition of vascular invasions inside a blood vessel. Each layer of cells or ECM molecule is depicted in a specific color code, where endothelial cells from the lung vasculature are denoted in red and those from the vascular invasion in orange. Note that tumor cells (CK8/18+) are tightly packed inside the vascular invasion, surrounded by FSP1+ cells, a LM/FN layer and a luminal oriented monolayer of endothelial cells (CD31+). CD45+ leukocytes are not in direct vicinity to the tumor cells but are present at the basal side of the vessel wall facing the parenchyma. Platelets (light blue circles) are found inside the vascular invasion underneath the FN/LM layer.
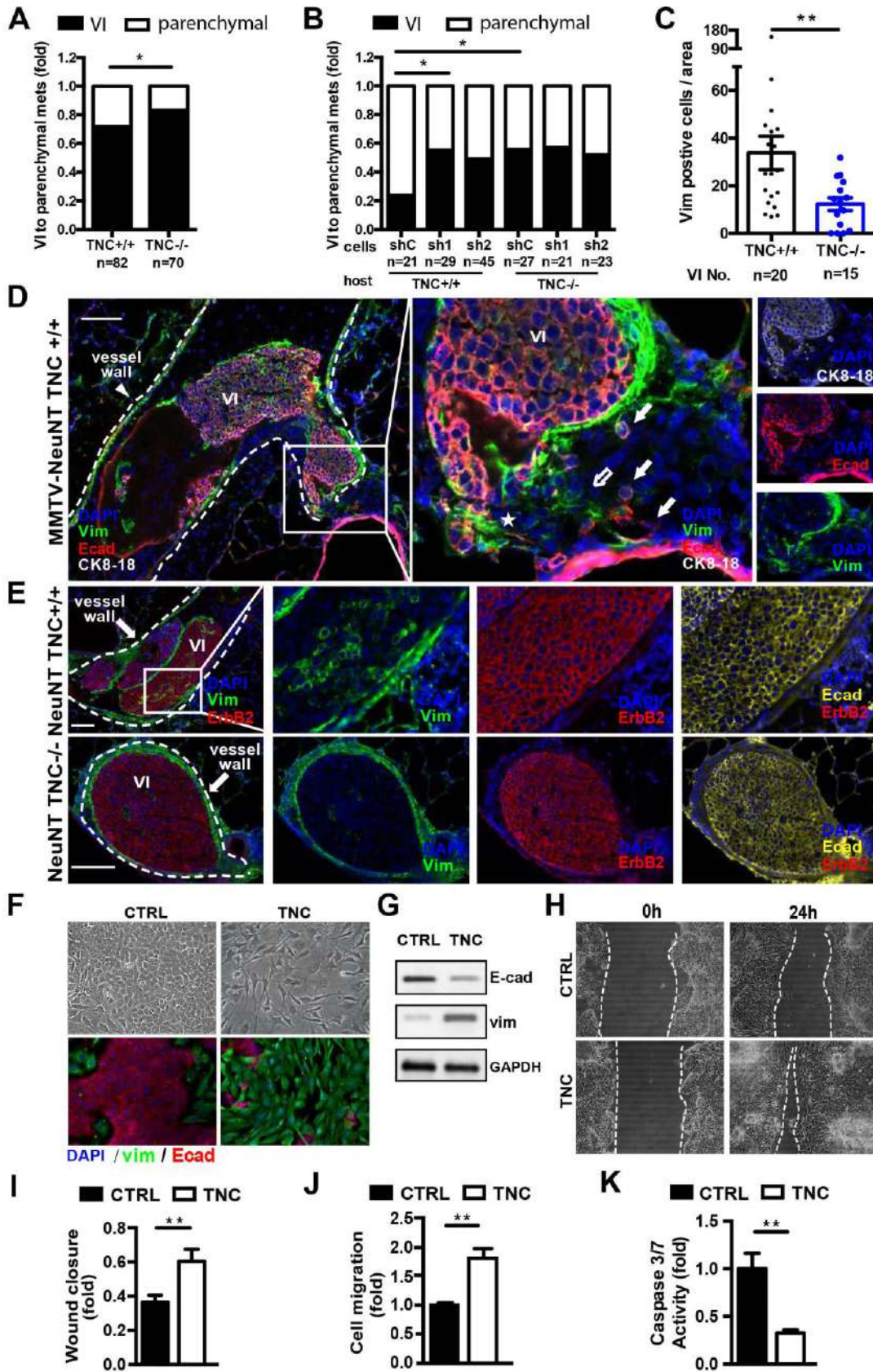
Figure 5

Figure 5. Tenascin-C promotes extravasation of tumor cells and epithelial cell plasticity **(A, B)** Proportion of vascular invasions (VI) to parenchymal metastasis in MMTV-NeuNT mice **(A)** (TNC +/+, N = 6 mice; TNC -/-, N = 6 mice) and in NT193 grafted mice **(B)** (shC in TNC +/+ mice (N = 5); sh1TNC in TNC +/+ mice (N = 4); sh2TNC in TNC +/+ mice (N = 7); shC in TNC -/- mice (N = 6); sh1TNC in TNC -/- mice (N = 5); sh2TNC in TNC -/- mice (N = 5). Mean ± SEM. Note, that either stromal or cancer cell derived TNC increases parenchymal metastasis. **(C)** Quantification of tumor cells expressing both vimentin (green) and ErbB2 (red) normalized per area of the vascular invasion (0.1 mm^2). MMTV-NeuNT (TNC +/+, N = 6 mice, n = 20 VI and TNC-/-, N = 4 mice, n = 15 VI). **(D, E)** Representative IF images of vimentin (green), E-cadherin (red) and CK8/18 (white) expression in vascular invasions from MMTV-NeuNT/TNC+/+ mice. White squares delineate areas of higher magnification. Note that tumor cells (CK8/18+) are invading the parenchymal lung tissue. Arrow points at single invading tumor cell with epithelilal characteristics (CK8/18+ and E-cadherin+). Empty arrow points at invading vimentin+ and E-cadherin- cell. Star points at an event at the invading front. Scale bar: 100 μm. **(E)** Representative IF images of cells expressing vimentin (green), ErbB2 (red) and E-cadherin (yellow) in vascular invasions of MMTV-NeuNT mice (TNC+/+ and TNC-/-). Scale bar: 100 μm. NT193 cells were treated with TNC for 24 hours before assessment of epithelial/mesenchymal plasticity by imaging (**F**), western blot (**G**), migration (**H-J**) and survival (**K**). **(F)** Phase contrast micrographs and IF images of E-cadherin (red) and vimentin (green). Nuclei are stained by DAPI (blue). Scale bar: 20 μm. **(G)** Detection of E-cadherin and vimentin by immunoblotting with GAPDH as loading control (one representative of three independent experiments is shown). **(H, I)** Wound closure assay, n = 14, five independent experiments with at least two replicates. Scale bar: 20 μm. (**J**)

Boyden chamber transwell migration assay. Prior to plating, cells were treated with TNC for 24 hours, n = 7, two independent experiments with at least triplicates. **(K)** Assessment of staurosporine (STS) - induced apoptosis by measuring caspase-3/7 activity, n = 9, three independent experiments in triplicates.
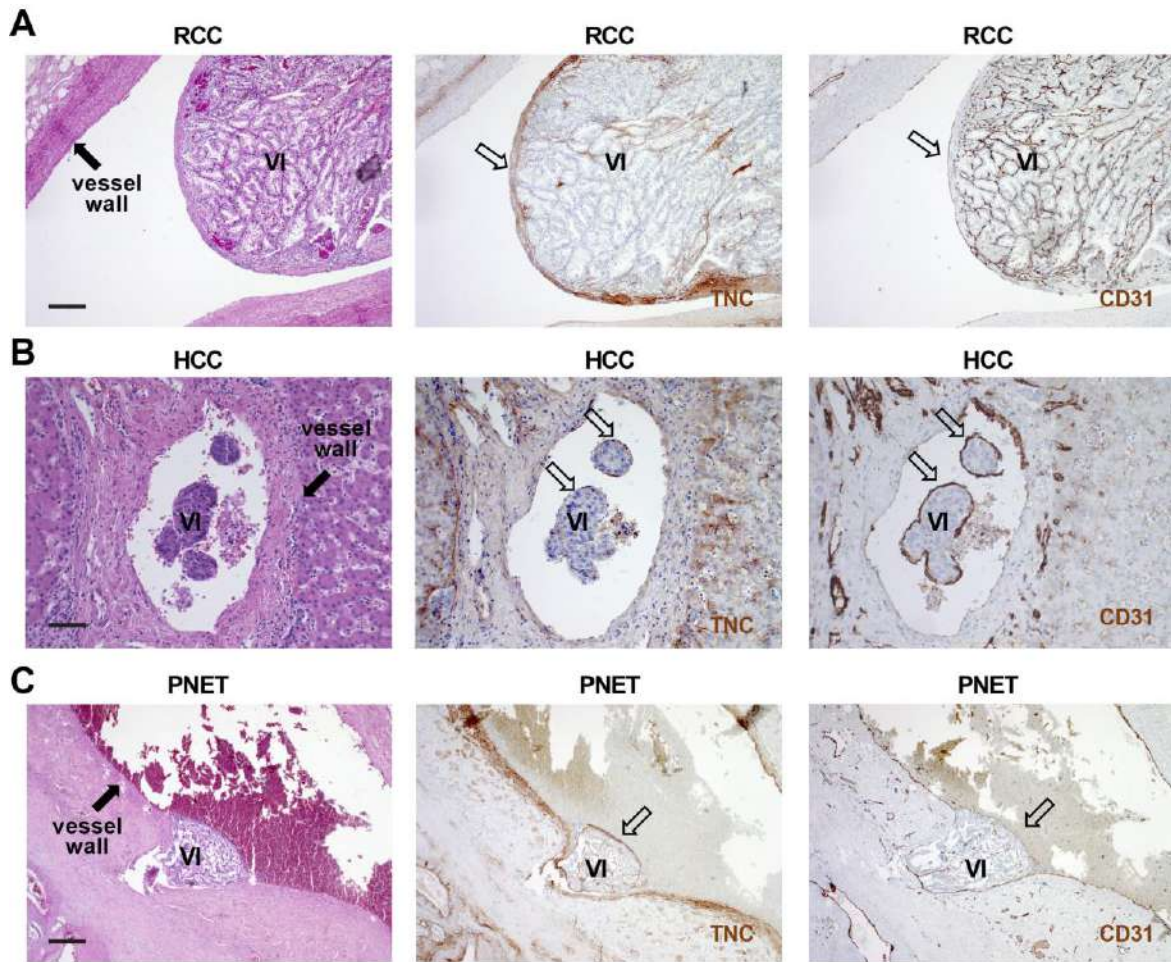
Figure 6 Circulating tumor cells in vascular invasions of human cancer are surrounded by endothelial cells and TNC Consecutive tissue sections from human RCC, HCC and PNET were stained for H&E, CD31 and TNC. Representative images are shown. Note that vascular invasions (VI) are surrounded by a luminal endothelial monolayer and express TNC beneath the endothelial layer (open arrows). Note, that tumor cell clusters were found to protrude into the lumen of blood vessels (filled arrows), in particular the renal veins (RCC), the portal vein and branches of the portal vein (HCC) and the stem or branches of the superior mesenteric vein (PNET). In PNET a thrombotic

reaction is observed at the luminal surface of the endothelium covering the vascular

invasion. Scale bar represents 50 μm.
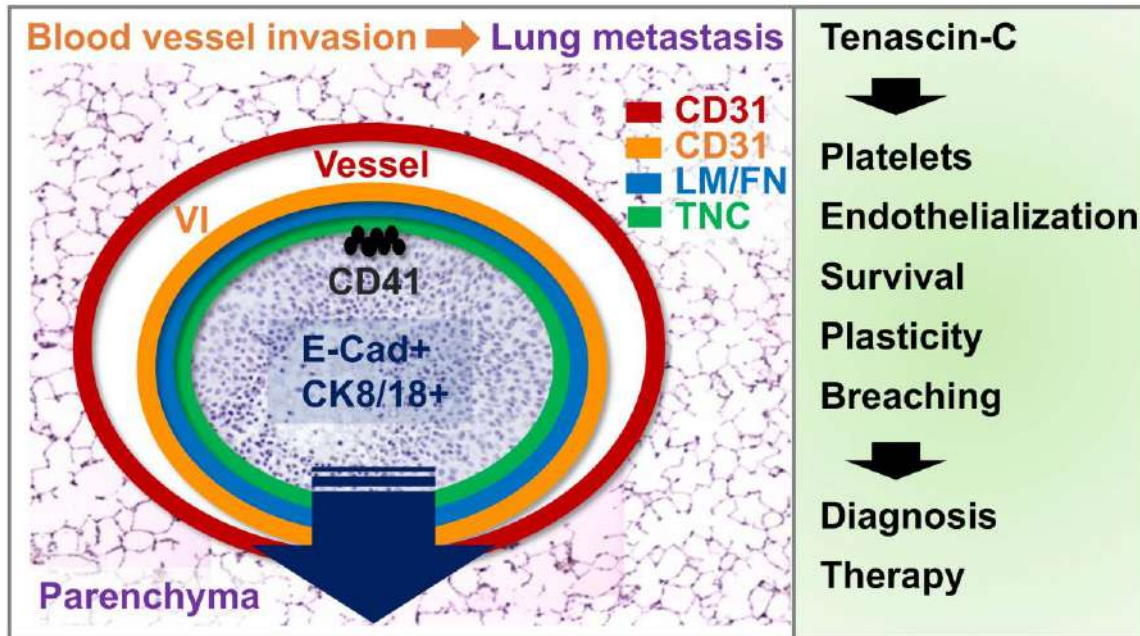
Figure 7 TNC promotes lung metastasis through tumor cell expansion and breaching from vascular invasions Here we describe vascular invasions in blood vessels as mini-organelle-like cargos. They are composed of a central core of tumor cells with cell junctions and epithelial characteristics (E-cadherin+ and CK8/18+). Some of the tumor cells proliferate thereby promoting tumor cell expansion inside the vascular invasion. The tumor cell nest is surrounded by Fsp1+ cells that are a likely source of TNC that is found facing the tumor cell nest. An ensheathing coat of an endothelial monolayer is separated from the TNC layer by other extracellular matrix, in particular laminin (LM) and fibronectin (FN). Platelets (CD41+) are eventually found deep inside the vascular invasion in close contact with the tumor cells. In the absence of TNC, the size of vascular invasions and parenchymal metastasis burden are reduced. By having compared tissues with and without TNC our results suggest multiple effects of TNC on vascular invasions such as enhancing abundance of platelets and, promoting endothelialization, survival, plasticity and breaching of tumor cells into the lung parenchyma. The endothelial layers of the vascular invasion and the blood vessel can form connections which may promote

breaching of the tumor cells. Epithelial plasticity of some tumor cells as indicated by vimentin expression may also contribute to breaching. The composition of vascular invasions offers opportunities for cancer patient stratification as in contrast to lymphatic vessels, vascular invasions in blood vessels express TNC and have an endothelial coat which could be a target of intervention therapies to preventing metastatic spread.

Supplemental information for Sun et al., "**Role of Tenascin-C in promoting lung metastasis through impacting vascular invasions"**

Supplemental Material and Methods

Supplemental Table S1 Patient information

Supplemental Table S2 Summary of vascular invasion characteristics in human cancers

Supplemental Table S3 List of antibodies

Supplemental Table S4 Primer sequences used for qPCR

Supplemental Figures S1 – S8

Supplementary Material and Methods

Human cancer tissue

Human cancer tissue (mammary carcinoma (MaCa), MaCa lung metastasis, renal cell carcinoma (RCC), hepatocellular carcinoma (HCC), pancreatic neuroendocrine tumor (PNET)) from two sites, the Medical University of Vienna/General Hospital Vienna (MUW) and the Hôpital Universitaire de Strasbourg Hautepierre (HUS) was analyzed (**Table S1, S2**). Patients underwent surgical treatment at the Department of Obstetrics and Gynecology and at the Department of Surgery/Division of Thoracic Surgery (MUW cohort), at the HUS for the pancreatic and hepatic tumors, and at the Nouvel Hôpital Civil for the renal tumors (HUS cohort). 30 cases of histologically proven invasive MaCa with metastasis to the lung were investigated. In addition, 35 breast cancer specimen were collected (November 2013 – October 2014) and selected according to clinical annotation of present vascular invasions (**Table S1**). Serial sections of 2 or 4 μm were prepared and stained with antibodies specific for TNC, Factor VIII, CD31, CD34, CD61 and podoplanin (D2-40) by using an automated stainer (BenchMark Ultra, Roche/Ventana). Analysis of staining results was performed by two pathologists independently (FO/RK, MUW cohort of breast cancer, AO/RK MUW cohort of RCC, GA/MPC, HUS cohort of breast cancer, GA/ZS, HUS cohort of RCC, HCC, PNET) in each center (**Table S1**)**.** Results are summarized in **Table S2**. Ethical approval for the procedures described has been granted.

Mice

MMTV-NeuNT female mice (FVB/NCrl background) with a mutated constitutively active form of rat ErbB2 (NeuNT), expressed under control of the mouse mammary tumor virus (MMTV) regulatory region [1], were provided by Gerhard Christofori (University of Basel,

Switzerland). Mice expressing NeuNT develop multifocal breast adenocarcinoma and lung metastasis. TNC +/- mice in the 129/Sv genetic background were generously donated by Reinhard Fässler [2]. Ten consecutive crosses with FVB/NCrl mice (Charles River) were done to homogenize the background. TNC +/- males were crossed with TNC +/- females to obtain TNC+/+ (WT) and TNC-/- (KO) littermates; MMTV-NeuNT males (FVB/NCrl background) were crossed with TNC+/- females to generate double-transgenic mice MMTV-NeuNT with a TNC+/+ and TNC-/- genotype, respectively. All mice were housed and handled according to the guidelines of INSERM and the ethical committee of Alsace, France (CREMEAS) (Directive 2010/63/EU on the protection of animals used for scientific purposes).

Animal experiments

For the syngeneic mouse model, 10^7 NT193 cells were diluted in 50 μL PBS and injected orthotopically into the left fourth mammary gland of FVB/NCrl mice. Mice were euthanized at indicated time points and breast tumors and lungs were snap frozen in liquid nitrogen for western blot and qPCR or embedded in O.C.T. (Sakura Finetek) or in paraffin for histological analysis and immunostaining.

Tissue analysis

The stereological analysis of the lung metastasis (index and number) was done as published [3]. Briefly, the left lung lobe was cut transversally into 2.0 mm thick parallel pieces, giving rise to a total of five to six pieces before paraffin embedding in parallel orientation, and cutting into 7 μm thick sections. In cases where no metastasis was found, 8 to 10 additional sections separated by 200 μm were analyzed.

HE staining

Lungs were prepared and fixed overnight in 4% PFA, dehydrated in 100% ethanol for 24 hours, embedded in paraffin, cut in 7 μm thick sections, dewaxed and rehydrated with 100% Toluene (2 washes of 15 minutes) then incubated in 100%–70% alcohol solutions (10 minutes each) followed by a final staining with hematoxylin (Surgipath) for 5 minutes and washing with tap water or followed by IHC. Sections were further processed with differentiation solution (1% HCl in absolute ethanol, for 7 seconds), followed by washing under tap water for 10 minutes. Sections were then incubated in eosin (Harris) for 10 seconds, rinsed and dehydrated in 70% - 100% alcohol baths with rapid dips in each bath before final wash in toluene for 15 minutes. Finally, tissue sections were embedded in Eukitt solution (Sigma).

Giemsa staining

Tissue was cut in 7 µm thick sections, dewaxed and stained with Giemsa (320310-0125, RAL) for 2 hours at 37°C. Sections were further processed in a 0.5% aqueous acetic acid solution, dehydrated and embedded in Eukitt solution.

Immunohistochemistry

Paraffin embedded tissue was rehydrated and the antigens were unmasked by boiling in 10 mM pH 6 citrate solution for 20 minutes. Cooled slides were washed and incubated in a peroxide solution (0.6% H_2O_2, 0.1% triton X-100 in PBS) to eliminate endogenous peroxidase activity. Non-specific binding sites were blocked with a blocking solution (5% normal goat serum in PBS) for one hour at room temperature (RT) and then avidin/biotin receptors were blocked by using the avidin/biotin blocking kit as recommended by the manufacturer (Vector). Slides were incubated with the first antibody overnight at 4°C in a humidified container. Next day, slides were washed and incubated for 45 minutes at

room temperature with a secondary antibody (coupled to biotin). The detection of peroxidase was done using the Elite ABC system (VECTASTAIN) with DAB (Vector) as substrate. Finally, tissue was stained with hematoxylin, dehydrated and the slide was mounted. Proliferation and apoptosis were quantified as events per area upon staining for Ki-67 and cleaved caspase-3, respectively.

Immunofluorescence staining

Tissue was air-dried and unspecific signals were blocked with blocking solution (5% normal goat or donkey serum in PBS) for one hour at room temperature. Tissue sections were incubated with the primary antibody overnight at 4°C in a humidified container (see **Table S4**). The following day the primary antibody was removed and tissue was incubated with a fluorescent secondary antibody for one hour at room temperature. Secondary goat or donkey antibodies for immunostainings were fluorescently labeled (1/1000): anti-mouse, anti-rabbit, anti-rat, anti-guinea pig and anti-goat IgG (Jackson Laboratory). Slides were washed and incubated with DAPI (Sigma) to visualize the nuclei (10 minutes at room temperature). Excess of dye was removed and tissue was embedded in the FluorSaveTM Reagent (Calbiochem). Fluorescent signal was analyzed with a Zeiss Axio Imager Z2 microscope. The staining procedure (fixation, blocking, antibody dilution) and image acquisition setting (microscope, magnification, light intensity, exposure time) were kept constant per experiment and between genetic conditions. Quantification of immunofluorescent microscopic images was done by the ImageJ (National Institutes of Health) software using a constant threshold. The expression of TNC was scored according to the extent and intensity of the whole tumor mosaic picture. A typical fibrillar TNC staining with the MTn12 antibody in the stroma around the tumor cells was considered as positive signal (no signal with the secondary antibody alone). The extent of TNC staining was scored by the percentage of the

positively stained area. The stained area in each region of interest was scored as 0 for staining less than 5 %, as 1 for 5–25 %, 2 for 25–50 %, 3 for 50–75 %, and 4 for more than 75 % of the stained area. The intensity of staining was scored as 0, 1, 2 and 3 representing no staining, mild (weak but detectable above control), moderate (distinct) and intense (strong) staining, respectively. The percentage of positively stained area and intensity of staining were multiplied to produce a weighted score [4].

qPCR analysis

Total RNA was prepared using TriReagent (Life Technologies) according to the manufacturer's instructions. RNA was reverse transcribed (MultiScribe reverse transcriptase, Applied Biosystems) and qPCR (real time quantitative polymerase chain reaction) was done on cDNA (diluted 1:5 in water) using a 7500 Real Time PCR machine (Applied Biosystems) with a SYBR green reaction mixture or Taqman reaction mixture (Applied Biosystems). Data were normalized by using a Taqman mouse *Gapdh* Endogenous Control (4333764T, Life Technology) and fold induction was calculated using the comparative Ct method (-ddCt). Primers used for qPCR are listed in **Table S4.**

Immunoblotting

Cell lysates were prepared in lysis buffer (25 mM Tris-HCl pH 7.6, 150 mM NaCl,1% NP-40, 1% sodium deoxycholate, 0.1% SDS) supplemented with protease inhibitor (Roche) and Phosphatase Inhibitor Cocktail (Santa Cruz). Protein concentration was determined with a Bradford Assay (BioRad). After addition of Laemmli buffer (Biorad), 20-30 μg protein lysate was separated by SDS-PAGE in precasted 4-20 % gradient gels (Biorad), transferred onto nitrocellulose membranes (Biorad) using TransBlot Turbo™ Transfer System (Biorad), blocked with 5 % Blocking-Grade blocker (Biorad) in 0.1% Tween 20-PBS and incubated with the primary (overnight at 4°C) and secondary antibodies (one

228

hour at RT) in 1.5 % Blocking-Grade Blocker in 0.1 %Tween 20-PBS. Secondary antibodies used for western blots were ECL horseradish peroxidase-linked (1/1000): anti-rat (NA935) and anti-rabbit (NA934V) (GE Healthcare). Protein bands were detected with the Amersham ECL Western Blotting detection reagent (GE Healthcare) or SuperSignal™ West Femto Maximum Sensitivity Substrate (ThermoFisher).

Immunofluorescence staining of cells

Cells were fixed in 4 % PFA for 10 minutes, permeabilized in PBS-Triton 0.1 % for 10 minutes, incubated with the primary antibody overnight at 4 °C, secondary antibody for one hour at RT, DAPI, mounted with FluorSaveTM Reagent (Calbiochem) and analyzed with a Zeiss Axio Imager Z2 microscope.

Cell culture

NT193 cells derived from a MMTV-NeuNT primary tumor [5] were cultured in DMEM medium with 4.5 g/L glucose (GIBCO) supplemented with 10 % of inactivated fetal bovine serum, penicillin (10 000 U/ml) and streptomycin (10 mg/ml). Cells were maintained at 37°C in a humidified atmosphere of 5 % CO_2 and were regularly analyzed by PCR for mycoplasma.

Transduction of cells

Silencing of *Tnc* in mouse cells was done by short hairpin (sh) mediated gene expression knock down (KD). Lentiviral particles with shRNA vectors (Sigma-Aldrich) specific for *Tnc* were used. sh1 (TRCN0000312137), sequence: 5'-CCGGCCCG GAACTGAATATGGGATTCTCGAGAATCCCATATTCAGTTCCGGGTTTTTG-3'; sh2 (TRCN0000312138), sequence: 5'-CCGGGCATCAACACAACCAGTCTAACT CGAGTTAGACTGGTTGTGTTGATGCTTTTTG-3'. Lentiviral particles encoding a non-

targeting shRNA vector were used as a control (SHC202V, Sigma-Aldrich). Transduced cells were selected with normal medium supplemented with 10 µg/ml puromycin (ThermoFisher) and the selection pressure was maintained in all in vitro experiments.

Spheroid assay

NT193 cells were seeded at 5000 cells per 100 µL together with TNC (10 µg/ml) or PBS-Tween-20 (0.01%) in 96 well plates with round bottom pre-coated with 10 µg/ml of poly-HEMA (Sigma) for 24 hours to allow spheroid formation and then cells were embedded in OCT for further immunostaining analysis.

Wound healing assay

NT193 cells (2×10^5) were grown to high confluency in 24-well plates for 24 hours. Confluent cell monolayers were treated two hours with mitomycin-C (Sigma) at 2 µg/ml to inhibit proliferation before application of a scratch wound with a pipet tip. Cell debris was removed by PBS washing before addition of serum-free medium supplemented with the indicated molecules. Images of the wounding area were acquired immediately after scratching and then in the same field after 24 hours. The relative wound closure was quantified by measuring the surface of the cell-free area at the time of injury and at the end point of the experiment.

Transwell migration assay

NT193 cells (5×10^5) were seeded for 7 hours in 60 mm dishes to adhere, then were starved overnight in serum-free medium. Cells were treated 24 hours with TNC at 10 µg/ml in serum-free medium before trypsinisation and seeding (3×10^4) in cell culture inserts (Corning Transwell, pore size 8.0µm), in serum-free condition. Medium containing 10% FBS was used as attractant. After 24 hours inserts were washed in PBS.

Cells were fixed in ice-cold methanol and stained with a 0,5% crystal violet solution. Non-migrating cells were removed with a cotton-tipped applicator. After several washes in distilled water, crystal violet was solubilised in methanol and absorbance measured at 595 nm.

Caspase3/7 activity assay

Caspase 3/7 activity assay (Promega) was performed according to the manufacturer's instructions. Briefly, 2000 cells/well were plated overnight in 96-well plates. Cells were treated as described for the indicated time period and then cell apoptosis was induced by staurosporine (1 μg/ml, Sigma) for 24 hours. To measure caspase 3/7 activity, 75 µL of caspase Glo 3/7 reagent was added to each well for one hour with constant shaking at room temperature. Luminescence was measured using a TriStar² LB942 multidetection microplate reader.

Preparation of washed platelets

Blood was drawn from the abdominal aorta of adult FVB/NCrl mice anesthetized intraperitoneally with a mixture of xylazine (20 mg/kg, Rompun, Bayer) and ketamine (100 mg/kg, Imalgene 1000, Merial). Platelets were washed using ACD-anticoagulated whole blood as previously described [6].

Table S1 Patient information

Number	G	Age (D)	Diagnosis	Grading, staging	Age (M)
1	F	60	MaCa IDC NST	G1, pT1c, pN0	65
2	F	43	Multifocal MaCa IDC NST	G1 and G2, pT2, pN1b-iii	49
3	F	49	MaCa IDC NST	G3, pT?, pN3b	50
4	F	68	Multifocal MaCa IDC NST	G2, pT2, pN1b-iii	78

5	F	64	MaCa ILC	G2, pT1c, pN0	70
6	F	57	Medullary carcinoma	pT2	67
7	F	38	MaCa IDC NST	G3, pT2, pN0	42
8	F	63	MaCa IDC NST	G3, pT1c	64
9	F	62	MaCa IDC NST	G2, pT2, pN1a, L1	63
10	F	53	MaCa IDC NST	G3, pT2, pN0	67
11	F	47	MaCa IDC NST	G2, pT2	54
12	F	58	MaCa IDC NST	G3, ypT1c, ypN1a, L0	60
13	F	81	MaCa IDC NST	pT2N1	
14	F	66	MaCa ILC	pT2N1	
15	F	74	MaCa ILC	pT2N1mi	
16	F	58	MaCa IDC NST	ypT2N1	
17	F	63	MaCa ILC	pT3N0	
18	F	70	MaCa IDC NST	ypT1aN0	
19	F	63	MaCa IDC NST	pT1cN0	
20	F	79	MaCa IDC NST	pT2N2	
21	F	59	MaCa IDC NST	pT2N0	
22	F	61	MaCa ILC	pT2N1	
23	F	70	MaCa IDC NST	pT4bN3a	
24	F	45	MaCa IDC NST	pT2N1	
25	F	47	MaCa IDC NST	pT2N1	
26	F	58	MaCa IDC NST	pT2cN1	
27	F	43	MaCa IDC NST	pT2N1	
28	F	52	MaCa IDC NST	pT4bN1a	
29	F	68	MaCa IDC NST	pT2N1	
30	F	64	MaCa IDC NST	pT1cN1a	
31	F	76	MaCa IDC NST	pT1cN0	
32	F	63	MaCa IDC NST	pT1cN0	
33	F	70	MaCa IDC NST	pT1cN1	
34	F	45	MaCa IDC NST	ypT2N0	
35	F	60	MaCa IDC NST	pT2N0	
36	F	34	MaCa IDC NST	pT2N1	
37	F	82	MaCa IDC NST	pT4aNx	
38	F	50	MaCa IDC NST	pT2N0	
39	F	50	MaCa ILC	pT3N1	
40	F	43	MaCa IDC NST	ypT1cN0	
50	F	79	MaCa IDC NST	pT2N1	
51	F	31	MaCa IDC NST	pT2N0	
52	F	51	MaCa IDC NST	pT1bN0	
53	F	83	MaCa IDC NST	pT1cN2a	
54	F	40	MaCa IDC NST	pT2N2a	
55	F	71	RCC	pT3aNxL1V1R0	
56	M	57	RCC	pT1bNxL0V1R0	
57	M	74	RCC	pT3aNxl	
58	F	19	RCC	pT3aN1L1V1R0	
59	M	53	RCC	pT4N1L1V1R2	
60	F	82	RCC	pT3aNXL0V0R0	
61	M	75	RCC	pT1aNXL0V1R0	
62	M	77	RCC	pT3aNxL0V0R0	
63	M	56	RCC sarcomatoid	pT3aNXL0V1R0	
64	M	58	HCC	pT4V1	
65	M	63	HCC	pT3bN0V1	
66	M	61	HCC	pT3bN0V1	

67	M	59	HCC	pT4N0V1	
68	M	75	HCC	pT4V1	
69	M	57	HCC	pT4N0V1	
70	M	58	HCC	pT4NXV1	
71	M	72	HCC	pT2N0M1	
72	M	58	HCC	pT4NXV1	
73	M	61	PNET G2	pT1cV1Pn1N0R0	
74	M	76	PNET G1	pT3V2Pn1R0N0	
75	M	63	PNET G2	pT3N0L0V1Pn1R0	
76	M	45	PNET G2	ypT3N1LXV1Pn1R1	
77	M	56	PNET G1	pT1N0V1L0Pn0R0	
78	M	77	PDAC	pT3N1R0	
79	M	62	PDAC	pT3N1R1M1	
80	F	67	PDAC	pT3N1R0	
81	M	66	PDAC	pT3N1M1R0	
82	M	60	PDAC (BC)	pT4N1M1R1	
83	F	79	PDAC	pT3N1L1V1Pn1R1*	
84	F	76	APBA	pT4N1R0	

Human cancer tissue from mammary carcinoma (MaCa) and associated lung metastasis of mammary carcinoma patients and, renal cell carcinoma (RCC), hepatocellular carcinoma (HCC), pancreatic neuroendocrine tumor (PNET) and pancreatic adenocarcinoma (PDAC) with annotation of tumor vascular invasions was analyzed as described in the methods section. Gender (F, female, M, male), age at diagnosis, grading (G1, G2, G3), staging (TNM classification, https://www.uicc.org/resources/tnm) is shown. APBA, Ampullary pancreato-biliary adenocarcinoma. PDAC (BC), biliary adenocarcinoma. For MaCa: Age at diagnosis (D), age at lung metastasectomy (M), grading (G1, G2, G3), staging (TNM classification, primary tumor site (pT), pathological lymph node involvement (pN) and distant metastatic spread (M), https://www.uicc.org/resources/tnm), IDC NST, invasive ductal carcinoma, no special type (according to WHO classification), ILC, invasive lobular carcinoma; ypT, tumor stage after chemotherapy; mi, micrometastasis. Results are summarized in **Table S2**.

Table S2 Summary of vascular invasion characteristics in human cancers

Number of cases w/ intravascular tumor cell nests	Number of cases w/ localization of tumor cell nests in blood or lymphatic vessels	Number of cases w/ intravascular tumor cell nests with endothelial ensheathing	Number of cases w/ intravascular tumor cell nests with TNC layer	Number of cases w/TNC expression in vessel wall	Number of cases w/ intravascular tumor cell nests, floating or attached phenotype
HCC (9)	Blood vessel (vein) (9/9)	9/9	9/9	9/9	attached (7/9)
RCC (9)	Blood vessel (vein) (9/9)	9/9	9/9	9/9	attached (9/9)
PNET (5)	Blood vessel (vein) (5/5)	5/5	5/5	4/5	attached (5/5)
PDAC (7)	Lymphatic vessel (7/7)	0/7	0/7	nd	floating (7/7)
Ductal invasive MaCa (29)	Lymphatic vessel (29/29)	0/29	0/25	nd	floating (29/29)
Lobular invasive MaCa (5)	Lymphatic vessel (5/5)	0/5	0/5	nd	floating (5/5)
MaCa (1/12)	Lymphatic vessel (1/12)	0/1	0/1	nd	floating (1/1)
MaCa lung metastasis (5/12)	Lymphatic vessel (5/12)	0/5	0/5	nd	floating (0/5)

Summary of immunohistochemical analysis of human carcinoma tissue and detection of intravascular tumor cell nests in hepatocellular carcinoma (HCC), renal cell carcinoma (RCC), pancreatic neuroendocrine tumors (PNET), pancreatic ductal adenocarcinoma (PDAC), invasive mammary carcinoma (MaCa) with previous annotation of vascular invasions and, not annotated MaCa and associatd lung metastasis (last two raws). Expression of TNC and presence of endothelial cells (flat nuclei in HE images, CD31 staining) in vascular invasions is depicted. Note that vascular invasions are either separated from the vessel wall and appear as floating structures or are connected to the vessel wall protruding into the vessel lumen (attached). Note further two groups of vascular invasions, one group with invasions into blood vessels of highly vascularized tumors (HCC, RCC, PNET) which are ensheathed by an endothelial monolayer and express TNC at the rim, similar to what has been seen in vascular invasions of the

murine MMTV-NeuNT and NT193 model. In the second group of tissues derived from PDAC, MaCa and MaCa lung metastasis, tumor cell nests were seen in lymphatic vessels that did not express TNC and lacked an endothelial cell layer. Note that the vessel wall expressed TNC where it had been investigated (see also **Fig. S7, S8**). nd, not determined.

Table S3 List of antibodies

Antigen	Host	Antibody name	Source	Dilution	Application
Akt	rabbit	4691	Cell Signaling	1/1000	WB
α-SMA	mouse	A2547	Sigma-Aldrich	1/400	IF
CD31	rat	550274	BD pharmigen	1/200	IF
CD31	mouse	JC/70A/M823	DAKO	1/20	IHC
CD31	rabbit	clone EP78/ AC-0083	Epitomics	manual	IHC (HUS)
CD34	mouse	Q-Bond 10	Novocastra	1/50	IHC (MUW)
CD41	rat	11024	Abcam	2µg/ml	IF
CD45	rat	550566	BD pharmigen	1/500	IF
CD61/platelet glycoprotein IIIa	mouse	Clone 2f2/ 161M-15	Cell Marque	Ready to use	IHC (MUW)
Cleaved caspase-3	rabbit	9661	Cell Signaling	1/600	IHC
Cytokeratin CK8/18	guinea pig	GP11	PROGEN	1/500	IF
D2-40/ podoplanin	mouse	322M-18	Cell Marque	Ready to use	IHC (MUW)
D2-40/ podoplanin	mouse	M3619	BenchMark Ultra, Roche/Ventana	manual	IHC (HUS)
E-cadherin	rat	13-1900	Life Technology	1/200 IF 1/1000 WB	IF, WB
ErbB2	rabbit	MA5-13675	ThermoFisher	1/50	IF
Factor VIII	rabbit	A082	DAKO	1/2000	IHC (MUW)
Fibronectin	rabbit	F3648	Sigma-Aldrich	1/200	IF
FSP1	rabbit	Mts1/S100a4	Ambartsumian, 1996	1/200	IF
GPIbβ	rat	RAM.1	Mangin, 2009	3µg/ml	IF
Ki-67	rabbit	RM-9106	ThermoFisher	1/600	IHC
Pan-laminin	rabbit	Ln6 7S	Simo et al.	1/2000	IF
TNC	rat	MTn12	Aufderheide, 1988	2µg/ml IF 0.4µg/ml WB	IF, WB
TNC	mouse	NCL-TENAS-C	Novocastra	1/50	IHC (MUW)
TNC	mouse	BC24	Sigma	1/4000	IHC
Vimentin	rabbit	2707-1	EPITOMICS	1/500 IF 1/1000 WB	IF, WB

IF, immunofluorescence staining; IHC, immunohistochemical staining; WB, western blot.
[5,7,8].

Table S4 Primer sequences used for qPCR

GENE	Forward primer	Reverse primer
E-cadherin	CAGCCTTCTTTTCGGAAGACT	GGTAGACAGCTCCCTATGACTG
vimentin	CCAACCTTTTCTTCCCTGAAC	TTGAGTGGGTGTCAACCAGA
slug	CTCACCTCGGGAGCATACAG	GACTTACACGCCCCAAGGATG
twist	AGTGTTTGGCAGGGGACA	CCCATCCCCTGGGTATCT
zeb1	GCCAGCAGTCATGATGAAAA	TATCACAATACGGGCAGGTG
fibonectin	GATGCCGATCAGAAGTTTGG	GGTTGTGCAGATCTCCTCGT
tenascin-C	CAGGGATAGACTGCTCTGAGG	CATTGTCCCATGCCAGATTT
MMP9	ACGACATAGACGGCATCCA	GCTGTGGTTCAGTTGTGGTG
PAI-1	GGCACCTTTGAATACTCAGGA	TTTCCCAGAGACCAGAACCA
Axin2	CTGCTGGTCAGGCAGGAG	TGCCAGTTTCTTTGGCTCTT
snail	Tapman probe, Hs00195591_m1, ThermoFisher	

References

1. Muller, W. J., Sinn, E., Pattengale, P. K., Wallace, R. & Leder, P. Single-step induction of mammary adenocarcinoma in transgenic mice bearing the activated c-neu oncogene. *Cell* **54,** 105–115 (1988).

2. Talts, J. F., Wirl, G., Dictor, M., Muller, W. J. & Fässler, R. Tenascin-C modulates tumor stroma and monocyte/macrophage recruitment but not tumor growth or metastasis in a mouse strain with spontaneous mammary cancer. *J. Cell. Sci.* **112 (Pt 12),** 1855–1864 (1999).

3. Nielsen, B. S. *et al.* A Precise and Efficient Stereological Method for Determining Murine Lung Metastasis Volumes. *The American Journal of Pathology* **158,** 1997–2003 (2001).

4. Shi, M. *et al.* Tenascin-C induces resistance to apoptosis in pancreatic cancer cell through activation of ERK/NF-κB pathway. *Apoptosis* **20,** 843–857 (2015).

5. Ambartsumian, N. S. *et al.* Metastasis of mammary carcinomas in GRS/A hybrid mice transgenic for the mts1 gene. *Oncogene* **13,** 1621–1630 (1996).

6. Cazenave, J.-P. *et al.* Preparation of Washed Platelet Suspensions From Human and Rodent Blood. in *Platelets and Megakaryocytes* **272,** 013–028 (Humana Press, 2004).

7. Aufderheide, E. & Ekblom, P. (7) Tenascin during gut development: Appearance in the mesenchyme, shift in molecular forms, and dependence on epithelial-mesenchymal interactions. (1988).

8. Mangin, P. H. *et al.* Identification of five novel 14-3-3 isoforms interacting with the GPIb-IX complex in platelets. *Journal of Thrombosis and Haemostasis* **7,** 1550–1555 (2009).

Supplemental figures
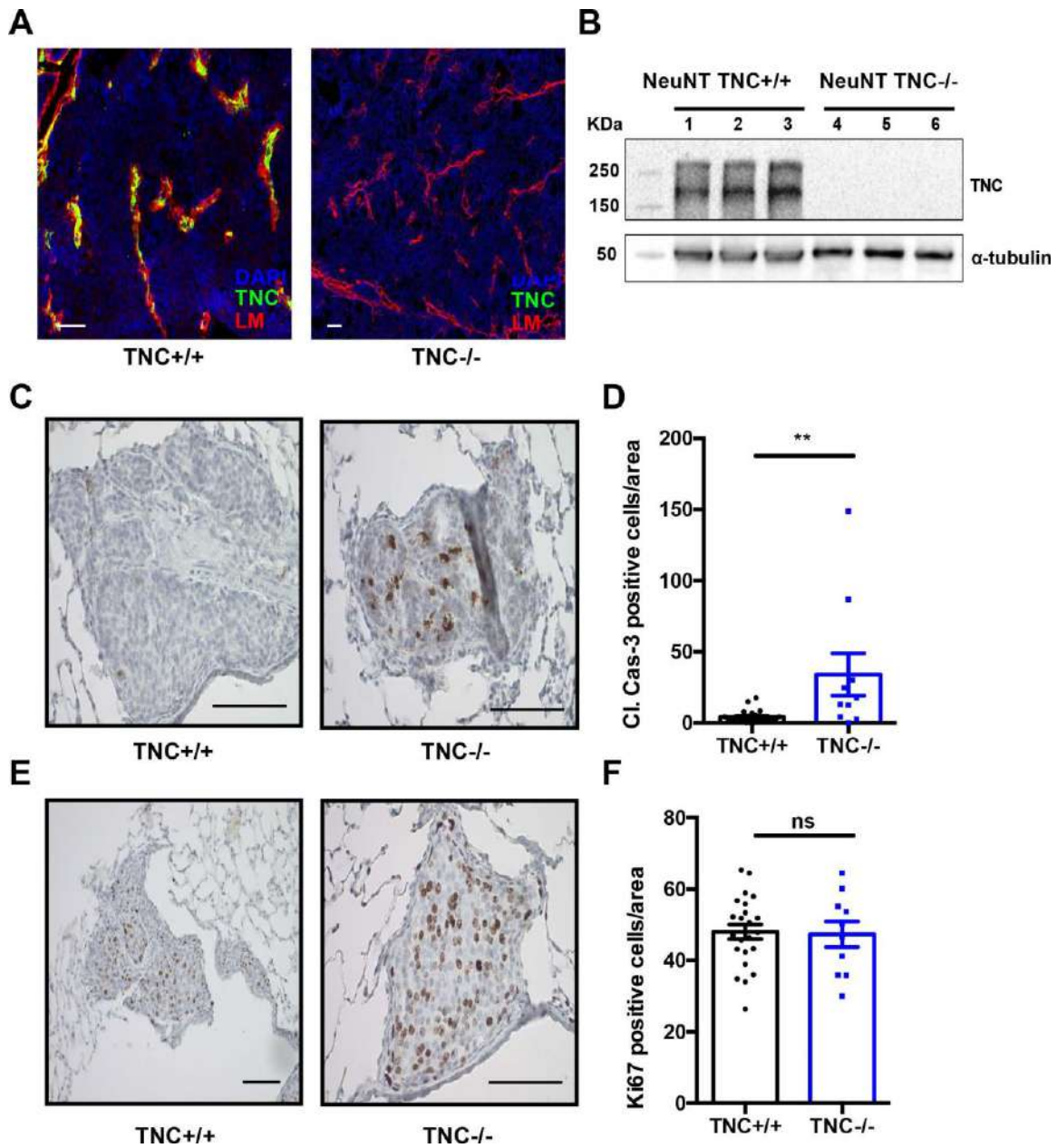
Figure S1. TNC promotes survival of cancer cells in parenchymal metastasis, yet not proliferation (A) Representative immunofluorescence (IF) images for TNC (green) and laminin (red) of primary tumors of MMTV-NeuNT mice (TNC+/+ and TNC-/-), respectively**. (B)** Representative immunoblot of TNC in MMTV-NeuNT tumors with α-

tubulin as control. Note, no detection of TNC in TNC-/- tumors. (**C-F)** Immunohistochemical (IHC) analysis for cleaved caspase-3 **(C)** and Ki67 **(E)** in parenchymal metastases (TNC +/+, N = 6 mice, n = 23 metastases; TNC -/-, N = 6 mice, n = 10 metastases). A dot represents the accumulated number of apoptotic **(D)** and proliferative cells **(F)** per area (0.1 mm^2) in parenchymal metastasis. Scale bar: 100 µm. Mean ± SEM.
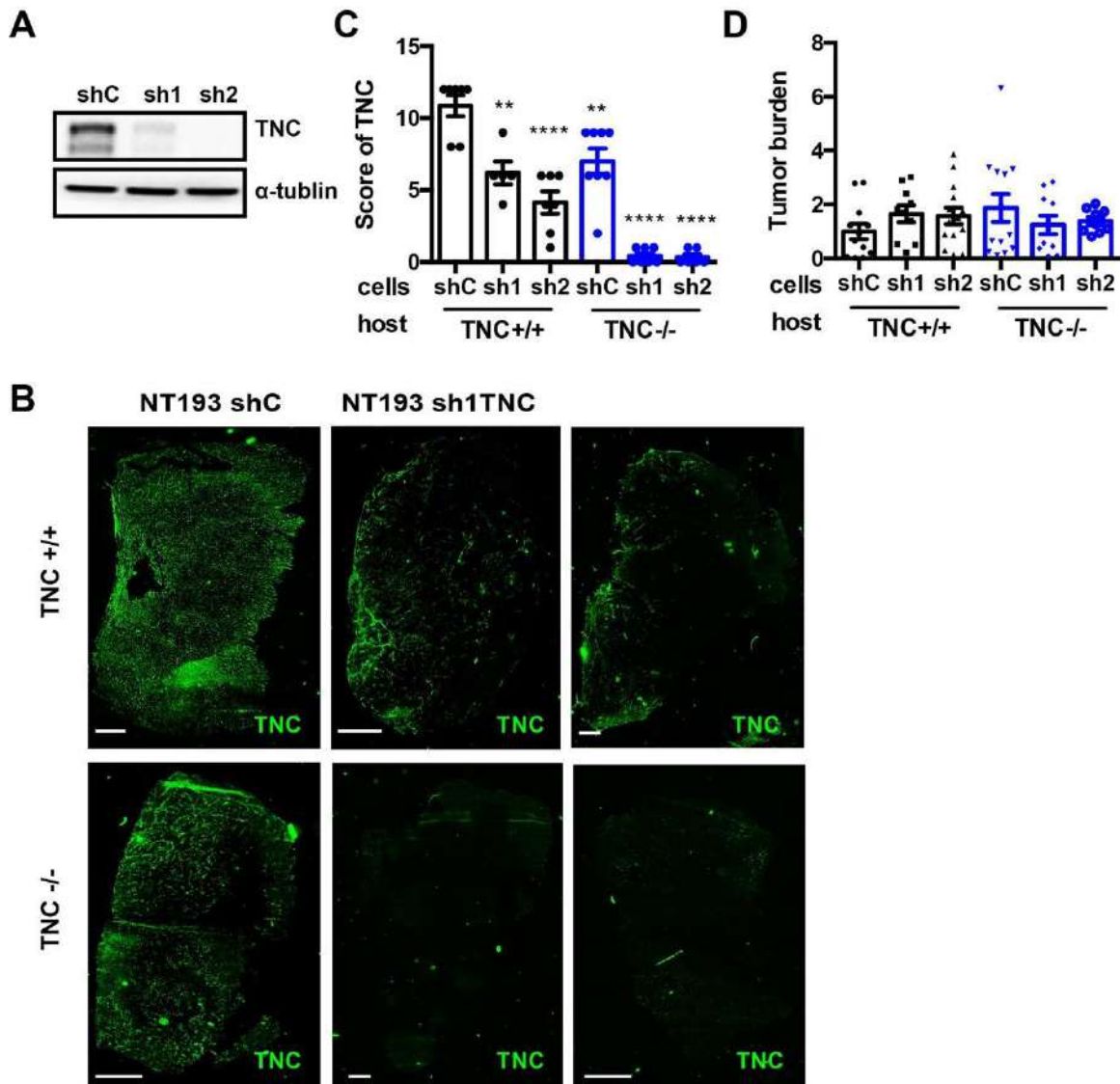
Figure S2. Knockdown of TNC in NT193 cells *in vitro* and in tumor cell grafts (A) Immunoblotting for TNC in cultured NT193 control (shC) and TNC knockdown cells (sh1 and sh2). Loading control, α-tubulin. **(B)** Representative mosaic IF images of TNC (green) in primary tumors, after engraftment of NT193 shC and TNC knockdown cells in the mammary fat pad of TNC+/+ and TNC-/- FVB mice, respectively. Scale bar: 1 mm. **(C)** TNC score in the primary tumor of each grafting condition (see material and methods

for details). N = 6 mice for each grafting condition. **(D)** Tumor burden (g) of TNC+/+ and TNC-/- FVB hosts after engraftment of NT193 sh control (shC), sh1TNC and sh2TNC cells (shC in TNC +/+ mice (N = 12); sh1TNC in TNC +/+ mice (N = 10); sh2TNC in TNC +/+ mice (N = 14); shC in TNC -/- mice (N = 13); sh1TNC in TNC -/- mice (N = 10); sh2TNC in TNC -/- mice (N = 9). Mean ± SEM.
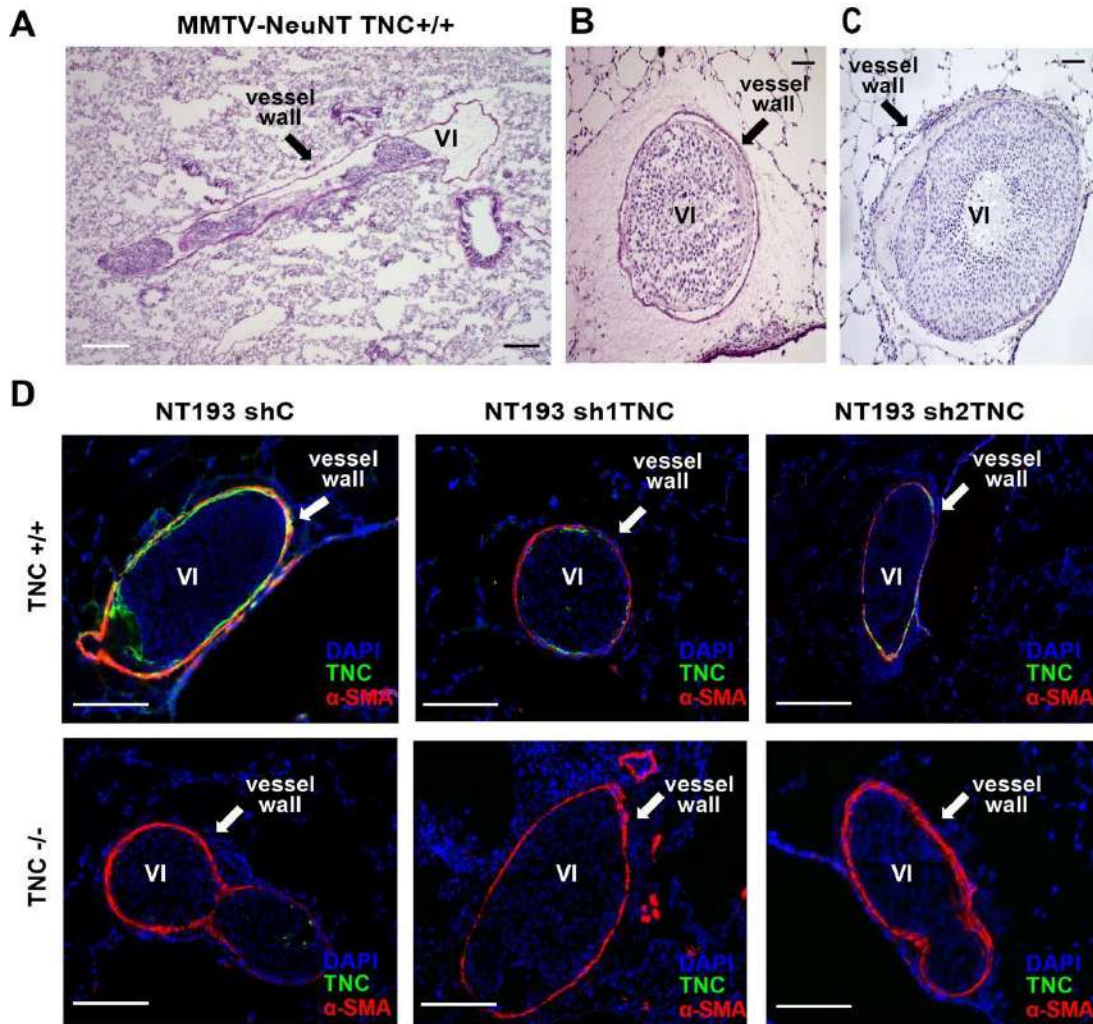
Figure S3. TNC expression in tumor vascular invasions (A - C) Representative HE images of vascular invasions (VI) in blood vessels of MMTV-NeuNT/TNC+/+ lung tissue. **(B, C)** Note that VI eventually can occlude the vessel lumen and that the central VI area can be necrotic as indicated by the absence of nucleated cells **(C)**. Scale bar: 200 μm **(A),** 50 μm **(B, C)**. **(D)** Representative IF images of TNC (green) in VI of lung tissue derived from NT193 tumor cell grafts. αSMA staining (red) marks blood vessels. Note, that TNC is expressed when the host (TNC+/+) expresses TNC yet not when the host lacks TNC (TNC -/-). Also in a TNC+/+ host shCTRL cells express lower TNC levels than in a WT host. Two images on the left (panel D) are already displayed in **Fig. 3C** and are

shown here again for comparison of TNC expression between the six conditions. Scale

bar: 100 μm.
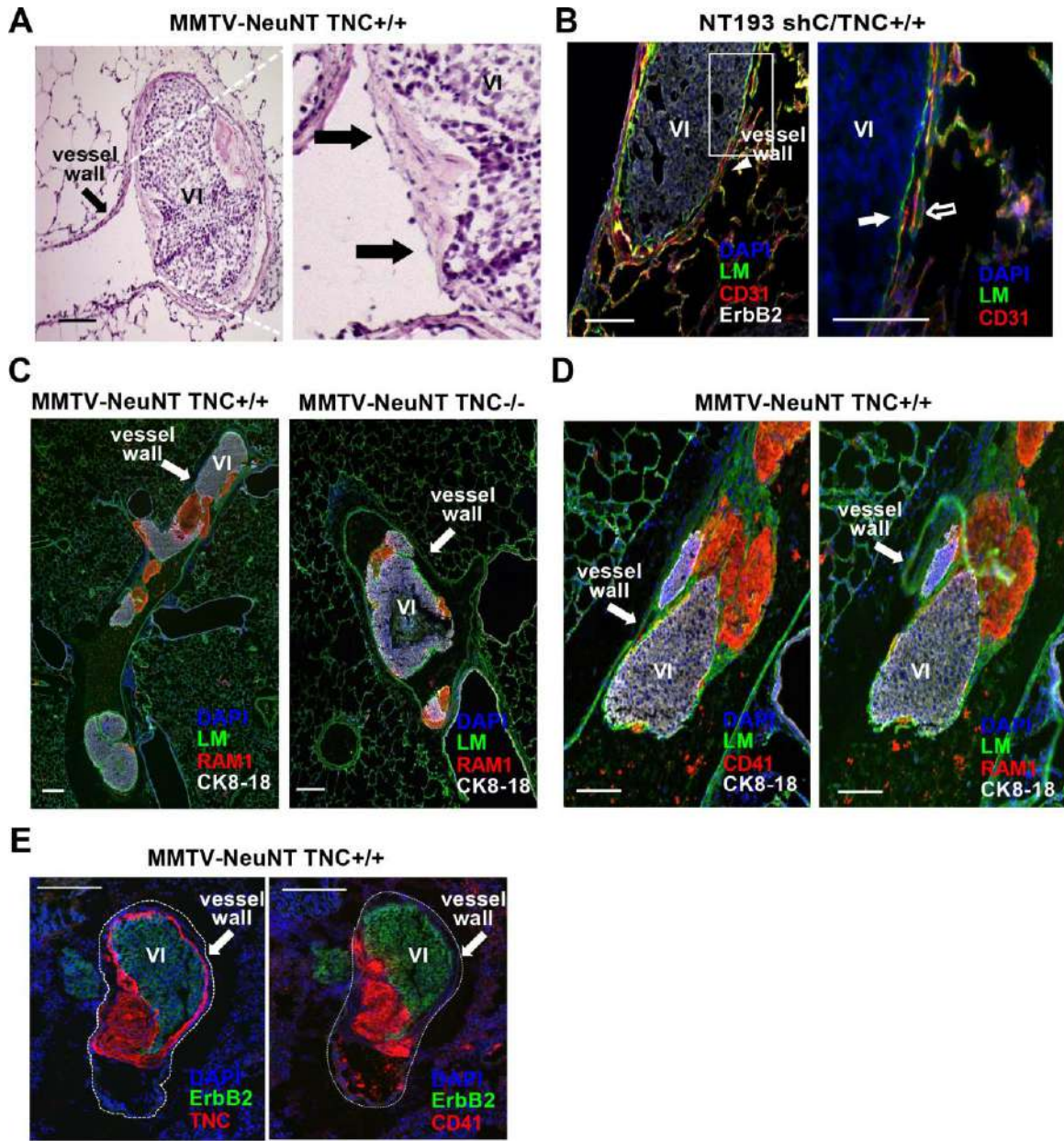
Figure S4

Figure S4. Presence of endothelial cells and platelets in vascular invasions (A) Representative HE images of vascular invasions (VI) of MMTV-NeuNT/TNC+/+ lung tumor tissue. Note a monolayer of cells with flat nuclei at the luminal border (arrow). A higher magnification is shown in the right panel. Scale bar: 100 µm. **(B)** Representative

IF image of endothelial cells (CD31+) in NT193 tumor derived vascular invasions. A higher magnification is shown in the right panel. The filled arrow points at the layer of endothelial cells that surround the tumor embolus, the empty arrow points at a blood vessel. Scale bar: 100 µm. (**C - E**) Representative IF images of platelets (RAM1 (Gp1b), CD41) together with laminin (LM) (**C, D**) or ErbB2 in vascular invasions of MMTV-NeuNT mice (TNC+/+ and TNC-/-). Note that platelets and tumor cells are enveloped by a common laminin layer **(C, D)**. Scale bar: 200 µm **(C)**, 100 µm **(D, E)**.
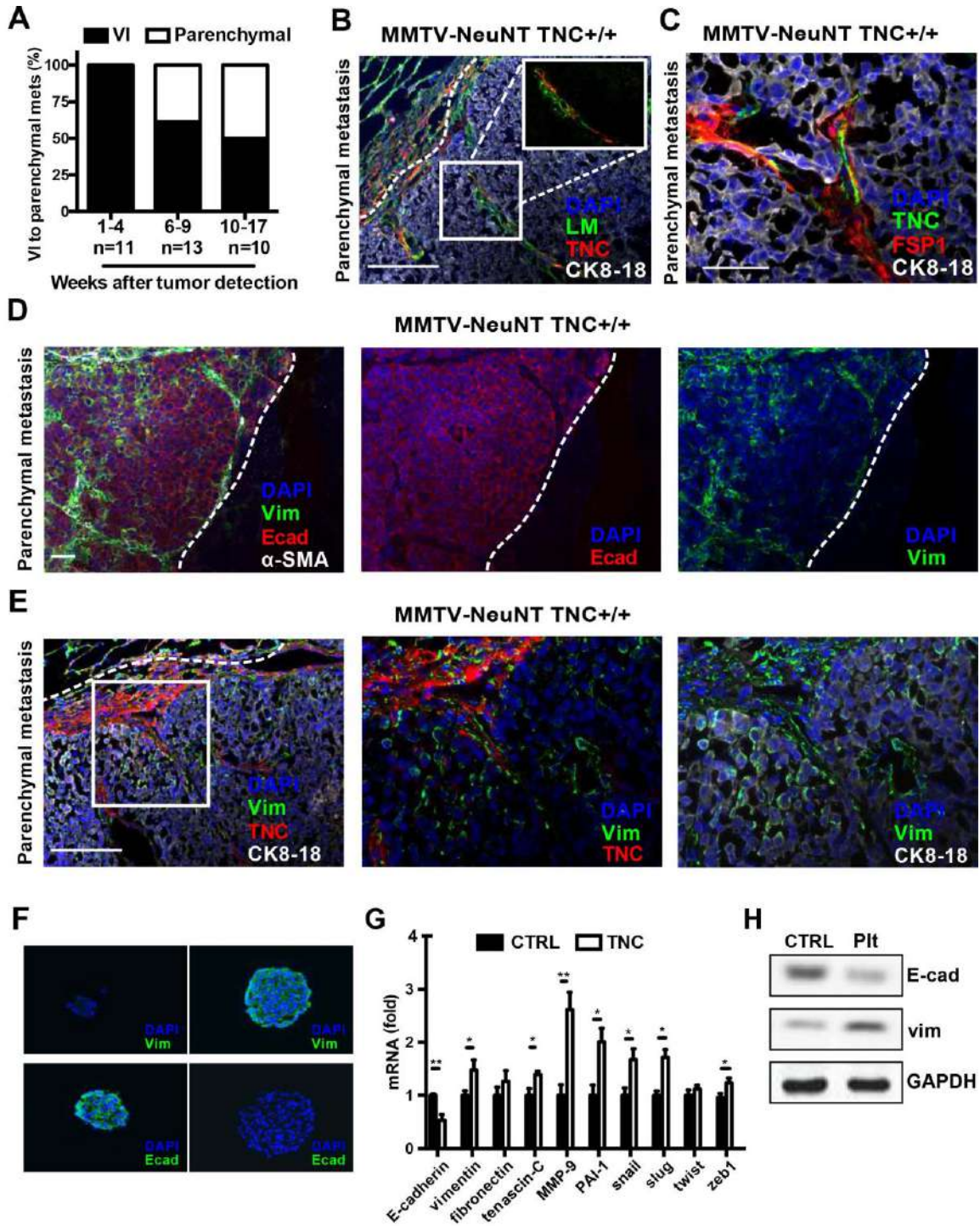
Figure S5

Figure S5. Kinetics of parenchymal lung metastasis and EMT-like phenotype in parenchymal metastasis of MMTV-NeuNT lung tissue and in cultured NT193 cells

(A) Proportion of vascular invasions (VI) and parenchymal lung metastases in MMTV-NeuNT mice sacrificed at distinct time points after first tumor detection. 1 - 4 weeks, N = 3 mice with a total of n = 11 VI; 6 - 9 weeks, N = 3 mice with n = 13 VI; 10 - 17 weeks, N = 3 mice with n = 10 VI. **(B-E)** Representative IF images of lung parenchymal metastases of TNC +/+ mice. White squares delineate fields of higher magnification. **(B)** Note that TNC (red) and laminin (green) form tumor matrix tracks inside and at the periphery of parenchymal metastases. Scale bar: 100 µm. **(C)** Note that FSP1 and TNC staining partially overlap. Scale bar: 50 µm. **(D)** Note that cells have a mixed phenotype as indicated by expression of E-cadherin and vimentin. Scale bar: 100 µm. **(E)** Note close vicinity of vimentin+ cells to TNC. Scale bar: 100 µm. Mean ± SEM. **(F)** IF images of E-cadherin and vimentin (green) of NT193 spheroids upon treatment with TNC for 24 hours. Cell nuclei stained with DAPI. Scale bar: 20 µm. **(G)** Relative expression (fold change) of the indicated genes in NT193 cells upon treatment with TNC for 24 hours (n = 5, five independent experiments) with normalization to GAPDH. **(H)** Detection of E-cadherin and vimentin expression by immunoblotting of lysates from NT193 cells treated with platelets (Plt) for 24 hours (n = 3, three independent experiments).

A MMTV-NeuNT TNC+/+; DAPI/Vim/ErbB2
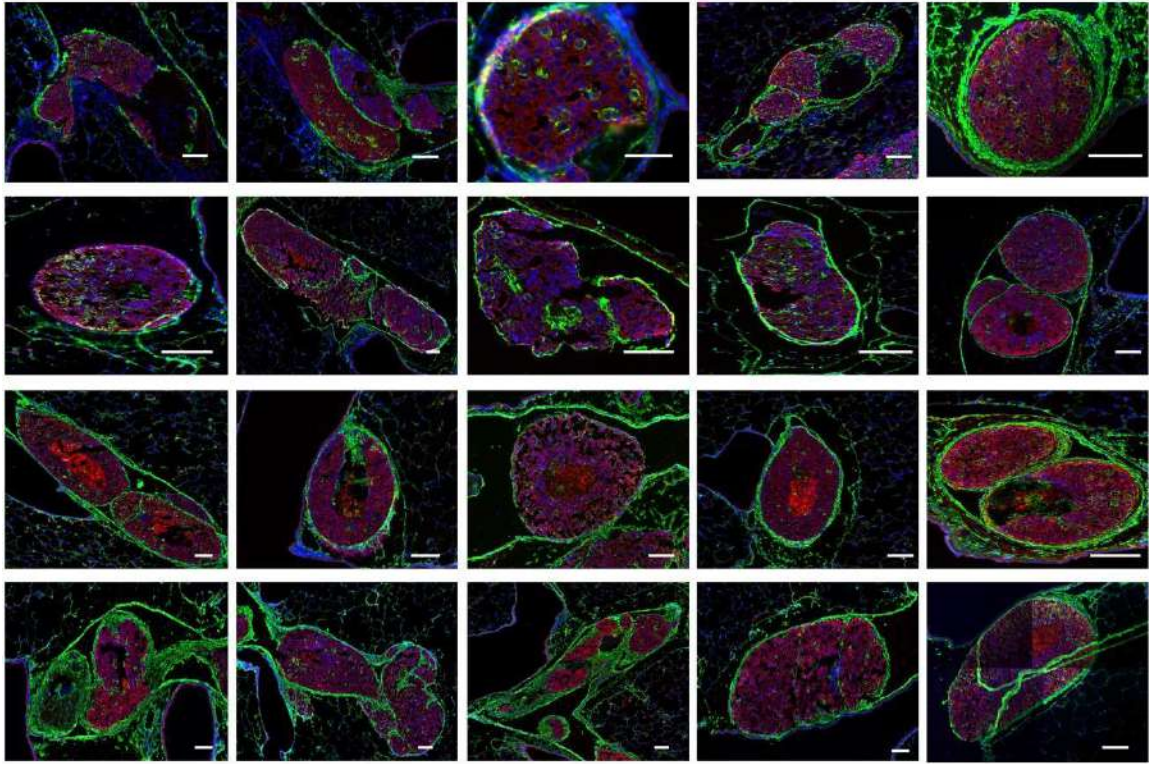
B MMTV-NeuNT TNC-/-; DAPI/Vim/ErbB2

250
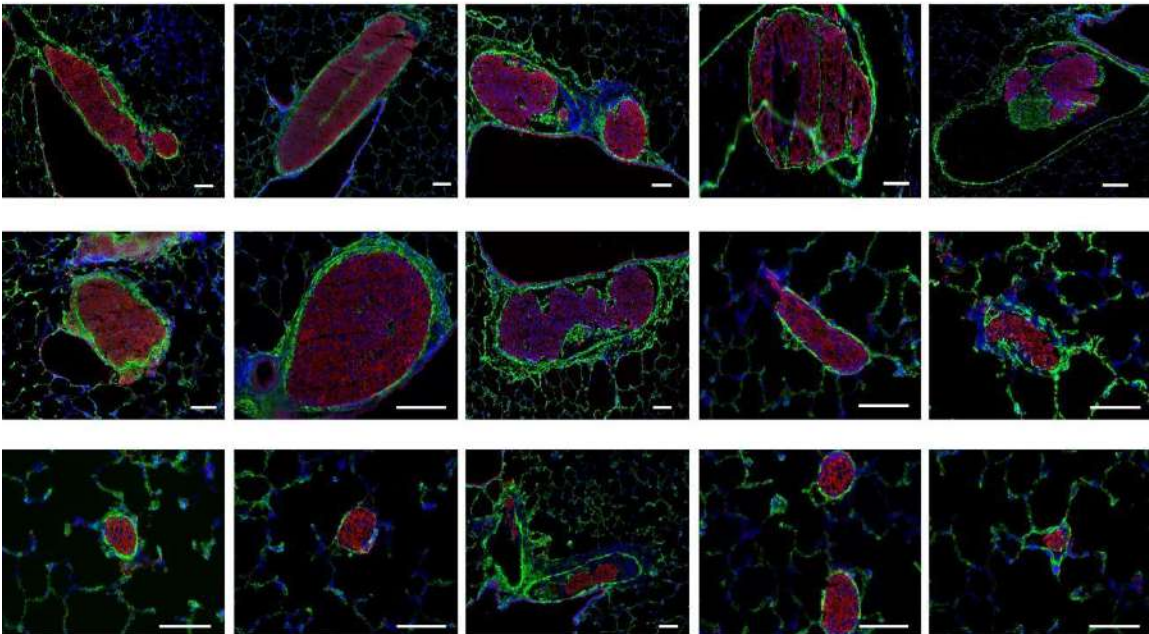
Figure S6. Cellular plasticity in MMTV-NeuNT vascular invasions (A, B)
Representative IF images of vimentin+ (green) and ErbB2+ (red) cells in vascular invasions of lung tissue from MMTV-NeuNT TNC +/+ (N = 6 mice, n = 20 VI) **(A)** and TNC -/- mice (N = 4 mice, n = 15 VI) **(B)**. Scale bar: 100 μm.
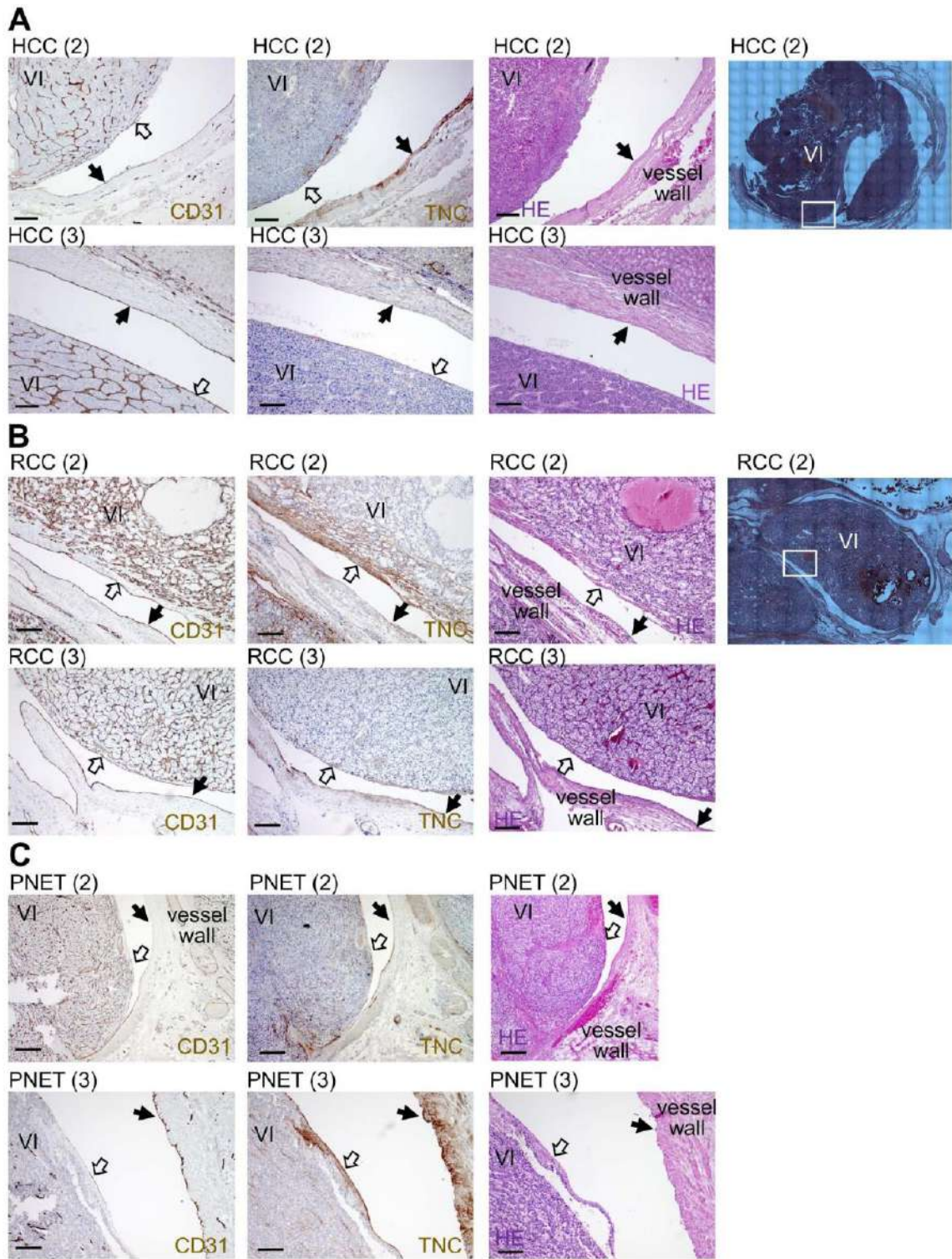
Figure S7 Vascular invasions in blood vessels of human cancer are characterized by endothelial cells and TNC expression Consecutive tissue sections from human

RCC, HCC and PNET were stained for HE, CD31 and TNC. Representative images including mosaic images (upper image in A and B) are shown that demonstrate filling of the invaded vessels (veins) (filled arrows). Note that vascular invasions (VI) are surrounded by a luminal endothelial monolayer and express TNC beneath the endothelial layer (open arrows). Scale bar represents 50 μm.
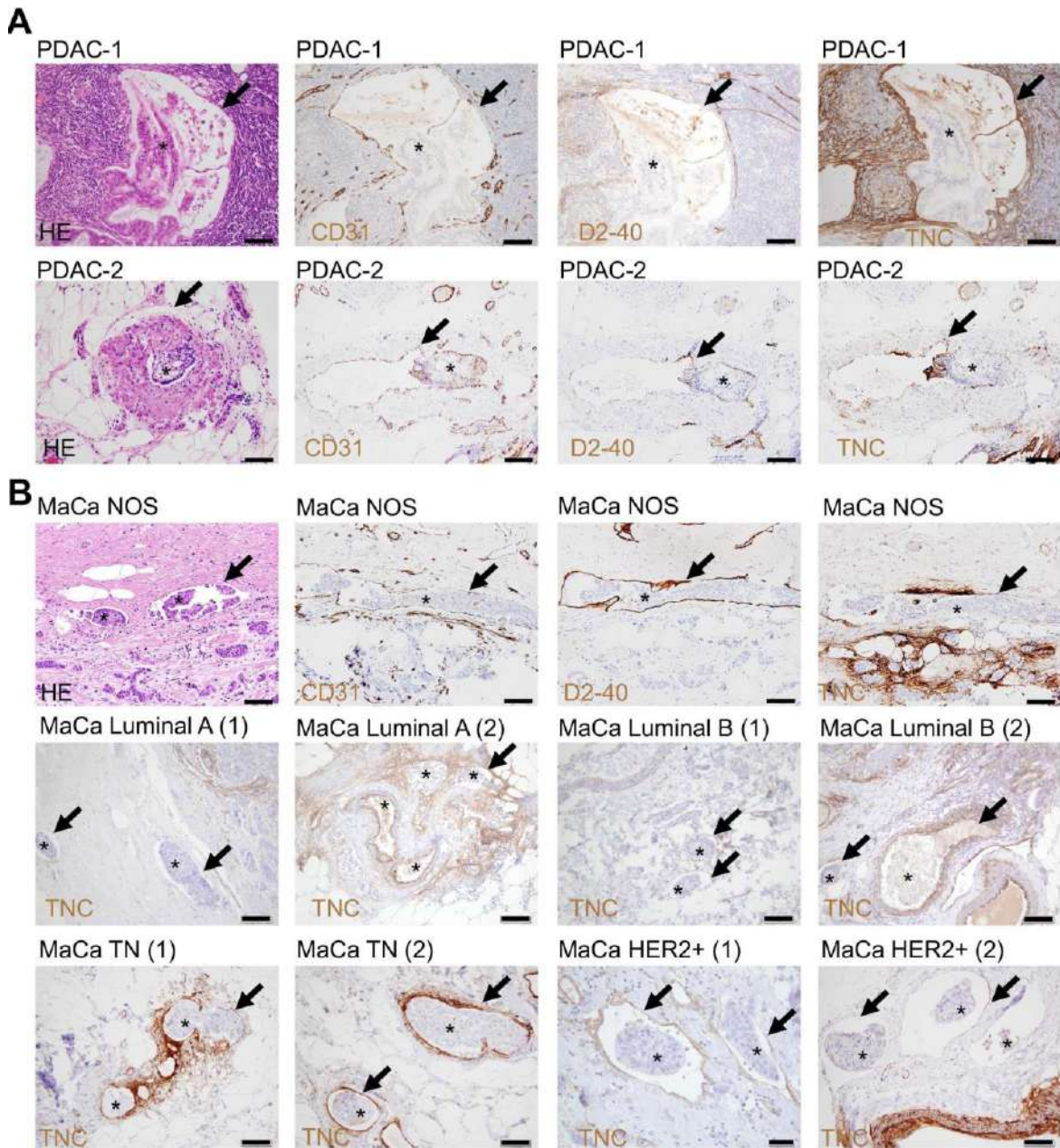
Figure S8 Tumor cell nests in lymphatic vessels of mammary and pancreatic adenocarcinomas Representative images of human invasive pancreatic ductal adenocarcinomas (PDAC) (**A**) and invasive mammary carcinomas (MaCa) (**B**) are shown upon staining with HE or antibodies specific for endothelial cells (CD31),

lymphatic vessels (D2-40) and TNC, respectively. Arrow points at infiltrated lymphatic vessel. As the tumor cell nests are found in lymphatic vessels they are desginated as lymphovascuar invasions (LVI) and marked with a star. Note that LVI are not enveloped by an endothelial monolayer, nor express TNC whereas the lymphatic vessel or the surrounding tissue can abundantly express TNC. Scale bars are 20 μm (Her2+ (1), TN (2)), 50 μm (PDAC (1), Luminal A (1/2), Luminal B (1/2), TN (1), Her2+ (2)) and 100 μm (PDAC (2), MaCa).

Appendix II

Manuscript: Tenascin-C promotes tumorigenesis in oral squamous cell carcinoma

In the carcinogen-driven tongue OSCC model with engineered levels of TNC we observed a pronounced effect of TNC on CD11c+ dendritic cells (DC) that were attracted by the TNC matrix potentially impairing CD8+ T cells that were less abundant in TNC expressing tumors. The tumor stroma is organized as tumor matrix tracks that have lymphoid-like characteristics where TNC generates a particular microenvironmental niche. In these niches TNC induces CCL21 in lymphatic endothelial cells (LEC) which attracts the DC into these niches. In consequence, CD8+ T cell function is presumably impaired. The tumor matrix tracks may also represent a physical shield thereby preventing entry of CD8+ T cells inside the tumor nests.
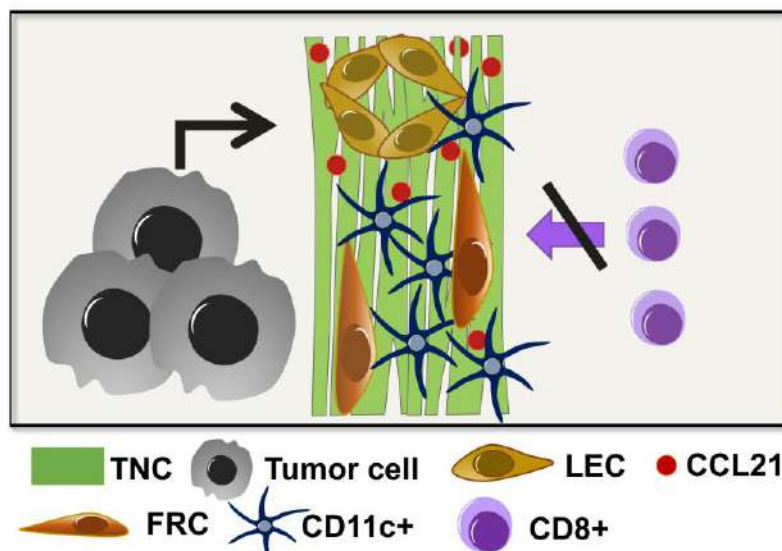
Figure 9 : Summary figure illustrating the lymphoid-like properties of TNC matrix tracks in an OSCC tongue tumor model. TNC is assembled into fibrillar parallel aligned matrix tracks together with other ECM molecules thereby surrounding the epithelial tumor cell nests. These matrix tracks have lymphoid-like properties as they are enriched by ERTR7+ fibroblastic reticular cells (FRC), lymphatic endothelial cells (LEC) and CCR7+ cells. TNC induces CCL21 in LEC and binds CCL21 thereby potentially generating an adhesive substratum for CD11c+ dendritic cells. These cells accumulate in the TNC matrix presumably causing the low number of CD8+ T cells in the tumor and local lymph nodes. This mechanism supports the idea of tumor cells generating a lymphoid-like immuno-tolerogenic TME, coined lymph node mimicry where we provide evidence of an important role of TNC as physical and signaling orchestrator (Shields et al., 2010).

Tenascin-C promotes tumorigenesis in oral squamous cell carcinoma

Caroline Spenlé[1]*, Thomas Loustau [1]*, **Devadarssen Murdamoothoo**[1], Pierre Bourdely[2], William Erne[1], Hélène Burckel[5], Alexandre Mariotte[1], Gérard Cremel[1], Stephanie Beghelli-de la Forest Divonne[3,4], Anne Sudaka[3,4], Nouhen K[3,4], Sebastian Schaub[3,4], Rekima S[3,4], Annick Klein[1], Christiane Arnold[1], Philippe Georgel[1], Michael van der Heyden[1], Georges Noel[5], Fabienne Anjuère[2]+, Ellen Van Obberghen-Schilling[3,4] + and Gertraud Orend G+

* equal contribution

+ equal corresponding authors

Address correspondence to Gertraud Orend, INSERM U1109, ImmunoRhumatologie Moléculaire (IRM), HOPITAL CIVIL, Institut d'Hématologie et d'Immunologie, 1, Place de l'Hôpital, 67091 Strasbourg, France, phone (direct): 0033 (0) 3 68 85 39 96, gertraud.orend@inserm.fr, https://u1109.wordpress.com/tumor-micro-environment/

[1] Université Strasbourg, INSERM U1109- MN3T, The Microenvironmental Niche in Tumorigenesis and Targeted Therapy, and The Tumor Microenvironment laboratory, Hopital Civil, Institut d'Hématologie et d'Immunologie, Fédération de Médecine Translationnelle de Strasbourg (FMTS), Strasbourg, France

[2] Université Côte d'Azur, CNRS, IPMC, Valbonne-Sophia Antipolis, France

[3] Université Côte d'Azur, CNRS, INSERM, iBV, France

[4] Centre Antoine Lacassagne, Nice 06189, France

[5] Centre Paul Strauss, Strasbourg, France

Abstract (250 words)

In the tumor microenvironment (TME) of head and neck tumors (HNSCC) the tumor promoting extracellular matrix (ECM) molecule tenascin-C (TNC) is highly expressed. Yet, how TNC impacts HNSCC is largely unknown. Therefore, we employed a carcinogen (4NQO)-induced murine tongue tumor model (OSCC) with abundant and no TNC and observed that TNC increases OSCC number, size and invasiveness and, impacts the immune cell infiltrate. Whereas TNC reduced total leukocyte numbers, Tregs were more abundant, suggesting a switch towards an immuno-tolerogenic TME. This correlates with poor dendritic cell (DC) infiltration of local lymph nodes. We demonstrate organization of TNC into tumor matrix tracks inside the stroma and describe their lymphoid-like properties. Whereas in WT tumors, DC poorly entered the tumor cell nests and mostly remained inside the matrix, they significantly invaded the tumor cell nests in the absence of TNC. Induction of CCL21 and, CCL21 binding to TNC could explain the observed attraction and adhesion of DC to TNC *in vitro* and *in vivo.* As tumor relapse represents a major problem upon radiotherapy we investigated OSCC upon irradiation and observed tumor regression accompanied by induction of TNC and, enforcement of the described lymphoid-like TME in the remaining tumor tissue. Relevance for the human disease is presented as leukocytes preferentially localize in TNC-rich stromal areas of HNSCC. Also, high TNC correlates with earlier tumor relapse upon radiotherapy. Altogether, TNC may be a driver of an immuno-tolerogenic lymphoid-like TME with a potential implication in rebound effects upon radiotherapy where CCL21 could be a target.

Introduction

Head and neck squamous cell carcinomas (HNSCC) are heterogeneous malignancies that arise in mucosal epithelia of the upper aero-digestive tract. Survival rates in Europe for patients with HNSCC are only 42% at 5 years (Grégoire et al., 2010). At least two genetic subclasses of HNSCCs can be distinguished, HPV-negative carcinomas and HPV-positive (mainly oropharyngeal) carcinomas which display improved clinical outcomes. For these tumors to develop and expand, malignant cells must overcome growth inhibitory signals from the surrounding tissue and escape immune surveillance mechanisms that repress cancer progression. This is achieved by promoting the conversion of the physiological microenvironment to a pro-tumoral state. Pro-tumoral conversion of the microenvironment is accompanied by major changes in the extracellular matrix (ECM), including the upregulation of certain ECM components that regulate cell adhesion/migration, distribution, activation and bioavailability of growth, angiogenic and immunomodulatory factors. Tenascin-C (TNC) is one such molecule that has been found to impact the progression of several tumor types through regulation of multiple cancer hallmarks including survival, proliferation, invasion, metastasis, angiogenesis and chronic inflammation (Chiquet-Ehrismann et al., 2014; Midwood et al., 2011, 2016). We have recently identified TNC as one of the major matrix proteins upregulated in the ECM of HNSCC-associated fibroblasts (Gopal et al., 2017), yet the precise roles of TNC in this disease have not yet been investigated.

In non-tumoral contexts TNC can activate an immune response by serving as a danger associated molecular pattern (DAMP) molecule, as recently described in rheumatoid arthritis where TNC binding to integrin $\alpha9\beta1$ and TLR4 triggers expression of pro-inflammatory cytokines and more severe inflammation (Midwood et al., 2009). Although TNC is mostly absent in normal tissues, it has been identified in reticular fibers of lymphoid tissues such as the thymus where it was proposed to regulate leukocyte maturation (Drumea-Mirancea et al., 2006). In cancer tissue, including insulinoma, colorectal carcinoma, glioma and breast cancer

(Rupp et al., 2016; Spenlé et al., 2015; Sun et al., submitted), we have observed TNC in matrix tracks that share certain features with reticular fibers and may play a role in targeting immune cell functions in cancer tissue (Midwood et al., 2011, 2016; Orend et al., 2014).

HNSCC is an immunosuppressive disease (Ferris, 2015). Hence, immunomodulatory therapies that overcome immune suppressive signals in patients with HNSCC have therapeutic promise. Indeed, several strategies that aim to restore antitumor immunity are currently under investigation in HNSCC. Among these, targeting the immune-checkpoint receptors or their ligands has shown clinical efficacy with durable long-lasting effects (Ferris, 2015; Sharma and Allison, 2015). However, only a fraction of patients (roughly 20%) respond. Hence, much progress is needed to improve our understanding of interactions between tumor cells and their host immune system, and in particular how immune cells interact physically and functionally with the neoplastic stroma in HNSCC, in order to predict treatment response and to provide a rational design for development of effective treatment combinations.

In the present study we used a carcinogen driven murine model with abundant or absent TNC to address the roles of TNC in squamous cell carcinomas of the oral cavity (OSCC). This is an interesting in vivo immunocompetent model for analyzing the mechanisms underlying carcinogen-induced reprogramming of the stromal environment and its consequence in head and neck cancer. It recapitulates the human disease with respect to histological features that characterize early steps of tumor progression in the tongue including dysplasia, in situ carcinomas and invasive carcinomas. Moreover, it displays genetic alterations similar to those observed with smoking exposure in HNSCC (Chung et al., 2004) and sequential changes in gene expression with relevance for human OSCC (Foy et al., 2016). Yet, this model has not been used so far to investigate the impact of the TME in OSCC. Here, we identified TNC as an important molecule of the TME of OSCC. Comparison of tumors in wildtype (WT) and TNC knockout (TNCKO) mice allowed us to demonstrate a

role for TNC in OSCC progression and suggest a mechanism by which the TNC-rich tumor matrix generates a lymphoid like tumor microenvironment (TME) with immuno-tolerogenic characteristics. We show that TNC in the tumor matrix tracks regulates the crosstalk with CCL21 and, positioning of infiltrating tumor-associated leukocytes thereby facilitating escape from immunosurveillance. This mechanism may provide targeting opportunities and, in addition is relevant in human HNSCC where a high TNC expression correlates with earlier tumor relapse upon radiotherapy.

Results

Human and mouse 4NQO-induced OSCC are associated with TNC upregulation

In non-tumoral human tongue tissue, TNC was barely expressed with a weak staining limited to the basement membrane and lamina propria (**Fig. 1A**). In all human OSCC examined, TNC expression was strongly upregulated in the tumor stroma region delaminated by the lamina propria and basement membrane and, intimately close to the cancer cells. TNC staining was often intense in the stroma between tumor epithelial islets (or nests) and showing specific organization with dense aligned tracks of ECM encapsulating areas of cohesive tumor epithelial cells. TNC was only rarely expressed in tumor epithelial cells (**Fig. 1A**).

To mimic the human OSCC pathological state in an immune-competent murine model we employed 4-Nitroquinoline 1-oxide (4NQO) to induce squamous cell carcinomas in the mucosal epithelial lining of the oral cavity of C57Bl6 mice. 4NQO is the most frequently used carcinogen for induction of OSCC and causes DNA adduct formation thus mimicking the effect of tobacco carcinogens (Kanojia and Vaidya, 2006). 4NQO induces premalignant and malignant lesions mainly in the tongue and esophagus when applied at low concentration through drinking water **(Fig. S1A, B)**. This model recapitulates the human disease with respect to histological features of each tumor progression step in the tongue, including intraepithelial dysplasia, in situ carcinomas and invasive tumors **(Fig. S1C)**. While its expression was very low or absent in tongue epithelium of non-treated mice, TNC expression became upregulated in the stroma area of 4NQO-induced OSCC **(Fig. 1B)**.

Tenascin-C is organized in tumor matrix tracks and enhances OSCC onset and progression

As TNC was expressed in the 4NQO-induced tumors we asked whether TNC had an impact on tumorigenesis in this model by comparing tumor formation in WT mice with that in TNC knockout (KO) mice. Whereas both genotypes developed tongue tumors (100% penetrance)

after exposure to 4NQO, TNCKO mice presented a reduced number of tumors with on average of one tumor per mouse in comparison to two tumors in WT mice **(Fig. 1C)**. In the absence of TNC, tongue tumors were significantly smaller than in WT mice **(Fig. 1D, E)**. Moreover, TNCKO mice did not develop invasive carcinomas, whereas a fraction of tumors in WT mice (18%) were invasive **(Fig. 1F)**.

By immunofluorescence staining (IF) we characterized the carcinogen-induced tumors and their stroma **(Fig. 1G and S1D)**. We found TNC to be organized in tumor matrix tracks together with other ECM molecules as laminin (LM), coll IV and fibronectin (FN) (**Fig. 1C**). These matrix niches, also rich in FSP1+ and αSMA+ cells, are separating areas of p63 positive tumor epithelial cells. Tumors were mostly differentiated adenocarcinomas as they expressed E-cadherin and no vimentin. They were highly vascularized as seen by CD31 staining. No difference in cell survival was apparent between genotypes after staining for cleaved-caspase 3 (**Fig. S1D**).

TNC regulates loco-spatial distribution of leukocytes and dendritic cells

Given that TNC plays a role in inflammation and that HNSCC are inflammatory cancers, we determined a potential impact of TNC on immune cell infiltration of the 4NQO-induced tumors by FACS. We observed significantly less leukocytes in tumors of TNC-expressing mice **(Fig. 2A)**. WT tumors contained in particular less cells positive for MHC class II and CD8. The abundance of other immune cell types was not statistically significantly affected by TNC (**Fig. 2A, S2A**). As lymph nodes play an important role in staging an immune response, by FACS we determined the immune cell infiltrate of local lymph nodes from 4NQO-induced tumor bearing mice. We observed an impact of TNC on CD11c+ DC and CD8+ T cells that were less abundant in lymph nodes from WT in comparison to TNCKO mice **(Fig. 2B, S2B)**. We confirmed this observation by IF staining showing less CD45+ and CD11c+ cells in the lymph nodes of the WT mice **(Fig. 2C, S2C).** This result suggests that TNC may be involved in impairing priming of DC and, potentially inactivating CD8+ T cell expansion. In contrast to the

local lymph nodes we did not see any difference in immune cell abundance in the spleens from tumor bearing mice of both genotypes **(Fig. S2D-G).**

To address how TNC may impact leukocytes, we investigated the loco-spatial distribution of CD45+ and CD11c+ cells in non-invasive tumors of both genotypes by IF. This experiment indeed revealed that TNC impacted CD45+ leukocyte infiltration, as CD45+ cells were preferentially present within the TNC-rich stromal areas in comparison to the tumor nests that were largely devoid of CD45+ cells. In the absence of TNC, more CD45+ leukocytes infiltrated the transformed epithelium of the tumors **(Fig. 3A, B)**. Similarly, we found CD11c+ cells highly enriched in the TNC-rich stromal areas of WT tumors with only few cells inside the tumor cell nests. This was particularly prominent in an invasive WT tumor, where we observed that CD11c+ cells were exclusively located in the TNC matrix **(Fig. S3A)**. Yet, in TNCKO tumors significantly more CD11c+ cells infiltrated the tumor cell nests **(Fig. 3C, D)**. Altogether, these observations suggest that TNC may attract and potentially sequester leukocytes, and in particular CD11c+ DC in the stroma, thereby blocking their entry into the tumorigenic epithelium and also their egress into the local lymph nodes.

In human tongue tumors CD45+ leukocytes are also preferentially localized in TNC-rich stroma

We next sought to examine the loco-spatial organization of infiltrating immune cells in human tumors. To do so, CD45 staining was performed on a set of 10 primary tongue tumors **(Table S1)**. Well differentiated, p16 negative, fibrotic and inflammatory tumors of the tongue were selected to most closely resemble those observed in the mouse OSCC model. We chose to carry out staining on large tumor sections encompassing both the tumor and peritumoral regions **(Fig. S3B, C)**, rather than on small tissue cores of carcinoma lobules in order to include staining of the fibrotic and inflammatory stromal compartment. Moreover, large sections allowed for a more complete examination of morphological features and to include heterogeneity of the tumors. For quantitative analysis, regions designated as tumor or stroma (based on histological criteria) were traced by a pathologist on 3 representative fields from

each tumor section. A typical example is displayed **(Fig. S3B, C)**. Across this set of tumors, tumor and stromal regions corresponded to 43% and 57% respectively of the total surface. CD45 staining in tumor and stromal regions was quantified, as detailed in the experimental procedures. CD45-staining covered 25% of the stromal regions whereas only 4% of the surface was stained in the tumor nest regions (**Fig. 3E, F, S3D**). TNC staining was performed on adjacent tumor sections to visualize expression levels, organization and spatial distribution of matrix proteins with respect to the infiltrating CD45+ cells. All tumors displayed high levels of TNC in the stroma **(Fig. 3E, S3C)**. As previously reported (Spenlé et al., 2015a), TNC was commonly organized in fibrillar tracks and, CD45+ cells appeared to be captured in these TNC matrix tracks **(Fig. 3E, S3C)**. We conclude from the analysis of human OSCC that tumor-infiltrating leukocytes are preferentially located in TNC-enriched stromal zones, similar to what we had seen in the carcinogen-induced tumors of the mouse.

Through induction of CCL21 and CCR7, TNC impacts adhesion of dendritic cells

As the chemokine CCL21 and its receptor CCR7 play a role in immune tolerance of the lymph node (ref) and have been implied in cancer (Shields, 2010, other paper Swartz lab) we investigated the expression of CCL21 and CCR7 by qRTPCR in the 4NQO-induced OSCC. We observed that both molecules are more expressed at mRNA level in WT than in TNCKO tumors **(Fig. S4A)**. This result was confirmed at protein level by tissue staining, where we found CCL21 and CCR7 predominantly expressed in the TNC matrix tracks of the WT tumors. In contrast, CCL21 and CCR7 were barely detectable in TNCKO tumors **(Fig. 4A-D)**. We investigated whether tumor cells may be a source of CCL21 as previously shown in another study (Shields 2010). Therefore, we used our newly established tumorigenic epithelial OSCC cell line from an invasive 4NQO-induced tumor (Spenlé et al., in preparation). Upon treatment with TNC we investigated CCL21 and CCR7 expression by qRTPCR and observed that OSCC cells do not express CCL21 (data not shown). In contrast, they express CCR7 and, TNC increased CCR7 levels in these cells (**Fig. 4E**). In search of the cellular source, we did co-staining of CCL21 with markers for fibroblasts (ERTR7, FSP1,

αSMA) or lymphatic endothelial cells (LEC) and, observed a complete signal overlap in LEC but not with other cells (**Fig. 4F,** data not shown**)**. Moreover, in TNCKO tumors LEC only poorly expressed CCL21 (**Fig. 4F**). To confirm that TNC induces CCL21 in LEC, we incubated hLEC with purified TNC and determined CCL21 expression by qRTPCR. This experiment confirmed that TNC can induce CCL21 mRNA levels in LEC (**Fig. 4G**). As TNC was shown to bind soluble molecules (De Laporte et al., 2013; Martino et al., 2014) we determined a potential interaction by surface plasmon resonance spectroscopy and, discovered that CCL21 binds TNC with a Kd of 5.8 x 10^{-8} M that is lower than CCL21 binding to CCR7 (**Fig. 4H)** (Lanati et al., 2010). Next, in a Boyden chamber migration assay we compared attraction of bone marrow derived DC (BMDC) towards FN, TNC or a combination of both substrata. We found that in combination with FN, TNC attracted BMDC (**Fig. 4I**). Altogether these results suggest that TNC attracts DC where CCL21 and in particular its binding to TNC may be relevant.

TNC impacts the generation of a lymphoid-like stroma with immuno-tolerogenic properties

So far we have shown that TNC attracts DC into the ECM-rich stromal area of the tumor, where LEC express CCL21. CCL21 may be involved in attracting DC *in vivo* into the stromal areas as we have seen attraction of DC by TNC *in vitro*. Now, we decided to explore in more detail the composition of the TNC-rich TME of the 4NQO-induced tumors. We investigated the abundance of fibroblast reticular cells (FRC), usually present in secondary lymphoid organs such as lymph nodes (Katakai et al., 2004) by staining for ERTR7 and, observed a selective and high abundance of these cells inside the TNC matrix (**Fig. 5A, B**). We also stained for gp38/podoplanin, a marker of lymphatic endothelial cells (LEC) and FRC, and observed expression in the TNC-rich stroma (**Fig. 5C,D**). In TNCKO tumors, these cells were also present in the stromal areas but the signal intensity was reduced. Upon quantification we confirmed less abundant ERTR7+ and gp38+ cells in the TNCKO tumors (**Fig. 5B, D**). Next, we measured the expression of immune cell markers and cytokines on extracted

OSCC tumors by qRTPCR. In presence of TNC, we found a significant increase in mRNA levels Foxp3 that can be expressed by Treg, as well as of TGFβ and IL-10, which are anti-inflammatory cytokines that again can be produced by Treg (ref). In contrast, the mRNA levels of pro-inflammatory cytokines produced by mature T cells such as IL-12 and IL-4, were reduced in tumors from WT mice in comparison to TNCKO mice (**Fig. 5E**). We also found a combined linear positive correlation of expression of CCL21 with TGFβ, and IL10, and a linear negative correlation of CCL21 with IL12 which suggests a potential interdependence and link to TNC (**Fig. 5F-H, S5**). Altogether, we have shown that the stromal areas in OSCC are characterized by the lymph node markers CCL21, CCR7, gp38 and ERTR7 and, that they express LMγ2, FN, Coll IV and TNC. These ECM molecules were previously described as constituents of reticular fibers in the thymus suggesting that the TNC-rich stroma in tumors may have similar properties as e.g. impacting immune cell education in an immuno-tolerogenic microenvironment (Drumea-Mirancea et al., 2006). This possibility is now supported by our results that showed that TNC affected positioning of DC away from the tumor cells inside the TNC rich stroma and upregulated immunosuppressive soluble factors.

Impact of radiotherapy

Radiotherapy is regularly used to treat OSCC tongue tumors that are inherently difficult to completely resect by surgery. Irradiation induces a proinflammatory tissue response and may trigger rebound effects (Spenlé et al., 2015b). But since only few tumor models exist to investigate the impact of irradiation on the TME, here we established a radiotherapy protocol for the carcinogen-induced tumor mice. We locally irradiated the lower part of the heads of the mice at 16 weeks after exposure to 4NQO, where we already observed lesions in some of the tongues, with one shot of 2Gy, sacrificed the mice at the end of the protocol and investigated the remaining tumor tissue. We observed that WT mice had on average only one tumor left after irradiation. Also the size of the remaining tumors was reduced, altogether suggesting that this treatment had caused tumor regression (**Fig. 6A, B**). That the applied dose of 2Gy irradiation was efficient, was also indicated by reduced proliferation in the

irradiated tumors (**Fig. 6D**). By staining for TNC, we noticed that its expression was higher in the irradiated tumors **(Fig. 6D)**. As TNC impacted the abundance of ERTR7+ FRC, we examined the remaining tumor tissue by IF. Indeed expression of ERTR7 also appeared to be enhanced **(Fig. 6E)**. We observed also an accumulation of CD45+ and CD11c+ cells in the stroma of WT tumors with a similar pronounced stroma-to-tumor-nest ratio as in the non-irradiated tumors suggesting that the properties of the tumor stroma is preserved upon irradiation **(Fig. S6A, B)**. Finally we noticed that upon irradiation the fraction of invasive tumors was increased, indicating that those tumors that were not destroyed now may progress faster **(Fig. S6C)**. These results suggest that this model can be used to address the impact of gamma irradiation on tumor destruction and its impact on the TME. Our results suggest that the lymphoid-like TME is not destroyed but rather enhanced upon radiotherapy which could explain the more invasive phenotype of the remaining tumors.

Surprisingly, in TNCKO mice no effect on tumor numbers nor size was seen which correlated with similar Ki67 staining intensities with and without irradiation **(Fig. 6B,C, Fig. S6D)**. Moreover, we did not see any obvious difference in ERTR7 staining between irradiated and non-irradiated TNCKO tumors (**Fig. S6E**) nor a change in the higher abundance of CD45+ and CD11c+ cells in the stroma in comparison to the WT tumors **(Fig. S6A, B)**. Finally, we noticed more non-differentiated tumors upon irradiation suggesting that irradiation may have had some effect on these tumors.

Finally, we asked whether our observations in murine OSCC have relevance for human HNSCC. Therefore, we investigated TNC expression in a cohort of HNSCC patients that had received radiotherapy where gene expression results are available from the relapsed tumors. We observed that TNC levels above the median correlate with earlier tumor relapse (**Fig. 6F**). Thus our results derived from the OSCC model may have relevance for HNSCC.

Discussion

The TME largely impacts tumor malignancy and potentially therapy outcome in HNSCC, yet we lack the molecular and mechanistic insight to better understand the roles of the TME in

this disease. Such information could be important to improve HNSCC therapy and patient survival. The lack of good *in vivo* models that allow recapitulating the impact of the TME in the human disease is also contributing to our poor knowledge. Here, we applied a well-established carcinogen-induced tongue tumor model and analyzed the cellular and matrix content of the TME and compared the results to human HNSCC. We confirmed published results that whereas most of the murine carcinogen-induced adenocarcinomas are not invasive, a few had invasive properties as seen in human HNSCC. The murine tumors were also highly infiltrated by immune cells resembling human HNSCC. In addition, the general organization of HNSCC into stromal areas surrounding tumor epithelial cell nests, as well as high proliferation and vascularization was also recapitulated in the murine tumors. The stromal areas were characterized by numerous fibroblasts expressing FSP1 or αSMA, again mimicking high abundance of fibroblasts in the stroma of the human tumors. We also found that TNC is highly expressed in the stromal areas of the carcinogen-induced tumors which again mimics HNSCC (Brüsehafer et al., 2016) and in particular human OSCC as we had shown here. Altogether, these observations suggest that the carcinogen-induced model recapitulates important features of HNSCC, including expression of FN (Gopal et al., 2017) and TNC. As TNC is a known promoter of tumor malignancy and is highly expressed in HNSCC, TNC may play an important role in this malignancy as key determinant of the TME (Midwood et al., 2016). To address this possibility we decided to use immune competent mice expressing or lacking TNC to induce OSCC by 4NQO and investigate the roles of TNC in tumorigenesis in detail. We observed that less and smaller tongue tumors occurred in the absence of TNC which were not invasive, suggesting that TNC promotes tumorigenesis also in this tumor model as was previously seen in other murine tumor models and in human cancers (Midwood et al., 2016; Saupe et al., 2013; Sun et al., submitted)).

Previously we observed that in several analyzed tumors, TNC is expressed in fibrillar ECM-rich stromal networks. In these networks, defined ECM molecules are expressed in parallel aligned fibrillar arrays providing niches for tumor cells, fibroblasts and leukocytes (Spenlé et al., 2015a). As the ECM molecules formed long contiguous fibrils, sometimes contacting

blood vessels with a connection to the blood circulation, we previously have hypothesized that they may act as transportation routes or tracks, hence the name "tumor matrix tracks" TMT (Spenlé et al., 2015a). We previously noted similarities of the tumor matrix tracks to reticular fibers in the thymus (Drumea-Mirancea et al., 2006; Spenlé et al., 2015b). In the tongue tumors now we also found that FN, Coll IV and LMγ2 are expressed together with TNC in fibrillar arrays reminiscent of what we had seen as matrix tracks in other tumors (Spenlé et al., 2015b). In the carcinogen-induced OSCC all stromal areas expressed TNC which is different to human HNSCC where all stroma is enriched in FN but not always in TNC (Gopal et al., 2017). This discrepancy may be linked to the heterogeneous causes of human OSCC and frequent high bacterial infiltration that is not mimicked in the murine model. Here, we provide novel information about the cellular content of these stromal niches. We found that cells expressing the reticular fiber markers CCR7, CCL21, ERTR7 and gp38, exclusively resided in the TNC rich stroma, supporting the observation that the tumor matrix tracks have similarities with reticular fibers. We wanted to know whether the absence of TNC has an impact on the organization of these niches and therefore investigated the TNCKO tumor tissue. We found that ERTR7, gp38, CCR7 and CCL21 were less prominent in the absence of TNC, suggesting that TNC may play a role in the composition and potentially, function of the tumor matrix tracks.

In support of this possibility, we observed an impact of TNC on leukocyte infiltration. The number of infiltrated leukocytes (as determined by FACS) was reduced in WT tumors in comparison to TNCKO tumors. Whereas the large majority of leukocytes was accumulated in the TNC rich stroma, only a few cells entered the tumor cell nests. This was in contrast to tumors not expressing the TNC protein, where leukocytes were less abundant in the stroma, but entered the tumor cell nests more numerously. We also saw less MHC II+ cells in the WT tumors and in particular less CD11c+ cells, suggesting that in a WT tumor, antigen presentation and priming of cytotoxic T cells (CTL) may be reduced. Indeed, we found less CD8+ T cells in the WT tumors. Also in the local lymph nodes of the tumor mice we saw less

CD11c+ and CD8+ T cells compared to the TNCKO conditions. In addition, TNC does not only lower the number of CD11C+ cells but also appears to attract them into the TNC-rich matrix tracks where the majority of DC were found. Only a few DC entered the tumor cell nests. This was again different in TNCKO tumors where less DC were present in the matrix, and more prominent in the tumor cell nests.

Here, we identified a mechanism that can explain how TNC promotes attraction of DC inside the tumor matrix tracks. TNC may regulate the loco-spatial abundance of DC through CCL21. Several evidences support this hypothesis. First, by using in vitro assays we showed that CCL21 attracted DC towards a TNC substratum. Second, we found that CCL21 directly binds to TNC which may increase the local concentration of CCL21 *in vivo*. Third, TNC also directly increases the expression of CCL21 in LEC as seen *in vitro* and *in vivo*. That TNC may impact attraction of DC in OSCC is supported by less CCL21 and fewer DC in the stromal areas of the TNCKO tumors.

Previously, it was published that some tumor cells can generate a lymphoid-like immuno-tolerogenic TME, a phenomenon that was called "lymph node mimicry". The authors linked these features to high expression of CCL21, which facilitated escape from immune surveillance (Shields et al., 2010). The authors further described the lymphoid-like TME to express CCR7, ERTR7 and gp38 and, to have immunosuppressive features. The authors interpreted these observations that tumor cells hide themselves in a lymphoid-like and immunosuppressive TME that they generate around themselves by expressing CCL21. But nothing was known about the ECM in this lymphoid-like TME. Our results shed new light on this concept where we demonstrate that TNC together with other ECM molecules form niches with lymphoid-like properties, the tumor matrix tracks, and that TNC is an essential molecule in defining the immunological properties of these niches by attracting leukocytes and in particular DC inside the tumor matrix tracks. As in Shields et al., (2010) CCL21 and CCR7 could be relevant in the OSCC model, as TNC increased expression of both

molecules. Yet, in the OSCC model LEC are the sole source of CCL21 and not the tumor cells as previously described (Shields 2010). A particular difference to the study by Shields et al., (2010) is the kinetics. In the carcinogen driven OSCC model tumors develop over 20 weeks which is different to the previously used grafting models that allow much less time for tumor development. One could easily imagine that this has an impact on the organization and subsequent function of the TME.

Altogether, our results suggest that TNC is impacting tumor immunity in OSCC at multiple levels. TNC negatively regulates the number of innate (DC) and adaptive (CD8+ T cells) immune cells and presumably reduces priming of effector cells in the lymph nodes. TNC may also enhance the number of immunosuppressive Treg, thereby potentially supporting an immuno-tolerogenic stroma. This has to be investigated in more detail in the future. Moreover, TNC facilitates attraction of DC in the stromal tumor matrix niches thereby physically separating them from the tumor cells. Our results suggest that TNC is an important factor in the described lymph node mimicry likely enhancing escape from immune surveillance **(Fig. 6G)**.

Besides surgical removal radiotherapy represents the major treatment of HNSCC, but often tumor relapse is observed. It is well known that radiotherapy induces an inflamed TME where TNC can be induced (Asparuhova et al., 2015; Spenlé et al., 2015b). We now document elevation of TNC expression in the carcinogen-induced OSCC. Here, we wanted to know whether TNC has an impact on the destruction of the tumor tissue by irradiation. Therefore, we irradiated mice of both genotypes with lesions and, found that the number and size of tumors in a WT mouse significantly reduced after irradiation which was accompanied by reduced proliferation. Surprisingly, in TNCKO mice irradiation did not affect tumor growth nor proliferation. Even if irradiation potentially had been applied before tumors have formed, irradiation may have changed the TME into a pro-tumorigenic one as was previously shown in a 4T1 grafting model (where TNC is one of the induced genes) (Asparuhova et al., 2015),

thereby potentially promoting tumor growth. But this apparently was not the case in the TNCKO condition as the tumors largely appear to be unaffected by irradiation. This raises the question whether TNC is a critical component of the irradiation-induced pro-tumorigenic TME. Future studies have to address this intriguing possibility. In the remaining WT tumors we observed that not only TNC, but also expression of ERTR7 increased upon irradiation. Moreover, the organization of the TME and the particular distribution of leukocytes inside the tumor matrix tracks was not destroyed by gamma irradiation suggesting a potential role of this TME in a rebound effect. Indeed, we saw more invasive tumors after irradiation. Future studies should focus on the description of the irradiation-induced TME as e.g. the ECM composition and tissue stiffening that were shown to be largely altered upon irradiation and promoted tumor progression in the aforementioned 4T1 model (Asparuhova et al., 2015). Altogether, our results suggest that irradiation may enhance the lymphoid-like TME in the remaining tumors and potentially the induction of a pro-tumorigenic TME in tumor free areas, thereby potentially enhancing tumor relapse and progression. This may have clinical relevance as in human HNSCC earlier tumor relapse upon radiotherapy correlates with higher TNC expression levels.

In summary, we have shown that the TME in the 4NQO-induced OSCC model phenocopies important aspects of the TME in the human disease, in particular local distribution of leukocytes in the stroma that is TNC rich. We further have shown that the TNC rich stroma has lymphoid-like properties and impacts attraction of leukocytes and in particular dendritic cells potentially through CCL21. Finally, we showed that the 4NQO-induced OSCC model is suitable to address the impact of radiotherapy on the TME. We conclude that this model is a relevant model to better understand the roles of the TME in HNSCC progression and radiotherapy. Finally, an improved knowledge about the roles of TNC in the TME of OSCC may provide novel angles for therapy.

References

Asparuhova, M.B., Secondini, C., Rüegg, C., and Chiquet-Ehrismann, R. (2015). Mechanism of irradiation-induced mammary cancer metastasis: A role for SAP-dependent Mkl1 signaling. Mol Oncol *9*, 1510–1527.

Brüsehafer, K., Manshian, B.B., Doherty, A.T., Zaïr, Z.M., Johnson, G.E., Doak, S.H., and Jenkins, G.J.S. (2016). The clastogenicity of 4NQO is cell-type dependent and linked to cytotoxicity, length of exposure and p53 proficiency. Mutagenesis *31*, 171–180.

Chiquet-Ehrismann, R., Orend, G., Chiquet, M., Tucker, R.P., and Midwood, K.S. (2014). Tenascins in stem cell niches. Matrix Biology *37*, 112–123.

Chung, C.H., Parker, J.S., Karaca, G., Wu, J., Funkhouser, W.K., Moore, D., Butterfoss, D., Xiang, D., Zanation, A., Yin, X., et al. (2004). Molecular classification of head and neck squamous cell carcinomas using patterns of gene expression. Cancer Cell *5*, 489–500.

De Laporte, L., Rice, J.J., Tortelli, F., and Hubbell, J.A. (2013). Tenascin C Promiscuously Binds Growth Factors via Its Fifth Fibronectin Type III-Like Domain. PLoS ONE *8*, e62076.

Drumea-Mirancea, M., Wessels, J.T., Müller, C.A., Essl, M., Eble, J.A., Tolosa, E., Koch, M., Reinhardt, D.P., Sixt, M., Sorokin, L., et al. (2006). Characterization of a conduit system containing laminin-5 in the human thymus: a potential transport system for small molecules. J Cell Sci *119*, 1396–1405.

Ferris, R.L. (2015). Immunology and Immunotherapy of Head and Neck Cancer. J Clin Oncol *33*, 3293–3304.

Foy, J.-P., Tortereau, A., Caulin, C., Le Texier, V., Lavergne, E., Thomas, E., Chabaud, S., Perol, D., Lachuer, J., Lang, W., et al. (2016). The dynamics of gene expression changes in a mouse model of oral tumorigenesis may help refine prevention and treatment strategies in patients with oral cancer. Oncotarget *7*, 35932–35945.

Gopal, S., Veracini, L., Grall, D., Butori, C., Schaub, S., Audebert, S., Camoin, L., Baudelet, E., Radwanska, A., Beghelli-de la Forest Divonne, S., et al. (2017). Fibronectin-guided migration of carcinoma collectives. Nat Commun *8*, 14105.

Grégoire, V., Lefebvre, J.-L., Licitra, L., Felip, E., and EHNS-ESMO-ESTRO Guidelines Working Group (2010). Squamous cell carcinoma of the head and neck: EHNS-ESMO-ESTRO Clinical Practice Guidelines for diagnosis, treatment and follow-up. Ann. Oncol. *21 Suppl 5*, v184-186.

Kanojia, D., and Vaidya, M.M. (2006). 4-nitroquinoline-1-oxide induced experimental oral carcinogenesis. Oral Oncol. *42*, 655–667.

Katakai, T., Hara, T., Sugai, M., Gonda, H., and Shimizu, A. (2004). Lymph Node Fibroblastic Reticular Cells Construct the Stromal Reticulum via Contact with Lymphocytes. J Exp Med *200*, 783–795.

Lanati, S., Dunn, D.B., Roussigné, M., Emmett, M.S., Carriere, V., Jullien, D., Budge, J., Fryer, J., Erard, M., Cailler, F., et al. (2010). Chemotrap-1: an engineered soluble receptor that blocks chemokine-induced migration of metastatic cancer cells in vivo. Cancer Res *70*, 8138–8148.

Martino, M.M., Briquez, P.S., Güç, E., Tortelli, F., Kilarski, W.W., Metzger, S., Rice, J.J., Kuhn, G.A., Müller, R., Swartz, M.A., et al. (2014). Growth Factors Engineered for Super-Affinity to the Extracellular Matrix Enhance Tissue Healing. Science *343*, 885–888.

Midwood, K., Sacre, S., Piccinini, A.M., Inglis, J., Trebaul, A., Chan, E., Drexler, S., Sofat, N., Kashiwagi, M., Orend, G., et al. (2009). Tenascin-C is an endogenous activator of Toll-like receptor 4 that is essential for maintaining inflammation in arthritic joint disease. Nat. Med. *15*, 774–780.

Midwood, K.S., Hussenet, T., Langlois, B., and Orend, G. (2011). Advances in tenascin-C biology. Cell. Mol. Life Sci. *68*, 3175–3199.

Midwood, K.S., Chiquet, M., Tucker, R.P., and Orend, G. (2016). Tenascin-C at a glance. J Cell Sci *129*, 4321–4327.

Rupp, T., Langlois, B., Koczorowska, M.M., Radwanska, A., Sun, Z., Hussenet, T., Lefebvre, O., Murdamoothoo, D., Arnold, C., Klein, A., et al. (2016). Tenascin-C Orchestrates Glioblastoma Angiogenesis by Modulation of Pro- and Anti-angiogenic Signaling. Cell Reports *17*, 2607–2619.

Saupe, F., Schwenzer, A., Jia, Y., Gasser, I., Spenlé, C., Langlois, B., Kammerer, M., Lefebvre, O., Hlushchuk, R., Rupp, T., et al. (2013). Tenascin-C Downregulates Wnt Inhibitor Dickkopf-1, Promoting Tumorigenesis in a Neuroendocrine Tumor Model. Cell Reports *5*, 482–492.

Sharma, P., and Allison, J.P. (2015). The future of immune checkpoint therapy. Science *348*, 56–61.

Shields, J.D., Kourtis, I.C., Tomei, A.A., Roberts, J.M., and Swartz, M.A. (2010). Induction of lymphoidlike stroma and immune escape by tumors that express the chemokine CCL21. Science *328*, 749–752.

Spenlé, C., Gasser, I., Saupe, F., Janssen, K.-P., Arnold, C., Klein, A., van der Heyden, M., Mutterer, J., Neuville-Méchine, A., Chenard, M.-P., et al. (2015a). Spatial organization of the tenascin-C microenvironment in experimental and human cancer. Cell Adh Migr *9*, 4–13.

Spenlé, C., Saupe, F., Midwood, K., Burckel, H., Noel, G., and Orend, G. (2015b). Tenascin-C: Exploitation and collateral damage in cancer management. Cell Adh Migr *9*, 141–153.

Talts, J.F., Wirl, G., Dictor, M., Muller, W.J., and Fässler, R. (1999). Tenascin-C modulates tumor stroma and monocyte/macrophage recruitment but not tumor growth or metastasis in a mouse strain with spontaneous mammary cancer. J. Cell. Sci. *112 (Pt 12)*, 1855–1864.

Material and methods

Human tumor samples and immunohistochemistry

Surgically removed tongue tumors embedded in paraffin wax blocks were retrieved from the archives of the Pathology Department of the Centre Antoine Lacassagne. Informed consent was obtained for all subjects. Patient characteristics are summarized in **Table S1**. Haematoxylin and eosin staining and immunohistochemical methods were performed on serial 4 µm deparaffinized TMA sections. CD45 staining was performed on a BenchMark Ulter automated slide staining system (Ventana Medical Systems, Inc., Roche Group, Tuscon, AZ) using monoclonal anti-CD45 (LCA) antibody (clone 2B11+PD7/26) according to instructions (UV/CC1M/16min @ 37°C) of the manufacturer (Cell Marque, Rocklin, CA). For TNC staining, intrinsic peroxidase was blocked by incubating sections with 3% hydrogen peroxide for 15 min and antigen retrieval was performed in EDTA buffer pH 9.0, in a de-cloaking chamber (Dako, S2367). Sections were blocked in 4 % goat serum for 1 hour, then incubated for 1 hour with mouse monoclonal anti-TNC antibody (clone BC24, Sigma-Aldrich 1/1000). After rinsing with PBS, sections were incubated with biotinylated secondary antibody (30 min), biotinylated goat anti-mouse IgG (30 min) then avidin-biotin complex (Vector Lab, VECTASTAIN ABC Kit, PK-4000). Staining was revealed with 3,3 '-Diaminobenzidine developing solution (Vector Lab, DAB, SK-4100) then sections were stained with hematoxylin and mounted with aqueous mounting medium.

Quantification of human staining

Stained slides were scanned on the Hamamatsu NanoZoomer 2.0-HT Digital slide scanner (40X mode). Scans were viewed and images acquired using the NDP.view2 software. For quantification, we developed a script (based on ImageJ) optimized to be used with interactive surfaces. Images (5X magnification, 3 per tumor) were projected on an interactive digital whiteboard for selection by pathologist of regions of interest (ROIs) corresponding to carcinoma cells (tumor) or stroma. These ROIs where extracted after color deconvolution and thresholding to quantify CD45 staining and hematoxylin. We then extracted the ratio of

area containing CD45 (holes are removed from hematoxylin image) per image and per ROI type.

4NQO model, irradiation and immunofluorescence

4-NQO (Sigma-Aldrich) was given to 8 week old WT and TNCKO (Talts et al., 1999) mice, that had been bred with C57Bl6 mice for more than 10 generation, in the drinking water at a final concentration of 100 µg/ml during 16 weeks (stock 5 mg/ml in propylene glycol). Mice were sacrificed at week 20 (or week 22 for the irradiation experiments) according to the ethical limit point. After sacrifice, tongue, neck lymph node, spleen and lung were collected and prepared for cryosectioning and IF analysis, mRNA or protein extraction. For irradiation experiment, mice were treated with 4-NQO for 16 weeks, then received one shot of 2Gy irradiation before feeding them with regular water until sacrifice.

For IF staining, unfixed frozen sections of 8 µm were incubated overnight directly with the primary antibodies (**Table S2**). Bound antibodies were visualized with anti-mouse, anti-rabbit or anti-rat secondary antibodies conjugated with Alexa 488 (Molecular Probe) or Cy3 (Jackson ImmunoResearch, UK). DAPI was used to visualize nuclei. After embedding in a glycerol/PBS/phenylenediamine solution, sections were examined using an AxioVision (Zeiss) microscope. Pictures were taken with an AxioCam MRm (Zeiss; Axiovision) camera. Control sections were processed as above with omission of the primary antibodies. For quantification of immune cells, ImageJ software was used. At least 2 sections of 5 different tumors/mice were quantified per condition. Number of immune cells was reported in correlation to the total number of DAPI positive cells.

Surface plasmon resonance spectroscopy

Surface plasmon resonance binding experiments were performed on a Biacore 2000 instrument (Biacore Inc.) at 25°C. TNC (Huang et al., 2001) was immobilized at high surface density (around 7000 resonance units) on an activated CM5 chip (Biacore Inc.) using a standard amine-coupling procedure according to the manufacturer's instruction. Soluble

molecules were added at a concentration of 10 µg/ml in 10 mM sodium acetate, pH 5.0, and at a flow rate of 5 µl/min for 20 min before addition of 1 M ethanolamine. CCL21 (0.5, o.87 and 2µg in 200µl) was added to the chip at pH 6.0 (10 mM MES, pH 6.0, 150 mm sodium chloride, 0.005% (v/v) surfactant P20), or at pH 7.4 (10mM HEPES, 150 mM sodium chloride, 0.005% (v/v) surfactant P20), at a flow rate of 10 µl/min. A blank CM5 chip was used for background correction. 10 mM glycine, pH 2.0, at 100 µl/min for 1 min was used to regenerate the chip surface between two binding experiments. A steady state condition was used to determine the affinity of CCL21 for TNC .The Dissociation constant (Kd) was determined using the 1:1 Langmuir association model as described by the manufacturer.

Flow cytometry/FACS

Tongue tumors, regional lymph nodes and spleens were excised from TNC+/+ and -/- mice. Tissues were inflated with digestion solution containing 1 mg/mL Collagenase D (Roche) and 0.2 mg/mL DNase I (Roche) 2% fetal bovine serum in RPMI, at 37°C for 2 hours. Upon completion of digestion, 92 µL of EDTA 54 mM was added and the samples were vortexed at maximal speed for 30 seconds. The resulting cell suspensions were passaged through a 70 µm and 40 µm cell strainer and treated with FACS buffer (PBS, 2% FBS, 1mM EDTA). After cells were counted and 2×10^6 cells per lymph node/spleen sample (1×10^6 cells for tumor sample) were stained with Aqua Live/Dead viability dye (Life Technologies) according the manufacturer's instructions. Cells were then incubated in blocking solution containing 2% FcBlock (eBiosciences, San Diego, CA) in FACS buffer, for 15 min at 4°C and then stained 30 minutes at 4°C with a standard panel of immunophenotyping antibodies: solution 1 with B220 (clone RA3-6B2, Biolegend), CD11c (clone HL3, BD biosciences), IA/IE (clone M5/114, BD biosciences). Solution 2 with CD8a (clone M1/69, ebioscience), CD45 (clone 30-F11, Biolegend), CD3e (clone 145-2C11, eBiosciences). Solution 3 with Gr1 (clone AL-21, BD Biosciences), CD11b (clone M1/70, BD Bioscience). Data was acquired with BD accuri C6 flow cytometer using BD accuri C6 software. Adjustments were done on the software at the beginning of each experiment.

Cell culture

LEC (ATCC), DC2.4 (Merck) and OSCC (Spenlé et al., in preparation) were cultured in EGCM (Dutscher), RPMI (Dutscher) and DMEM-F12 (Dutscher) respectively with 10% Fetal Bovine Serum (FBS, Sigma-Aldrich), 100 U/ml penicillin, 100 µg/ml streptomycin and 40 U/ml gentamicin at 37°C and 5% CO_2. OSCC cells were supplemented with hydrocortisone (Sigma) 50 µg/ml. Cells were starved with medium containing 1% FBS overnight before treatment with TNC (10 µg/ml) or seeding cells on FN or FN/TNC substrata.

Coating with purified ECM molecules

Purification of FN and TNC and coating of cell culture dishes was done using protocols as previously described (Huang and al., 2001). Briefly, FN and TNC were coated in 0.01% Tween 20-PBS at 1 µg/cm² before saturation with 10 mg/ml heat inactivated BSA in PBS.

RNA extraction and real-time quantitative PCR:

Frozen tongue tumors, hLEC and DC2.4 were disolved in the TRizol reagent for total RNA extraction. cDNAs were synthesized from 1000 µg of total RNA using random primers and Moloney murine leukemia virus reverse transcriptase. The cDNA was used for quantitative real-time PCR in an Mx3005P Real-Time PCR System (Thermo Fisher Scientific). Reactions were carried out in duplicate for all conditions using a Sybr Green Master mix ((Thermo Fisher Scientific) or Fast Taqman mix (Thermo Fisher Scientific) and expression of GAPDH mRNA was used as endogenous control in the comparative cycle threshold method. Primer sequences were used for qPCR determination (**Table S3**).

Statistical analysis

For all data, Gaussian distribution was tested by the d'Agostino-Pearson normality test. When data followed a Gaussian distribution, statistical differences were analyzed by unpaired t-test (with Welch's correction in case of unequal variance) or ANOVA one-way with Tukey post-test. Otherwise, the Mann Whitney test or a non-parametric ANOVA followed by

Dunns post-test were used to verify significance of the observed differences. All statistical analyses were performed using the GraphPad Prism software. Mean ± SEM. p values < 0.05 were considered as statistically significant, *$p < 0.05$; **$p < 0.01$; ***$p < 0.001$; ****$p < 0.0001$.

Figure 1

A. Human OSCC — TNC — Non tumor area / Tumor area

B. 4NQO-induced OSCC — LMγ2 TNC — Non tumor area / Tumor area

C. Tumors per mouse — TNC+/+ / TNC-/- **

D. TNC+/+ / TNC-/-

E. Tumor size (mm²) — TNC +/+ / TNC -/- *

F. TNC+/+ / TNC-/- — differentiated / non-differentiated / invasive

G. TNC / p63 — Laminin — Collagen IV — Fibronectin (FN) — TNC+/+ / TNC-/-
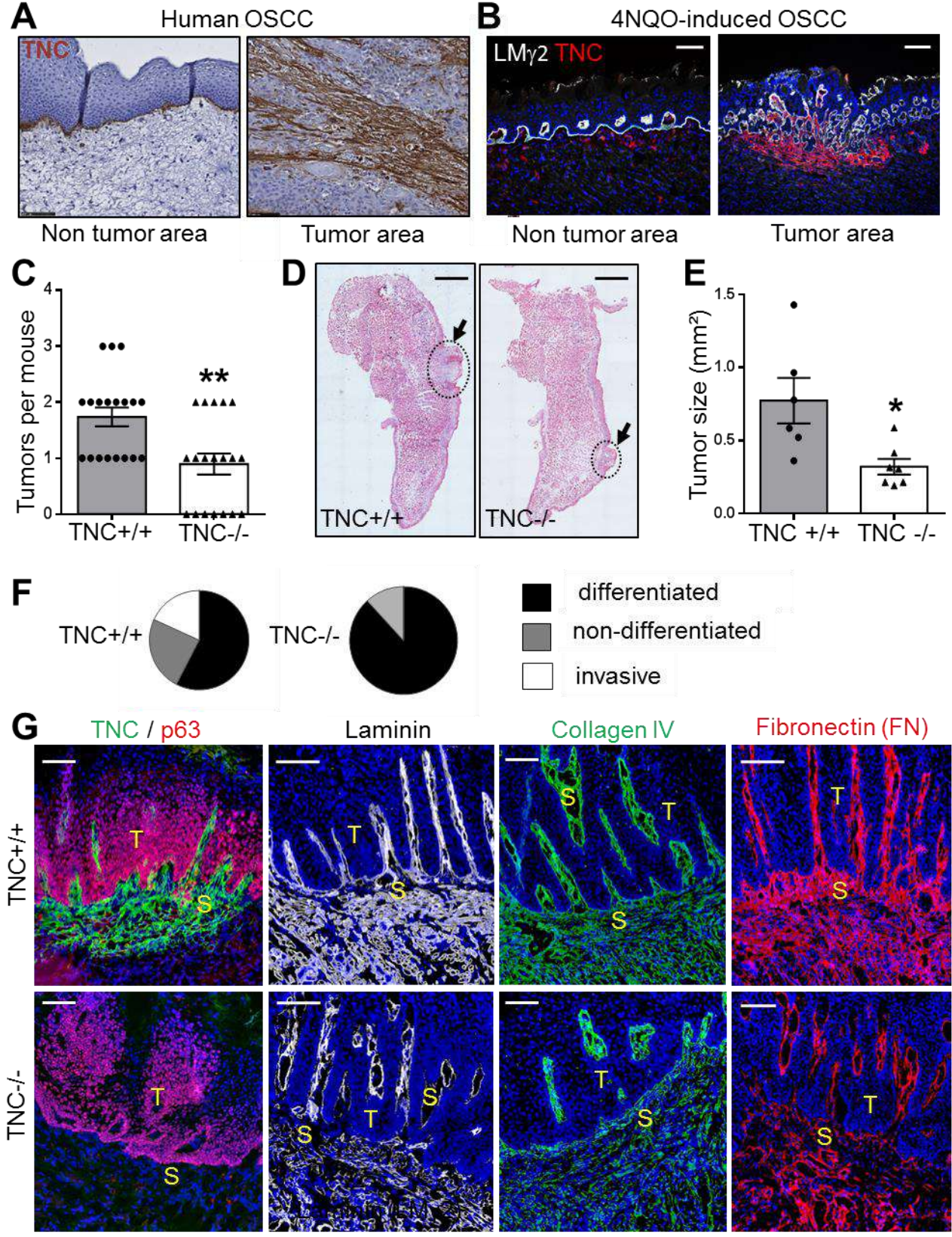
Figure 1 TNC overexpression in human HNSCC and association of TNC, assembled into matrix tracks, with tumor incidence and progression in a murine OSCC model

(A) Representative images of IHC staining for TNC in non tumoral and tumoral areas of a human tongue tumor. Scale bar, 100µm. **(B)** Representative images of IF staining for laminin gamma 2 (LMγ2, white) and TNC (red) in non tumoral and tumoral areas of 4NQO-induced tongue lesions in TNC+/+ mice. Scale bar, 50µm. **(C)** Quantification of tongue tumors in TNC+/+ and TNC-/- mice. Mean ± SEM, N = 19 per group. Mann-Whitney test, ** $p < 0.01$. **(D)** Representative composite images of cross sections from tongues of TNC+/+ and -/- mice after HE staining. The black arrows and circles indicate the tongue tumor. Scale bar, 1000 µm. **(E)** Quantification of tumor size from HE stained images. N = 6 TNC +/+ mice; N = 7 TNC -/- mice. n = 8-10 images per tongue. Mean ± SEM, Mann-Whitney test, * $p < 0.05$. **(F)** Classification of tongue tumors of TNC +/+ and -/- mice. Lesions from WT and TNCKO mice (n = 19 per genotype) were scored according to their histological features as differentiated squamous cell adenocarcinoma (black), non-differentiated in situ carcinoma (grey) or invasive carcinoma (white). **(G)** Representative images of IF staining. Note that TNC is organized in tracks inside the stroma clearly separating p63 positive epithelial tumor cells. TNC, fibronectin (FN), collagen IV and laminin (LMγ2) are juxtaposed inside the stromal matrix tracks. Scale bar, 100 µm. T = Tumor cell nest (p63+); S = Stroma, (p63-).

Figure 2

A — Tumor

Number of viable cells in extracted tumor

☐ TNC +/+
▨ TNC -/-

Gr1-/CD11b+
Gr1+/CD11b+
CD45+/CD3-/CD8+
CD45+/CD3+/CD8+ *
CD45+/CD3+/CD8-
MHC II+/ B220+
MHC II+/CD11c+
MHC II+ **
CD45+ **

0 1000 2000 5000 10000

B — Lymph node

Number of viable cells in lymph node

☐ TNC +/+
▨ TNC -/-

Gr1-/CD11b+
Gr1+/CD11b+
CD45+/CD3-/CD8+
CD45+/CD3+/CD8+ *
CD45+/CD3+/CD8-
MHC II+/ B220+
MHC II+/CD11c+ **
MHC II+
CD45+

0 5000 15000 25000 30000 40000

C

TNC +/+   TNC -/-

Lymph nodes — TNC LM CD11c

Lymph nodes — TNC

Lymph nodes — CD11c

Figure 2 FACS analysis reveals less leukocytes and MHC II+ cells in OSCC tumors expressing TNC

(A) Bar graph representation of the flow cytometry analysis of immune cell populations in the extracted OSCC tumors of TNC +/+ (n = 5) and -/- (n = 6) mice. Leukocyte (CD45+), MHC II+ cells and CD8+ T cells (CD45+/CD3+/CD8+) are more abundant in TNC -/- tongue tumors. Mann-Whitney test, * p < 0.05, ** p < 0.01. **(B)** Bar graph representation of the flow cytometry analysis of immune cell populations in the lymph nodes of TNC +/+ (n = 5) and -/- (n = 6) tumor mice. Note that CD8+ T cells (CD45+/CD3+/CD8+) and dendritic cells (MHC II+/CD11c/B220-) are less abundant in regional lymph nodes of TNC +/+ tumor mice. Mann-Whitney test, * p < 0.05, ** p < 0.01. **(C)** Representative IF images of lymph node tissue for laminin (white), TNC (green) and CD11c (red) in tumor bearing WT and TNCKO mice. Scale bar, 100 µm.
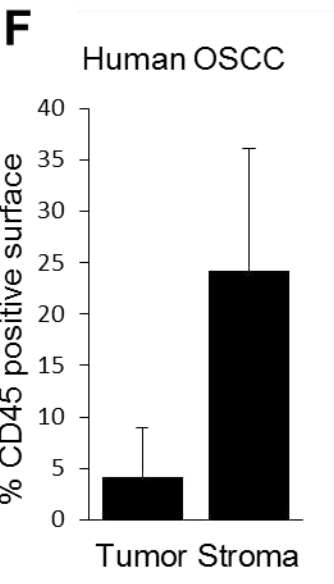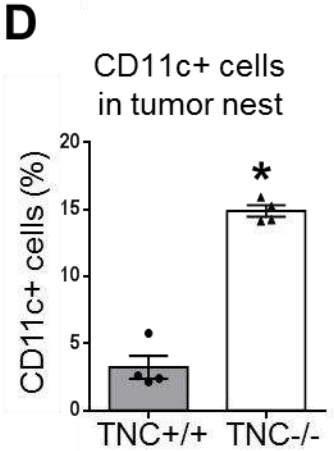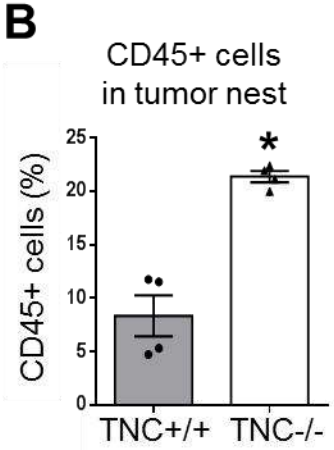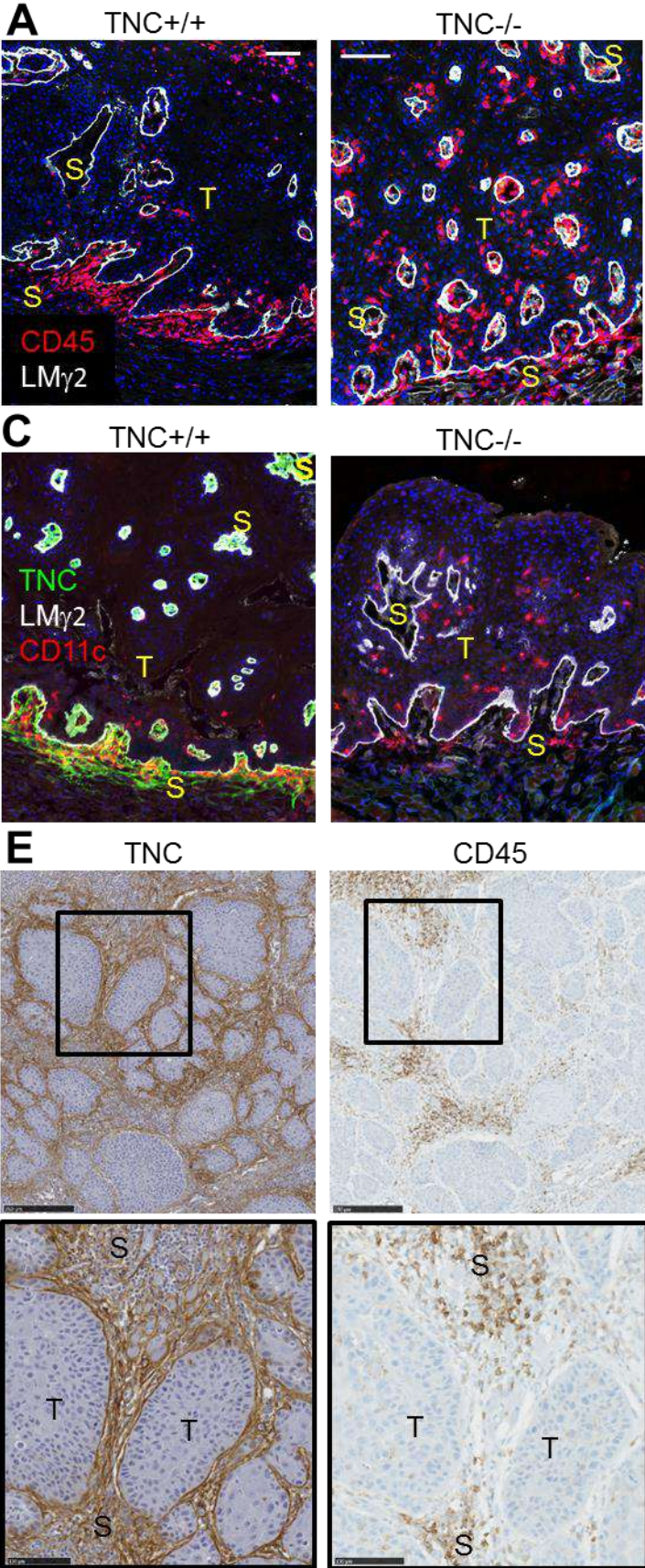
Figure 3

Figure 3 Enrichment of leukocytes and dendritic cells in TNC-rich stromal areas of the carcinogen-induced OSCC

(A) Representative images of CD45 IF staining and **(B)** quantification of CD45+ cells in the tumor nest of TNC +/+ and TNC -/- mice. **(C)** IF staining for CD11c and TNC and **(D)** quantification of CD11c+ cells in the tumor nest of TNC +/+ and TNC -/- mice. Scale bar, 100 µm. T, Tumor; S, Stroma. The histograms corresponds to mean values (± SEM) from 4 mice per genotype and 8-10 images per tumor. Mann-Whitney test, * $p < 0.05$. **(E)** Representative IHC staining of TNC and CD45 in serial whole sections of a human tongue tumor. Scale bar, 200 µm. **(F)** Quantification of CD45+ cells in tumor epithelial nests and stroma (n = 10 tumors, 3 regions per tumor). Mean, +/-Standard Deviation.

Figure 4
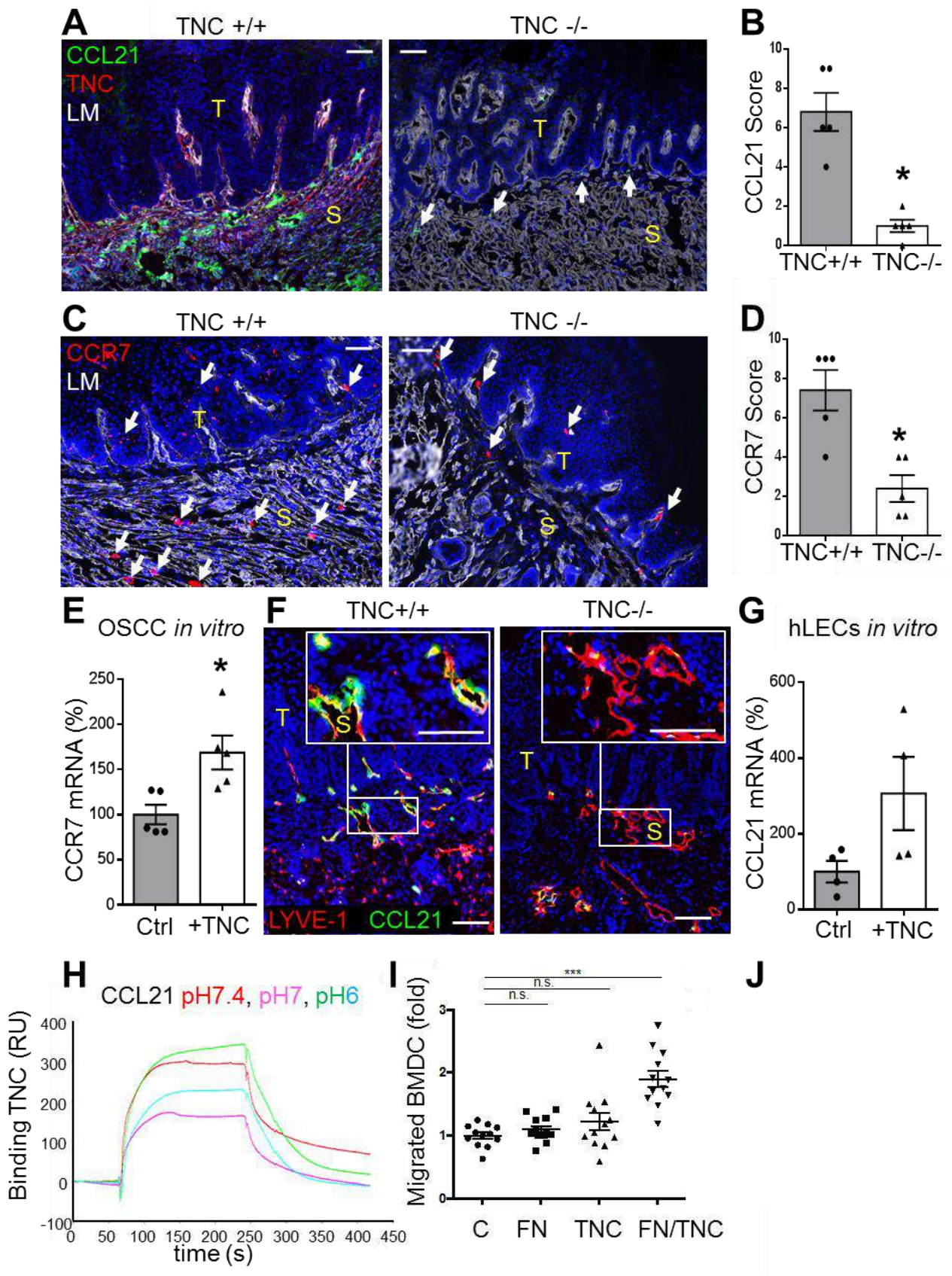
Figure 4 Lymphoid-like properties of TNC-rich stromal areas in the murine OSCC

Representative IF images for CCL21 **(A)** and CCR7 **(C)**. Scale bar, 100 µm; T, Tumor; S, Stroma. Semi-quantitative measurement of CCL21 **(B)** and CCR7 **(D)** in tongue tumors of TNC +/+ and -/- mice. Mean ± SEM from 5 mice per genotype and 8-10 individual images per tumor. Mann-Whitney test; * p < 0.05. **(E)** mRNA levels (qRTPCR) of CCR7 in OSCC cells treated *in vitro* for 24 hours with medium containing TNC (10 µg/mL). (N = 3 independent experiments); Mann-Whitney test, mean ± SEM, * p < 0.05. **(F)** Representative IF images for Lyve-1 (red) and CCL21 (green), showing colocalisation of these molecules. Scale bar, 100 µm; T, Tumor; S, Stroma. **(G)** Stimulation of human lymphatic endothelial cells (hLECs) with soluble TNC (24 hours) induces CCL21 expression (qRTPCR). Means ± SEM. **(H)** Binding of soluble CCL21 to TNC as measured by surface plasmon resonance spectrometry. Kd (1/s)=0.0231; KD(M)=6,78e-08; KA(1/M)=1.47E+07 **(I)** Quantification of migration of Bone Marrow derived dendritic cells (BMDC) towards FN, TNC or both in the presence of CCL21 for 2 hours in comparison to a not coated surface **(C)**. Data derive from 4 independent experiments (n = 9 wells) and are represented as normalized individual values (fold increase of cell number for each condition compared to migration towards medium alone (no coating condition). Mann-Whitney test, ns = not significant, ***p < 0.001.

Figure 5

A TNC +/+   TNC -/-

B

C TNC +/+   TNC -/-

D

E Ratio TNC +/+ to TNC-/-

F

G

H
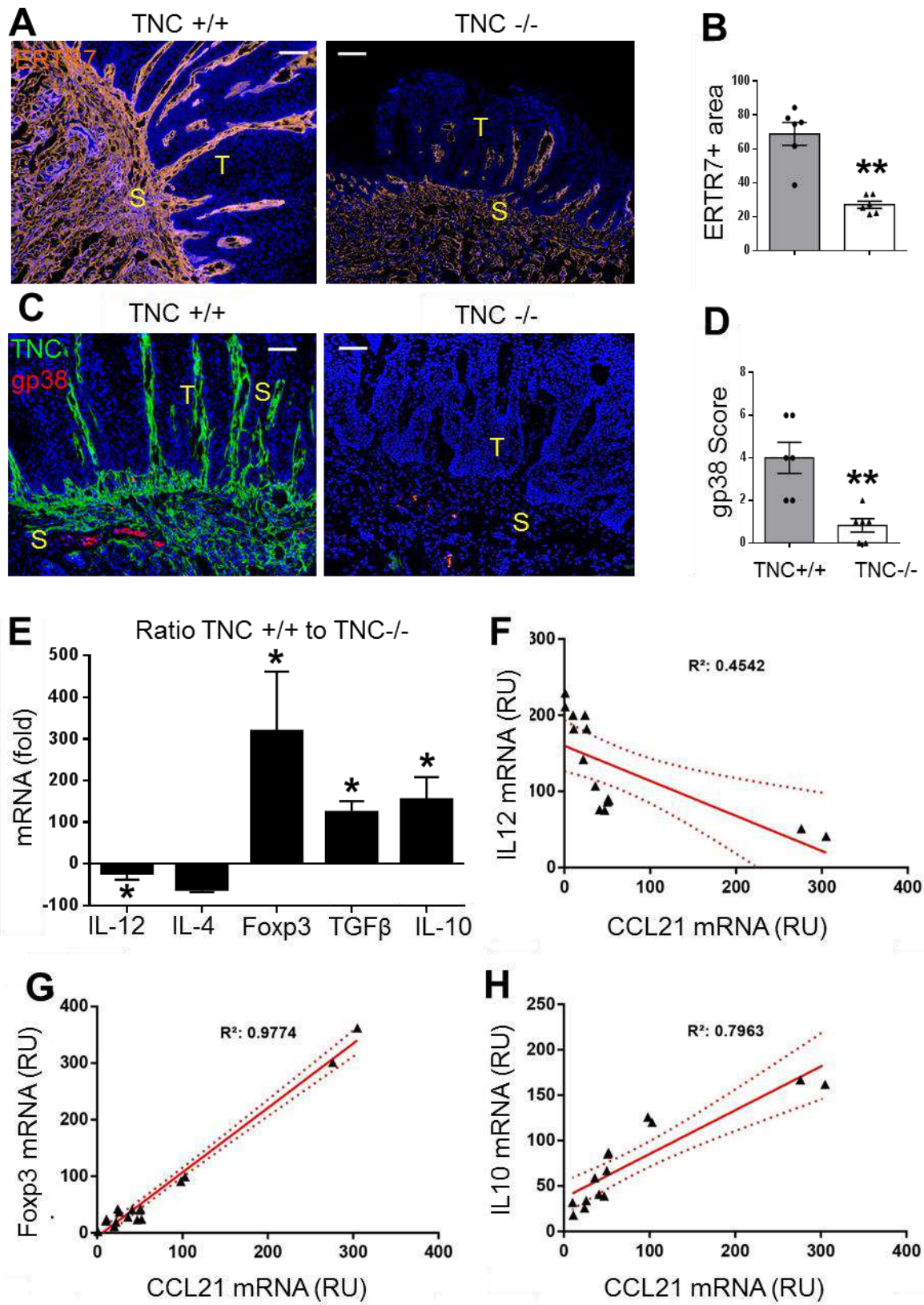
Figure 5 Immuno-tolerogenic like properties of TNC expressing murine OSCC

Representative IF images for ERTR7 **(A)** and gp38 **(C)** in OSCC tumors from both genotypes. Scale bar, 100 μm; T, Tumor; S, Stroma. Semi-quantitative measurement of ERTR7 **(B)** and gp38 **(D)** in tumors of TNC +/+ (n = 5) and -/- (n = 5) mice with 8-10 individual images per tumor. Mean ± SEM, Mann-Whitney test, ** $p < 0.01$. **(E)** The mRNA levels as determined by qRTPCR and expressed as ratio of TNC+/+ versus TNC-/- for the indicated molecules in tumors from both genotypes (n = 5). Mean ± SEM. Mann-Whitney test, * $p < 0.05$. **(F – H)** Linear regression curves indicating expression of CCL21 in correlation to the indicated molecules in tumors from both genotypes, n = 13.

Figure 6

A
TNC +/+   TNC -/-
IR
NIR

B

□ TNC +/+
□ TNC -/-

Tumor number per mouse

NIR   IR   NIR   IR

C

■ TNC +/+
□ TNC -/-

Tumor size (mm²)

*   *   *

NIR   IR   NIR   IR

D

TNC +/+

NIR   IR

TNC
Ki67

E

TNC +/+

NIR   IR

ERTR7   ERTR7

T
S   T

T
S

F

HNSCC with radiotherapy

Relapse free survival

TNC low, n= 54
TNC high, n= 54

HR = 1,5
p = 0,018

3 years   5 years

0   500   1000   1500   2000   2500
days

G

1.   2.   4.
3.

TNC   Tumor cell   LEC   CCL21
FRC   CD11c+   CD8+
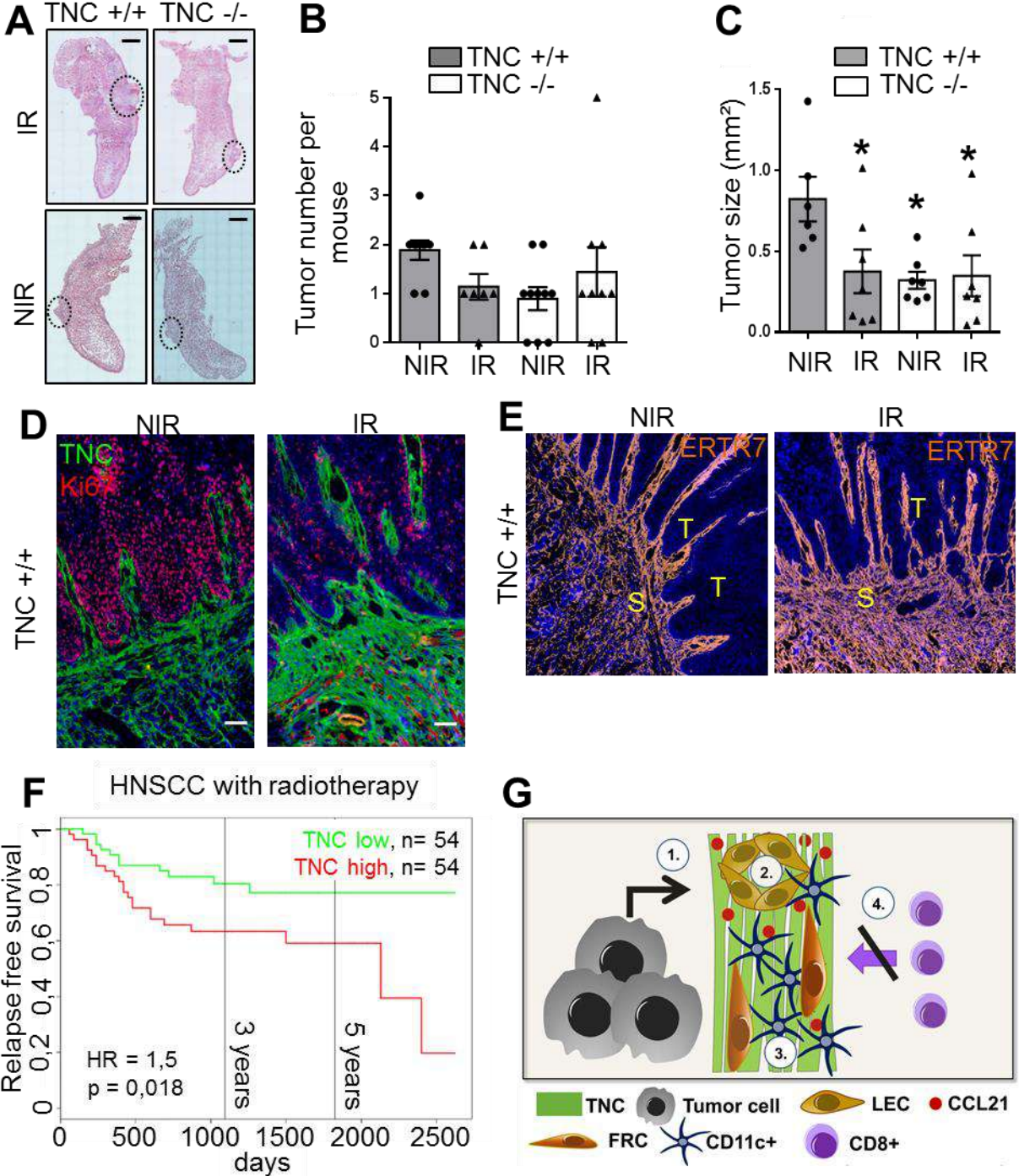
Figure 6 Radiotherapy effects in the murine OSCC model and working hypothesis

(A) Representative HE stained images of cross sections (composite) from tongues of both genotypes with (IR) or without (NIR) 2Gy irradiation. Tumors are encircled. Scale bar, 1000 µm. **(B, C)** Quantification of tumor numbers and size upon radiotherapy. TNC +/+, IR and NIR n = 6; TNC -/-, IR and NIR n = 7 with 8-10 images per tumo. Mean ± SEM. Mann-Whitney test.* p < 0.05. **(D, E)** Representative IF images of WT tumors with and without irradiation for Ki67 and TNC **(D)** and ERTR7 **(E).** Scale bar, 100 µm. T, Tumor; S, Stroma. **(F)** Kaplan Meier analysis of HNSCC patient survival after radiotherapy until tumor relapse and expression of TNC above or below the median. Hazard ratio (HR) = 1,5; p = 0,018; n = 54 per group. **(G)** Summary. In a tumor, TNC is expressed by tumor or other cells where TNC is assembled into fibrillar parallel aligned matrix tracks together with other ECM molecules such as FN, LMγ2 and Coll IV. This stroma (surrounding the epithelial tumor cell nests) is rich in ERTR7+ fibrolastic reticular cells (FRC) and gp38/podoplanin+ cells, resembling the organisation of reticular fibres in the thymus (1.). Also LYVE-1+ lymphatic endothelial cells (LEC) reside in the TNC matrix where TNC induces expression of CCL21 by LEC (2.). CCL21 can bind to TNC and thereby potentially creates a gradient and sticky substratum for CD11c+ DC that enter the matrix tracks where they accumulate (3.). Thus, DC may not be able to leave the tumor and enter the local lymph nodes and may fail to prime CD8+ T cells. In consequence the number of CD8+ T cells is reduced in the lymph nodes as well as in the tumor. The tumor matrix tracks may also represent a physical shield thereby preventing entry of CD8+ T cells inside the tumor nests (4.). This mechanism supports the idea of tumor cells generating a lymphoid-like immuno-tolerogenic TME (Shields et al., 2010). Here we provide evidence that TNC is an important factor of this lymphoid-like TME and document some immuno-tolerogenic properties.

Supplemental figures
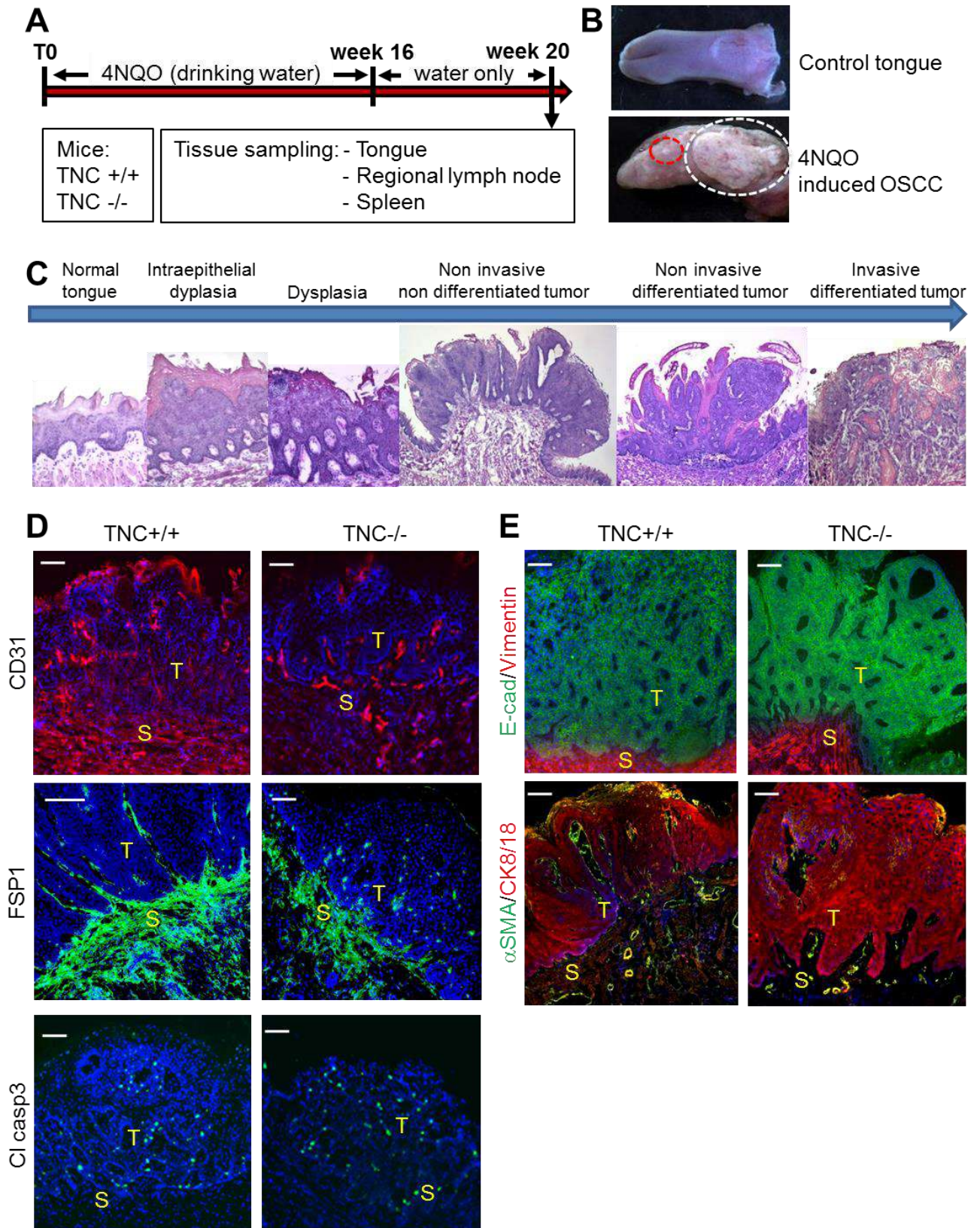
Figure S1

Supplementary Figure 1   4NQO protocol and characterization of early lesions in WT and TNCKO mice

(A) Schematic representation of the experimental carcinogen treatment protocol indicating the kinetics and tissue sampling for analysis. **(B)** Representative image of a control tongue and a tongue with a tumor at the end of the carcinogen treatment protocol. White and red circles represent an invasive and non-invasive tumor, respectively. **(C)** Representative images illustrating the kinetics of the disease in a WT mouse. In our study, only non-invasive tumors were investigated of both genotypes. **(D, E)** Representative IF images for the indicated molecules. Scale bar, 100 µm. T, Tumor; S, Stroma.

Figure S2
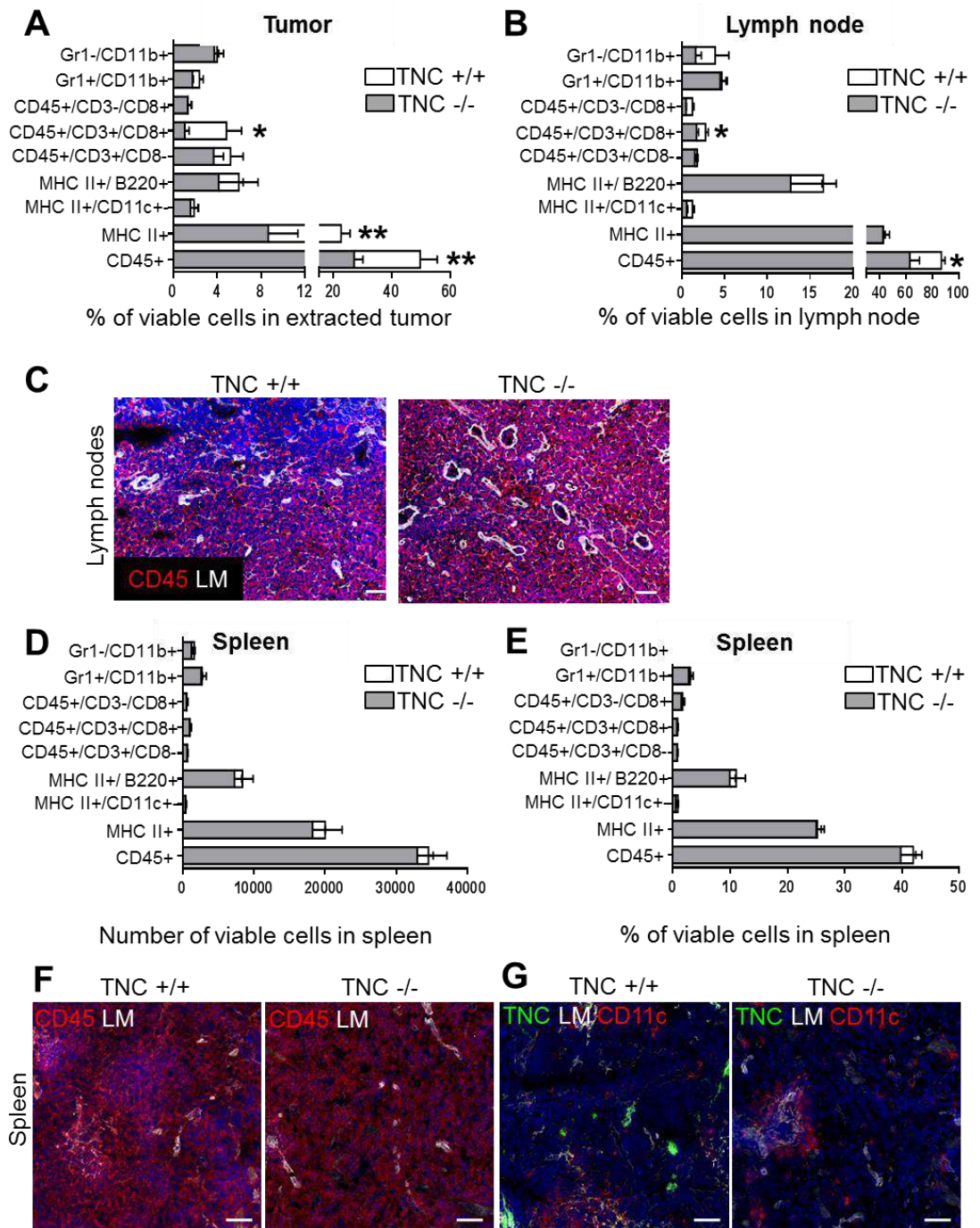
Supplementary Figure 2 FACS immunoprofiling and tissue staining of tumors, local lymph nodes and spleen

(A, B, D, E) Bar graph representation of the flow cytometry analysis of immune cell populations in the extracted OSCC tumors **(A)**, local lymph nodes **(B)** and spleens **(D, E)** of TNC +/+ (n = 5) and -/- (n = 6) tumor bearing mice represented as percentage of the total viable cells in the tissue sample **(A, B, E)** or as real counts **(D)**. Mann-Whitney test, * p < 0.05, ** p < 0.01. **(C, F, G)** IF images for the indicated molecules in representative lymph nodes **(C)** and spleen **(F, G)**. Scale bar, 100 μm.

Figure S3

A Invasive 4NQO OSCC

LMγ2 TNC CD11c

B Invasive human OSCC

CD45

HE   CD45   TNC

Tumor 3

Tumor 8

Tumor 10

D

% CD45 positive staining in stroma

Tumor number
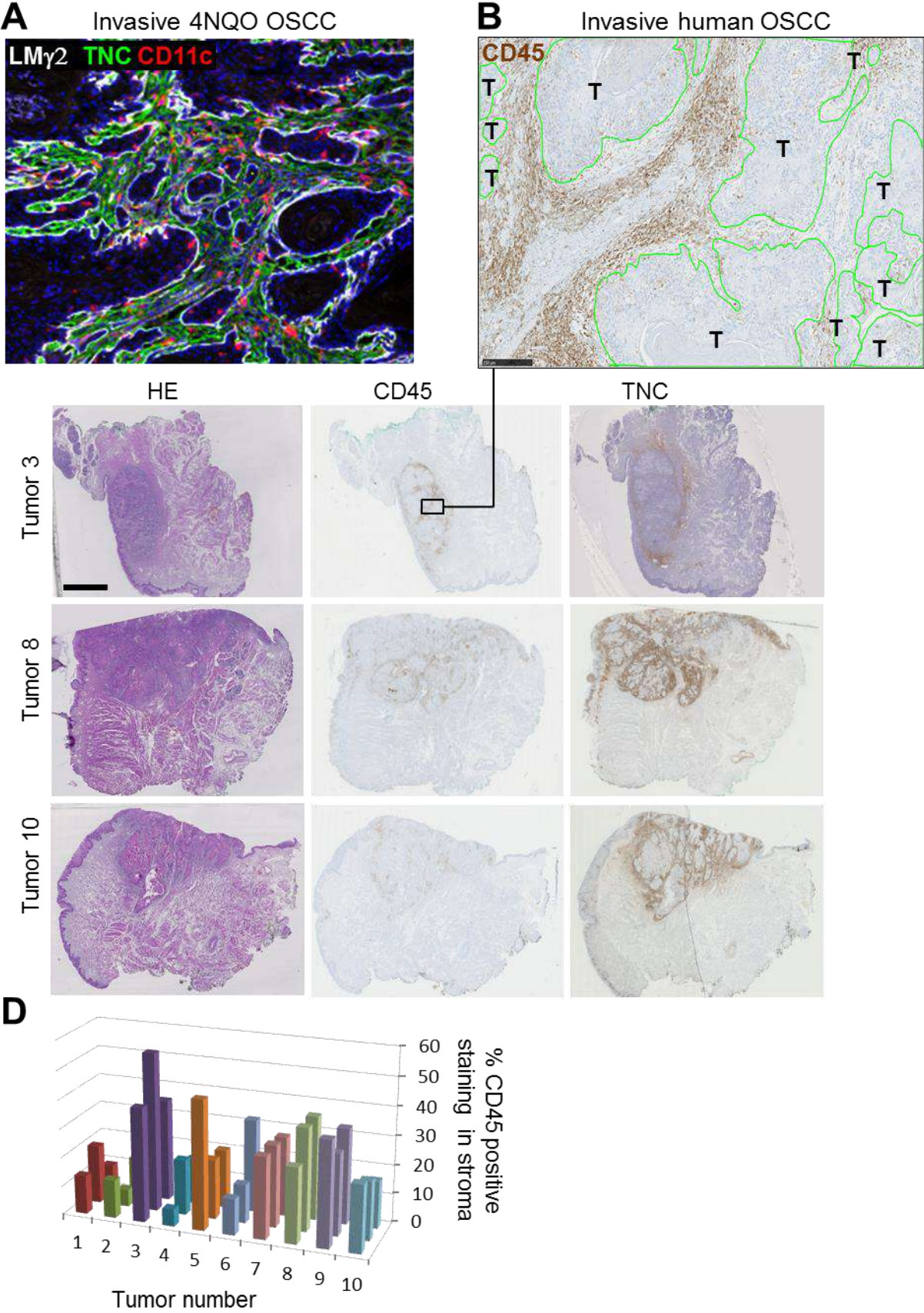
Supplementary Figure 3   Analysis of CD11c and CD45 expression in murine and human OSCC

(A) Representative IF image of an invasive murine WT tumor for the indicated molecules. Note that CD11c+ cells are exclusively present inside the TNC rich stroma. Scale bar, 100 μm. **(B)** Representation of a human OSCC upon staining for CD45. Areas designated as tumor regions are circled in green, the remaining area corresponds to stroma. Scale bar, 250 μm. **(C)** Staining of CD45 and TNC in sections from 3 representative primary tongue tumors used for quantitative analysis (tumor numbers indicated above images). Insert in tumor 3 depicts one of 3 fields selected for quantification and shown in panel B. Scale bar, 5 μm. **(D**) Results correspond to values obtained from 3 individual images per tumor. Numbers of the 10 tumors are indicated below.

Figure S4
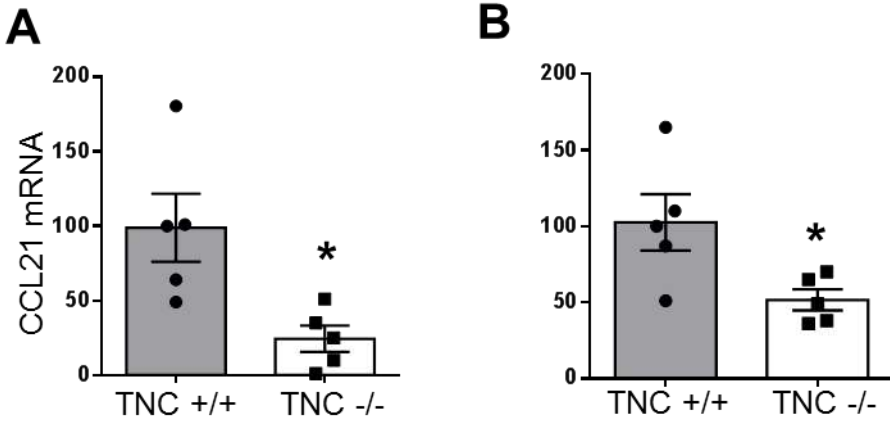
Supplementary Figure 4 Expression of CCL21 and CCR7 in murine OSCC

The mRNA levels of CCL21 **(A)** and CCR7 **(B)** from tongue tumors of TNC +/+ (n = 5) and TNC -/- (n = 5) mice were determined by qRTPCR. Means ± SEM. Mann-Whitney test, * $p < 0.05$.

Figure S5
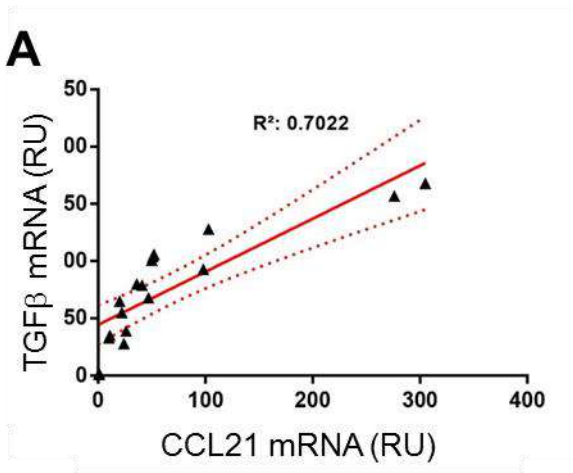
Supplementary Figure 5 mRNA expression of CCL21 is correlated with TGFβ mRNA expression

(A) Linear regression curves indicating expression of CCL21 in correlation to TGFβ expression in extracted tumors from both genotypes, n = 13.

Figure S6
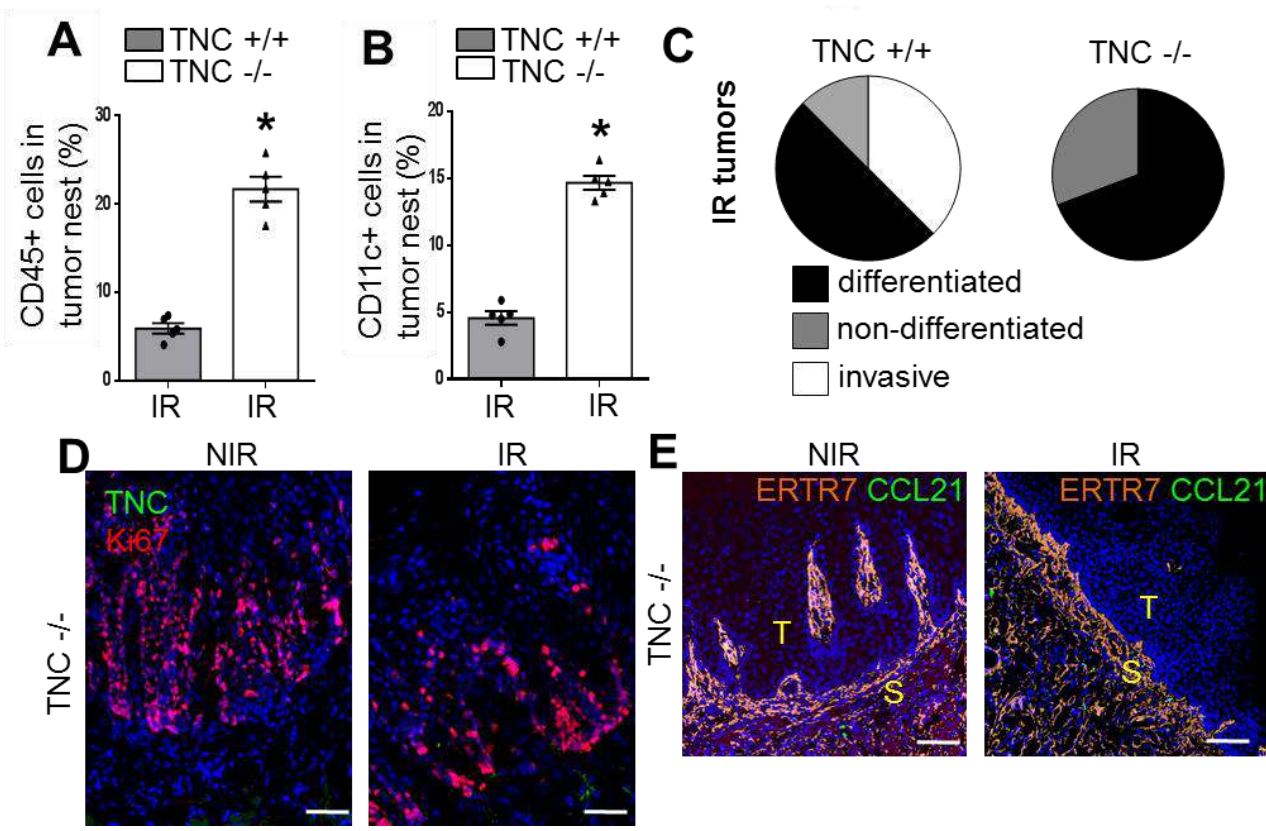
Supplementary Figure 6 Spatial localization of immune cells and characterization of TNC-/- irradiated tumoral and stroma area

(A, B) Quantification of CD45+ (A) and CD11c+ cells (B) in the tumor nests of TNC +/+ (n = 5) and TNC -/- mice (n = 5), 8-10 images per tumor. Mean ± SEM, Mann-Whitney test, * p < 0.05. **(C)** Classification of the tongue tumors upon 2Gy irradiation. Lesions from WT and TNCKO mice (n = 19 per genotype) were scored according to their histological features as non-differentiated   (black), differentiated (grey) or invasive carcinoma (white). **(D, E)** Representative IF images of the indicated molecules in the irradiated tumors. Scale bar, 100 μm. T, Tumor; S, Stroma.

Table S1 Characteristics of HNSCC patient cohort

Patient	Age at diagnosis (yr)	Sex	Smoking status	Alcohol	Stage (PTN)
1	44	M	never	no	PT3N0
2	70	M	current	former	PT1N0
3	69	F	current	no	PT2N0
4	69	F	former	no	PT1N1
5	73	M	current	-	PT2N0
6	62	F	current	yes	PT4N1
7	84	F	current	no	PT2N1
8	81	F	never	no	PT2N1
9	45	F	never	no	PT1N0
10	75	M	current	no	PT1N0

Mean age at diagnosis was 67.2 +/- 13.5 (range: 44-84). Smoking status and alcohol consumption corresponds to the self-reported status of patients when available. The pathologic stage (PTNM) is the classification of the tumor based on microscopic examination of the tumor by a pathologist, after it has been surgically resected.

Table S2: Protein quantification scoring and CCL21 expression quantification as example

CCL21/CCR7/gp38 quantification criteria	
Stained area in each region of interest	
0	No expression
1	Basal expression (BE)
2	BE < area ≤ 2x BE
3	Area > 2x BE
Intensity staining	
0	negative (no staining)
1	mild (weak)
2	moderate (distinct)
3	intense (strong)

TNC WT				TNC KO			
Mouse ID	Area	Intensity	CCL21 Score	Mouse ID	Area	Intensity	CCL21 Score
3418	3	3	9	3671	0	0	0
3689	3	3	9	3680	1	1	1
3725	2	2	4	3724	1	2	2
3696	2	3	6	3669	1	1	1
3399	3	2	6	3681	1	1	1

Disclosure of potential conflict of interest

Authors contribution

CS established the carcinogen model, CS and TL applied and investigated the model. CS, HB and GN developed the irradiation protocol. DM, PB, WE, HB, AM, GC, SBFD, AS, KN, SS, SR, RK, CA and MvH performed experiments, analyzed and interpreted the data. AS and EVO supervised the analysis of the human HNSCC tissues. CS, TL, EVO and GO wrote the manuscript. EVO, FA, CS and GO conceptualized and supervised the study. Grants to EVO and GO financed the study.

Acknowledgements

Appendix III

Tumor Biology and Immunology

Cancer Research

Tenascin-C Promotes Tumor Cell Migration and Metastasis through Integrin α9β1–Mediated YAP Inhibition

Zhen Sun[1,2,3,4], Anja Schwenzer[1,2,3,4], Tristan Rupp[1,2,3,4], Devadarssen Murdamoothoo[1,2,3,4], Rolando Vegliante[1,2,3,4], Olivier Lefebvre[1,2,3,4], Annick Klein[1,2,3,4], Thomas Hussenet[1,2,3,4], and Gertraud Orend[1,2,3,4]

Abstract

Tenascin-C is an extracellular matrix molecule that drives progression of many types of human cancer, but the basis for its actions remains obscure. In this study, we describe a cell-autonomous signaling mechanism explaining how tenascin-C promotes cancer cell migration in the tumor microenvironment. In a murine xenograft model of advanced human osteosarcoma, tenascin-C and its receptor integrin α9β1 were determined to be essential for lung metastasis of tumor cells. We determined that activation of this pathway also reduced tumor cell–autonomous expression of target genes for the transcription factor YAP. In clinical specimens, a genetic sig-

nature comprising four YAP target genes represents prognostic impact. Taken together, our results illuminate how tumor cell deposition of tenascin-C in the tumor microenvironment promotes invasive migration and metastatic progression.

Significance: These results illuminate how the extracellular matrix glycoprotein tenascin-C in the tumor microenvironment promotes invasive migration and metastatic progression by employing integrin α9β1, abolishing actin stress fiber formation, inhibiting YAP and its target gene expression, with potential implications for cancer prognosis and therapy. *Cancer Res; 78(4); 950–61. ©2017 AACR.*

Introduction

The extracellular matrix (ECM) molecule tenascin-C (TNC) that is highly expressed in the tumor microenvironment represents an active component of cancer tissue. Its high expression correlates with worsened patient survival prognosis in several

[1]INSERM U1109 - MN3T, The Microenvironmental Niche in Tumorigenesis and Targeted Therapy, Hôpital Civil, Institut d'Hématologie et d'Immunologie, Strasbourg, France. [2]Université de Strasbourg, Strasbourg, France. [3]LabEx Medalis, Université de Strasbourg, Strasbourg, France. [4]Fédération de Médecine Translationnelle de Strasbourg (FMTS), Strasbourg, France.

Z. Sun, A. Schwenzer, and T. Rupp contributed equally to this article.

Current address for Z. Sun: Tongji Cancer Research Institute, Tongji Hospital, Tongji Medical College in Huazhong, University of Science and Technology, Wuhan, Hubei, China; Department of Gastrointestinal Surgery, Tongji Hospital, Tongji Medical College in Huazhong, University of Science and Technology, Wuhan, Hubei, China; current address for A. Schwenzer: Kennedy Institute of Rheumatology, Nuffield Department of Orthopaedics, Rheumatology and Musculoskeletal Sciences, University of Oxford, Oxford, UK; and current address for T. Rupp: Porsolt, Research Laboratory, Z.A. de Glatigné, 53940 Le Genest-Saint-Isle, France.

Corresponding Author: Gertraud Orend, INSERM, 1, Place de l'Hopital, Strasbourg 67091, Cedex, France. Phone: 0033-0-3-68-85-39-96; E-mail: gertraud.orend@inserm.fr

cancer types (1). TNC promotes multiple events in cancer progression as recently demonstrated in a multistage neuroendocrine tumorigenesis model with abundant and no TNC. It was shown that TNC enhances tumor cell survival, proliferation, invasion, and lung metastasis. Moreover, TNC increases Notch signaling in breast cancer (2). TNC also promotes stromal events such as the angiogenic switch and the formation of more but leaky blood vessels involving Wnt signaling and inhibition of Dickkopf1 (DKK1) in a neuroendocrine tumor model (3, 4) and Ephrin-B2 signaling in a glioblastoma (GBM) model (5). TNC networks can have similarities with reticular fibers in lymphoid organs (6) and may alter the biomechanical properties of cancer tissue (7), in particular increase tissue stiffening (8). TNC also impairs actin stress fiber formation (9) and regulates gene expression, which may affect cell behavior and tumor malignancy (10).

The actin polymerization state is interpreted by the cell through two cotranscription factors, megakaryoblastic leukemia 1 (MKL1, myocardin-related transcription factor MRTF-A, MAL; ref. 11) and yes activating protein (YAP; refs. 12, 13). Under poorly adhesive conditions, cells fail to polymerize actin and subsequently cannot form actin stress fibers. MKL1 binds to globular G-actin monomers and remains sequestered in the cytoplasm. In consequence, MKL1 cannot reach nuclear serum response factor (SRF) or DNA sequences to induce gene transcription (14, 15), and MKL1-dependent genes remain silent.

YAP and TAZ (transcriptional coactivator with PDZ-binding motif) proteins are integral parts of the Hippo signaling pathway that is important for organ growth control during development and is often found to be deregulated in cancer

AACR

(16). Recently, YAP and TAZ were demonstrated to transduce mechanical and cytoskeletal cues with actin stress fibers promoting their nuclear translocation (17). Nuclear YAP/TAZ can activate gene expression through binding to the TEAD (TEA domain transcription factors) family of transcription factors (17), thus controlling gene expression upon cell adhesion.

Here, we analyzed the underlying mechanisms and consequences of poor cell adhesion by TNC. We demonstrate that TNC downregulates gene expression through inhibition of actin stress fibers, which in turn abolishes MKL1 and YAP activities in tumor cells. TNC itself is downregulated by a negative feedback loop due to inactive MKL1 and YAP. We further show that integrin α9β1 and inactive YAP are instrumental for TNC to promote tumor cell migration in an autocrine and paracrine manner. This has relevance for metastasis as knockdown of *TNC* or *ITGA9* decreases lung metastasis, which is associated with increased YAP target gene expression. Finally, poor expression of three YAP target genes (*CTGF*, *CYR61*, and *CDC42EP3*) identifies a group of osteosarcoma and GBM patients with worst prognosis when TNC levels are below the median expression. To our knowledge, this is the first report that provides a full view on a signaling pathway initiated by TNC, employing integrin α9β1, subsequently destroying actin stress fibers, inhibiting YAP, and abolishing target gene expression, thus promoting cell migration and lung metastasis. This information could be of prognostic and therapeutic value.

Materials and Methods

More details can be found in the Supplementary Information section.

Cell culture

Human GBM T98G (ATCC, CRL-169), U87MG (ATCC, HTB-14), and osteosarcoma KRIB (v-Ki-*ras*–transformed human osteosarcoma cells; ref. 18), previously used (9, 19), were cultured up to 10 passages after defrosting in DMEM (Gibco) 4.5 g/L glucose with 10% FBS (Sigma-Aldrich), 100 U/mL penicillin and 100 μg/mL streptomycin, and 40 μg/mL gentamicin at 37°C and 5% CO_2. The absence of mycoplasmas was regularly checked by quantitative real-time PCR (qPCR) according to the manufacturer's instructions (Venor GeMClassic; Minerva BioLabs). Cells were starved with 1% FBS overnight before drug treatment with 30 μmol/L lysophosphatidic acid (LPA; H_2O, Santa Cruz Biotechnology), 5 μmol/L Latrunculin B (LB; DMSO, Calbiochem), 2 μmol/L Jasplakinolide (Jasp; DMSO; Santa Cruz Biotechnology), and 10 μmol/L Y27632 (DMSO; Selleck Chemicals), respectively, or seeding on surfaces coated with purified horse serum–derived fibronectin (FN) or, FN plus purified recombinant human TNC for 24 hours in DMEM containing 1% FBS.

Animal experiments

KRIB control (shCTRL) and *TNC* and *ITGA9* knockdown cells (shTNC, shITGA9; 10×10^6), diluted in 100 μL PBS, were subcutaneously injected in the left upper back of nude mice (Charles River) and sacrificed 5 weeks later. The tumor size was measured every 7 days with a digital caliper and was calculated using the formula $S = a \times b$, where b is the longest axis and a is the

perpendicular axis to b. Upon extraction, the tumor weight was determined with a digital balance. The tumor and the smallest lung lobe of each mouse were directly frozen in liquid nitrogen and further analyzed by qPCR. Experiments with animals were performed according to the guidelines of INSERM and the ethical committee of Alsace, France (CREMEAS), with the reference number of the project AL/73/80/02/13 and the mouse house E67-482-21.

Coating with purified ECM molecules

FN and TNC were coated in 0.01% Tween 20-PBS at 1 μg/cm² before saturation with 10 mg/mL heat-inactivated BSA/PBS (3, 9).

RNA isolation and qPCR

Total RNA was isolated from cells by using TriReagent (Life Technologies) according to the manufacturer's instructions, reverse transcribed, and used for qPCR with primers listed in Supplementary Table S1.

Immunoblotting

Cells were lysed in RIPA buffer (150 mmol/L NaCl, 1.0% IGEPAL CA-630, 0.5% sodium deoxycholate, 0.1% SDS, and 50 mmol/L Tris, pH 8.0), separated by polyacrylamide gel electrophoresis, blotted onto nitrocellulose membrane using the Trans-Blot Turbo RTA Mini Nitrocellulose Transfer Kit (BioRad) and incubated with primary and horseradish peroxidase–coupled secondary antibodies before signal detection with the Amersham ECL detection reagent.

Immunofluorescence staining

Cells were fixed in 4% paraformaldehyde (PFA) for 10 minutes and permeabilized in PBS-Triton 0.1% for 10 minutes, incubated with the anti-YAP antibody and a secondary fluorophore-coupled antibody, and analyzed with a Zeiss Axio Imager Z2 microscope. At least 150 cells in duplicates per condition were quantified.

Lentiviral transduction of cells

Silencing of *MKL1*, *TNC*, and *ITGA9* was done by short hairpin (sh)–mediated gene expression knockdown (see Supplementary Table S2). MISSION lentiviral transduction particles (Sigma-Aldrich) or MISSION nontarget shRNA control transduction particles (SHC002V; Sigma-Aldrich) with an MOI of 1 were used, and transduced cells were selected with 2.5, 10, and 1 μg/mL puromycin for *MKL1*, *TNC*, and *ITGA9* knockdown, respectively. Stable knockdown was determined at RNA level by qPCR and protein level by immunoblotting.

Transfection and RNAi

Plasmids encoding YAP (YAP-WT), constitutively active YAP (CA-YAP, S127A mutant; ref. 20) and non-TEAD interacting YAP (DN-YAP, S127A-S94A mutant; ref. 20), and MKL1-WT (pEF full-length hemagglutinin-tagged MAL HA) and N-terminal deleted constitutively active CA-MKL1 (pEF HAΔN MAL) were provided by Guido Posern (Halle-Wittenberg University, Halle, Germany). Plasmids were transiently transfected (JetPEI, Polyplus), and the siRNA reagent system (sc-45064; Santa Cruz Biotechnology) for reducing expression of *YAP*, *MKL1*, *ITGA9*, and *SDC4* was used according to the manufacturer's

310

Sun et al.

instruction. Note that cells with stable expressing of CA-YAP could not be established.

Luciferase reporter assay

Cells were transiently transfected (JetPEI, Polyplus) with the pGL3-5 x MCAT(SV)-49 plasmid (provided by I. Farrance, University of Maryland School of Medicine, Baltimore) encoding 5 x MCAT (TEAD binding sites) or 3DA.Luc plasmid (provided by Guido Posern, Halle-Wittenberg University, Halle, Germany) encoding *FOS*-derived SRF-binding sites together with the pRL-TK (TK-*Renilla*) plasmid for normalization. Cells were lysed and analyzed by the Dual-Luciferase reporter assay system (Promega) and a BioTek Luminometer EL800. Firefly luciferase activity was normalized to internal *Renilla* luciferase control activity.

Migration and invasion assays

For 2D migration, 2×10^5 cells were seeded in a 50 mm lumox dish (SARSTEDT). Real-time phase contrast images were taken with a Zeiss microscope (Axiovert observation) every 15 minutes for 24 hours. Migration of individual cells in the first 12 hours (10 cells in each field, 2 fields per condition) was analyzed with the ImageJ software. For Boyden chamber transwell migration or invasion assays, 2×10^4 cells were plated onto the upper chamber of a transwell filter with 8 μm pores (Greiner Bio-one) that had been coated on the upper side with FN and FN/TNC (1 μg/cm^2), growth factor–reduced Matrigel (0.5 mg/mL; Corning), or rat tail type 1 collagen gel (2.5 mg/mL; BD Biosciences) as described (21, 22). Note that 10% FBS in the lower chamber was used as chemoattractant. Cells at the lower side were fixed with 4% PFA in PBS, stained with DAPI (Sigma D9542), photographed, and abundance was quantified using the ZEN Blue software (Zeiss).

Patient survival analysis

The patient dataset GSE21257 (osteosarcoma) and GSE42669 (GBM) available in the Gene Expression Omnibus (GEO) Database (http://www.ncbi.nlm.nih.gov/gds) were used. Microsoft Excel was used to extract the expression values of a small number of genes (probesets) and was compared with the clinical data from GEO. Survival analysis was performed using SPSS23.0 and the Kaplan–Meier survival procedure.

Statistical analysis

All experiments were performed at least 3 times independently with at least two to three replicates per experiment. For all data, Gaussian distribution was tested by the d'Agostino-Pearson normality test. Statistical differences were analyzed by the unpaired *t* test (with Welch's correction in case of unequal variance) or ANOVA one-way with Tukey post-test for Gaussian dataset distribution. Statistical analysis and graphical representation were performed using GraphPad Prism. GSEA (23) was used to analyze enrichment of the YAP/TAZ/TEAD target genes (24) and MKL1 target genes (25) in the TNC-specific gene expression signature (10). *P* values < 0.05 were considered as statistically significant (mean ± SEM; *P* values: *, $P < 0.05$; **, $P < 0.01$; ***, $P < 0.001$; and ****, $P < 0.0001$).

Results

TNC inhibits actin stress fiber formation on a mixed FN/TNC substratum

FN and TNC are often coexpressed and act as accomplices in cell adhesion where TNC counteracts the adhesive properties of FN (9, 26, 27). To set the stage for the subsequent mechanistic analysis, we determined how low cell adhesion to FN implemented by TNC affects actin dynamics and downstream gene expression in two previously used human tumor cell lines derived from GBM (T98G) and osteosarcoma (KRIB; refs. 9, 28). Whereas most experiments were performed with KRIB cells, some were reproduced in T98G cells (Supplementary Figures). We found that both cells were round and adhered less on the FN/TNC substratum (Supplementary Fig. S1A–S1C). Western blot upon fractionation into monomeric G-actin and polymerized F-actin revealed less F-actin in both cells grown on FN/TNC compared with FN (Supplementary Fig. S1D–S1F). TRITC-phalloidin staining showed no actin stress fibers on FN/TNC (Supplementary Fig. S1G and S1H).

A TNC repression signature negatively correlates with MKL1- and YAP-responsive genes

Because TNC inhibits actin stress fibers and actin stress fibers regulate MKL1 and YAP/TAZ (11–13), we asked whether TNC modulates MKL1 and/or YAP activities. Therefore, we searched for a potential correlated expression of genes that are regulated by TNC (10) and genes that are regulated by MKL1/SRF (25) or YAP/TAZ (24), respectively. We used publicly available mRNA expression data and Gene Set Enrichment Analysis (GSEA) and found that both gene sets are significantly negatively correlated with a gene signature that is downregulated by TNC in T98G cells (Fig. 1A and B; ref. 10). By qPCR, we evaluated TNC substratum–specific gene expression and found that in contrast to *FOS*, that is increased on FN/TNC, a selection of known MKL1-regulated genes (tropomyosin-1/*TPM1*, *TPM2*, ZYX/Zyxin, *FOSL1*/Fos-related antigen 1, *CDC42EP3*/CDC42 effector protein-3, *TNC*; refs. 29– 31) and YAP-regulated genes (*CTGF*/CCN2, CYR61/CCN1, DKK1/Dickkopf-1, *GLI2*/GLI family zinc finger 2; ref. 32) was indeed lowered on the FN/TNC substratum in both cells (Fig. 1C; Supplementary Fig. S1I). Whereas TAZ mRNA level was slightly enhanced in T98G (yet not in KRIB), YAP protein levels consistently were not affected by the FN/TNC substratum in either cell (Fig. 1D; Supplementary Fig. S1J). In contrast, MKL1 protein levels were reduced on FN/TNC in both cells, suggesting that TNC blocks expression of MKL1 but not of YAP (Fig. 1E; Supplementary Fig. S1K).

TNC blocks (non–SRF-mediated) MKL1 target gene expression through repression of MKL1

MKL1 can induce SRF-dependent and -independent gene expression (11, 15). We addressed whether MKL1/SRF-dependent transcription is potentially impaired by TNC in T98G (Supplementary Fig. S2A–S2G) and KRIB cells (Supplementary Fig. S2H–S2M) by measuring SRF-driven luciferase activity in cells grown on FN or FN/TNC and noticed similar activities, suggesting that TNC does not inhibit the SRF-dependent function of MKL1 (Supplementary Fig. S2A and S2H). Then, we used loss-of-function (LOF) and gain-of-function (GOF) approaches employing shRNAs to reduce MKL1 expression and overexpression of a constitutive active CA-MKL1 molecule,
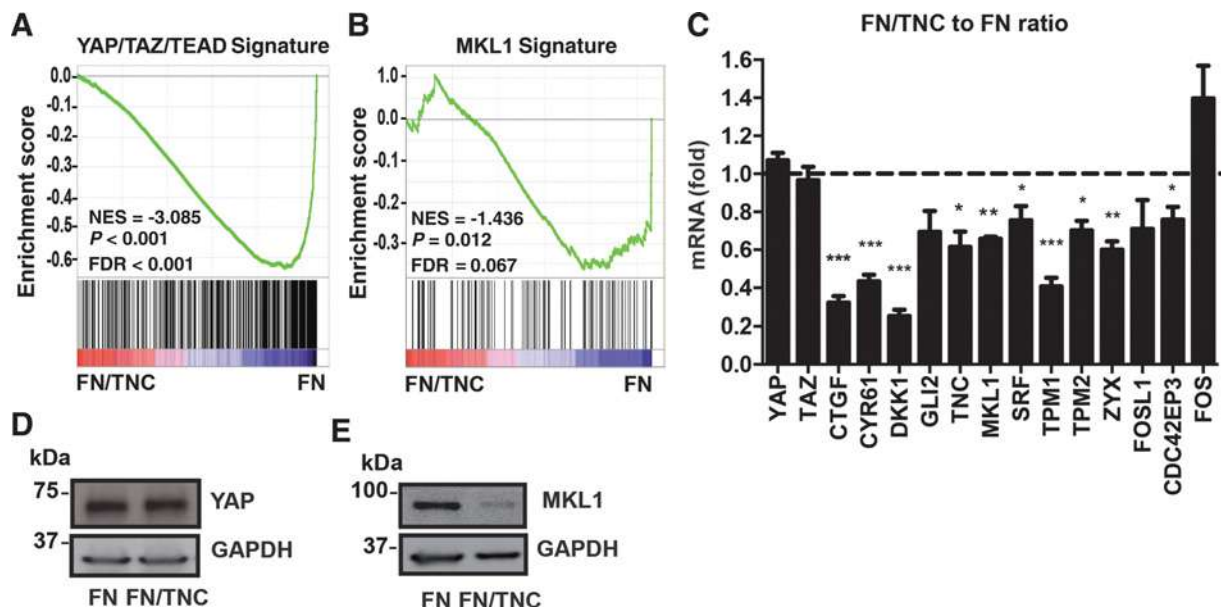
311

Figure 1.
Impact of TNC on MKL1 and YAP target gene expression. GSEA reveals a significant anticorrelation between TNC and a YAP/TAZ (**A**) and a MKL1/SRF (**B**) gene expression signature, respectively. The normalized enrichment score (NES) and the false discovery rate (FDR) q value assessing the significance of enrichment are indicated. **C,** Gene expression by qPCR of selected genes in KRIB cells upon growth on FN or FN/TNC ($n = 9$) is expressed as relative ratio of values on FN/TNC versus FN. **D** and **E,** Immunoblotting for YAP and MKL1 in KRIB cells on FN or FN/TNC. In all figures, $n = 9$ and $n = 6$ represent three independent experiments with three replicates and two replicates, respectively (mean ± SEM).

respectively (Supplementary Fig. S2B, S2C, S2I, and S2J). Whereas knockdown of *MKL1* caused reduced expression of all tested MKL1 target genes (Supplementary Fig. S2D and S2K), CA-MKL1 induced SRF-luciferase activity, indicating MKL1 responsiveness (Supplementary Fig. S2E). CA-MKL1 significantly induced *CTGF*, *CDC42EP3*, *TNC*, *DKK1*, and *TPM1*, yet not *CYR61* in both cells (Supplementary Fig. S2F and S2L). Whereas *CTGF* and *CYR61* remained unaffected, transient expression of CA-MKL1 increased gene expression of *CDC42EP3*, *TNC*, *DKK1* (only T98G), and *TPM1* significantly on FN/TNC in both cells (Supplementary Fig. S2G and S2M). These results suggest that TNC downregulates some genes such as *TPM1*, *TNC*, *CDC42EP3*, and *DKK1* through impairing MKL1 functions. In contrast, other genes such as *CTGF* and *CYR61* are repressed by TNC through another mechanism.

TNC represses genes in tumor cells through abolishing YAP activity by cytoplasmic retention

To analyze whether TNC inhibits the YAP cotranscriptional functions, we measured luciferase activity driven by the transcription factor TEAD, which requires active YAP (17). Indeed, luciferase activity was reduced in both cells grown on FN/TNC compared with FN (Fig. 2A; Supplementary Fig. S3A). Because YAP protein levels were equal on both substrata (Fig. 1D; Supplementary Fig. S1J), excluding regulation by TNC at expression level, we investigated whether TNC may impair YAP nuclear translocation (17). We assessed YAP subcellular localization by staining cells for YAP. Indeed, whereas YAP was nuclear in the large majority of both cells plated on FN, YAP remained mostly cytoplasmic in cells on FN/TNC even 24 hours after plating, which resembles cells in the absence of FBS, a condition that blocks YAP function (Fig. 2B and C; Supple-

mentary Fig. S3B–S3E; ref. 33). Thus, on FN/TNC, nuclear translocation of YAP is impaired, which could explain inactivation of YAP cotranscription function.

To determine regulation of genes by TNC through YAP in more detail, we used LOF and GOF approaches by transiently expressing inhibitory (DN-YAP) or activating (CA-YAP) YAP molecules (Fig. 2D and E; Supplementary Fig. S3F and S3G). We addressed YAP transactivation function with a TEAD-luciferase assay and observed high TEAD-luciferase activity upon transfection of CA-YAP (Fig. 2F; Supplementary Fig. S3H). CA-YAP also significantly increased *CTGF*, *CYR61*, *CDC42EP3*, and *TNC* gene expression. In contrast, neither *DKK1* nor *TPM1* were induced by CA-YAP, indicating that these genes are not regulated by YAP (Fig. 2G; Supplementary Fig. S3I). To investigate whether TNC downregulates genes through impairment of YAP, we used transient expression of CA-YAP and looked for gene expression on FN/TNC. We noticed in both cells that expression of *CTGF*, *CYR61*, *CDC42EP3*, and *TNC* was increased. Again, expression of *DKK1* was poorly affected in both cells (Fig. 2H; Supplementary Fig. S3J). These results suggest that TNC reduces expression of *CTGF*, *CYR61*, and *CDC42EP3* by inhibiting YAP. Moreover, we showed for the first time that YAP regulates *TNC* expression.

TNC downregulates YAP target gene expression through blocking actin stress fibers

As TNC affects the actin cytoskeleton and abolishes MKL1 and YAP target gene expression, we asked whether and how TNC-regulated genes respond to actin dynamics. We treated both cells with Latrunculin B (LB) causing disassembly of actin filaments into monomeric G-actin (34), Jasplakinolide (Jasp) to stabilize F-actin and inhibit stress fibers (35), and

312

Sun et al.
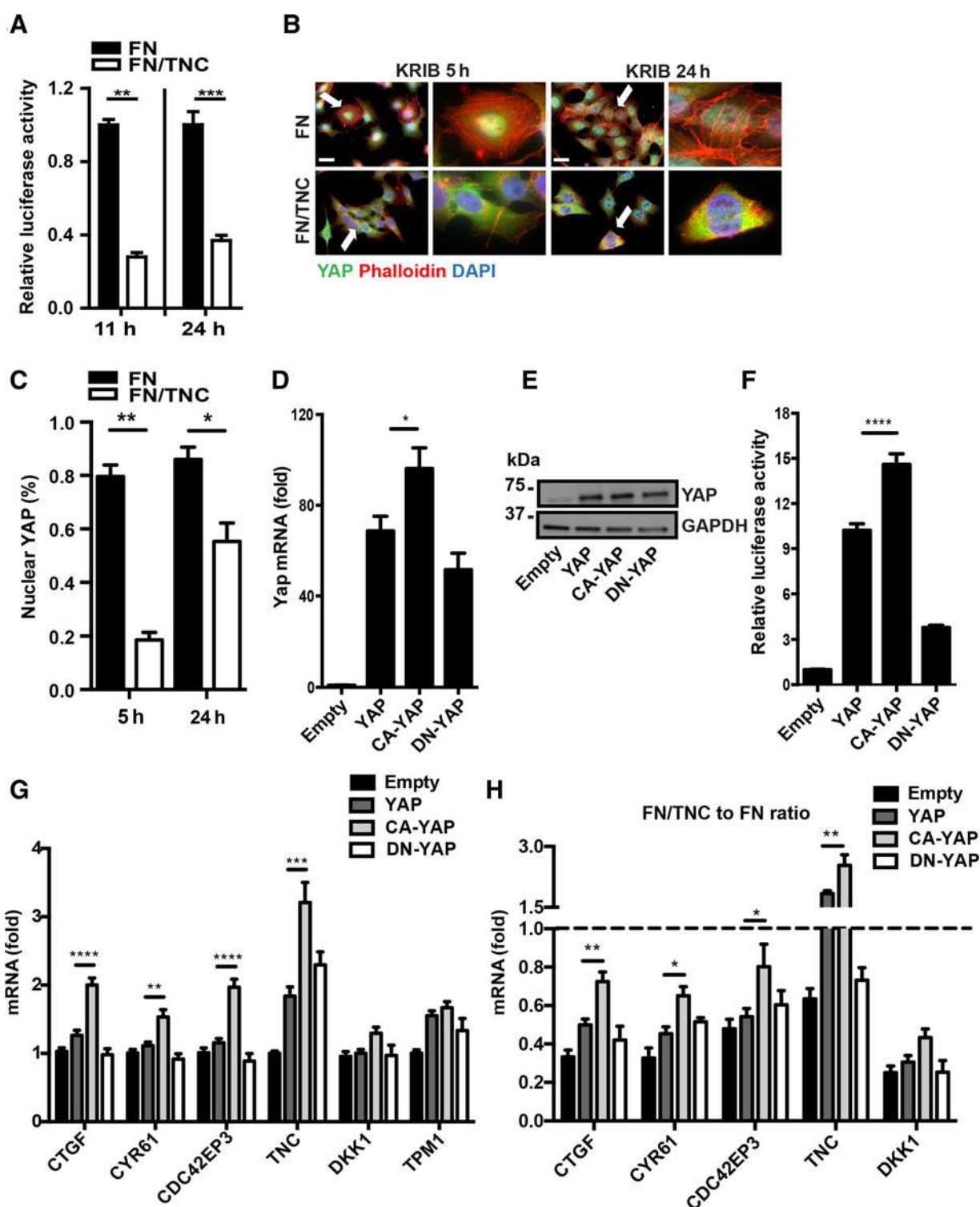
Figure 2.
An FN/TNC substratum impairs YAP target gene expression by cytoplasmic retention of YAP. Results for KRIB cells are shown. **A,** TEAD luciferase assay of cells grown on FN or FN/TNC. **B,** Representative images of YAP (green), polymerized actin (phalloidin, red), and nuclei (DAPI, blue) in cells upon growth on FN or FN/TNC. The arrow points at the cell of higher magnification on the right. Scale bar, 5 μm. **C,** Quantification of cells with nuclear YAP on the indicated substrata represented as percentage of all cells. **D,** YAP expression in cells by qPCR upon transfection of empty vector (CTRL) or YAP expression constructs. **E,** Immunoblotting for YAP and GAPDH upon transient transfection of cells with YAP expression plasmids. **F,** TEAD luciferase assay upon transfection of YAP expression plasmids. **G,** Gene expression analysis by qPCR upon transient expression of YAP expression plasmids in cells grown on plastic. **H,** Ratio of gene expression on FN/TNC versus FN as determined by qPCR upon transient transfection of YAP expression plasmids ($n = 9$, except for **C** ($n = 6$); mean ± SEM).

313
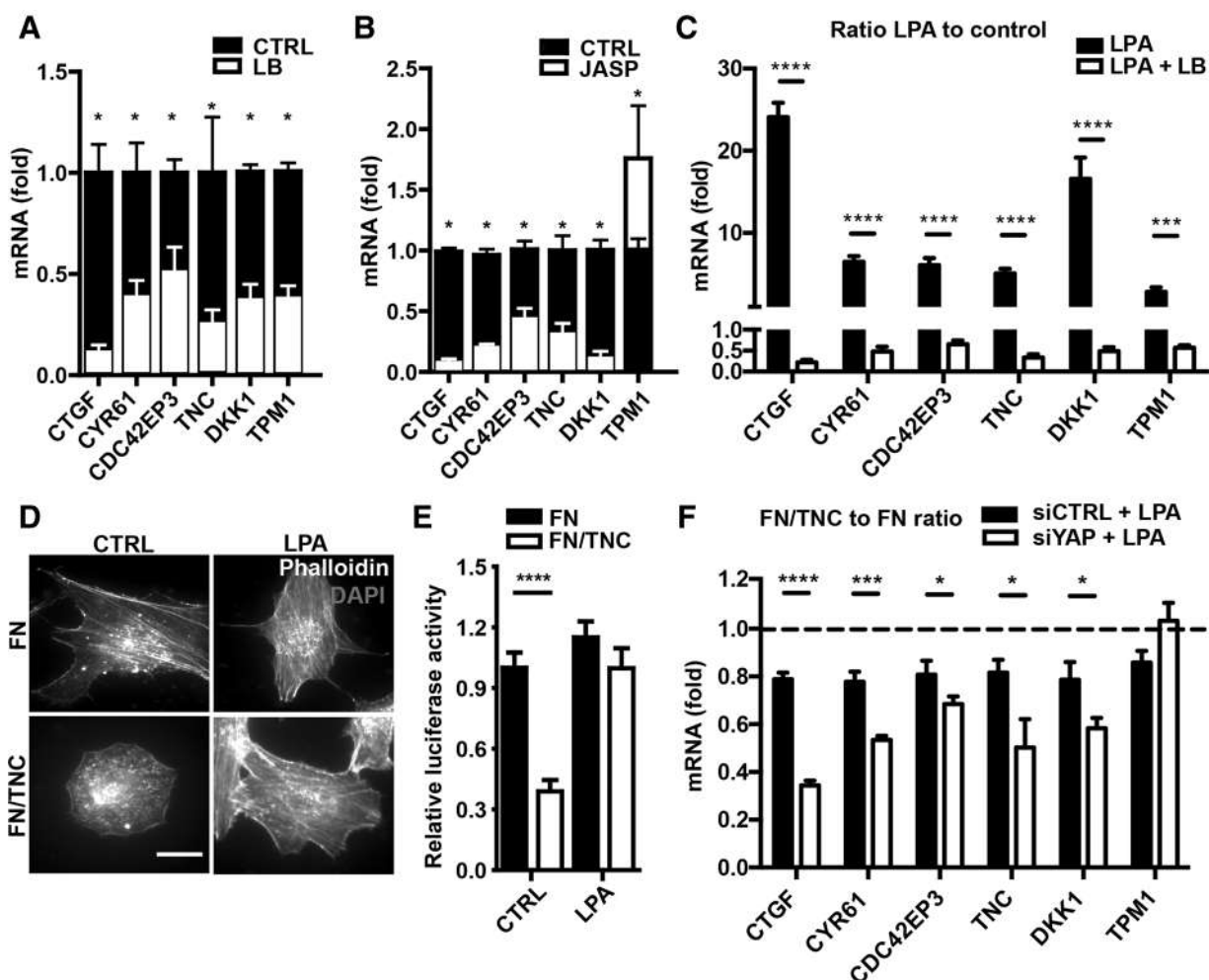
Figure 3.
Actin polymerization–dependent expression of TNC-downregulated genes. Results for KRIB cells are shown. **A–C,** Gene expression analysis by qPCR of TNC target genes upon treatment with LB (**A**), Jasp (**B**), or LPA plus LB (**C**) after 5 hours ($n = 6$, three experiments in duplicates). **D,** Representative images of polymerized actin (phalloidin, white) and nuclei (DAPI) of cells on FN or FN/TNC with or without LPA treatment after 5 hours. Scale bar, 5 μm. **E,** TEAD luciferase assay upon growth on FN or FN/TNC with or without LPA for 24 hours ($n = 12$, four experiments in triplicates). **F,** Gene expression analysis by qPCR upon treatment with LPA and siYAP and growth on FN or FN/TNC. Relative expression is depicted as a ratio of values on FN/TNC versus FN ($n = 9$; mean ± SEM).

LPA to induce actin stress fibers (Supplementary Fig. S4A and S4B; ref. 36) before measuring gene expression. LB blocked expression of all tested genes in both cells (Fig. 3A; Supplementary Fig. S4C). Whereas Jasp blocked *CTGF*, *CYR61*, *CDC42EP3*, *TNC*, and *DKK1* expression, *TPM1* was even increased over control conditions by Jasp (Fig. 3B; Supplementary Fig. S4D), suggesting that F-actin is sufficient to drive *TPM1* expression but not expression of the other five TNC target genes, which may require actin stress fibers. Indeed, the actin stress fiber inducer LPA triggered actin stress fiber formation in KRIB cells plated on FN/TNC, as well as TEAD-driven luciferase and expression of all tested genes in both cells and on a FN/TNC substratum (Fig. 3C–F; Supplementary Fig. S4E–S4G). These results suggest that actin stress fibers are important regulators of the TNC-repressed genes. To prove that the LPA effect is due to its role in actin stress fiber formation (as LPA can also have other downstream effectors;

ref. 37), we treated cells with LPA together with LB, generating G-actin, and measured gene expression (Supplementary Fig. S4A). We observed that LB abolished LPA-induced expression of all tested genes, which indicates that LPA bypasses TNC gene repression through its impact on actin stress fiber formation (Fig. 3C; Supplementary Fig. S4E). Importantly, *TNC* expression itself is regulated by actin stress fibers as LPA induces and Jasp blocks *TNC* expression, respectively (Fig. 3A–C; Supplementary Fig. S4C–S4E).

We used LPA to induce target gene expression on FN/TNC (Fig. 3D) and then investigated whether inhibition of YAP (Supplementary Fig. S4H) could revert the LPA effect. Indeed, siYAP abolished expression of all LPA-restored genes on FN/TNC except *TPM1* (not a YAP target gene) in both cells (Fig. 3F; Supplementary Figs. S4G and S5A–S5L). This result suggests that TNC represses YAP target genes through inhibition of actin stress fibers.

314

Sun et al.

TNC promotes 3D migration through integrin α9β1 by blocking actin stress fibers and inactivating YAP

As TNC impairs actin stress fiber formation and YAP-dependent gene expression, we wanted to know whether this has an effect on cell migration. We monitored mobility by time-lapse microscopy in KRIB cells and observed that the total migration distance was lower on FN/TNC than on FN (Fig. 4A and B, videos 1 and 2). By using a 3D Boyden chamber migration assay, we observed that more KRIB cells moved to the other side of the filter when cells were placed on the FN/TNC substratum in comparison with FN at the 6- and 24-hour time points (Fig. 4C). A similar observation was made for T98G cells (Supplementary Fig. S6A and S6B). We demonstrated that the TNC-containing substratum did not affect T98G and KRIB cell proliferation even not upon treatment with LPA (Supplementary Fig. S6C). Moreover, TNC-induced migration was not affected by proliferation as migration was similar upon treatment with proliferation-inhibitory Mitomycin-C (Supplementary Fig. S6D). Altogether, these observations suggest that TNC promotes transwell migration of KRIB and T98G cells.

As LPA restored cell spreading through induction of actin stress fibers, we asked whether LPA had an impact on transwell migration. Indeed, LPA reduced migration of KRIB cells on FN/TNC to levels as on FN (Fig. 4D). Thus, actin stress fibers counteract TNC-induced transwell migration, suggesting that impairment of stress fibers is important for migration by TNC. Cells with a round cell shape can migrate in an amoeboid manner where active Rho-kinase (ROCK) is crucial (38). We chemically inhibited ROCK and observed that ROCK is required for transwell migration by TNC, as Y27632 blocked migration from FN/TNC in the Boyden chamber experiment (Fig. 4D).

Now, we addressed a potential interdependence with MKL1 and/or YAP. Therefore, we added LPA to KRIB cells with knockdown of *MKL1* or *YAP* and measured Boyden chamber migration. Whereas knockdown of *MKL1* did not alter KRIB cell migration on FN/TNC in the presence of LPA, knockdown of *YAP* restored transwell migration (Fig. 4E and F). To substantiate a link to actin stress fibers, we stained KRIB cells with phalloidin upon growth on FN/TNC and addition of LPA and transfection of siYAP or expression of DN-YAP and CA-YAP, respectively. Whereas LPA induced actin stress fibers on FN/TNC, this did not occur in KRIB cells with siYAP or expressing DN-YAP (Fig. 3D; Supplementary Fig. S6E and S6F). We conclude that siYAP abolishes the stress fiber–inducing effect of LPA. We further noticed that CA-YAP restored actin stress fibers on FN/TNC and abolished TNC-induced transwell migration. This was not the case with DN-YAP or WT-YAP (Fig. 4G; Supplementary Fig. S6F). We conclude that TNC promotes transwell migration through blocking actin stress fibers and YAP.

Next, we addressed which upstream regulators such as syndecan-4 (9) or integrin α9β1, a receptor for TNC (39, 40), are mediating TNC-induced migration. We lowered gene expression by siRNA and shRNA, respectively, and confirmed reduced expression of *SDC4* and the *ITGA9* chain (Supplementary Fig. S6G–S6J). Reduced levels of *SDC4* (mimicking cell rounding by TNC; ref. 28) did not abolish LPA-specific migration on FN/TNC, suggesting that inactivation of syndecan-4 by TNC is not relevant for TNC transwell migration (Fig. 4H). In contrast, transient knockdown of *ITGA9* induced actin stress fibers on FN/TNC and abolished TNC-specific transwell migration in

KRIB cells, pointing at integrin α9β1 as relevant TNC receptor (Fig. 4H; Supplementary Fig. S6E).

As TNC transwell migration occurs in the absence of actin stress fibers, and the knockdown of *ITGA9* and of *YAP* impaired actin stress fibers and TNC-specific migration, we wanted to know whether TNC downregulates YAP target genes through integrin α9β1. By qPCR, we indeed observed that the *ITGA9* knockdown in KRIB cells increased expression of all tested TNC target genes on FN/TNC, reaching levels close to FN (Fig. 4I).

In addition, we analyzed whether TNC potentially also enhances transwell migration through an autocrine mechanism. Therefore, we measured Boyden chamber migration in control (shCTRL) and *TNC* knockdown (shTNC) KRIB cells (Supplementary Fig. S6I) and found less *TNC* knockdown cells moving through the uncoated filter than shCTRL cells, suggesting that endogenously made TNC is important (Fig. 4J). Next, we addressed whether TNC affects invasion through Matrigel and/or a type 1 collagen gel with a pore size that was shown to favor amoeboid migration (21, 22), respectively. We observed that less KRIB cells passed through Matrigel than through the collagen gel–coated substratum, yet Matrigel invasion was independent of TNC. In contrast, 3D migration through the collagen gel was TNC dependent as it was reduced upon *TNC* knockdown (Fig. 4K). We conclude that endogenously expressed TNC as well as a TNC substratum induces α9β1 signaling and promotes amoeboid-like transwell migration.

TNC and integrin α9β1 promote lung metastasis of osteosarcoma cells, associated with low levels of YAP target gene expression

We tested whether signaling by TNC and integrin α9β1 influences expression of YAP target genes and migration *in vivo* by generating KRIB cells with a knockdown of *TNC* and the *ITGA9* chain, respectively, and grafted cells subcutaneously into nude mice (Supplementary Fig. S6I and S6J). We noticed stable knockdown of both genes in the arising tumors (Supplementary Fig. S7A and S7B) and that knockdown of *TNC* or *ITGA9* reduced tumor growth (Fig. 5A and B). In addition, KRIB cells disseminated and formed lung metastasis, as assessed by the appearance of macrometastasis and expression of human *GAPDH* by qPCR. We observed that knockdown of either gene, *TNC* or *ITGA9*, reduced lung metastasis (Fig. 5C and D; Supplementary Fig. S7C). A potential *in vivo* effect of TNC and/or integrin α9β1 on YAP target gene expression was addressed by measuring gene expression in KRIB tumors with knockdown of *TNC* or *ITGA9*, respectively. We observed that sh2TNC tumors displayed reduced tumor weight and less metastasis, and significantly increased expression of all tested TNC target genes (Fig. 5E). This was not the case for sh1TNC tumors (Fig. 5B and E). Also in human U87MG GBM cell–derived tumors, where TNC promoted tumor growth (5), TNC increased YAP target gene expression (Supplementary Fig. S7D). Most importantly, in *ITGA9* knockdown KRIB tumors, gene expression of *CTGF*, *CYR61*, and *CDC42EP3* was significantly increased (Fig. 5F).

Predictive value of TNC-regulated genes *CTGF*, *CYR61*, and *CDC42EP3* for cancer patient survival

By having established a link of TNC to enhanced migration through abolishing YAP activity and increasing osteosarcoma metastasis, we asked now whether this information could be of relevance for cancer patient survival. We analyzed expression of a

315
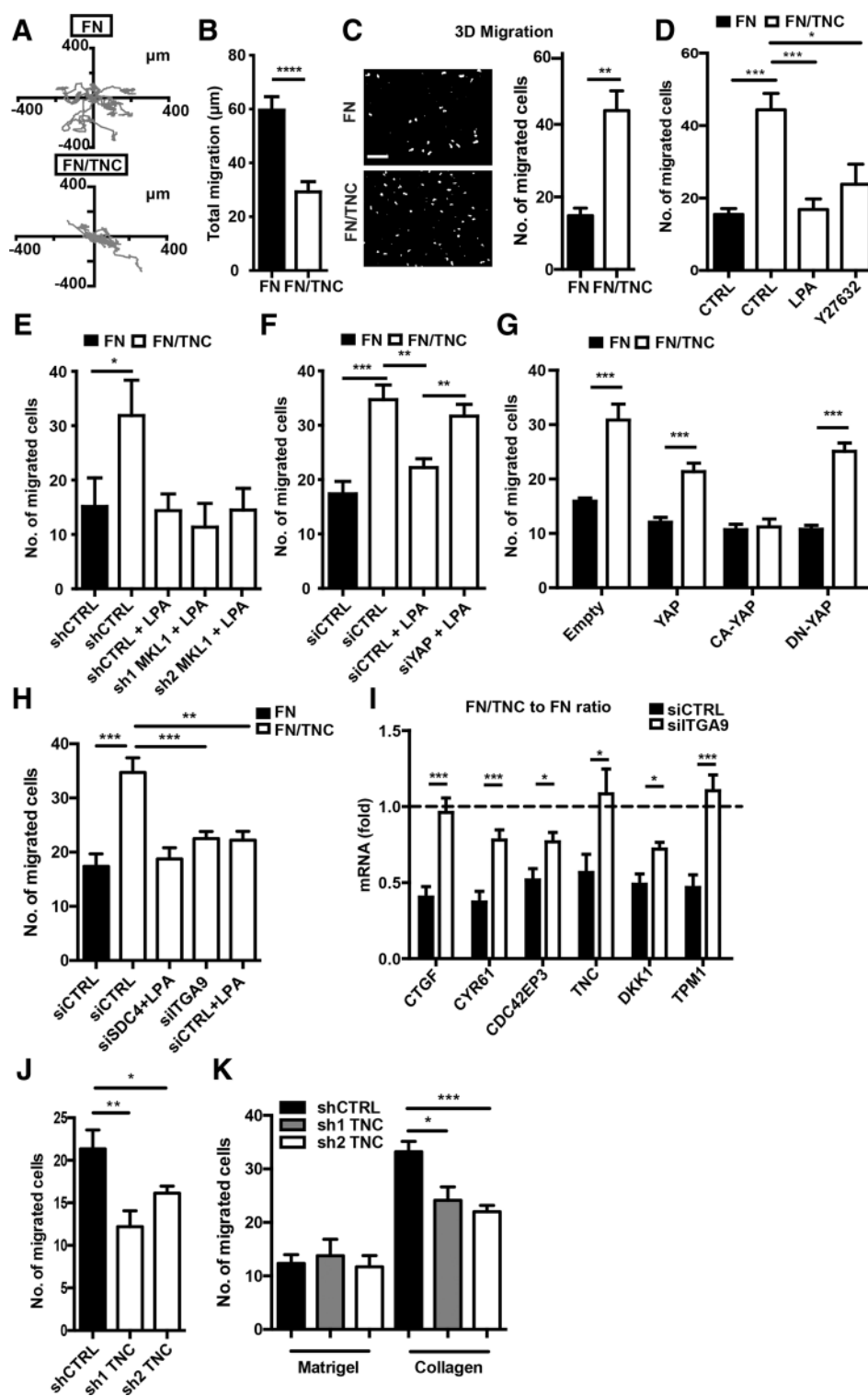
Figure 4.
TNC promotes transwell migration through integrin α9β1 and requires inactive YAP. Results for KRIB cells are shown. Assessment of 2D migration (**A** and **B**) showing the movement of individual cells during 12-hour live imaging (**A**) and transwell migration 24 hours after seeding on FN or FN/TNC (**C**), and upon treatment with LPA or Y27632 (**D**), or knockdown of the following genes, *MKL1* (**E**), *YAP* (**F**), *ITGA9* (**H**), *SDC4* (**I**), and *TNC* (**J**), respectively, and upon overexpression of YAP molecules (**G**). Scale bar, 20 μm. **I,** mRNA levels of the indicated genes upon knockdown of *ITGA9* expressed as a ratio of values for FN/TNC versus FN. **K,** Quantification of invasion of shCTRL and shTNC cells through Matrigel- and collagen gel–coated transwells after 24 hours [*n* = 6, except for **G** (*n* = 7, three experiments with at least duplicates) and **F**, **H**, **I**, and **K** (*n* = 9); mean ± SEM].

316

Sun et al.
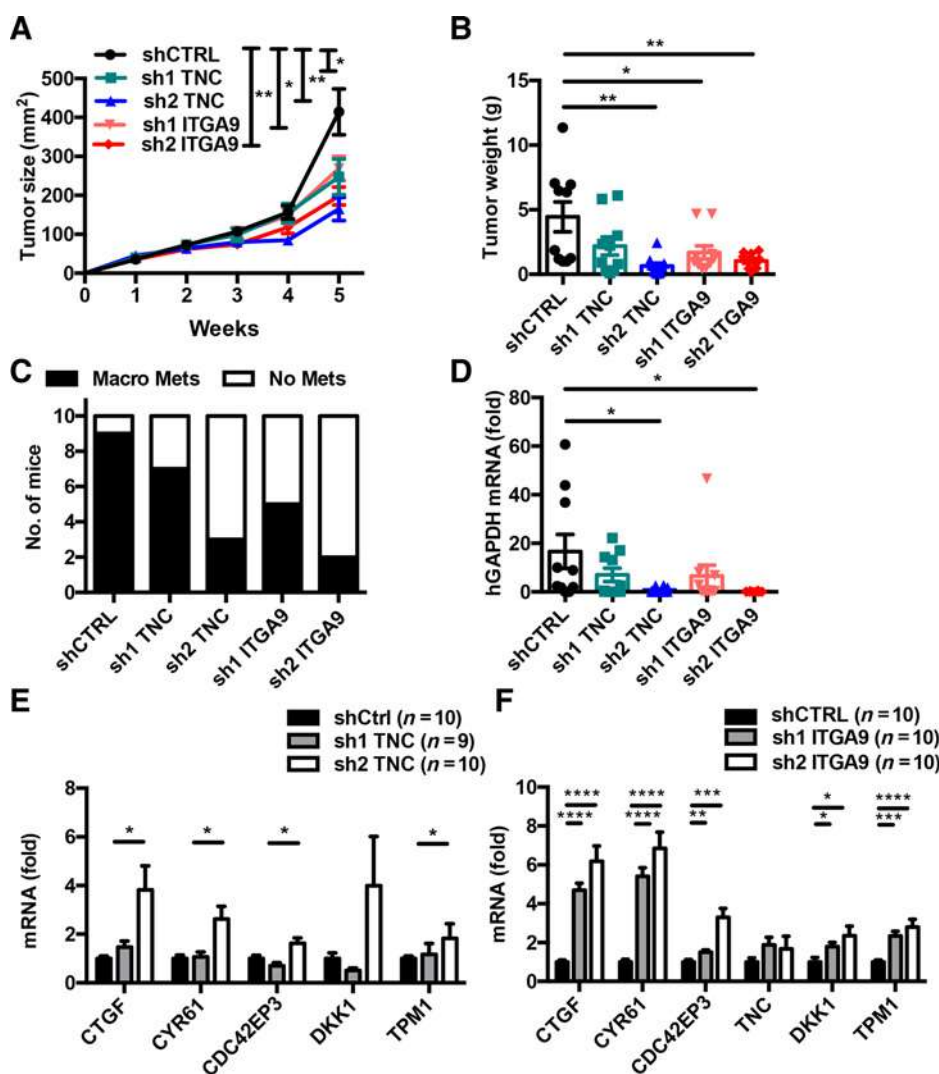
Figure 5.
TNC and integrin α9β1 increase subcutaneous tumor growth, enhance lung metastasis, and reduce YAP target gene expression *in vivo*. Results for KRIB cells are shown. Growth curves (**A**) and weight (**B**) of subcutaneous tumors arising from control, *TNC,* and *ITGA9* knockdown cells are shown. **C,** Number of mice with and without lung macrometastasis in each group. **D,** Metastatic burden is determined by measuring human *GAPDH* in lung tissue of tumor-bearing mice (fold change, qPCR). **E** and **F,** Gene expression levels (qPCR) of the indicated genes in tumors derived from shCTRL, shTNC (**E**), and shITGA9 cells. Ten tumors per group (**A–F**), except for sh1TNC (9 tumors; **E**) mean ± SEM.

YAP signature (41) that was downregulated by TNC (10) in a publicly available mRNA expression dataset of osteosarcoma patients ($n = 53$; GSE 21257) and patient survival (42), but noticed no link (unpublished observation). Yet, when we used the three genes *CTGF, CYR61,* and *CDC42EP3* together, which are strongly repressed by TNC in our cellular and two animal models, we noticed a shorter metastasis-free survival of patients with tumors exhibiting abundant TNC yet below the median tumor level (Fig. 6A; ref. 28). No correlation was seen in tumors with TNC levels above the median (Fig. 6B). Moreover, neither low nor high expression of each gene alone or in different combinations had any predictive value (Supplementary Fig. S8). We also analyzed expression levels of the three-gene signature in a cohort of 46 GBM patient–derived tumor xenografts (PDX) where the gene signature of the experimental tumors correlated with invasiveness and worsened overall GBM patient survival (43). We observed that PDX tumors that had lower expression of *CTGF, CYR61,* and *CDC42EP3* in a context of abundant but TNC expression below the median represent a group of GBM patients with worsened progression-free survival (Supplementary Fig. S9A and S9B). Low expression of either gene alone or in combinations

of three had no relevance for patient prognosis (Supplementary Fig. S10). Altogether, we identified a short list of TNC-downregulated YAP target genes with correlation to worse prognosis in osteosarcoma and GBM patients.

Discussion

By using LOF and GOF approaches (Supplementary Table S3; Supplementary Fig. S9C), here we have shown a novel function of TNC in cancer. Our results suggest that TNC/integrin α9β1 signaling destroys actin stress fibers, thus inhibiting YAP, which promotes migration with amoeboid-like properties and metastasis. In addition to surface-adsorbed TNC, endogenously expressed TNC also promotes transwell migration, suggesting an autocrine, in addition to a paracrine, TNC/integrin α9β1 signaling loop. This mechanism may be relevant in tumors as we observed an increased expression of YAP target genes in grafted osteosarcoma cell–derived tumors upon knockdown of *TNC* and *ITGA9,* respectively. Remarkably, knockdown tumors also caused less lung metastasis, suggesting that TNC/integrin α9β1 signaling is enhancing lung metastasis. Our observations suggest that TNC
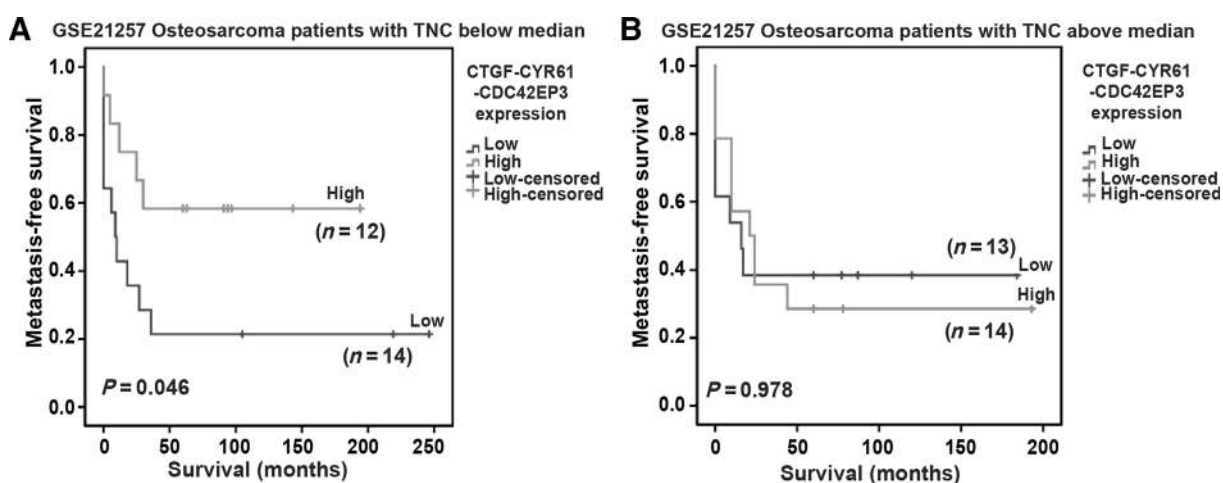
Figure 6.
The Kaplan–Meier survival analysis in osteosarcoma patients. The Kaplan–Meier survival analysis of patients with osteosarcoma upon stratification into tumors with abundant *TNC* expression below the median (**A**) and above the median (**B**) in combination with low (below the median) and high (above the median) expression of *CTGF*, *CYR61*, and *CDC42EP3*. The number of patients in each group is indicated within brackets, and *P* values indicate the significance of survival differences between the groups of individuals by the log-rank test.

matters in tumors as soon as it is expressed where promotion of tumor cell migration may be an important and early mechanism driving tumor malignancy (Fig. 7).

As it was incompletely understood how TNC regulates gene expression and migration through cell adhesion, here we have revisited the effect of TNC on cell adhesion in the context of FN. TNC competes syndecan-4 binding to FN, thus blocking integrin α5β1–mediated cell adhesion and actin stress fiber formation (9), which results in a protumorigenic gene expression profile and repression of multiple cell adhesion–associated genes (10). Here, we have identified the two actin cytoskeleton sensors MKL1 and YAP to be impaired by TNC, which leads to repression of target genes. We identified three groups of genes that TNC represses through its impact on MKL1 (*TPM1*), YAP (*CTGF*, *CYR61*) or MKL1, and YAP (*CDC42EP3*, *TNC*, and *DKK1*). Most importantly, through inhibition of YAP, TNC promotes transwell migration (Fig. 7; Supplementary Fig. S9C).

TNC migration has amoeboid-like properties (38) as cells migrate through a collagen gel in a TNC-dependent manner, whereas invasion through Matrigel is unaffected by TNC. Moreover, cells display an amoeboid-like phenotype such as a round morphology, lack of actin stress fibers and focal adhesions, inactive FAK and paxillin (9, 10, 28, 44, 19), and ROCK dependence (38), as inhibition of ROCK blocked TNC-mediated transwell migration. We have identified integrin α9β1 as novel upstream regulator of TNC-induced migration. Integrin α9β1 is known as receptor for TNC (39), and the TNC/integrin α9β1 interaction was recently shown to play a role in attraction of prostate cancer cells to bone tissue (45). Yet nothing was known how this interaction affects gene expression, cell migration, or metastasis. Here, we have demonstrated for the first time that integrin α9β1 is promoting amoeboid-like migration by TNC. Moreover, we link migration by TNC through integrin α9β1 to destruction of actin stress fibers and inhibition of YAP, which may be relevant for metastasis, as knockdown of either molecule reduces lung metastasis of grafted osteosarcoma cells.
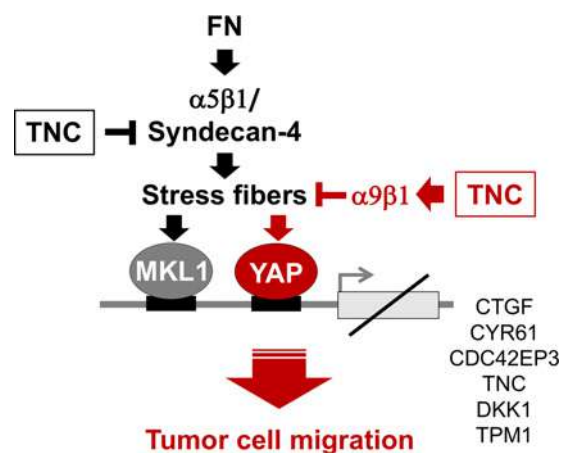
Figure 7.
Summary of TNC effects on actin polymerization, gene expression, and tumor cell migration. Upon cell adhesion to FN through integrin α5β1/syndecan-4, cells establish actin stress fibers. MKL1 and YAP are two sensors of actin dynamics. In the presence of actin stress fibers, both molecules are translocated to the nucleus where they act as cotranscription factors. TNC impairs actin polymerization and actin stress fiber formation in cells grown on FN by inhibiting integrin α5β1/syndecan-4 signaling (10). As we showed here, TNC also inhibits actin stress fiber formation through integrin α9β1. By GOF and LOF experiments, we discovered that TNC downregulates some genes through impairing MKL1 (*TPM1*) or YAP (*CTGF*, *CYR61*) or MKL1 and YAP (*TNC*, *CDC42EP3*, and *DKK1*). TNC impairs MKL1 expression and nuclear translocation of YAP, respectively. Integrin α9β1 signaling is induced by a TNC substratum as well as by tumor cell–expressed TNC, suggesting an autocrine and paracrine mechanism of action. TNC/integrin α9β1 signaling causes YAP impairment and repression of YAP target genes *CTGF*, *CYR61*, and *CDC42EP3*, thus promoting transwell migration. Our results indicate that inhibition of YAP is a prerequisite for TNC-induced amoeboid-like migration. This mechanism may have clinical relevance as patients with osteosarcoma that have abundant yet *TNC* levels below the median together with low levels of *CTGF*, *CYR61*, and *CDC42EP3* have worst prognosis.

318

Sun et al.

In tumor tissue, TNC is often coexpressed together with FN and other ECM molecules forming matrix tracks that serve as niches for tumor and stromal cells (6). These matrix-dense areas may increase tissue stiffness and cellular tension due to multiple integrin-binding opportunities. Indeed, in GBM, high TNC levels were correlated with increased tissue stiffness (8). TNC may locally reduce cellular tension by counteracting adhesive signals by inhibiting syndecan-4 or activating integrin α9β1 (Fig. 7). In addition, we have shown that TNC downregulates its own expression. Thus, TNC is an ideal candidate to balancing cellular tension in cancer tissue.

We had investigated whether expression of TNC-downregulated genes correlates with cancer patient survival. Indeed, low expression of three YAP target genes, *CTGF*, *CYR61*, and *CDC42EP3* (that are strongly repressed by TNC in our *in vitro* and *in vivo* models), correlates with worst prognosis of patients with osteosarcoma and GBM when TNC is below the median expression. It has to be stressed that these TNC levels are still considerably high, as normal tissue poorly, if at all, expresses TNC (28). High TNC levels are correlated with bad patient survival (46), and lower TNC levels are presumed to indicate a better prognosis (10, 47). Yet, some patients with lower TNC levels are still at high risk to die of their cancer, suggestive of a subgroup of yet unidentified patients with bad prognosis. Our result provides an opportunity to predict prognosis of osteosarcoma and glioma patients with moderate TNC expression, in particular when PDX expression data for GBM are available. Although tumors grown in a patient and in a mouse obviously differ, it is remarkable that the expression data from the PDX tumors have predictive value for GBM patient prognosis. Altogether, GBM patients with moderate TNC expression below the median, which usually are not considered to have a bad prognosis, may be recognized thanks to combined low expression of *CTGF*, *CYR61*, and *CDC42EP3* in their PDX. Similarly, our predictive gene expression signature may allow identifying osteosarcoma patients with worse prognosis and in need of more forceful treatment.

As TNC expression is regulated by MKL1 and YAP, ablation of these activities may be considered for targeting TNC expression and its tumor-promoting effects. Yet, our results suggest that inhibition of YAP may be detrimental, as cells with inactive YAP may be highly motile and metastatic in a TNC context. We believe that integrin α9β1 provides a better targeting opportunity, as inhibiting integrin α9β1 reduces tumor cell migration and metastasis.

Disclosure of Potential Conflicts of Interest

No potential conflicts of interest were disclosed.

Authors' Contributions

Conception and design: Z. Sun, A. Schwenzer, T. Rupp, T. Hussenet, G. Orend
Development of methodology: Z. Sun, A. Schwenzer, T. Rupp
Acquisition of data (provided animals, acquired and managed patients, provided facilities, etc.): Z. Sun, A. Schwenzer, T. Rupp, D. Murdamoothoo, R. Vegliante, O. Lefebvre
Analysis and interpretation of data (e.g., statistical analysis, biostatistics, computational analysis): Z. Sun, A. Schwenzer, T. Rupp, D. Murdamoothoo, R. Vegliante, G. Orend
Writing, review, and/or revision of the manuscript: Z. Sun, A. Schwenzer, T. Rupp, G. Orend
Administrative, technical, or material support (i.e., reporting or organizing data, constructing databases): Z. Sun, T. Rupp
Study supervision: G. Orend
Other (financing of study): G. Orend

References

1. Midwood KS, Chiquet M, Tucker RP, Orend G. Tenascin-C at a glance. J Cell Sci 2016;129:4321–7.
2. Oskarsson T, Acharyya S, Zhang XH-F, Vanharanta S, Tavazoi SF, Morris PG, et al. Breast cancer cells produce tenascin C as a metastatic niche component to colonize the lungs. Nat Med 2011;17:867–74.
3. Saupe F, Schwenzer A, Jia Y, Gasser I, Spenlé C, Langlois B, et al. Tenascin-C downregulates Wnt inhibitor dickkopf-1, promoting tumorigenesis in a neuroendocrine tumor model. Cell Rep 2013;5:482–92.
4. Langlois B, Saupe F, Rupp T, Arnold C, Van der Heyden M, Orend G, et al. AngioMatrix, a signature of the tumor angiogenic switch-specific matrisome, correlates with poor prognosis for glioma and colorectal cancer patients. Oncotarget 2014;5:10529–45.
5. Rupp T, Langlois B, Koczorowska MM, Radwanska A, Sun Z, Hussenet T, et al. Tenascin-C orchestrates glioblastoma angiogenesis by modulation of pro- and anti-angiogenic signaling. Cell Rep 2016;17:2607–19.
6. Spenlé C, Gasser I, Saupe F, Janssen KP, Arnold C, Klein A, et al. Spatial organization of the tenascin-C microenvironment in experimental and human cancer. Cell Adh Migr 2015;9:4–13.
7. Imanaka-Yoshida K, Aoki H. Tenascin-C and mechanotransduction in the development and diseases of cardiovascular system. Front Physiol 2014;5.
8. Miroshnikova YA, Mouw JK, Barnes JM, Pickup MW, Lakins JN, Kim Y, et al. Tissue mechanics promote IDH1-dependent HIF1α-tenascin C feedback to regulate glioblastoma aggression. Nat Cell Biol 2016;18:1336–45.
9. Huang W, Chiquet-Ehrismann R, Moyano JV, Garcia-Pardo A, Orend G. Interference of tenascin-C with syndecan-4 binding to fibronectin blocks cell adhesion and stimulates tumor cell proliferation. Cancer Res 2001; 61:8586–94.
10. Ruiz C, Huang W, Hegi ME, Lange K, Hamou MF, Fluri E. Differential gene expression analysis reveals activation of growth promoting signaling pathways by tenascin-C. Cancer Res 2004;64:7377–85.
11. Miralles F, Posern G, Zaromytidou AI, Treisman R. Actin dynamics control SRF activity by regulation of its coactivator MAL. Cell 2003; 113:329–42.
12. Dupont S, Morsut L, Aragona M, Enzo E, Giulitti S, Cordenonsi M, et al. Role of YAP/TAZ in mechanotransduction. Nature 2011;474:179–83.
13. Wada KI, Itoga K, Okano T, Yonemura S, Sasaki H. Hippo pathway regulation by cell morphology and stress fibers. Development 2011;138: 3907–14.
14. Olson EN, Nordheim A. Linking actin dynamics and gene transcription to drive cellular motile functions. Nat Rev Mol Cell Biol 2010;11:353–65.

319

15. Gurbuz I, Ferralli J, Roloff T, Chiquet-Ehrismann R, Asparuhova MB. SAP domain-dependent Mkl1 signaling stimulates proliferation and cell migration by induction of a distinct gene set indicative of poor prognosis in breast cancer patients. Mol Cancer 2014;13:22.

16. Zhao B, Li L, Lei Q, Guan KL. The Hippo-YAP pathway in organ size control and tumorigenesis: an updated version. Genes Dev 2010;24: 862–74.

17. Halder G, Dupont S, Piccolo S. Transduction of mechanical and cytoskeletal cues by YAP and TAZ. Nat Rev Mol Cell Biol 2012;13:591–600.

18. Berlin Ö, Samid D, Donthineni-Rao R, Akeson W, Amiel D, Woods VL. Development of a novel spontaneous metastasis model of human osteosarcoma transplanted orthotopically into bone of athymic mice. Cancer Res 1993;53:4890–5.

19. Lange K, Kammerer M, Hegi ME, Grotegut S, Dittmann A, Huang W, et al. Endothelin receptor type B counteracts tenascin-C-induced endothelin receptor type A-dependent focal adhesion and actin stress fiber disorganization. Cancer Res 2007;67:6163–73.

20. Lamar JM, Stern P, Liu H, Schindler JW, Jiang ZG, Hynes RO. The Hippo pathway target, YAP, promotes metastasis through its TEAD-interaction domain. Proc Natl Acad Sci U S A 2012;109:E2441–50.

21. Lehmann S, te Boekhorst V, Odenthal J, Bianchi R, van Helvert S, Ikenberg K, et al. Hypoxia induces a HIF-1-dependent transition from collective-to-amoeboid dissemination in epithelial cancer cells. Curr Biol 2017;27:392–400.

22. Wolf K, Alexander S, Schacht V, Coussens LM, von Andrian UH, van Rheenen J, et al. Collagen-based cell migration models in vitro and in vivo. Semin Cell Dev Biol 2009;20:931–41.

23. Subramanian A, Tamayo P, Mootha VK, Mukherjee S, Ebert BL, Gillette MA, et al. Gene set enrichment analysis: a knowledge-based approach for interpreting genome-wide expression profiles. Proc Natl Acad Sci U S A 2005;102:15545–50.

24. Zhao B, Ye X, Yu J, Li L, Li W, Li S, et al. TEAD mediates YAP-dependent gene induction and growth control. Genes Dev 2008;22:1962–71.

25. Descot A, Hoffmann R, Shaposhnikov D, Reschke M, Ullrich A, Posern G. Negative regulation of the EGFR-MAPK cascade by actin-MAL-mediated Mig6/Errfi-1 induction. Mol Cell 2009;35:291–304.

26. Chiquet-Ehrismann R, Kalla P, Pearson CA, Beck K, Chiquet M. Tenascin interferes with fibronectin action. Cell 1988;53:383–90.

27. Van Obberghen-Schilling E, Tucker RP, Saupe F, Gasser I, Cseh B, Orend G. Fibronectin and tenascin-C: accomplices in vascular morphogenesis during development and tumor growth. Int J Dev Biol 2011;55:511–25.

28. Lange K, Kammerer M, Saupe F, Hegi ME, Grotegut S, Fluri E, et al. Combined lysophosphatidic acid/platelet-derived growth factor signaling triggers glioma cell migration in a tenascin-C microenvironment. Cancer Res 2008;68:6942–52.

29. Selvaraj A, Prywes R. Expression profiling of serum inducible genes identifies a subset of SRF target genes that are MKL dependent. BMC Mol Biol 2004;5:13.

30. Lee SM, Vasishtha M, Prywes R. Activation and repression of cellular immediate early genes by serum response factor cofactors. J Biol Chem 2010;285:22036–49.

31. Asparuhova MB, Ferralli J, Chiquet M, Chiquet-Ehrismann R. The transcriptional regulator megakaryoblastic leukemia-1 mediates serum response factor-independent activation of tenascin-C transcription by mechanical stress. FASEB J 2011;25:3477–88.

32. Seo E, Basu-Roy U, Gunaratne PH, Coarfa C, Lim DS, Basilico C, et al. SOX2 regulates YAP1 to maintain stemness and determine cell fate in the osteo-adipo lineage. Cell Rep 2013;3:2075–87.

33. Calvo F, Ege N, Grande-Garcia A, Hooper S, Jenkins RP, Chaudhry SI, et al. Mechanotransduction and YAP-dependent matrix remodelling is required for the generation and maintenance of cancer-associated fibroblasts. Nat Cell Biol 2013;15:637–46.

34. Wakatsuki T, Schwab B, Thompson NC, Elson EL. Effects of cytochalasin D and latrunculin B on mechanical properties of cells. J Cell Sci 2001;114: 1025–36.

35. Visegrády B, Lőrinczy D, Hild G, Somogyi B, Nyitrai M. The effect of phalloidin and jasplakinolide on the flexibility and thermal stability of actin filaments. FEBS Lett 2004;565:163–6.

36. Nobes CD, Hall A. Rho, rac, and cdc42 GTPases regulate the assembly of multimolecular focal complexes associated with actin stress fibers, lamellipodia, and filopodia. Cell 1995;81:53–62.

37. Willier S, Butt E, Grunewald TGP. Lysophosphatidic acid (LPA) signalling in cell migration and cancer invasion: a focussed review and analysis of LPA receptor gene expression on the basis of more than 1700 cancer microarrays. Biol Cell 2013;105:317–33.

38. Pan?ková K, Rösel D, Novotný M, Brábek J. The molecular mechanisms of transition between mesenchymal and amoeboid invasiveness in tumor cells. Cell Mol Life Sci 2010;67:63–71.

39. Yokosaki Y, Matsuura N, Higashiyama S, Murakami I, Obara M, Yamakido M. Identification of the ligand binding site for the integrin alpha9 beta1 in the third fibronectin type III repeat of tenascin-C. J Biol Chem 1998;273: 11423–8.

40. Kon S, Uede T. The role of α9β1 integrin and its ligands in the development of autoimmune diseases. J Cell Commun Signal 2017 Oct 3. Epub ahead of print.

41. Zanconato F, Forcato M, Battilana G, Azzolin L, Quaranta E, Bodega B, et al. Genome-wide association between YAP/TAZ/TEAD and AP-1 at enhancers drives oncogenic growth. Nat Cell Biol 2015;17:1218–27.

42. Buddingh EP, Kuijjer ML, Duim RAJ, Bürger H, Agelopoulos K, Myklebost O, et al. Tumor-infiltrating macrophages are associated with metastasis suppression in high-grade osteosarcoma: a rationale for treatment with macrophage activating agents. Clin Cancer Res 2011;17:2110–9.

43. Joo KM, Kim J, Jin J, Kim M, Seol HJ, Muradov J, et al. Patient-specific orthotopic glioblastoma xenograft models recapitulate the histopathology and biology of human glioblastomas in situ. Cell Rep 2013;3:260–73.

44. Orend G, Huang W, Olayioye MA, Hynes NE, Chiquet-Ehrismann R. Tenascin-C blocks cell-cycle progression of anchorage-dependent fibroblasts on fibronectin through inhibition of syndecan-4. Oncogene 2003;22:3917–26.

45. San Martin R, Pathak R, Jain A, Jung SY, Hilsenbeck SG, Pin?a-Barba MC, et al. Tenascin-C and integrin α9 mediate interactions of prostate cancer with the bone microenvironment. Cancer Res 2017;77:5977–88.

46. Midwood KS, Hussenet T, Langlois B, Orend G. Advances in tenascin-C biology. Cell Mol Life Sci 2011;68:3175–99.

47. Ishihara A, Yoshida T, Tamaki H, Sakakura T. Tenascin expression in cancer cells and stroma of human breast cancer and its prognostic significance. Clin Cancer Res 1995;1:1035–41.

320

Cancer Research

The Journal of Cancer Research (1916-1930) | The American Journal of Cancer (1931-1940)

AAC⊖R American Association for Cancer Research

Tenascin-C Promotes Tumor Cell Migration and Metastasis through Integrin α9β1–Mediated YAP Inhibition

Zhen Sun, Anja Schwenzer, Tristan Rupp, et al.

Updated version	Access the most recent version of this article at: doi:10.1158/0008-5472.CAN-17-1597
Supplementary Material	Access the most recent supplemental material at: http://cancerres.aacrjournals.org/content/suppl/2017/12/19/0008-5472.CAN-17-1597.DC1

Cited articles	This article cites 45 articles, 18 of which you can access for free at: http://cancerres.aacrjournals.org/content/78/4/950.full#ref-list-1

E-mail alerts	Sign up to receive free email-alerts related to this article or journal.
Reprints and Subscriptions	To order reprints of this article or to subscribe to the journal, contact the AACR Publications Department at pubs@aacr.org.
Permissions	To request permission to re-use all or part of this article, use this link http://cancerres.aacrjournals.org/content/78/4/950. Click on "Request Permissions" which will take you to the Copyright Clearance Center's (CCC) Rightslink site.

Appendix IV

Cell Reports

Tenascin-C Orchestrates Glioblastoma Angiogenesis by Modulation of Pro- and Anti-angiogenic Signaling

Graphical Abstract
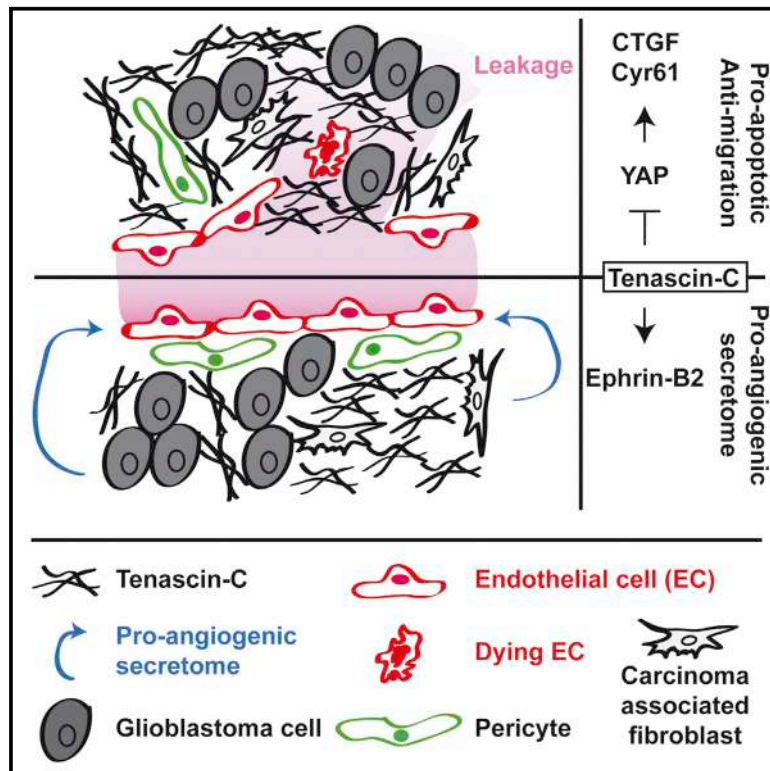
Authors

Tristan Rupp, Benoit Langlois, Maria M. Koczorowska, ..., Oliver Schilling, Ellen Van Obberghen-Schilling, Gertraud Orend

Correspondence

gertraud.orend@inserm.fr

In Brief

Rupp et al. report a dual role for tenascin-C that results in a poorly functional glioblastoma vasculature. Tenascin-C blocks YAP pro-survival signaling in endothelial cells through direct contact. In glioblastoma cells, tenascin-C induces a pro-angiogenic secretome that correlates with poor glioma patient survival. Targeting the ephrin-B2/EPHB4 axis impairs tenascin-C pro-tumoral activities.

Accession Numbers

PXD005217

Highlights

- Contact with tenascin-C blocks YAP signaling and endothelial cell behavior

- Tenascin-C induces ephrin-B2 and a pro-angiogenic secretome in glioblastoma cells

- Inhibiting ephrin-B2 signaling impairs tenascin-C pro-angiogenic activities

- The tenascin-C secretome signature correlates with poor glioma patient prognosis

CrossMark

CellPress

Tenascin-C Orchestrates Glioblastoma Angiogenesis by Modulation of Pro- and Anti-angiogenic Signaling

Tristan Rupp,[1,2,3,4,9] Benoit Langlois,[1,2,5,4,9] Maria M. Koczorowska,[5,6,7] Agata Radwanska,[8] Zhen Sun,[1,2,3,4]
Thomas Hussenet,[1,2,3,4] Olivier Lefebvre,[1,2,3,4] Devadarssen Murdamoothoo,[1,2,3,4] Christiane Arnold,[1,2,3,4]
Annick Klein,[1,2,3,4] Martin L. Biniossek,[5] Vincent Hyenne,[1,2,3,4] Elise Naudin,[1,2,3,4] Ines Velazquez-Quesada,[1,2,3,4]
Oliver Schilling,[5,6,7] Ellen Van Obberghen-Schilling,[8] and Gertraud Orend[1,2,3,4,10,*]
[1]The Microenvironmental Niche in Tumorigenesis and Targeted Therapy, INSERM U1109 - MN3T, 3 Avenue Molière, 67200 Strasbourg,
France
[2]Université de Strasbourg, 67000 Strasbourg, France
[3]LabEx Medalis, Université de Strasbourg, 67000 Strasbourg, France
[4]Fédération de Médecine Translationnelle de Strasbourg (FMTS), 67000 Strasbourg, France
[5]Institute of Molecular Medicine and Cell Research, University of Freiburg, 79104 Freiburg, Germany
[6]BIOSS Centre for Biological Signalling Studies, University of Freiburg, 79104 Freiburg, Germany
[7]German Cancer Consortium (DKTK), German Cancer Research Center (DKFZ), 69120 Heidelberg, Germany
[8]iBV, INSERM, CNRS, Université Côte d'Azur, 06108 Nice, France
[9]Co-first author
[10]Lead Contact
*Correspondence: gertraud.orend@inserm.fr
http://dx.doi.org/10.1016/j.celrep.2016.11.012

SUMMARY

High expression of the extracellular matrix component tenascin-C in the tumor microenvironment correlates with decreased patient survival. Tenascin-C promotes cancer progression and a disrupted tumor vasculature through an unclear mechanism. Here, we examine the angiomodulatory role of tenascin-C. We find that direct contact of endothelial cells with tenascin-C disrupts actin polymerization, resulting in cytoplasmic retention of the transcriptional coactivator YAP. Tenascin-C also downregulates YAP pro-angiogenic target genes, thus reducing endothelial cell survival, proliferation, and tubulogenesis. Glioblastoma cells exposed to tenascin-C secrete pro-angiogenic factors that promote endothelial cell survival and tubulogenesis. Proteomic analysis of their secretome reveals a signature, including ephrin-B2, that predicts decreased survival of glioma patients. We find that ephrin-B2 is an important pro-angiogenic tenascin-C effector. Thus, we demonstrate dual activities for tenascin-C in glioblastoma angiogenesis and uncover potential targeting and prediction opportunities.

INTRODUCTION

Angiogenesis is a crucial mechanism driving vessel formation from pre-existing blood vessels. In the tumor microenvironment (TME), the angiogenic behavior of endothelial cells (ECs) relies on dynamic interactions between stromal and tumor cells and their extracellular matrix (ECM) and soluble factors (Bissell and Radisky,

2001). The balance of angio-modulatory molecules secreted by tumor and stromal cells, drives vessel expansion that results in a highly tortuous vasculature that promotes tumor invasion and metastasis (Hanahan and Weinberg, 2011). Exploiting this knowledge for tumor targeting, with the intention of starving the tumor or normalizing the vessels for better drug delivery, at best results in poor improvement of cancer patient survival (Jain, 2014).

In the TME, ECM molecules surrounding tumor and stromal cells exert both scaffolding and signaling roles. ECM molecules trigger cell signaling through activation of specific cell adhesion receptors, modulate access to soluble factors, and alter the mechanical properties of the tissue (Hynes, 2009). Moreover, ECM molecules can have both pro- and anti-angiogenic effects (Campbell et al., 2010). Tenascin-C (TNC) is a selectively expressed glycoprotein. Despite prominent expression in the embryo, TNC is mostly absent from healthy tissues. However, TNC is highly expressed in pathological contexts, including cancer, where angiomodulatory functions have been described (Midwood et al., 2011). In the RIP1-Tag2 neuroendocrine tumor model (Hanahan, 1985), TNC contributes to the angiogenic switch and is highly induced during the early stages of tumor progression together with a list of expressed ECM genes, defined as the AngioMatrix signature, that correlates with poor prognosis in glioma patients (Langlois et al., 2014). High TNC levels are also correlated with higher tumor vessel density, decreased pericyte coverage, and vessel leakiness, suggesting that TNC plays multiple roles in angiogenesis with potentially opposing functions (Saupe et al., 2013). Beyond apparently contradictory results (reviewed in Midwood et al., 2011, 2016; Orend et al., 2014), the molecular mechanisms underlying these functions remain unclear.

Here, we examine the effects of TNC on tumor angiogenesis, uncovering a direct anti-angiogenic effect on ECs and a paracrine pro-angiogenic effect on tumor cells and cancer-associated
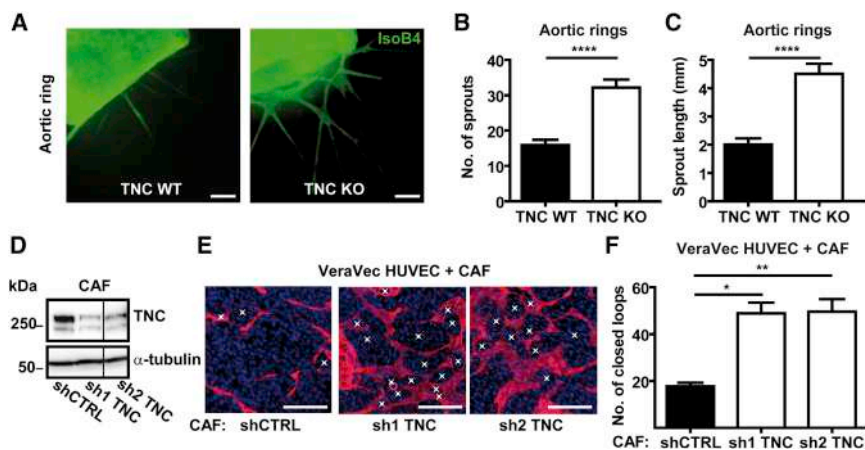
Figure 1. TNC Represses Angiogenic Sprouting and Tubulogenesis

(A) Representative images of vessel sprouts from TNC WT and TNC KO aortic rings upon staining with isolectin B4 (scale bar, 150 μm).

(B and C) Quantification of the number (B) and length (C) of aortic sprouts. Bars represent mean ± SEM. n = 9 mice per genotype; TNC WT, 105 aortic rings; TNC KO, 123 aortic rings.

(D) Immunoblot of CAF shCTRL, sh1 TNC, and sh2 TNC for TNC and α-tubulin.

(E and F) Tubulogenesis in a coculture assay of VeraVec HUVECs with CAF shCTRL, sh1 TNC, or sh2 TNC after 7 days; representative images (scale bar, 200 μm) (E) and quantification of the number of endothelial closed loops (F) are shown. Vessel-like structures were stained with an anti-CD31 antibody (red). Nuclei are visualized upon staining with DAPI (blue).

Values are mean ± SEM from three independent experiments with three replicates. See also Figure S1.

fibroblasts (CAFs). We identify ephrin-B2 as major factor induced by TNC in glioblastoma cells that promotes angiogenesis. This information is of potential interest, since blocking TNC-driven aberrant vascularization may combat tumor progression.

RESULTS

Inhibitory Effect of Tenascin-C on Vessel Sprouting

To determine the dependence of sprouting angiogenesis on TNC expression, we used aortic rings prepared from TNC wild-type (WT) and TNC knockout (KO) mice in which TNC expression was detected by immunoblotting (Figure S1A). Endothelial sprouts were composed of ECs and mural cells positively stained by immunofluorescence (IF) analysis for isolectin B4 and α smooth muscle actin (α-SMA), respectively (Figure S1B). We observed that the number and length of endothelial sprouts was higher in the absence of TNC, suggesting a negative effect of TNC on vessel formation in this assay (Figures 1A–1C). We next analyzed the impact of TNC on physiological angiogenesis in the retina of WT and TNC KO mice. Importantly, we did not detect TNC expression in WT retinas by IF (Figure S1C). Whereas the expansion of the vascular network (at postnatal day 5.5 [P5.5]) was slightly reduced (<5%, p = 0.0435) in TNC KO retinas, the number of branching points and the endothelial filopodia density remained similar, suggesting that TNC plays a minor role if any in this physiological angiogenic process (Figures S1D–S1J).

Fibroblasts have been described to promote tumor angiogenesis. They are also a prominent source of TNC in cancer (Kalluri and Zeisberg, 2006). We used a recently described 3D tubulogenesis model in which coculture of CAFs with ECs mimics their proximity in a tumor (Ghajar et al., 2013). Here, human CAFs, as provider of TNC and engineered to express reduced TNC levels by small hairpin RNA (shRNA) (Figure 1D), were coseeded together with human umbilical vein endothelial cells (HUVECs). We observed that TNC-deficient CAFs induced more closed EC loops than control CAFs (Figures 1E and 1F). None of the five hu-

man EC types tested (Figures S1K and S1L) or bovine aortic endothelial cells (BAECs) (unpublished data) expressed TNC at the protein level in normal culture conditions. Moreover, stimulation by different ECM substrata or treatment with pro-angiogenic vascular endothelial growth factor A (VEGFA) and the TNC-inducing molecule transforming growth factor β1 (TGF-β1) (Scharenberg et al., 2014) (Figures S1L and S1M) did not induce TNC in HUVECs, suggesting that TNC secreted by CAFs repressed endothelial tubulogenesis in the coculture assay.

Direct Exposure to Tenascin-C Represses Tubulogenesis, Adhesion, and Migration of Endothelial Cells

So far, our results suggest that expression of TNC negatively influences endothelial sprouting and tubulogenesis, which could be a result of a direct interaction with TNC. To address whether contact between ECs and TNC had an impact on tubulogenic activity, we plated HUVECs and BAECs on Matrigel together with purified recombinant TNC. Both the length of HUVEC capillary-like structures and the number of closed loops were reduced by TNC in a dose-dependent manner (Figures 2A–2C). TNC also reduced the number of closed loops formed by BAECs (Figures S2A and S2B). Thus, TNC contact has a negative influence on the tubulogenic behavior of ECs.

As both adhesion and migration are involved in tubulogenesis (Lamalice et al., 2007), we analyzed the effect of TNC on these processes in ECs. Indeed, HUVEC and BAEC adhesion was impaired by a TNC substratum compared to fibronectin (FN) or type I collagen (Col I) (Figures 2D–2F). In addition, cell migration of HUVECs and BAECs was reduced in a wound-healing assay in a TNC dose-dependent manner (Figures 2G–2J). Moreover, invasion of HUVECs through a Col I gel was repressed by TNC (Figures 2K and 2L).

Pericyte recruitment around newly formed blood vessels constitutes an important step in vessel maturation. Tumor blood vessels display less pericyte coverage, which contributes to vessel leakiness (McDonald and Choyke, 2003), and this effect is

enhanced by TNC in an insulinoma mouse model (Saupe et al., 2013). We addressed if and how TNC affects human brain vascular pericyte (HBVP) behavior. Whereas pericytes expressed TNC, which can be enhanced by TGF-β (Figure S2C), we observed that similarly to ECs, only a few pericytes adhered to the TNC substratum (Figures 2D and 2M). Furthermore, wound closure of a pericyte monolayer was largely impaired by TNC in a dose-dependent manner (Figures 2N and 2O), suggesting a similar inhibitory effect of TNC on pericyte migration.

Tenascin-C Impairs Survival of Endothelial Cells

We also investigated if and how TNC affected EC proliferation using an MTS incorporation assay. Whereas HUVECs and BAECs proliferated on FN and Col I over 3 days, their growth only slightly increased on TNC in the same time frame, demonstrating an inhibitory effect of TNC (Figures 3A and 3B) that was dose dependent (Figure S3A). In contrast to ECs, despite delayed cell adhesion on TNC, the growth of pericytes over time was unaffected by TNC (Figure 3C).

In the TME, cells interact with their ECM in a 3D context. Moreover, 3D models exhibit properties such as mechanical compliance and immobilization of growth factors that are closer to the complexity found in tissues (Beacham et al., 2007). Here, we generated a 3D cell-derived matrix (CDM) as described previously (Beacham et al., 2007) (Figure S3B) that was assembled by mouse embryonic fibroblasts (MEFs) derived from TNC KO (TNC−) or TNC WT (TNC+) mice. We confirmed that CDM from TNC KO MEFs was devoid of TNC and that both CDMs presented a similar fibrillar ECM network comprising FN, periostin, and Col I (Figure S3C). Growth of both EC types tested (HUVECs and BAECs) was higher on TNC -deficient CDM than on the CDM containing the TNC protein (Figures 3D and 3E). Similarly BAEC growth was reduced on CDM generated by CAFs with TNC knockdown (KD) (shTNC) when compared with control (shCTRL) cells (Figure S3D), whereas pericyte growth was unaffected (Figure 3F). These findings recapitulate the inhibitory effect of TNC on the growth of ECs on a 2D TNC substratum.

Inhibition of cell growth by TNC could depend on an altered balance of survival and proliferation, which we tested by plating HUVECs on either purified ECM coatings or CDM. Indeed, TNC-containing substrata increased EC apoptosis, as illustrated by the increased number of cleaved-caspase-3-positive nuclei in the presence of TNC (Figures 3G and 3H). Assessing proliferation by bromodeoxyuridine (BrdU) incorporation revealed a reduction on TNC in comparison to FN and Col I (Figure 3I). Thus, ECs exposed to TNC are prone to apoptosis and show a reduced proliferation rate. This could have an impact on endothelium function, which we tested in an in vitro Boyden chamber permeability assay. We observed that the TNC substratum increased dextran-FITC diffusion across the endothelial monolayer over that of the other ECM coatings (Figure S3E), suggesting that TNC may alter endothelial monolayer integrity in vitro.

Tenascin-C Impairs YAP Signaling through Repression of Actin Polymerization, Causing Downregulation of Pro-angiogenic Molecules and Cell Growth

Signaling associated with the actin cytoskeleton status plays an important role during angiogenesis (Bayless and Johnson, 2011).

Since TNC affects the organization of the actin cytoskeleton in fibroblasts and tumor cells (Midwood et al., 2011), we tested its effect on actin polymerization in ECs. We observed that whereas actin stress fibers are present in HUVECs on Col I and FN substrata, these structures were poorly detectable on TNC (Figures 4A and S4A). Similarly, only few actin stress fibers were seen on CDM containing TNC (TNC+) which was in contrast to cells seeded on CDM lacking TNC (TNC−), where we observed abundant actin stress fiber formation (Figure S4B). Quantification of the relative abundance of filamentous/polymerized (F) versus globular/non-polymerized (G) actin upon fractionation (Posern et al., 2002) showed that 5 hr after seeding on TNC, the ratio of F-actin to G-actin in HUVECs was largely reduced in comparison to FN or Col I (Figures 4B and 4C).

YAP (Yes-associated protein), a sensor of cell shape and regulated by the actin cytoskeleton, acts as a transcriptional integrator of extracellular stimuli (Halder et al., 2012). Upon actin polymerization, YAP translocates into the nucleus, where it binds to members of the TEAD family of transcription factors and induces gene expression (Calvo et al., 2013). We studied subcellular localization of YAP and observed that whereas 85% of HUVECs plated on FN exhibited nuclear YAP, only 12% of cells plated on TNC had nuclear YAP, similar to cells grown on FN in low serum in which YAP is mainly sequestered in the cytoplasm (Calvo et al., 2013) (Figures 4D and 4E).

Connective tissue growth factor (CTGF) and cysteine-rich protein 61 (Cyr61), two pro-angiogenic molecules that promote migration and survival of ECs (Brigstock, 2002), are direct YAP target genes (Halder et al., 2012). qRT-PCR revealed that expression of CTGF and Cyr61 was downregulated in HUVECs grown on the TNC substratum in comparison to FN (Figure 4F). To address whether downregulation of YAP target genes and inhibition of actin polymerization by TNC are functionally linked, we treated HUVECs with lysophosphatidic acid (LPA) to rescue actin stress fiber formation (Siess et al., 1999). Indeed, LPA induced spreading and stress fiber formation (Figure S4C) in the majority of HUVECs plated on TNC (Figure S4D). LPA-induced cell spreading was further associated with a significant increase in HUVEC growth on TNC (Figure 4G) and an elevated expression of CTGF (Figure 4H) and Cyr61 (Figure S4F). The LPA effect was due to a restoration of YAP activity, since it was reversed by YAP KD (Figures 4H, 4I, S4E, and S4F). These results suggested that adhesion to a TNC substratum represses actin polymerization, nuclear localization of YAP, expression of pro-angiogenic factors, and EC growth.

Induction of a Pro-angiogenic Secretome in Tumor Cells and Fibroblasts by Tenascin-C

To analyze a potential paracrine angiogenic activity of TNC, we investigated the effect of TNC on the secretome of glioblastoma (GBM) cells, which abundantly express TNC. We collected conditioned media (CM) from three independent GBM cell lines, namely U87MG, U118MG, and U373MG, that had been grown 48 hr on CDM containing (TNC+) or lacking TNC (TNC−) and then assessed the impact of these CM on HUVEC survival and tubulogenesis. We confirmed by an MTS assay that the CM derived from a similar number of cells (Figure S5A) and that CM of U87MG, U118MG, and U373MG exposed to TNC (present
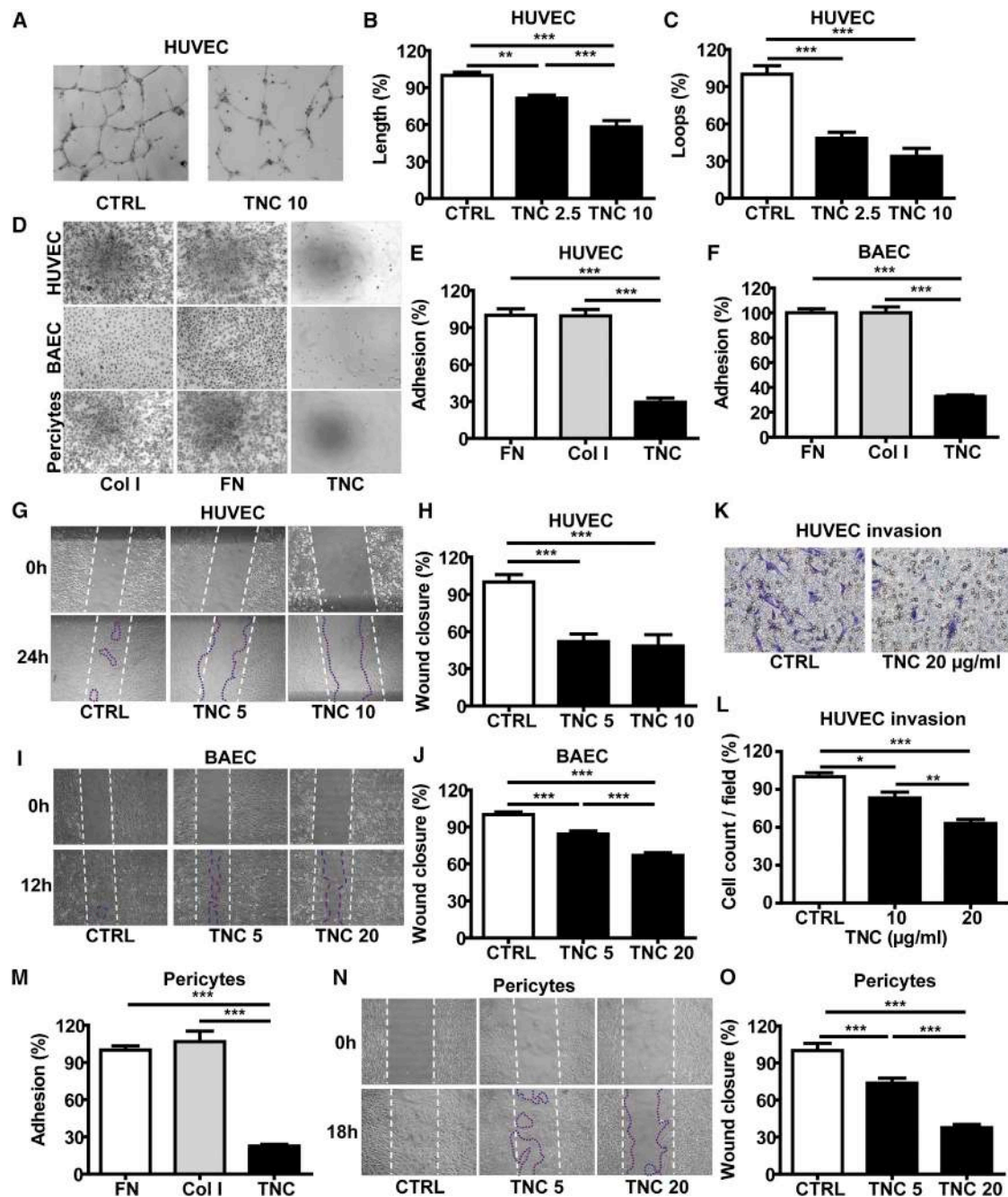
Figure 2. TNC Impairs EC Tubulogenesis, Adhesion, and Migration In Vitro

(A–C) Endothelial network formation in TNC dependence. (A) Representative images of HUVECs 7 hr after plating on Matrigel together with 10 μg/mL TNC or 0.01% Tween 20-PBS as control (CTRL) followed by quantification of the length of capillary like structures (B) and the number of endothelial closed loops (C). Values are mean ± SEM from three independent experiments with five replicates.

(D–F) Representative pictures (D) of HUVEC, BAEC, and pericyte adhesion upon plating cells for 1 hr on wells coated with Col I, FN, and TNC at 1 μg/cm^2 (HUVECs) and 2 μg/cm^2 (pericytes and BAECs) followed by quantification of adherent cells (E and F). Values are mean ± SEM from three independent experiments with six replicates.

(G–J) Wound closure of HUVECs, 24 hr (G and H) and BAECs, 12 hr (I and J) was quantified upon addition of TNC (5, 10, or 20 μg/mL) or 0.01% Tween 20-PBS (CTRL). Values are mean ± SEM from three independent experiments with four replicates.

(K and L) Representative pictures (K) and quantification (L) of HUVEC invasion through Col I gels containing or not containing TNC after 24 hr. Values are mean ± SEM from three independent experiments with three to four replicates.

(legend continued on next page)
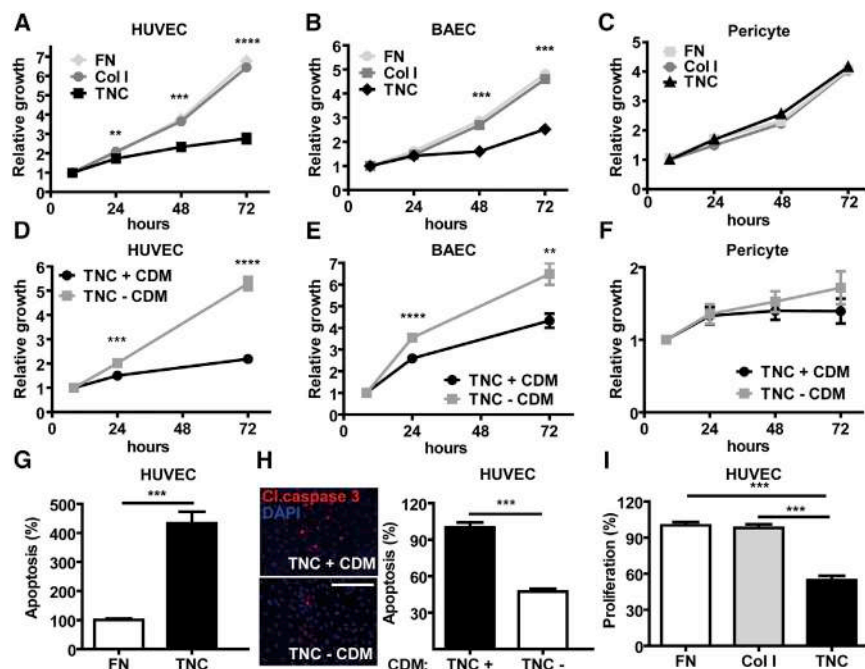
Figure 3. TNC Reduces EC Survival and Proliferation

(A–F) MTS assay for HUVECs (A and D), BAECs (B and E), and pericytes (C and F) upon plating on the indicated ECM molecules (1–2 $\mu g/cm^2$) (A–C) or on CDM derived from TNC KO (TNC−) or WT MEFs (TNC+) (D–F) for up to 72 hr. (A–C) Values are mean ± SEM from five independent experiments with five replicates. (D–F) Values are mean ± SEM in HUVECs (five independent experiments with five or six replicates), BAECs (three independent experiments with three replicates), and pericytes (four independent experiments with six replicates).

(G and H) Assessment of HUVEC apoptosis after 72 hr upon growth on ECM-coated wells (G) or CDM containing (TNC+) or lacking TNC (TNC−). Representative images of IF staining for cleaved caspase-3 (red) and nuclei with DAPI (blue); scale bar, 100 μm (H). Values are mean ± SEM from three independent experiments with four replicates. Four random fields were quantified per replicate.

(I) Assessment of HUVEC proliferation after 48 hr upon growth on ECM-coated wells. Values are mean ± SEM of three independent experiments with six replicates.

See also Figure S3.

in CDM) increased EC loop formation (Figures 5A and S5B). Analysis of cell survival using incorporation of ethidium bromide and acridine orange revealed that the secretome of TNC-exposed GBM cells enhanced HUVEC survival (Figure 5B). An MTS incorporation assay further demonstrated that the TNC-induced secretome increased growth of HUVECs and BAECs (Figures 5C and S5C). Moreover, whereas CM from U87MG cells with a KD of TNC (shRNA) (Figure S5D) did not affect U87MG cell growth (Figure S5E), this CM reduced HUVEC loop numbers on Matrigel (Figures 5D and 5E). Thus, the KD approach confirmed that TNC regulates the expression and secretion of pro-angiogenic molecules in GBM cells.

Next, we determined whether TNC potentially induced a pro-angiogenic secretome also in stromal cells such as fibroblasts. We prepared CM from CAFs that were grown on CDM containing TNC (TNC+) or not (TNC−), which did not affect relative cell growth (Figure S5F). We measured HUVEC cell growth and HUVEC Matrigel tubulogenesis upon addition of these CM. Whereas loop formation was unaffected (Figure S5G), we noticed that HUVEC growth was increased by CM of CAFs exposed to the TNC-rich CDM (Figure 5E). To analyze a potential paracrine mechanism on sprouting angiogenesis, we used a coculture assay (Figure S5H) in which HUVECs and telomerase immortal-ized fibroblasts (TIFs) expressing high or low levels of TNC (KD for TNC [shRNA]) (Figure S5I) were physically separated. Whereas the number of HUVEC sprouts was not different, their length was significantly reduced upon coculture with shTNC

TIFs (Figures 5F and S5J). This result suggests that fibroblasts can also secrete diffusible factors that stimulate HUVEC sprouting in a TNC-dependent manner. In summary, TNC triggers secretion of pro-angiogenic factors in fibroblasts and GBM cells that enhance EC survival, proliferation, and tubulogenesis.

Proteomic Analysis of the Glioblastoma Cell-Derived Secretome Reveals that Pro-angiogenic Ephrin-B2 Is Induced by Tenascin-C

To determine the molecular identity of the pro-angiogenic secretome, we analyzed the CM from U87MG cells exposed to CDM expressing or lacking TNC by quantitative proteomics, employing chemical stable isotope labeling (Shahinian et al., 2014). The secretome comprised a mixture of human and mouse proteins, originating from U87MG, and the MEFs used to generate the CDM. To discriminate between human and mouse proteins, a combined mouse and human database was used for analysis, and only proteins with at least one unique peptide were considered. A total of 1,613 proteins, including 951 human and 662 mouse proteins, were identified and quantified (PX: PXD005217). Changes in protein abundance upon growth on a TNC-containing CDM were expressed as fold-change (Fc) values (log_2) (Table S1) according to Tholen et al. (2013). For U87MG-originating proteins, the distribution of Fc values was close to normal (Figure S6A). To distinguish proteins with altered abundance, we chose a log_2 Fc cutoff of 0.58 for an increase and −0.58 for a decrease in abundance by more than 1.5-fold.

(M) Quantification of adherent pericytes upon plating for 1 hr on wells coated with Col I, FN, and TNC at 2 $\mu g/cm^2$. Values are mean ± SEM from three independent experiments with six replicates.

(N and O) Representative pictures (N) and quantification (O) of pericyte wound closure after 18 hr upon addition of TNC (5 or 20 $\mu g/mL$) or 0.01% Tween 20-PBS (CTRL). Values are mean ± SEM from three independent experiments with four replicates.
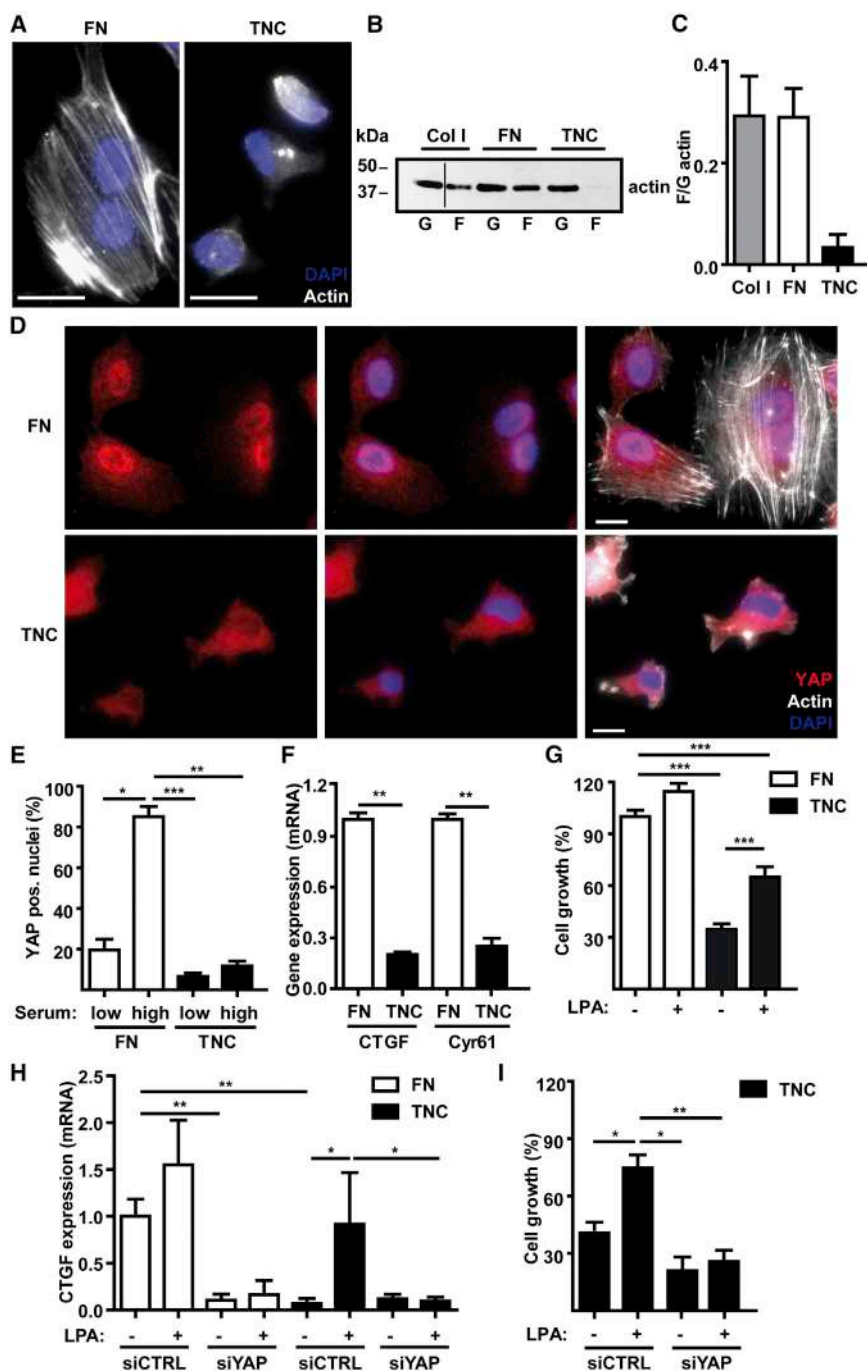
See also Figure S2.

Figure 4. TNC Represses Actin Polymerization and YAP Nuclear Shuttling in ECs

(A) Representative images of actin polymerization (phalloidin, white) and nuclei (DAPI, blue) of HUVECs upon growth on FN or TNC for 5 hr in full medium (scale bar, 5 μm).

(B and C) Analysis of G-actin (globular) and F-actin (fibrillar) in HUVECs by immunoblotting upon plating on the indicated substrata for 5 hr in full medium. (C) Quantification of the immunoblotting signals expressed as F/G actin ratio (three independent experiments).

(D) Representative images of YAP (red), polymerized actin (phalloidin, white), and nuclei (DAPI, blue) of HUVECs upon growth on FN or TNC for 5 hr (scale bar, 5 μm).

(E) Quantification of YAP-positive nuclei normalized to DAPI-positive nuclei. 30–40 cells were counted in four to six randomly chosen fields per condition. Values are mean ± SEM, described as a percentage of YAP-positive nuclei, from three independent experiments with three replicates.

(F) qRT-PCR analysis of the YAP target genes CTGF and Cyr61 in HUVECs upon growth on FN or TNC for 24 hr in full medium (five independent experiments).

(G) Assessment of HUVEC growth (MTS assay) upon treatment with 10 μM lysophosphatidic acid (LPA) 48 hr after seeding on the FN or TNC substratum (1 μg/cm^2) in full medium. Values are mean ± SEM from four independent experiments with four replicates.

(H) qRT-PCR analysis of CTGF YAP target gene expression in HUVECs upon treatment with LPA and small interfering RNA (siRNA) for YAP (siYAP) or controls (siCTRL) 24 hr after growth on FN or TNC in full medium (five independent experiments).

(I) Growth analysis (MTS assay) of HUVECs transfected with siCTRL or siYAP RNA upon treatment with LPA for 48 hr and growth on TNC (1 μg/cm^2) in full medium. Relative growth of HUVECs was normalized to transfected cells with siCTRL and to cells seeded on FN. Values are mean ± SEM from four independent experiments with three replicates.
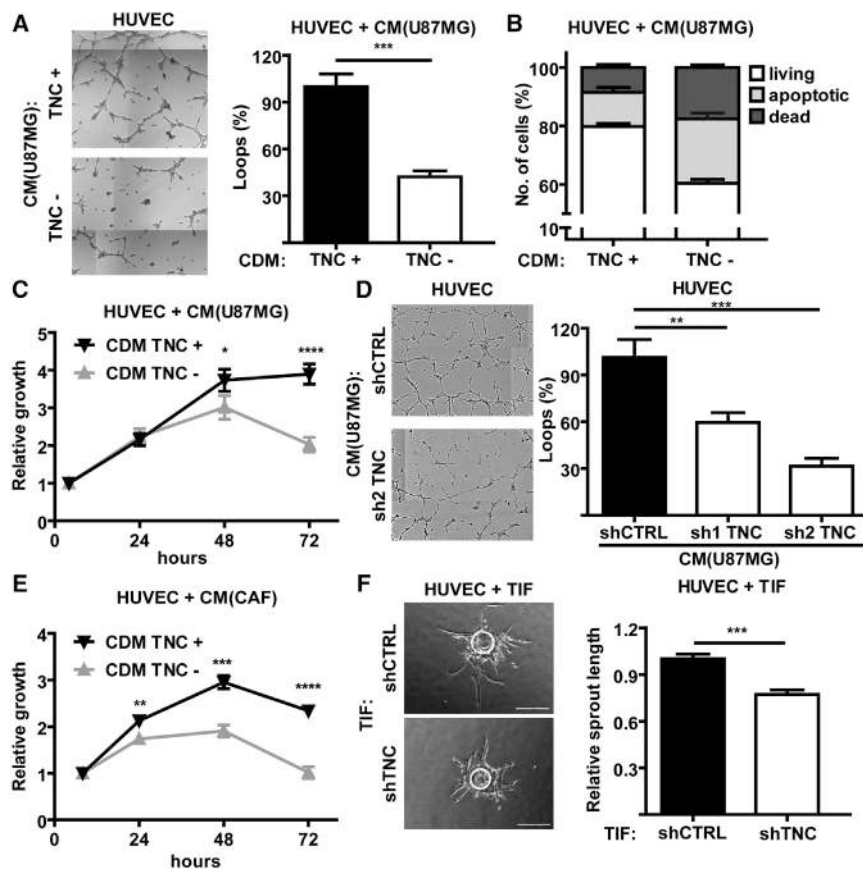
See also Figure S4.

induced CM. Among a selected list of human proteins (Figure 6A), we validated that ephrin-B2 is overexpressed in CM from U87MG cells exposed to TNC (Figure 6B). Ephrin-B2 has been assigned a pro-angiogenic role (Abéngozar et al., 2012), raising the possibility that ephrin-B2 is a target of TNC-increased angiogenesis. We also detected higher ephrin-B2 levels in CM from U118MG and U373MG cells that had been grown on TNC-containing CDM (Figure S6B). Finally, ephrin-B2 protein and mRNA levels were also higher in U87MG shCTRL cells compared to shTNC KD cells (Figures S6C and S6D).

To test ephrin-B2 as effector molecule of TNC-promoted angiogenesis, we targeted ephrin-B2-driven signaling using the

Moreover, we focused on secreted proteins and found 65 U87MG-originating proteins upregulated by more than 1.5-fold upon growth on a TNC-containing CDM, while 156 proteins were downregulated (Table S2).

Using gene ontology analysis, no apparent angiogenic assignment of secreted proteins regulated by TNC was noted (data not shown). Given the demonstrated pro-angiogenic activity of the secretome, we specifically searched our proteomic data for pro-angiogenic proteins with increased abundance in the TNC-

Figure 5. TNC-Educated CM from GBM Cells or CAFs Promotes Angiogenesis In Vitro

(A) Number of closed loops upon growth of HUVECs (7 hr) on Matrigel and treatment with CM from U87MG cells grown on CDM from MEFs expressing (TNC+) or lacking TNC (TNC−). Values are mean ± SEM from three independent experiments with four or five replicates.

(B) Assessment of HUVEC viability after 48 hr by EB/AO staining upon addition of CM derived from U87MG cells grown on CDM deposited by MEFs expressing (TNC+) or lacking TNC (TNC−). Bars represent the percentage of viable, apoptotic, and dead cells (with SEM) from three independent experiments with three replicates.

(C) Assessment of HUVEC growth (MTS assay) upon treatment with CM derived from U87MG cells grown on CDM from MEFs expressing (TNC+) or lacking TNC (TNC−). Values are mean ± SEM from three independent experiments with six replicates.

(D) Quantification of endothelial closed loops of HUVECs upon growth on Matrigel for 7 hr with CM derived from U87MG shCTRL, sh1 TNC, and sh2 TNC cells. Values are mean ± SEM from three independent experiments with five replicates.

(E) MTS assay for HUVECs treated with CM derived from CAFs grown on CDM from MEFs expressing (TNC+) or lacking TNC (TNC−). Values are mean ± SEM from three independent experiments with six replicates.

(F) Quantification and representative pictures of sprout length of HUVECs adsorbed to beads in coculture with TIF shCTRL and TIF shTNC 3 days after embedding into a fibrin gel. Scale bar, 200 μm. Values are mean ± SEM (TIF shCTRL, 47 beads; TIF shTNC, 46 beads) from three independent experiments. See also Figure S5.

small tyrosine kinase inhibitor NVP-BHG712 to block its receptor, EPHB4 (Martiny-Baron et al., 2010). We observed that NVP-BHG712 treatment impaired the promoting effect of the TNC-instructed CM on EC invasion and tubulogenesis, reaching control levels (Figures 6C, 6D, and S6E). Moreover KD of ephrin-B2 in U87MG (Figure S6F) also repressed the pro-tubulogenic effect of the TNC-instructed secretome, reaching control levels (Figure S6G). Although the CAF-derived TNC-instructed secretome also promoted growth and sprouting of ECs (Figure 5E), we did not observe increased expression of ephrin-B2 by TNC in these cells (Figure S6H), suggesting a TNC-specific effect on GBM cells. Our results demonstrate that the ephrin-B2/EPHB4 axis conveys the pro-angiogenic activity of the TNC-induced CM of GBM cells.

Ephrin-B2 is either membrane bound, released into extracellular vesicles, or secreted as a soluble molecule upon proteolytic cleavage (Ji et al., 2013; Pasquale, 2010). By fractionation followed by immunoblotting, we detected ephrin-B2 in the soluble fraction and not in extracellular microvesicles or exosomes (Figure S6I), suggesting a cleavage-dependent mechanism for its release into the CM. To address which protease potentially released ephrin-B2, we used inhibitors for metalloproteinases (MMPs) (broad spectrum), ADAMs, and γ-secretase, covering the major proteases known to cleave ephrin-B2 (Ji et al.,

2013; Pasquale, 2010). Whereas inhibition of γ-secretase did not have an effect on ephrin-B2 release, inhibition of ADAM10/17 and MMPs repressed ephrin-B2 release into the CM (Figure S6J).

In Experimental Glioblastoma, Tenascin-C Promotes a Poor Functional Vasculature and Reduces Ephrin-B2 Expression

TNC is highly expressed in human glioma, which is mimicked in glioblastoma xenograft models (Herold-Mende et al., 2002). We analyzed the TNC expression pattern in intracranial and subcutaneous U87MG tumor xenografts using species-specific anti-TNC antibodies. In both models, TNC was mainly expressed by tumor cells (Figures S7A and S7B) and blood vessels were largely embedded in a TNC-rich matrix (Figures S7C and S7D), thus suggesting a potential role of TNC proximity in poor vessel integrity (see below).

To validate the functional significance of the TNC/ephrin-B2 axis in GBM angiogenesis, we analyzed tumor growth and angiogenesis in U87MG tumors derived from subcutaneous grafting of control and TNC KD cells. TNC did not affect the in vitro growth of these cells on a TNC substratum or in spheroids (Figures S7E–S7G). Tumors grown for 55 days were smaller (as deduced by their weight and volume) upon grafting of TNC KD cells, and
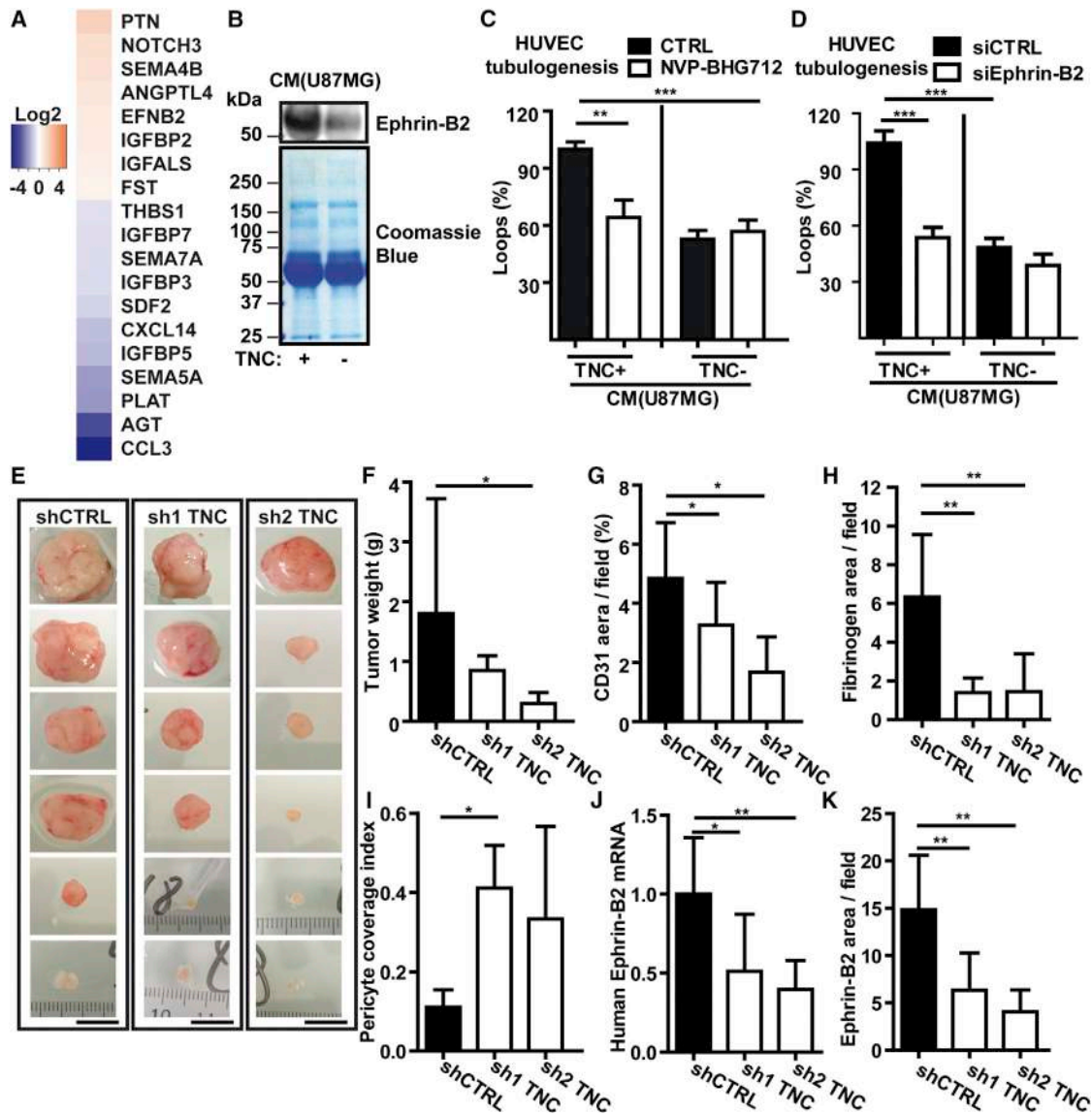
Figure 6. TNC-Derived Upregulated Secretome Promotes Angiogenesis through Ephrin-B2/EPHB4

(A) Heatmap representing selected candidates in the TNC-derived U87MG secretome. Data are shown in log2 scale with representation of upregulated proteins in orange and downregulated proteins in blue. PTN, pleiotrophin; NOTCH3, neurogenic locus notch homolog protein 3; SEMA, semaphoring; EFNB2, ephrin-B2; ANGPTL4, angiopoietin-like 4; IGFALS, insulin-like growth factor binding protein, acid labile subunit; FST, follistatin; CXCL14, chemokine (C-X-C motif) ligand 14; IGFBP, insulin-like growth factor-binding protein; TSP1, thrombospondin-1; PLAT, tissue plasminogen activator; AGT, angiotensinogen; CCL3, chemokine (C-C motif) ligand 3; SDF2, stromal cell-derived factor 2.

(B) Immunoblotting for human ephrin-B2 of TNC-educated CM from U87MG cultivated for 48 hr on CDM of MEFs expressing (TNC+) or lacking TNC (TNC−). Coomassie-blue-stained gel serves as control for equal protein loading.

(C and D) Assessment of HUVEC closed loop formation 7 hr after seeding on Matrigel together with (C) TNC-educated CM derived from U87MG cells treated with the EPHB4 inhibitor NVP-BHG712 (500 nM) and (D) upon ephrin-B2 KD (siRNA). Values are mean ± SEM from three independent experiments and four or five replicates.

(E and F) Pictures of six representative tumors (E) and weight of U87MG shCTRL and shTNC subcutaneous tumors (F). Values are mean ± SD; n = 9 tumors per condition with one tumor per mouse.

(G) Blood vessel density measured as CD31 signal in six fields per tumor. Values are mean ± SD; n = 6 tumors per condition.

(H) Blood vessel leakiness assessed by quantification of the FBG signal per field measured in six random fields per tumor. Values are mean ± SD; n = 6 tumors per condition.

(I) Pericyte blood vessel coverage assessed by measuring combined signals for CD31 and NG2 per field, with six fields per tumor. Values are mean ± SD; n = 6 tumors per condition.

(legend continued on next page)

331

this effect was significant in sh2 TNC cells (Figures 6E, 6F, and S7H) and was correlated with reduced TNC expression. Whereas no difference in host-derived (murine) TNC expression was seen, tumor cell-derived (human) TNC expression was lower in shTNC tumors, indicating that the TNC KD was active in vivo (Figures S7I and S7J). These results showed that TNC promoted U87MG tumor growth.

By CD31 staining, we observed that blood vessels were more numerous in control tumors than in TNC KD tumors (Figure 6G). Given its close proximity to blood vessels (Figure S7D), TNC may affect vessel function. Assessing the expression of fibrinogen (FBG) that spills out into the surrounding tissue from tumor vessels as a readout for vessel leakiness, we determined either the covered FBG surface or the leakiness score, which includes the relative abundance of leakage sites (Figures S7K and S7L). We observed that vessels were more leaky in control tumors than in TNC KD tumors (Figures 6H and S7M). We also analyzed pericyte abundance and coverage of blood vessels by tissue staining for NG2 and observed fewer pericytes and a lower pericyte coverage index in control tumors (Figures 6I, S7N, and S7O).

Analysis of ephrin-B2 expression in U87MG tumors revealed that whereas murine ephrin-B2 was not different (Figure S7P), human ephrin-B2 mRNA and protein levels were significantly higher in control tumors than in TNC KD tumors (Figures 6J, 6K, and S7Q). Thus, TNC promotes ephrin-B2 expression in GBM cells, which correlates with more but less functional blood vessels.

Combined Tenascin-C and Ephrin-B2 as well as the Tenascin-C-Dependent Protein Signature Correlate with Poor Glioma Patient Survival

It was already known that TNC mRNA levels correlate with worsened overall survival (Midwood et al., 2011) and that ephrin-B2 protein levels correlate with lower progression-free survival of GBM patients (Tu et al., 2012). We now revisited the expression of these two molecules using publicly available transcriptome data of two larger cohorts from The Cancer Genome Atlas (TCGA) comprising 745 glioma patients with 540 GBM and 205 low-grade glioma (LGG) specimens to determine how combined expression of TNC and ephrin-B2 or expression of our identified TNC-upregulated list of 65 proteins (Table S2) correlated with patient survival. This analysis substantiated published results and demonstrated that high ephrin-B2 expression correlates with shorter overall survival of LGG and GBM patients (Figures S8A and S8B). In addition TNC, which was found to be one of the most overexpressed genes in GBM, ranging in the top 2% of overexpressed genes with a 36-fold higher level in the GBM patients (Figure S8C), was also correlated with shorter survival in GBM and LGG patients (Figures S8D and S8E). Moreover, the prediction power largely increased when the combined expression of ephrin-B2 and TNC was used (Figures 7A and 7B). Furthermore, by patient stratification using a cutoff for

assignment into high and low averages of gene expression of the TNC signature, we observed that higher expression of the 65 upregulated candidates was correlated with shorter survival of GBM and LGG patients (Figures 7C and 7D). However, there was no correlation between our signature and prognosis of patients with head and neck squamous cell carcinoma; breast, colon, lung, and ovarian cancers; or melanoma (Figures S9A–S9F), demonstrating a selected specificity of this signature for glioma malignancy. Our results thus demonstrate that the combined expression of ephrin-B2 and TNC as well as the TNC-derived signature has a strong negative prognostic value for survival of LGG and GBM patients that is higher than that observed for TNC and ephrin-B2 alone.

Inhibition of EPHB4 Reduces Glioblastoma Vessel Formation and Growth

Finally, we assessed a potential anti-tumorigenic effect of EPHB4 inhibition in GBM by intraperitoneal administration of the specific EPHB4 kinase inhibitor NVP-BHG712 in U87MG-tumor-bearing mice (Martiny-Baron et al., 2010). We observed a significantly reduced tumor growth (Figure 7E), a reduced proliferation index (Figure 7F), and a decrease in vessel density (Figure 7G) in treated mice. We conclude that targeting the ephrin-B2/EPHB4 axis has treatment potential for GBM.

In summary, our study shows that TNC stimulates the angiogenic properties of fibroblasts and GBM cells by altering the composition of their secretomes. We revealed ephrin-B2 as novel pro-angiogenic factor that is upregulated by TNC in GBM cells in vitro and in vivo. Furthermore, ephrin-B2 notably conveys TNC pro-angiogenic activity. This might be relevant for treating GBM patients, as blocking EPHB4 reduced GBM growth. In contrast, a direct interaction with TNC interferes with EC survival, proliferation, and tubulogenesis, thus counteracting the pro-angiogenic paracrine activities of TNC. We describe YAP as a novel downstream target that is impaired by the anti-adhesive activity of TNC. Cytoplasmic sequestration of YAP by TNC results in repression of pro-angiogenic genes. Thus, a concurrent action of direct and paracrine responses to TNC in the TME could determine whether ECs react by thriving or dying (Figure 7H).

DISCUSSION

Some studies have investigated a potential role of TNC in tumor angiogenesis, but mechanistic insight was lacking (reviewed in Orend et al., 2014). Here, we used several state-of-the-art angiogenesis models to comprehensively address the roles of TNC in tumor angiogenesis. We demonstrated independent pro- and anti- angiogenic effects of TNC. It is remarkable that TNC is mostly absent from healthy arteries or veins (Kimura et al., 2014; Mustafa et al., 2012) as well as from remodeling angiogenic tissues such as the endometrium or placenta (Mustafa

---

(J and K) Ephrin-B2 levels in U87MG shCTRL and TNC KD tumors. (J) Human ephrin-B2 mRNA levels (qRT-PCR analysis). Values are mean ± SD; n = 9, 8, and 6 tumors for shCTRL, sh1 TNC, and sh2 TNC cells, respectively. (K) Ephrin-B2 quantification by tissue staining. Values are mean ± SD; n = 6 tumors per condition and ten fields per tumor.
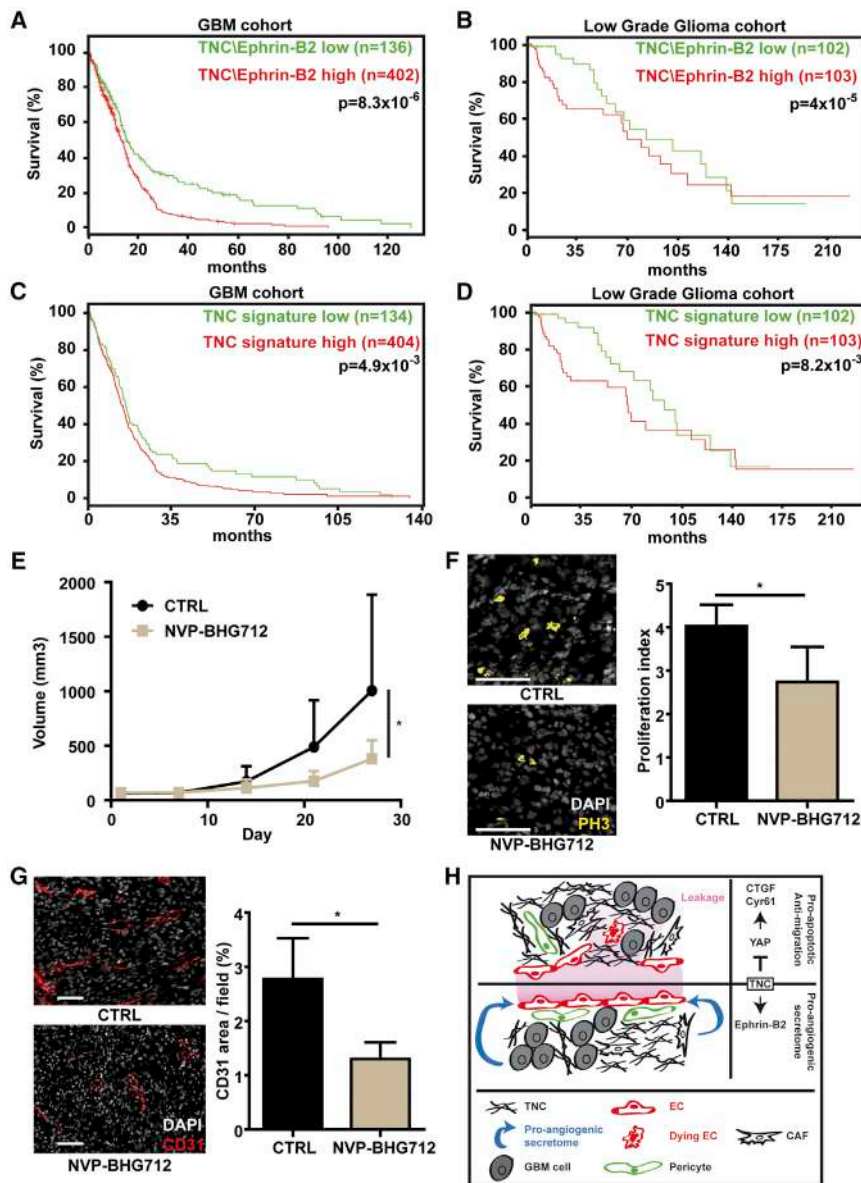See also Figures S6 and S7 and Tables S1 and S2.

Figure 7. The TNC-Induced Upregulated Secretome and Combined Ephrin-B2/Tenascin-C Expression Are Highly Correlated with Poor Glioma Patient Survival

(A–D) Kaplan-Meier survival analysis of glioma patients from TCGA cohorts. Patients were stratified according to the median average expression of TNC and ephrin-B2 (A and B) and the 65 genes in the TNC upregulated signature (C and D) as high if the value was above the cutoff and as low if the value was below the cutoff. The number of patients in each group is indicated within brackets, and p values indicate the significance of survival differences between the groups of individuals by log-rank test.

(E) Impact of EPHB4 inhibition on U87MG xenograft tumor growth (E) using NVP-BHG712. Values are mean ± SD; n = 5 mice in the control group, n = 6 mice in the NVP-BHG712 group.

(F and G) Pictures and quantification of proliferation index (F) and blood vessel density (G) measured as the fraction of PH3- or CD31-positive cells in six fields per tumor. Values are mean ± SD; n = 5–6 tumors per condition.

(H) Schematic representation of the dual effect of TNC on the TME. In a paracrine manner, TNC promotes tumor angiogenesis by induction of a pro-angiogenic secretome in CAFs and GBM cells. Ephrin-B2 is an important pro-angiogenic molecule induced by TNC in GBM cells. TNC impairs EC survival and migration and pericyte migration, which together may lead to endothelium remodeling and thus contribute to vessel leakage. YAP is repressed by TNC in ECs, thus downregulating pro-angiogenic CTGF and Cyr61, which may promote EC death.

See also Tables S1 and S2.

any of the six analyzed EC cell types, even upon stimulation with TGF-β1, a factor that triggers TNC expression in fibroblasts and pericytes (Scharenberg et al., 2014). However, in a tumor, ECs experience direct contact with TNC provided by perivascular or tumor cells, potentially resulting in endothelium remodeling and subsequent vessel leakage. This possibility is supported by Fujimoto et al. (2016), who demonstrated an enhanced permeability of blood vessels in a model of subarachnoid hemorrhaging upon injection of purified TNC. However, similar experiments in normal mice did not induce vessel permeability or leakiness (Fujimoto et al., 2016). TNC expression around blood vessels also impairs vessel regeneration in the ischemic liver (Kuriyama et al., 2011) and might counteract vessel stability in the CNS (Bicer et al., 2010). These data suggest that whereas normal vessels may be resistant to TNC-induced damage, TNC, accumulated during diseases, affects vessel remodeling and vessel functionality. This is now confirmed in the U87MG xenograft model, where we have shown that TNC reduces vessel maturation, resulting in increased blood vessel leakage. As in RIP1Tag2 tumors (Saupe et al., 2013), we observed that TNC impairs pericyte

et al., 2012), yet TNC can be highly expressed in angiogenic conditions found in chronic inflammatory tissues, wound healing, and cancer (reviewed in Orend et al., 2014). Outgrowth of aortic sprouts expressing TNC and cocultures of ECs with CAFs (expressing abundant or lowered TNC) revealed an inhibitory effect of TNC on endothelial tubulogenesis. Moreover, TNC reduces survival and inhibits proliferation and migration of ECs, which may be related to poor cell adhesion to TNC and subsequent anoikis. In some tumor types, including glioma, TNC levels increase with tumor grade (Herold-Mende et al., 2002; Saupe et al., 2013). Whereas TNC is weakly expressed around blood vessels in LGG, perivascular TNC is frequent in GBM (Martina et al., 2010; Mustafa et al., 2012). Thus, in cancer tissue, TNC may influence EC behavior due to its close proximity. Interestingly, in cell culture, we could not detect expression of TNC in

coverage in U87MG tumors. Thus, dynamic TNC expression can induce vascular remodeling and tumor vessel leakage.

We find that TNC impairs EC adhesion, thus blocking actin polymerization into actin stress fibers. How cells interpret this particular adhesion is not completely understood. YAP/TAZ signaling acts as a sensor of cell adhesion and actin polymerization and regulates migration and proliferation (Halder et al., 2012). YAP/TAZ are translocated into the nucleus upon actin polymerization and thus trigger gene transcription (Halder et al., 2012). Here, we find that TNC directly represses EC proliferation through impaired YAP nuclear translocation, likely contributing to the anti-angiogenic effects of TNC. In support of this possibility, we demonstrated that TNC downregulates expression of the pro-angiogenic YAP target genes CTGF and Cyr61 (Brigstock, 2002). Moreover, repression of YAP target genes and inhibition of proliferation by TNC occurs through YAP, since restoration of cell spreading and actin polymerization on TNC by LPA increases cell growth, which is inhibited by KD of YAP.

We also analyzed paracrine mechanisms and focused on gliomas where high TNC expression correlates with malignancy (Midwood et al., 2011). We observed that TNC triggers secretion of soluble factors in three different human GBM cell lines and that this secretome promotes survival, proliferation, and tubulogenesis of ECs. Our mass spectrometric analysis showed that the secretome of TNC-instructed U87MG cells differs from that of cells not educated by TNC. Among 221 differently expressed molecules, 65 were upregulated, and their combined expression correlates with poor patient survival in two large cohorts of LGG and GBM patients. Thus, expression of these factors could be valuable for glioma (and in particular LGG) patient survival prediction.

We identified pro-angiogenic ephrin-B2 (Abéngozar et al., 2012) as an important target of TNC in the U87MG signature, and we validated this in vivo. Ephrins, transmembrane signaling proteins, play an important role in physiological and tumor angiogenesis, which applies in particular to ephrin-B2 and its receptor, EPHB4 (Pasquale, 2010). Using a pharmacological EPHB4 inhibitor (Martiny-Baron et al., 2010), we demonstrated its important role in TNC-induced pro-angiogenic paracrine signaling. This appears to be specific to GBM cells, since TNC did not increase ephrin-B2 in CAFs. Ephrin-B2 has been described to activate EPHB4 through membrane-mediated cell-cell contact (Pasquale, 2010) that may involve exosomes where ephrin-B2 is abundant (Ji et al., 2013). Ephrin-B2 can also be released upon proteolytic cleavage by MMP2 and MMP9 (Lin et al., 2008), ADAMs, or γ-secretase (Pasquale, 2010). We showed that ephrin-B2 acts as a soluble factor in the TNC-dependent secretome and is released from U87MG cells by MMPs and ADAM10/17. Previously it was shown that high expression of ephrin-B2 or EPHB4 correlates with low progression-free survival (Tu et al., 2012) and that high levels of TNC have been linked to shorter overall survival of glioma patients (Midwood et al., 2011). Importantly, here we found not only that the expression of ephrin-B2 or TNC alone correlates with poor overall survival in two large cohorts of LGG and GBM but also that concomitant high expression of TNC and ephrin-B2 has an even more significant predictive value.

Our results showed for the first time that inhibition of EPHB4 reduces GBM tumor growth and angiogenesis, as had previously been seen for other tumors (Abéngozar et al., 2012; Martiny-Baron et al., 2010). Thus, pharmacological targeting of the TME by compounds that block TNC-induced pro-angiogenic signals such as EPHB4 may be useful in blocking GBM tumor angiogenesis and growth.

In conclusion, our study reveals cellular and molecular mechanisms underlying the multiple effects of TNC during tumor angiogenesis. Whereas TNC exerts direct anti-angiogenic activity toward ECs, TNC also controls paracrine pro-angiogenic signals conveyed by tumor cells and CAFs. These opposing effects provide contrasting angiomodulatory functions of TNC in the TME, where its expression promotes the assembly of denser but less functional tumor blood vessels. The TNC-regulated pro- and anti-angiogenic signature, in particular ephrin-B2, may open innovative pharmacological opportunities to counteract TNC activity in GBM.

EXPERIMENTAL PROCEDURES

Animal Experiments

In the GBM xenograft model, 5×10^6 U87MG control (shCTRL) and knockdown cells (shTNC) were diluted in 100 μL PBS and injected subcutaneously in the left upper back of nude mice (Charles River Laboratories); after 55 days, mice were sacrificed. Analysis of EPHB4 inhibition on tumor development was done by subcutaneously engrafting 5×10^6 U87MG shCTRL cells into nude mice. Animals were grouped randomly when tumors reached an average size of 70 mm^3. NVP-BHG712 (diluted in DMSO) was applied daily by intraperitoneal injection for 4 weeks at 10 mg/kg. DMSO alone was applied as control. Tumor size was measured every 3 or 7 days with a caliper, and tumor volume was calculated using the formula $V = (a^2 * b)/2$, where b is the longest axis and a is the perpendicular axis to b. Tumor tissue was snap frozen in liquid nitrogen or directly embedded in O.C.T. and further analyzed by qRT-PCR and immunostaining. For GBM intracranial xenograft tumors, 1×10^6 U87MG cells were injected into nude mice and tumors were collected after 35 days. Tumor tissues were directly embedded in O.C.T. for further analysis by immunostaining. Experiments with animals were performed according to the guidelines of INSERM and the ethical committee of Alsace, France (CREMEAS).

Vascular Coculture Assay

The protocol from Ghajar et al. (2013) was adapted. Briefly, CAF control (shCTRL) or KD for TNC (shTNC) cells were seeded at a density of 50,000 cells per well in 96-well culture plates together with VeraVec HUVECs at a 5:2 ratio. The cell mixture was suspended in ECGM medium. During the 7 days of coculture in ECGM, the medium was replenished every 2 days. Then, cells were fixed and stained with a CD31 antibody and DAPI. Total closed loops were counted using ZEN Blue software (Carl Zeiss) as a readout for network complexity. Three independent experiments were done, with six replicates per experiment.

Statistical Analysis

All in vitro and ex vivo experiments were performed at least three times independently using at least three biological replicates per experiment (except for qPCR, which used one biological replicate). Statistical analysis and graphical representation were done using GraphPad Prism or R. p values < 0.05 were considered as statistically significant ($*p < 0.05$; $**p < 0.01$; $***p < 0.001$; $****p < 0.0001$).

ACCESSION NUMBERS

The accession number for the mass spectrometry proteomics data reported in this paper is PX: PXD005217.

SUPPLEMENTAL INFORMATION

Supplemental Information includes Supplemental Experimental Procedures, eleven figures, and two tables and can be found with this article online at http://dx.doi.org/10.1016/j.celrep.2016.11.012.

AUTHOR CONTRIBUTIONS

T.R., B.L., E.V.O.-S., O.S., and G.O. designed the experiments; T.R., B.L., M.M.K., A.R., S.Z., D.M., I.V.-Q., and O.L. performed experiments and analyzed the data; C.A., A.K., M.L.B., V.H., and E.N. provided technical assistance; T.H. provided scientific support; E.V.O.-S and O.S. critically reviewed the manuscript; and T.R. and G.O. wrote the manuscript.

REFERENCES

Abéngozar, M.A., de Frutos, S., Ferreiro, S., Soriano, J., Perez-Martinez, M., Olmeda, D., Marenchino, M., Cañamero, M., Ortega, S., Megias, D., et al. (2012). Blocking ephrinB2 with highly specific antibodies inhibits angiogenesis, lymphangiogenesis, and tumor growth. Blood *119*, 4565–4576.

Bayless, K.J., and Johnson, G.A. (2011). Role of the cytoskeleton in formation and maintenance of angiogenic sprouts. J. Vasc. Res. *48*, 369–385.

Beacham, D.A., Amatangelo, M.D., and Cukierman, E. (2007). Preparation of extracellular matrices produced by cultured and primary fibroblasts. Curr. Protoc. Cell Biol. *Chapter 10*, Unit 10.9.

Bicer, A., Guclu, B., Ozkan, A., Kurtkaya, O., Koc, D.Y., Necmettin Pamir, M., and Kilic, T. (2010). Expressions of angiogenesis associated matrix metalloproteinases and extracellular matrix proteins in cerebral vascular malformations. J. Clin. Neurosci. *17*, 232–236.

Bissell, M.J., and Radisky, D. (2001). Putting tumours in context. Nat. Rev. Cancer *1*, 46–54.

Brigstock, D.R. (2002). Regulation of angiogenesis and endothelial cell function by connective tissue growth factor (CTGF) and cysteine-rich 61 (CYR61). Angiogenesis *5*, 153–165.

Calvo, F., Ege, N., Grande-Garcia, A., Hooper, S., Jenkins, R.P., Chaudhry, S.I., Harrington, K., Williamson, P., Moeendarbary, E., Charras, G., and Sahai, E. (2013). Mechanotransduction and YAP-dependent matrix remodelling is required for the generation and maintenance of cancer-associated fibroblasts. Nat. Cell Biol. *15*, 637–646.

Campbell, N.E., Kellenberger, L., Greenaway, J., Moorehead, R.A., Linnerth-Petrik, N.M., and Petrik, J. (2010). Extracellular matrix proteins and tumor angiogenesis. J. Oncol. *2010*, 586905.

Fujimoto, M., Shiba, M., Kawakita, F., Liu, L., Shimojo, N., Imanaka-Yoshida, K., Yoshida, T., and Suzuki, H. (2016). Deficiency of tenascin-C and attenuation of blood-brain barrier disruption following experimental subarachnoid hemorrhage in mice. J. Neurosurg. *124*, 1693–1702.

Ghajar, C.M., Peinado, H., Mori, H., Matei, I.R., Evason, K.J., Brazier, H., Almeida, D., Koller, A., Hajjar, K.A., Stainier, D.Y.R., et al. (2013). The perivascular niche regulates breast tumour dormancy. Nat. Cell Biol. *15*, 807–817.

Halder, G., Dupont, S., and Piccolo, S. (2012). Transduction of mechanical and cytoskeletal cues by YAP and TAZ. Nat. Rev. Mol. Cell Biol. *13*, 591–600.

Hanahan, D. (1985). Heritable formation of pancreatic beta-cell tumours in transgenic mice expressing recombinant insulin/simian virus 40 oncogenes. Nature *315*, 115–122.

Hanahan, D., and Weinberg, R.A. (2011). Hallmarks of cancer: the next generation. Cell *144*, 646–674.

Herold-Mende, C., Mueller, M.M., Bonsanto, M.M., Schmitt, H.P., Kunze, S., and Steiner, H.-H. (2002). Clinical impact and functional aspects of tenascin-C expression during glioma progression. Int. J. Cancer *98*, 362–369.

Hynes, R.O. (2009). The extracellular matrix: not just pretty fibrils. Science *326*, 1216–1219.

Jain, R.K. (2014). Antiangiogenesis strategies revisited: from starving tumors to alleviating hypoxia. Cancer Cell *26*, 605–622.

Ji, H., Greening, D.W., Barnes, T.W., Lim, J.W., Tauro, B.J., Rai, A., Xu, R., Adda, C., Mathivanan, S., Zhao, W., et al. (2013). Proteome profiling of exosomes derived from human primary and metastatic colorectal cancer cells reveal differential expression of key metastatic factors and signal transduction components. Proteomics *13*, 1672–1686.

Kalluri, R., and Zeisberg, M. (2006). Fibroblasts in cancer. Nat. Rev. Cancer *6*, 392–401.

Kimura, T., Shiraishi, K., Furusho, A., Ito, S., Hirakata, S., Nishida, N., Yoshimura, K., Imanaka-Yoshida, K., Yoshida, T., Ikeda, Y., et al. (2014). Tenascin C protects aorta from acute dissection in mice. Sci. Rep. *4*, 4051.

Kuriyama, N., Duarte, S., Hamada, T., Busuttil, R.W., and Coito, A.J. (2011). Tenascin-C: a novel mediator of hepatic ischemia and reperfusion injury. Hepatology *54*, 2125–2136.

Lamalice, L., Le Boeuf, F., and Huot, J. (2007). Endothelial cell migration during angiogenesis. Circ. Res. *100*, 782–794.

Langlois, B., Saupe, F., Rupp, T., Arnold, C., van der Heyden, M., Orend, G., and Hussenet, T. (2014). AngioMatrix, a signature of the tumor angiogenic switch-specific matrisome, correlates with poor prognosis for glioma and colorectal cancer patients. Oncotarget *5*, 10529–10545.

Lin, K.-T., Sloniowski, S., Ethell, D.W., and Ethell, I.M. (2008). Ephrin-B2-induced cleavage of EphB2 receptor is mediated by matrix metalloproteinases to trigger cell repulsion. J. Biol. Chem. *283*, 28969–28979.

Martina, E., Degen, M., Rüegg, C., Merlo, A., Lino, M.M., Chiquet-Ehrismann, R., and Brellier, F. (2010). Tenascin-W is a specific marker of glioma-associated blood vessels and stimulates angiogenesis in vitro. FASEB J. *24*, 778–787.

Martiny-Baron, G., Holzer, P., Billy, E., Schnell, C., Brueggen, J., Ferretti, M., Schmiedeberg, N., Wood, J.M., Furet, P., and Imbach, P. (2010). The small molecule specific EphB4 kinase inhibitor NVP-BHG712 inhibits VEGF driven angiogenesis. Angiogenesis *13*, 259–267.

McDonald, D.M., and Choyke, P.L. (2003). Imaging of angiogenesis: from microscope to clinic. Nat. Med. *9*, 713–725.

Midwood, K.S., Hussenet, T., Langlois, B., and Orend, G. (2011). Advances in tenascin-C biology. Cell. Mol. Life Sci. *68*, 3175–3199.

Midwood, K.S., Chiquet, M., Tucker, R.P., and Orend, G. (2016). Tenascin-C at a glance. J. Cell Sci.

Mustafa, D.A.M., Dekker, L.J., Stingl, C., Kremer, A., Stoop, M., Sillevis Smitt, P.A.E., Kros, J.M., and Luider, T.M. (2012). A proteome comparison between physiological angiogenesis and angiogenesis in glioblastoma. Mol. Cell. Proteomics *1*, M111.008466.

Orend, G., Saupe, F., Schwenzer, A., and Midwood, K. (2014). The Extracellular Matrix and Cancer: Regulation of Tumor Cell Biology by Tenascin-C (iConcept Press).

Pasquale, E.B. (2010). Eph receptors and ephrins in cancer: bidirectional signalling and beyond. Nat. Rev. Cancer *10*, 165–180.

335

Posern, G., Sotiropoulos, A., and Treisman, R. (2002). Mutant actins demonstrate a role for unpolymerized actin in control of transcription by serum response factor. Mol. Biol. Cell *13*, 4167–4178.

Saupe, F., Schwenzer, A., Jia, Y., Gasser, I., Spenlé, C., Langlois, B., Kammerer, M., Lefebvre, O., Hlushchuk, R., Rupp, T., et al. (2013). Tenascin-C downregulates wnt inhibitor dickkopf-1, promoting tumorigenesis in a neuro-endocrine tumor model. Cell Rep. *5*, 482–492.

Scharenberg, M.A., Pippenger, B.E., Sack, R., Zingg, D., Ferralli, J., Schenk, S., Martin, I., and Chiquet-Ehrismann, R. (2014). TGF-β-induced differentiation into myofibroblasts involves specific regulation of two MKL1 isoforms. J. Cell Sci. *127*, 1079–1091.

Shahinian, H., Loessner, D., Biniossek, M.L., Kizhakkedathu, J.N., Clements, J.A., Magdolen, V., and Schilling, O. (2014). Secretome and degradome profiling shows that Kallikrein-related peptidases 4, 5, 6, and 7 induce TGFβ-1 signaling in ovarian cancer cells. Mol. Oncol. *8*, 68–82.

Siess, W., Zangl, K.J., Essler, M., Bauer, M., Brandl, R., Corrinth, C., Bittman, R., Tigyi, G., and Aepfelbacher, M. (1999). Lysophosphatidic acid mediates the rapid activation of platelets and endothelial cells by mildly oxidized low density lipoprotein and accumulates in human atherosclerotic lesions. Proc. Natl. Acad. Sci. USA *96*, 6931–6936.

Tholen, S., Biniossek, M.L., Gansz, M., Gomez-Auli, A., Bengsch, F., Noel, A., Kizhakkedathu, J.N., Boerries, M., Busch, H., Reinheckel, T., and Schilling, O. (2013). Deletion of cysteine cathepsins B or L yields differential impacts on murine skin proteome and degradome. Mol. Cell. Proteomics *12*, 611–625.

Tu, Y., He, S., Fu, J., Li, G., Xu, R., Lu, H., and Deng, J. (2012). Expression of EphrinB2 and EphB4 in glioma tissues correlated to the progression of glioma and the prognosis of glioblastoma patients. Clin. Transl. Oncol. *14*, 214–220.

336

Résumé

La ténascine-C (TNC), protéine de la matrice extracellulaire, favorise la progression tumorale et la métastase par des mécanismes pas totalement élucidés. J'ai utilisé un nouveau modèle de progression tumorale de la glande mammaire basé sur une approche de greffe de cellules tumorales orthotopiques syngéniques et j'ai ainsi identifié la TNC comme un régulateur important de la croissance tumorale. L'expression concomitante de la TNC par les cellules de l'hôte et les cellules tumorales induit une régression de la tumeur en induisant une signature de présentation d'antigène. Cette signature a été corrélée avec une meilleure survie des patientes atteintes de cancer du sein. D'autre part, la TNC exprimée par les cellules tumorales induit également l'expression de CXCL12 au sein de la tumeur, piégeant les lymphocytes CD8+ dans des travées de matrice enrichies avec le CXCL12 lié à la TNC. L'inhibition du récepteur de CXCL12, le CXCR4 provoque une régression tumorale qui s'accompagne d'un afflux important de lymphocytes T CD8+ et d'une augmentation de la mort cellulaire au sein du lit tumorale. La séquestration des lymphocytes T cytotoxiques par la TNC dans les travées de matrice peut avoir une implication importante dans le développement et l'utilisation des nouvelles immunothérapies ciblant l'activité des cellules effectrices du système immunitaire.

Mots clés : Ténascine-C, Lymphocytes T CD8+, CXCL12, Immunité anti-tumorale, Présentation d'antigène

Résumé en anglais

The extracellular matrix molecule tenascin-C (TNC) promotes tumor progression and metastasis by poorly understood mechanisms. I used a novel breast progression model based on a syngeneic orthotopic tumor cell grafting approach and identified TNC as an important regulator of tumor growth. I document that TNC promotes the battle between tumor regression and growth, where combined expression of tumor cell- and host-derived TNC induces tumor cell rejection. Tumor cell-derived TNC may elicit regression by induction of an antigen presenting signature (APS) expressed by the host, which correlates with better breast cancer patient survival. Tumor-cell derived TNC also triggers CXCL12 expression, thereby causing trapping of CD8+ T cells in the surrounding TNC matrix tracks. TNC binds CXCL12, and combined TNC/CXCL12 attracts and immobilizes CD8+ T cells. Inhibition of the CXCL12 receptor CXCR4 causes tumor regression that is accompanied by massive infiltration of CD8+ T cells and cell death inside the tumor cell nests. Altogether, TNC-triggered CXCL12 signaling may dampen CD8+ T cell function where physical trapping of CD8+ T cells in the TNC matrix may have implications for immune cell therapies. Our results and new tumor model, offer novel opportunities for preclinical cancer research and cancer patient therapy, by triggering the "good" and blocking the "bad" actions of TNC. In particular, overcoming the immune suppressive action of TNC, through inhibition of CXCR4, could be a useful approach.

Keywords: Tenascin-C, CD8+ T cells, CXCL12, Tumor immunity, Antigen presentation